UNIVERSITE D'AIX-MARSEILLE

UNIVERSITE DE SHANGHAI

ED 352-PHYSIQUE ET SCIENCES DE LA MATIERE

School of Materials Science and Engineering

MADIREL

Thèse présentée pour obtenir le grade universitaire de docteur

Discipline : Physique et Sciences de la Matière
Spécialité : Matière Condensée et Nanosciences

Wei LIU

Etude de l'ordre atomique et du volume molaire dans la phase binaire sigma par approches DFT et CALPHAD

Investigations of the atomic order and molar volume in the binary sigma phase by DFT and CALPHAD approaches

Soutenue le 11/12/2017 devant le jury :

Prof. Li-Jun ZHANG	Central South University	Rapporteur
Prof. Qing-Miao HU	Chinese Academy of Sciences	Rapporteur
Prof. Zhi LIU	Shanghai university	Examinateur
Prof. Jun LUO	Shanghai university	Examinateur
Prof. Pascal BOULET	Aix Marseille university	Directeur de thèse
Prof. Marie-Christine RECORD	Aix Marseille university	Directeur de thèse
Prof. Xiao-Gang LU	Shanghai university	Directeur de thèse

Numéro national de thèse/suffixe local : 2017AIXM0001/001ED62

Résumé de la thèse en français

Les phases topologiquement compactes (TCP) ne sont pas uniquement des précipités préjudiciables que l'on rencontre dans de nombreux matériaux structuraux. Ces phases peuvent être précieuses pour l'optimisation de ces matériaux ou des supraconducteurs fonctionnant à hautes températures. Cependant, leurs propriétés physiques n'ont pas encore été suffisamment étudiées.

En tant que phase TCP type, la phase sigma suscite un grand intérêt. De nombreux travaux ont déjà été reportés sur ses propriétés cristallographiques, physiques et thermodynamiques, en particulier le volume molaire et l'ordre atomique (c'est-à-dire la distribution des constituants atomiques ou la préférence d'occupation des sites non-équivalents de sa structure cristalline). L'ordre atomique affecte un grand nombre de propriétés importantes des phases TCP, comme le volume molaire, le module d'élasticité isostatique, l'enthalpie de formation, etc. Cependant, jusqu'à ce jour, pour la plupart des bases de données thermodynamiques, l'information sur l'occupation du site n'a pas été prise en compte lors des évaluations. Cette insuffisance rend les données moins fiables et limite les échanges entre les bases de données thermodynamiques et les autres bases de données telles que celles contenant les volumes molaires ou les mobilités. De fait toute mise à jour des bases de données thermodynamiques modifie l'occupation des sites et les autres bases de données doivent être modifiées.

L'objectif principal du présent travail est de déterminer les facteurs d'influence sur l'ordre atomique et l'effet de l'ordre atomique sur les propriétés de la phase sigma, telles que le volume molaire, le module d'élasticité isostatique et l'enthalpie de formation. La modélisation thermodynamique et le calcul du volume molaire de la phase sigma binaire ont ensuite été réalisés en utilisant la méthode CALPHAD combinée à des calculs de premier principe.

Dans la section 1, nous présentons, dans une première partie, de façon systématique les caractéristiques générales et les applications de la phase intermétallique. Elle comprend des composés de valence normaux, des composés électroniques, des phases interstitielles, des composés interstitiels, des phases TCP et des superstructures. Dans une deuxième partie, nous présentons de manière détaillée la structure cristalline, le domaine d'homogénéité et les systèmes présentant la phase sigma. Cette phase cristallise dans une structure tétragonale (groupe spatial: $P4_2/mnm$) avec 30 atomes répartis sur cinq sites non équivalents, à savoir 2a, 4f, $8i_1$, $8i_2$ et 8j comme présenté sur les figures 1.1 et 1.2. La phase sigma est signalée comme existant dans 49 systèmes binaires différents. Pour autant que nous le sachions, la phase sigma est le phase intermétallique qui présente le plus large domaine de non stoechiométrie. Enfin, nous

mentionnons brièvement le paramètre de l'ordre à longue distance et le paramètre d'électronégativité.

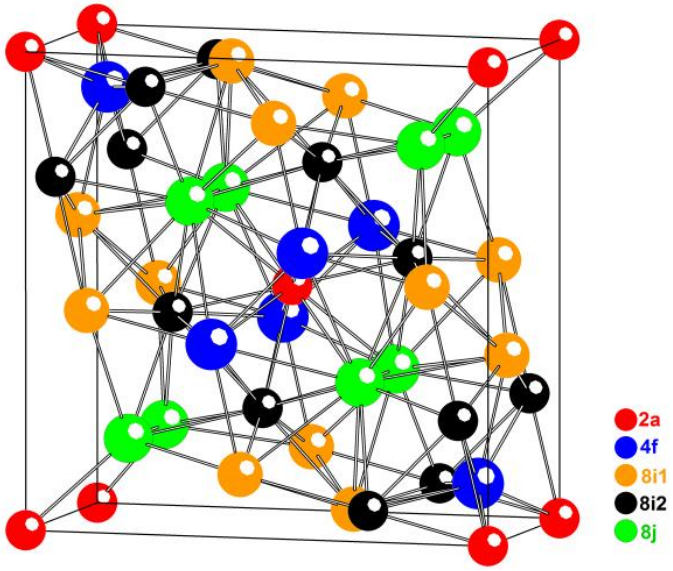

Figure 1.1: Structure cristalline de la phase sigma avec différents atomes occupant les différents sites cristallins, 2a, 4f, $8i_1$, $8i_2$ et 8j.

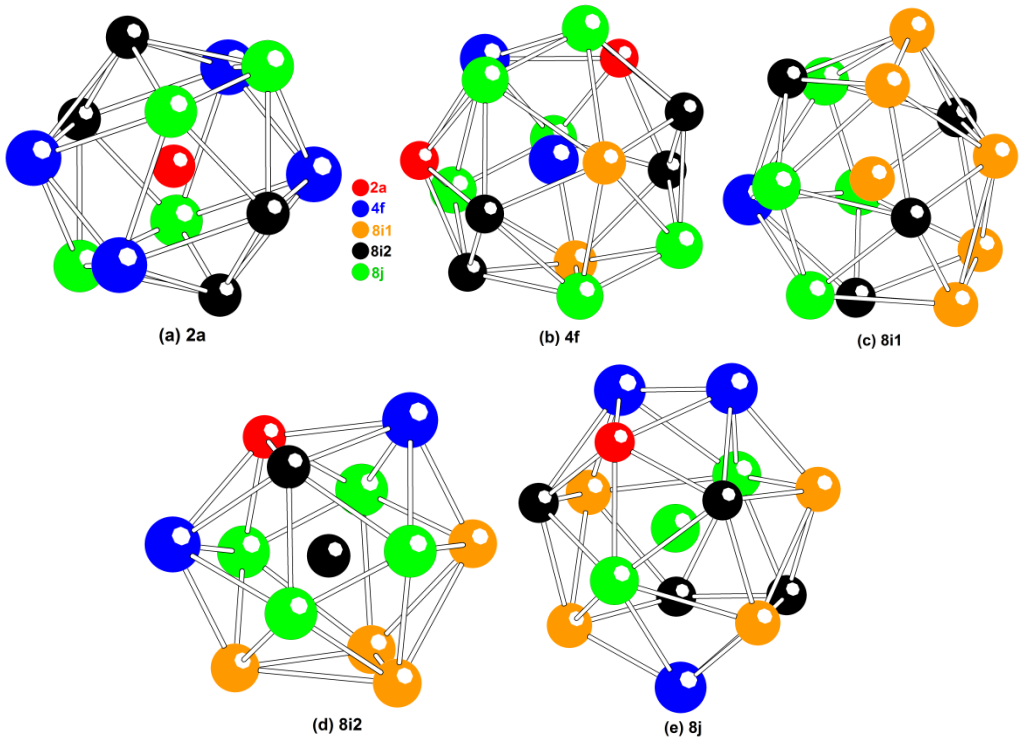

Figure 1.2: Coordination du polyèdre autour de cinq sites non-équivalents de la structure de la phase sigma avec différents atomes sur les différents sites cristallins, 2a, 4f, $8i_1$, $8i_2$ et 8j.

Dans la section 2, nous présentons les méthodes de calcul utilisées dans ce travail, à savoir les calculs de premiers principes et l'approche CALPHAD. Les calculs de premiers principes sont basés sur la théorie de la fonctionnelle de la densité (DFT). Les codes utilisés sont EMTO-CPA (Orbitales exactes de Muffin-Tin – approximation du potentiel cohérent) et VASP (Vienna Ab initio Simulation Package). Les calculs EMTO-CPA facilitent principalement les calculs pour les alliages désordonnés. Les calculs VASP sont pour les structures ordonnées. Nous avons également combiné la théorie Bader des atomes dans les molécules (AIM) avec les calculs VASP pour analyser la charge atomique et le volume atomique de la phase sigma. En ce qui concerne l'approche CALPHAD, différents modèles de volume sont présentés : le modèle de volume pour les substances pures à la pression atmosphérique, le modèle de volume pour les phases en solution à la pression atmosphérique, le modèle de pression et le modèle d'énergie de Helmholtz. Le logiciel utilisé Thermo-Calc est également présenté. Il permet grâce à un ensemble de bases de données de calculer toutes sortes d'équilibres entre phases, de diagrammes de phases et de transformations de phase et de réaliser des évaluations thermodynamiques.

Dans la section 3, nous apportons de nouvelles idées sur les facteurs d'influence de l'ordre atomique (c'est-à-dire la distribution des constituants atomiques ou la préférence d'occupation du site sur les sites non équivalents d'une structure cristalline) dans la phase sigma binaire. Les premiers arguments indiquent que les atomes à grande taille ou pauvres en électrons d occupent préférentiellement des sites à grand nombre de coordination (CN), à savoir 4f, $8i_1$ et 8j; les atomes de petite taille ou riches en électrons d occupent préférentiellement des sites avec un petit CN, à savoir 2a et $8i_2$. Cependant, la conclusion ci-dessus, en se limitant au facteur de taille et au nombre d'électrons de valence, ne peut pas expliquer de manière satisfaisante les occupations du site mesurées ou l'ordre atomique.

Dans le présent travail, nous avons calculé les volumes atomiques et les charges atomiques des éléments constitutifs de 32 composés définis stoechiométriques (c'est-à-dire l'ensemble complet des configurations ordonnées) dans les systèmes de phase sigma binaire en utilisant les calculs VASP combinés avec la théorie des atomes de Bader dans Molécules (AIM). Les résultats des calculs montrent que le facteur de taille, le nombre d'électrons de valence et le nombre total d'orbitales électroniques sont les trois facteurs qui influencent l'ordre atomique de la phase sigma.

Sur la base de ce qui précède, nous classons les phases sigma binaires A-B (l'atome A a toujours une taille plus grande que l'atome B, c'est-à-dire V(A)>V(B)) en fonction de la configuration électronique des éléments constitutifs. Il y a six catégories différentes telles que présentées à la figure 3.1, à savoir les catégories SMe, SMs-SMe, LAs, LAs-SMe, LAs-LAe et A-Al (A=Nb, Ta), où SMe et LAe indiquent que l'atome A a un nombre plus petit ou plus grand d'électrons de valence que l'atome B, respectivement; SMs et LAs indiquent que l'atome A a un nombre total d'orbitales électroniques plus petit ou plus grand que l'atome B, respectivement.

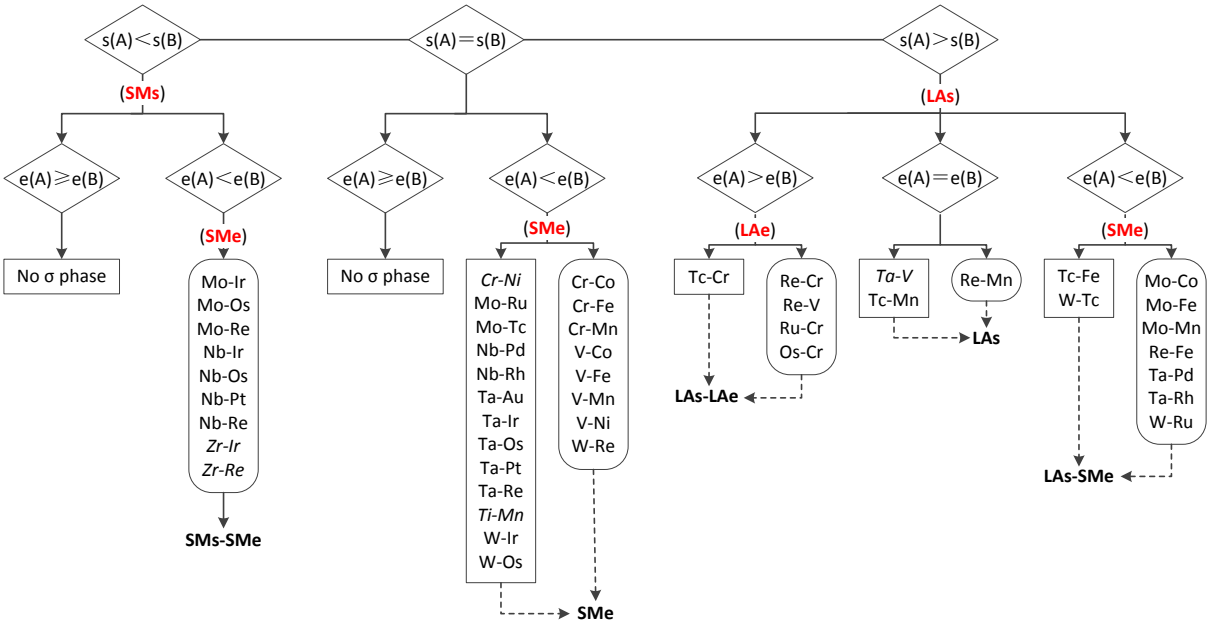

Figure 3.1 : Systèmes binaires A-B (V(A)>V(B)) répartis en differentes categories selon la configuration électronique des éléments constitutifs.

La figure 3.2 et la figure 3.3 présentent le volume atomique en fonction de la charge atomique des éléments constitutifs dans des configurations ordonnées des composés sigma. Elles font apparaître l'ordre suivant pour la taille des cinq sites non équivalents : $4f_{(CN15)}>8i_{1(CN14)}>8j_{(CN14)}>8i_{2(CN12)}>2a_{(CN12)}$.

En outre, la figure 3.2 indique que, entre les deux éléments constitutifs de la phase sigma, celui avec un plus petit nombre total d'orbitales électroniques ou un plus petit nombre d'électrons de valence a tendance à perdre des électrons; celui avec un plus grand nombre total d'orbitales électroniques ou un plus grand nombre d'électrons de valence a tendance à gagner des électrons ; et la figure 3.3 indique qu'en général, les atomes sur les sites 2a et $8i_2$ ont tendance à gagner des électrons et les atomes sur les sites 4f, $8i_1$ et 8j ont tendance à perdre des électrons. Ainsi, en général, entre les deux éléments constitutifs de la phase sigma, celui qui a un nombre total d'orbitales électroniques plus petit ou un nombre d'électrons de valence plus petit préfère occuper des sites avec CN grand (4f, $8i_1$ et 8j) et celui qui a un nombre total d'orbitales électroniques plus grand ou un plus grand nombre d'électrons de valence préfère occuper des sites avec CN petit (2a et $8i_2$). En outre, nous avons dissocié les effets des facteurs d'influence sur l'ordre atomique de la phase sigma en combinant les résultats avec les occupations mesurées du site reportées dans la littérature. L'effet dissocié des facteurs électroniques conduit à l'ordre atomique suivant: LAs: $8i_{2(A)}>2a_{(A)}>8i_{1(A)}>4f_{(A)}/8j_{(A)}$; SMs: $4f_{(A)}/8j_{(A)}>8i_{1(A)}>2a_{(A)}>8i_{2(A)}$; LAe: $8i_{2(A)}>2a_{(A)}>4f_{(A)}>8i_{1(A)}>8j_{(A)}$; SMe: $8j_{(A)}>8i_{1(A)}>4f_{(A)}>2a_{(A)}>8i_{2(A)}$. L'ordre atomique d'un système spécifique est un compromis entre les facteurs d'influence que sont, la taille et les facteurs électroniques.

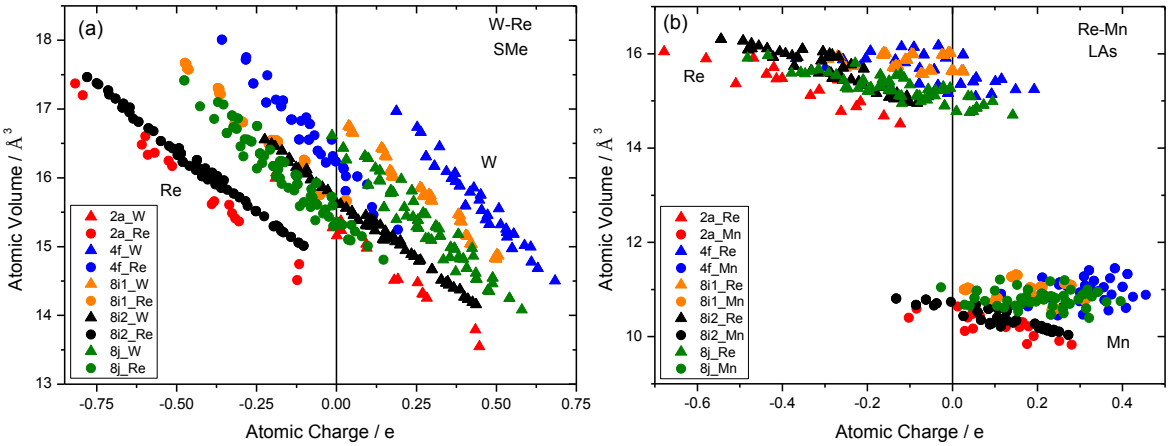

Figure 3.2: Volume atomique en fonction de la charge atomique des éléments constitutifs dans l'ensemble complet (2^5 = 32) des configurations ordonnées ($W_2W_4W_8W_8W_8$, $Re_2W_4W_8W_8W_8$ etc.) des phases sigma W-Re et Re-Mn calculé en utilisant VASP et l'approche AIM de Bader.

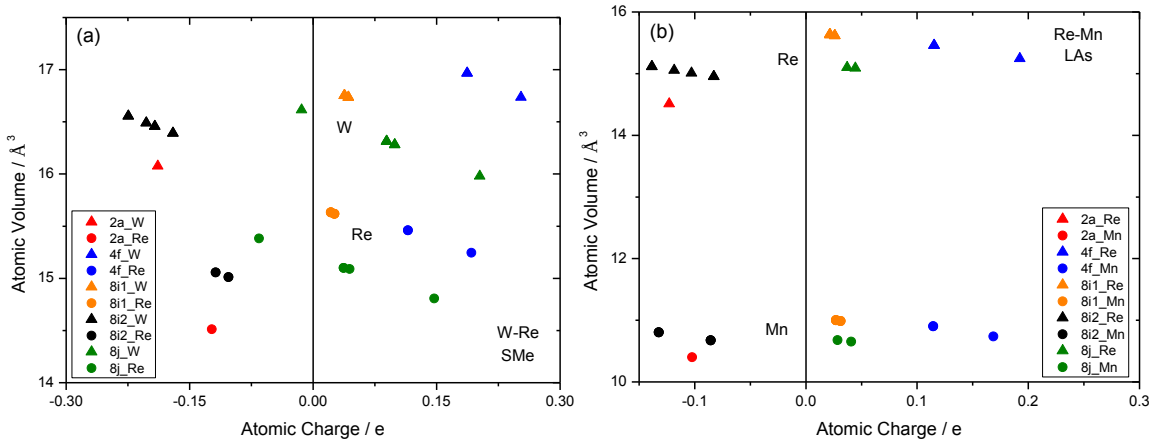

Figure 3.3: Volume atomique en fonction de la charge atomique des éléments purs dans la structure de la phase sigma hypotétique calculée à l'aide de VASP et de l'approche AIM de Bader. Chaque figure contient 30 points mais certains se chevauchent.

Dans la section 4, nous avons systématiquement clarifié l'influence de l'ordre atomique (c'est-à-dire la distribution des constituants atomiques ou la préférence d'occupation des sites sur les sites non équivalents d'une structure cristalline) sur l'enthalpie de formation, le module d'élasticité isostatique et le volume molaire de la phase sigma binaire. Les calculs de ces propriétés par la méthode des premiers principes ont été réalisés pour 19 systèmes de phase sigma binaire avec des ordres atomiques différents basés sur l'occupation du site déterminée expérimentalement ainsi que sur les états hypothétiques ordonnés et désordonnés en utilisant la méthode EMTO-CPA. L'occupation des sites pour la phase sigma A_2B dans les états ordonnés et désordonnés est donnée dans le tableau 4.1. Les résultats des calculs de l'enthalpie de formation et du module d'élasticité isostatique montrent qu'à 0K, la phase sigma dans l'état ordonné présente une enthalpie de formation plus faible et un module d'élasticité isostatique

plus grand que ceux calculés pour un état moins ordonné, comme indiqué dans les tableaux 4.2 et 4.3.

Tableau 4.1: Structure cristalline de la phase sigma avec affectation de l'occupation du site de l'atome A correspondant aux composés ordonnés et désordonnés A_2B et $A_xB_{(1-x)}$ (V(A)>V(B), où V(A) et V(B) sont les volumes molaires des éléments A et B dans leur structure sigma hypothétique déterminés à partir des évaluations CALPHAD).

Groupe d'espace	$P4_2/mnm$ (no. 136)				
Position de Wyckoff	2a	4f	$8i_1$	$8i_2$	8j
Nombre de coordination (CN)	12	15	14	12	14
Etat totalement ordonné (A_2B)	0	1	1	0	1
Etat désordonné (A_xB_{1-x})	x	x	x	x	x

Tableau 4.2: différence de taille entre les éléments constitutifs (A et B) et enthalpie de formation (Hf) de la phase sigma A66.7B33.3 dans les états ordonnés et désordonnés calculés par la méthode EMTO-CPA à 0 K.

catégorie	A-B	$(V_A-V_B)/V_A$	Hf, kJ/mol		catégorie	A-B	$(V_A-V_B)/V_A$	Hf, kJ/mol	
			ordonné	désordonné				ordonné	désordonné
SMe	Cr-Mn	0.0147	-7.88	-1.37	SMs-SMe	Nb-Ir	0.2126	-69.05	-43.13
SMe	Cr-Fe	0.0588	-15.62	-5.04	LAs-SMe	Mo-Mn	0.2386	-13.08	13.68
SMe	V-Mn	0.1052	-16.67	-6.77	LAs-SMe	Mo-Co	0.3087	-29.83	4.27
SMe	Cr-Co	0.1053	-18.79	-7.79	LAs	Re-Mn	0.2006	-15.53	9.68
SMe	V-Fe	0.1453	-29.54	-13.90	LAs-LAe	Re-V	0.1065	-23.29	-13.54
SMe	V-Ni	0.1739	-27.26	-12.35	LAs-LAe	Ru-Cr	0.1298	-9.94	
SMe	V-Co	0.1876	-37.06	-19.56	LAs-LAe	Re-Cr	0.1887	-18.09	1.32
SMs-SMe	Mo-Re	0.0476	-11.33	-3.87	X-Al	Nb-Al	0.143	-39.69	-10.63
SMs-SMe	Mo-Os	0.0856	-28.18	-13.85	X-Al	Ta-Al	0.1454	-30.54	0.97

Tableau 4.3: module d'élasticité isostatique (B_0) et volume molaire correspondant (Vm) pour la phase sigma $A_{66.7}B_{33.3}$ calculés par EMTO_CPA dans les états ordonné et désordonné à 0 K.

A_xB_y	B_0, Gpa		Vm, 10^{-6} m^3/mol	
	ordonné	désordonné	ordonné	désordonné
$Cr_{66.7}Co_{33.3}$	251.345	242.347	6.799	6.869
$Cr_{66.7}Fe_{33.3}$	257.813	249.913	6.801	6.855
$Cr_{66.7}Mn_{33.3}$	255.737	250.914	6.921	6.950
$V_{66.7}Co_{33.3}$	206.275	195.199	7.467	7.566
$V_{66.7}Fe_{33.3}$	212.796	203.138	7.491	7.562
$V_{66.7}Mn_{33.3}$	209.324	203.167	7.643	7.675

$V_{66.7}Ni_{33.3}$	195.071	183.190	7.588	7.700
$Mo_{66.7}Os_{33.3}$	283.269	274.343	9.478	9.491
$Mo_{66.7}Re_{33.3}$	273.023	268.617	9.644	9.614
$Nb_{66.7}Ir_{33.3}$	222.794	207.189	10.345	10.417
$Mo_{66.7}Co_{33.3}$	246.252	225.691	8.482	8.771
$Mo_{66.7}Mn_{33.3}$	250.635	232.845	8.633	8.808
$Re_{66.7}Mn_{33.3}$	330.679	311.432	8.310	8.539
$Re_{66.7}Cr_{33.3}$	319.851	306.083	8.493	8.706
$Re_{66.7}V_{33.3}$	296.475	288.341	8.794	8.994
$Nb_{66.7}Al_{33.3}$	151.447	136.561	10.493	10.870
$Ta_{66.7}Al_{33.3}$	169.286	152.224	10.505	10.944

D'autre part, l'étude du volume molaire pour la phase sigma s'est faite sous deux aspects. Tout d'abord, les volumes molaires calculés par rapport à la composition de la phase sigma montrent que les composés sigma en état désordonné ne sont pas conformes à la relation linéaire volume-composition. L'écart peut être négatif ou positif selon la tendance à la perte ou au gain d'électrons des deux éléments constitutifs tels qu'ils sont présentés dans le tableau 4.4. Pour les catégories SMe et SMs-SMe, les composés présentent une déviation négative, car l'atome A tend à perdre des électrons; Pour les catégories LAs et LAs-LAe, les composés présentent une déviation négative, car l'atome A tend à gagner des électrons. Pour la catégorie LAs-SMe, cela dépend des facteurs électroniques (c.-à-d. des facteurs LAs et SMe). Ensuite nous avons comparé le volume molaire calculé des composés sigma binaires des états hypotétiquement ordonnés et désordonnés tels que présentés dans le tableau 4.5. Les résultats montrent que l'effet de l'ordre atomique sur le volume molaire de la phase sigma dépend de la configuration électronique des deux éléments constitutifs. Nous avons constaté que lorsqu'on augmente (ou diminue) le nombre total d'orbitales électroniques de l'atome A (ou l'atome B) ou diminue (ou augmente) le nombre d'électrons de valence de l'atome A (ou de l'atome B), la différence de volume ($\Delta V=V_{désordonné}-V_{ordonné}$) augmente comme indiqué sur la figure 4.1. Les facteurs SMe et LAs augmentent la différence de volume ($\Delta V=V_{désordonné}-V_{ordonné}$); Les facteurs LAe et SMs diminuent la différence de volume.

Tableau 4.4: Déviation par rapport à la relation linéaire composition-volume des phases sigma binaires calculés par EMTO-CPA dans les structures désordonnées (EMTO-CPA-x%) de la figure 2.

Catégories	Systèmes				Déviation (x %)	
					Négative	Positive
X-Al	Nb-Al	Ta-Al			✘	
SMe	Cr-Co	Cr-Fe	Cr-Mn		✘	
	V-Co	V-Fe	V-Mn	V-Ni		
SMs-SMe	Nb-Ir	Mo-Re	Mo-Os		✘	
LAs-SMe	Mo-Co	Mo-Mn				✘

LAs	Re-Mn				✘
LAs-LAe	Os-Cr	Re-Cr	Re-V	Ru-Cr	✘

Tableau 4.5: différence de volume molaire ($\Delta Vm=V_{disorder}-V_{order}$) entre états désordonnés et ordonnés de la phase sigma binaire A-B (V(A)>V(B) calculée par la méthode EMTO-CPA.

X-Al $\Delta Vm, 10^{-7}$ m^3/mol	Nb-Al ($4d^45s^1$-$3s^23p^1$) 3.80	Ta-Al ($5d^36s^2$-) 4.37		
LAs $\Delta Vm, 10^{-7}$ m^3/mol	Re-Mn ($5d^56s^2$-$3d^54s^2$) 2.26			
SMe $\Delta Vm, 10^{-7}$ m^3/mol	V-Mn ($3d^34s^2$-$3d^54s^2$) 0.31 Cr-Mn ($3d^54s^1$-$3d^54s^2$) 0.28	V-Fe (-$3d^64s^2$) 0.71 Cr-Fe (-$3d^64s^2$) 0.55	V-Co (-$3d^74s^2$) 0.99 Cr-Co (-$3d^74s^2$) 0.70	V-Ni (-$3d^84s^2$) 1.12
SMs-SMe $\Delta Vm, 10^{-7}$ m^3/mol	Nb-Ir ($4d^45s^1$-$5d^76s^2$) 0.73 Mo-Re ($4d^55s^1$-$5d^56s^2$) -0.30	 Mo-Os (-$5d^66s^2$) 0.12		
LAs-SMe $\Delta Vm, 10^{-7}$ m^3/mol	Mo-Mn ($4d^55s^1$-$3d^54s^2$) 1.76	Mo-Co (-$3d^74s^2$) 2.88		
LAs-LAe $\Delta Vm, 10^{-7}$ m^3/mol	Re-V ($5d^56s^2$-$3d^34s^2$) 2.01	Re-Cr (-$3d^54s^1$) 2.13		

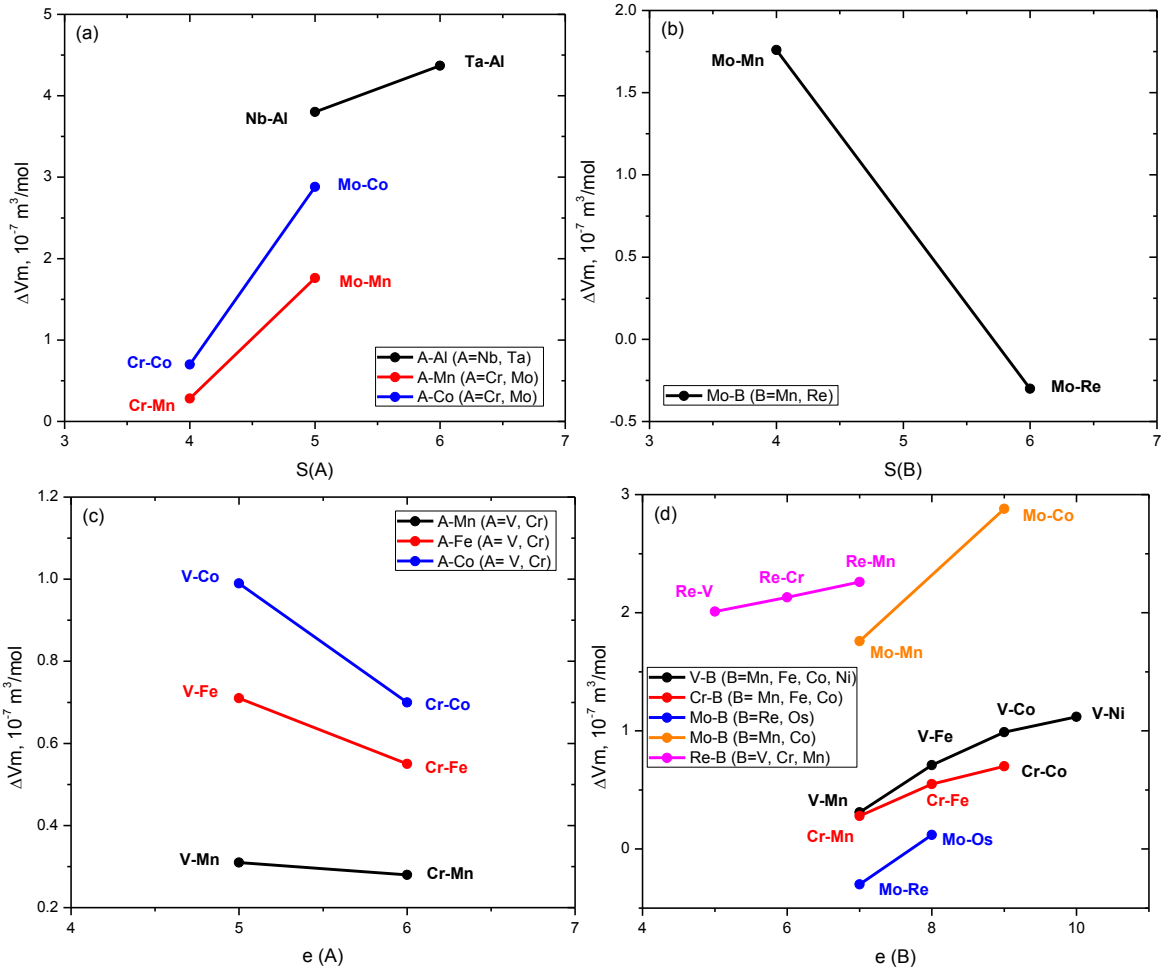

Figure 4.1: différence de volume molaire ($\Delta Vm=V_{désordonné}-V_{ordonné}$) entre les états désordonnés et ordonnés de la phase sigma binaire A-B (V(A)>V(B)) calculée par la méthode EMTO-CPA par rapport à: (a) le nombre total d'orbitales électroniques de l'élément A, S (A); (b) le nombre total d'orbitales électroniques de l'élément B, S (B); (c) le nombre d'électrons de valence de l'élément A, e (A); (d) le nombre d'électrons de valence de l'élément B, e (B).

Dans la section 5, le volume molaire de la phase sigma a été modélisé et évalué à la température ambiante et à la pression atmosphérique pour les systèmes binaires concernant 21 éléments de transition Au, Co, Cr, Fe, Ir, Mn, Mo, Nb, Ni, Os, Pd , Pt, Re, Rh, Ru, Ta, Tc, Ti, V, W et Zr ainsi qu'un élément du bloc p Al en utilisant l'approche CALPHAD. Le modèle de volume proposé dans ce travail exprime le volume molaire d'une phase sigma non stoechiométrique en tant que moyenne linéaire des volumes des éléments constitutifs dans leur structure sigma hypothetique. Des paramètres de modèle raisonnables ont été obtenus et donnent une description raisonnable de la plupart des données expérimentales, cf. par exemple les résultats de la figure 5.1. Les paramètres du modèle sont présentés dans le tableau 5.1. À titre de comparaison, les volumes des 21 éléments de transition dans la structure sigma ont été calculés en utilisant des calculs de premier principe. Les résultats illustrent une cohérence raisonnable avec les valeurs évaluées, comme le montre la figure 5.2.

Tableau 5.1: Quantités molaires évaluées pour des éléments purs dans la structure de la phase sigma comparés aux résultats de calculs de premiers principes.

	V_m, 10^{-6} m^3/mol			V_m, 10^{-6} m^3/mol			V_m, 10^{-6} m^3/mol	
Elément	CALPHAD	First-principles	Elément	CALPHAD	First-principles	Elément	CALPHAD	First-principles
Au	10.100	11.248	Nb	10.770	11.313*	Ru	8.400	8.573*
Co	6.540	6.658*	Ni	6.650	6.689*	Ta	10.800	11.127*
Cr	7.310	7.003*	Os	8.650	8.922*	Tc	8.770	8.842*
Fe	6.880	7.137*	Pd	9.100	9.514	Ti	--	10.298*
Ir	8.480	9.128	Pt	9.000	9.808	V	8.050	8.109*
Mn	7.203	6.446*	Re	9.010	9.121*	W	9.600	9.782*
Mo	9.460	9.585*	Rh	8.200	8.808	Zr	--	13.775*

* Les données de Crivello et al. confirmées dans le présent travail.

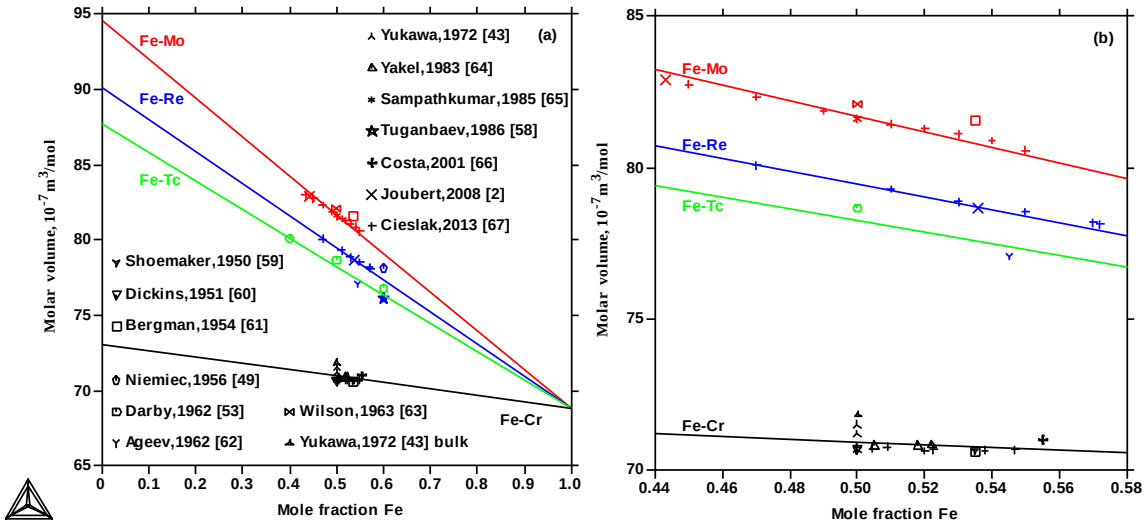

Figure 5.1: Volumes molaires calculés des phases sigma Fe-X (X = Cr, Mo, Re, Tc) comparées aux données expérimentales. (b) est une partie élargie de (a). Notez que pour une phase sigma, la même couleur est attribuée à la fois à la ligne calculée et aux données expérimentales.

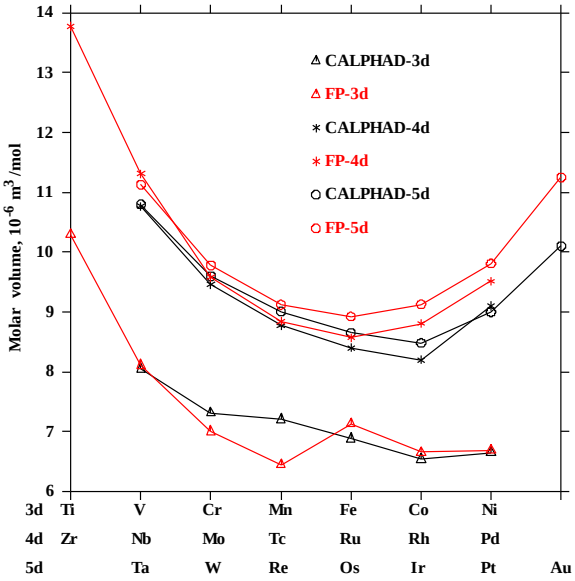

Figure 5.2: Quantités molaires évaluées des éléments de transition dans la structure de la phase sigma comparés aux résultats des calculs de premiers principes (FP).

Dans la section 6, la préférence du site de la phase sigma binaire a été calculée en utilisant l'approche CALPHAD combinée aux calculs de premiers principes. La phase sigma a été décrite par le formalisme d'énergie des composés (CEF) avec un modèle à 5 sous-réseaux (SL) utilisant l'enthalpie de l'ensemble complet des configurations ordonnées directement à partir des calculs de premiers principes. Les résultats des calculs sont présentés à la figure 6.1. Nous avons constaté que l'occupation du site de la phase sigma peut être prédite en utilisant la méthode CALPHAD combinée aux calculs de premiers principes. Pour certains systèmes, on peut obtenir des bases de données auto-

cohérentes sans aucun paramètre d'interaction en utilisant la description complète en sous-réseaux. Pour certains autres systèmes, les paramètres évalués sont nécessaires même pour être en accord avec les occupations du site.

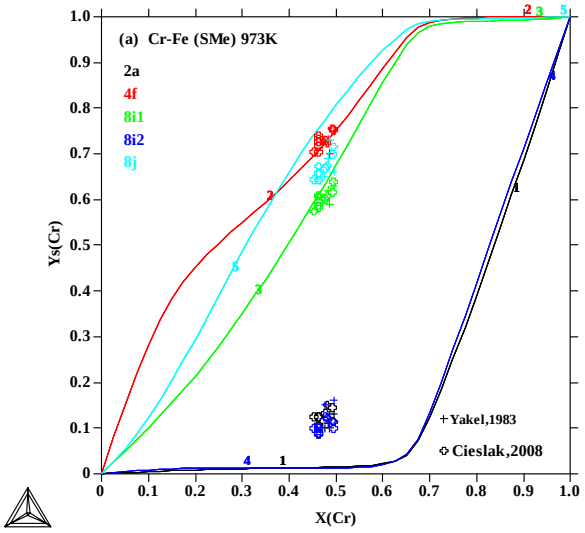

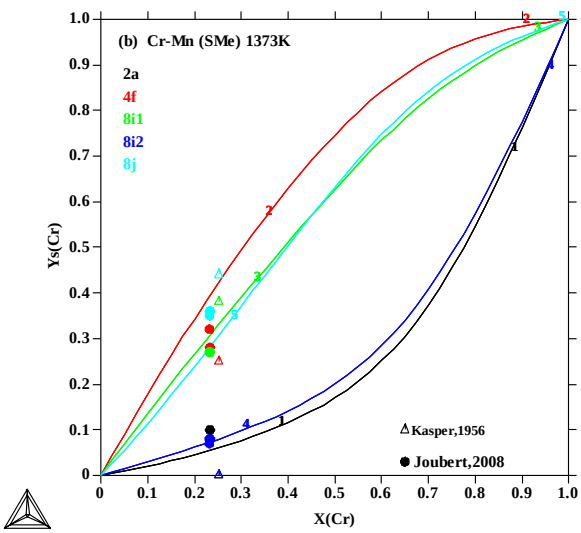

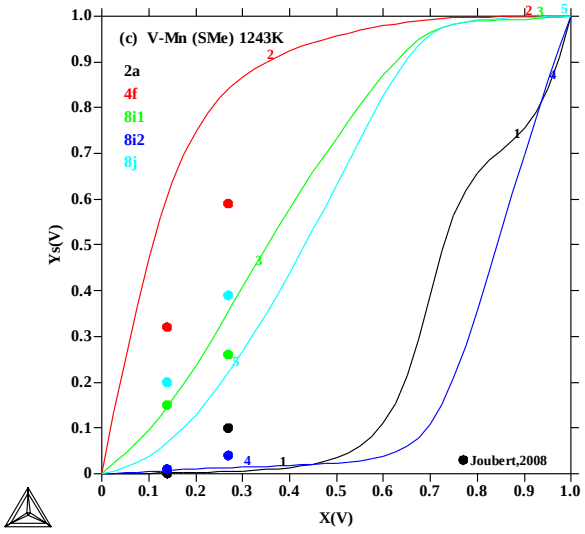

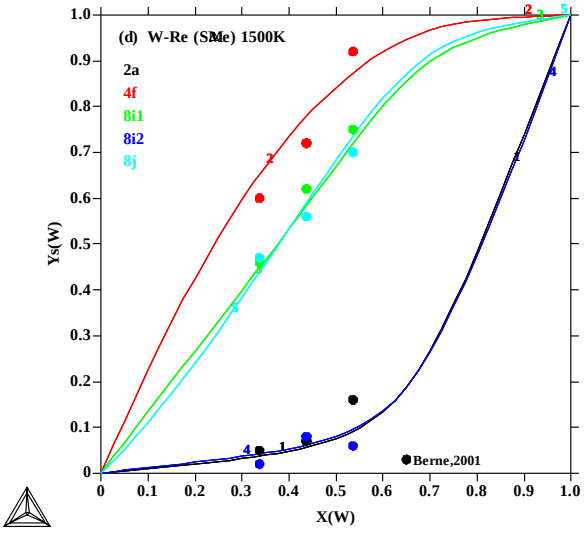

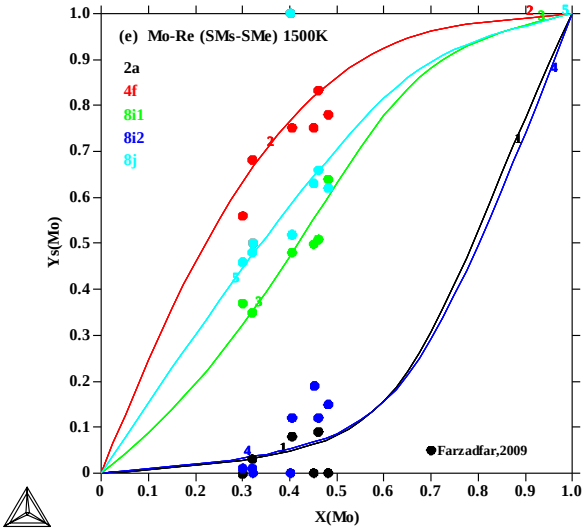

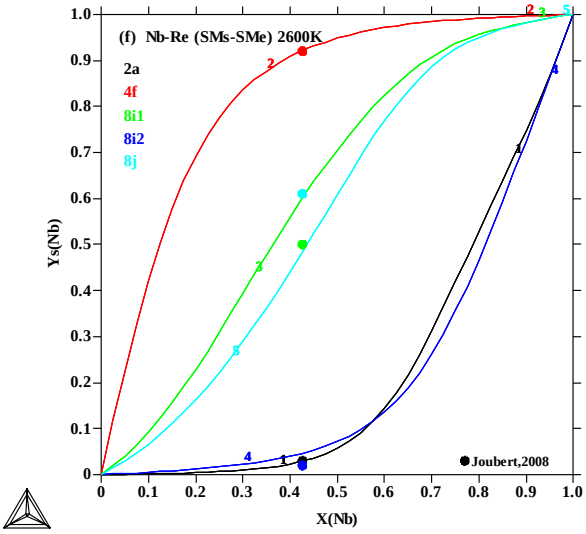

Figure 6.1: Occupation du site, Ys (A), en fonction de la fraction molaire de l'atome A, X (A), calculée en utilisant des calculs VASP comparée aux données expérimentales de la littérature. Les résultats de calcul des systèmes contenant Re proviennent de Crivello et al. à l'exception du système Mo-Re, pour lequel nos propres résultats de calcul sont utilisés.

En conclusion, dans le présent travail, les propriétés physiques de la phase sigma axées sur l'ordre atomique, le volume molaire ont été systématiquement étudiées en utilisant les calculs de premiers principes et la méthode CALPHAD combinée aux données expérimentales de la littérature.

Tout d'abord, nous avons effectué des calculs VASP associés à l'analyse de Bader sur 12 systèmes de phase sigma typiques. Ainsi, nous avons obtenu le volume atomique et la charge atomique correspondante des atomes constitutifs pour chaque système dans l'ensemble complet de configurations ordonnées de la phase sigma, et à partir de ces résultats sont clairement apparus l'effet de la tendance au gain ou à la perte d'électrons des deux éléments constitutifs et la différence de taille entre les cinq sites non équivalents du cristal.

On pu constater que, outre le facteur de taille et le nombre d'électrons de valence, le nombre total d'orbitales électroniques est le troisième facteur qui affecte l'ordre atomique de la phase sigma. Les occupations du site expérimental sont les résultats d'une concurrence et d'une coopération entre les trois facteurs influents. En outre, nous avons dissocié les effets des facteurs d'influence sur l'ordre atomique pour la phase sigma binaire. Toutes les occupations des sites correctement mesurées peuvent être expliquées en utilisant nos découvertes.

Deuxièmement, nous avons étudié l'influence de l'ordre atomique sur l'enthalpie de formation, le module d'élasticité isostatique et le volume molaire de la phase sigma binaire. Nous avons trouvé que dans l'état ordonné à 0K, la phase sigma a une faible enthalpie de formation et un grand module d'élasticité isostatique; l'influence de la composition sur le volume molaire de la phase sigma dépend de la tendance à la perte ou au gain d'électrons des deux éléments constitutifs; l'influence de l'ordre atomique sur le volume molaire de la phase sigma dépend de la configuration électronique des deux éléments constitutifs.

Troisièmement, nous proposons un modèle pour décrire le volume molaire de la phase sigma non stoechiométrique en tant que moyenne linéaire des volumes de ses éléments constitutifs dans leur structure sigma hypothétique. Le modèle linéaire proposé peut reproduire de manière satisfaisante la plupart des données expérimentales de la littérature. Après une évaluation systématique des données de la littérature, la base de données du volume molaire des phases sigma binaire à température ambiante et pression atmosphérique impliquant 20 éléments (Al, Au, Co, Cr, Fe, Ir, Mn, Mo, Nb, Ni, Os, Pd, Pt, Re, Rh, Ru, Ta, Tc, V et W) a été obtenu en utilisant l'approche CALPHAD. La méthode adoptée peut être étendue aux systèmes multi-composants et réduit les n^3 inconnues pour les composés extrêmes à n valeurs pour n éléments dans une phase sigma de n-composants. Un autre avantage pratique est que le

développement de la base de données de volume pour ces phases sigma peut être séparé des bases de données thermodynamiques.

Enfin, nous avons discuté de la prédiction de l'occupation du site de la phase sigma. La méthode CALPHAD combinée aux calculs des premiers principes est un bon moyen de prédire les préférences d'occupation des sites de la phase sigma, mais pour certains systèmes les paramètres évalués sont nécessaires.

Résumé

La phase sigma peut servir de prototype de phases topologiquement compactes (TCP), car la phase sigma possède une large gamme d'homogénéité et il existe de nombreuses données expérimentales disponibles pour la phase sigma. Dans le présent travail, les propriétés physiques, comprenant l'ordre atomique, le volume molaire, l'enthalpie de formation et le module d'élasticité isostatique, de la phase sigma binaire ont été étudiées en utilisant les calculs de premiers principes et la méthode CALPHAD combinée aux données expérimentales de la littérature.

Tout d'abord, nous avons constaté que l'ordre atomique (c'est-à-dire la distribution du constituant atomique ou la préférence d'occupation du site sur les sites non équivalents d'une structure cristalline) de la phase sigma est affecté par le facteur de taille et la configuration électronique des éléments constitutifs. En outre, nous avons dissocié les effets de ces facteurs d'influence sur l'ordre atomique. Ensuite, nous avons mis en évidence un effet de l'ordre atomique sur l'enthalpie de formation, le module d'élasticité isostatique et le volume molaire. A l'état ordonné à 0K, la phase sigma a une faible enthalpie de formation et un grand module d'élasticité isostatique. L'influence de l'ordre atomique sur le volume molaire de la phase sigma dépend de la configuration électronique des deux éléments constitutifs. Par ailleurs, la base de données des volumes molaires des phases sigma binaires a été construite, ce qui devrait grandement faciliter la conception du matériau. Enfin, nous avons discuté de la prédiction de l'occupation du site de la phase sigma en utilisant la méthode CALPHAD combinée aux calculs de premiers principes.

Mots clés: phase sigma, ordre atomique, volume molaire, enthalpie de formation, module d'élasticité isostatique, calculs de premiers principes, DFT, CALPHAD

Abstract

The sigma phase can serve as a prototype of topologically close-packed (TCP) phases, as the sigma phase bears a broad homogeneity range and there are numerous experimental data available for the sigma phase. In the present work, physical properties, including atomic order, molar volume, enthalpy of formation and bulk modulus, of the binary sigma phase were investigated by using first principles calculations and CALPHAD method combining with the experimental data from the literature.

Firstly, we found that the atomic order (i.e. atomic constituent distribution or site occupancy preference on nonequivalent sites of a crystal structure) of the sigma phase is affected by the size factor and electron configuration of the constituent elements. Furthermore, we have dissociated the effect of the individual influencing factor on atomic order. Secondly, the atomic order is found affecting physical properties, such as enthalpy of formation, bulk modulus and molar volume. When in the ordered state at 0K, the sigma phase shows a low enthalpy of formation and a large bulk modulus. The influence of atomic order on the molar volume of the sigma phase depends on the electron configuration of the two constituent elements. Thirdly, the molar volume database of the binary sigma phase has been built up within the CALPHAD framework, which can greatly facilitate material design. Finally, we tentatively discussed the site occupancy prediction of the sigma phase by using the CALPHAD method combined with first-principles calculations.

Keywords : sigma phase, atomic order, molar volume, enthalpy of formation, bulk modulus, first-principles calculations, DFT, CALPHAD

Acknowledgements

I would like to express my sincerely gratitude to all those who helped me during the writing of my thesis.

Firstly, no words can fully express my gratitude to my supervisors Prof. Xiao-Gang LU, Prof. Pascal BOULET and Prof. Marie-Christine RECORD for their continuous support of my PhD study. Prof. Xiao-Gang LU gives me the greatest help. He paid a lot of efforts on my papers and thesis from selecting the topic to discussion until the final revision. Teacher's kindness like sea is hard to repay in one's lifetime. Prof. LU is very passionate about research with rigorous academic attitude, which deeply impressed and influenced me. From him, I see the precious qualities as a scientific researcher. In life, he is our friend, and the unpretentious and approachable personality is our role model. Not only to guide our academic research, but also to teach us how to behave as a human being. The influence of these precious characters will not be erased from my whole life. I would like to extend my most heartfelt thanks and the highest respect to Prof. LU.

I also would like to thank my beloved Prof. Pascal BOULET and Prof. Marie-Christine RECORD. They gave me a great deal of help in my life and my studies. As a foreigner in a different country, I do feel the warmth of home. They passed me the most unselfish concern and dedication. At the same time, the rigorous academic attitude and profound knowledge are deeply affected me. They spend a lot time on me for numerous discussions and revision of my thesis and papers. I will never forget their kindness and selfless help. I hope they could accept my sincere thanks.

My sincere thanks also go to Prof. Hong-Bin WANG, Prof. Yan-Lin HE, who provided me an opportunity to start the research journey, and Prof. Qing-Miao HU who provided us the calculation software, taught me how to use it and patiently answered the questions I met during research. With their help, everything goes easier.

I would like to thank my fellow labmates and teachers in both Shanghai University and Aix-Marseille University for their help and all the fun we have had. Also I am grateful to all of my friends in both China and France who accompanied, cared and encouraged me.

Besides, I would like to thank the rest of my thesis committee: Prof. Zhi LIU, Prof. Jun LUO and Prof. Li-Jun ZHANG, for their insightful comments and encouragement, but also for the hard questions which incented me to widen my research from various perspectives.

Last but not least, I would like to thank my family: my parents, my sister and my boyfriend for supporting me spiritually throughout writing the thesis and my life in general.

Contents

Introduction

TCP phases are not only important precipitates in a lot of technological significant materials. Applications of TCP phases have also been highlighted as high-temperature structural and superconducting materials. However, their physical properties have not yet been sufficiently investigated.

As a typical TCP phase, the investigation of the sigma phase has attracted great interests. There are numerous investigations on its crystallographic, physical and thermodynamic properties, especially molar volume and atomic order (i.e. atomic constituent distribution or site occupancy preference on nonequivalent sites of a crystal structure). The atomic order affects lots of important properties of the TCP phases, like molar volume, bulk modulus, enthalpy of formation etc. However, so far, for most thermodynamic databases, the site occupancy information was not considered during the assessments. Thus it makes the databases less reliable and limits the integration between thermodynamic databased and other databases, like molar volume databases and mobility databases. Any updates of thermodynamic databases may predict different site occupancies and other databases have to change correspondingly.

The focus of the present work is to clarify the influencing factors on atomic order and the effect of atomic order on the properties of the sigma phase, including molar volume, bulk modulus and enthalpy of formation. Then thermodynamic and molar volume modeling of the binary sigma phase are investigated and discussed by using the CALPHAD method combined with first-principles calculations to facilitate material design.

1. Generality

1.1 Intermetallic phase

An alloy is a mixture of metals or a mixture of a metal and another element obtained by smelting, sintering or other methods. Alloys are defined by a metallic bonding character [1]. Alloys are usually classified as solid solution and intermetallic. A solid solution is a homogeneously mixed solid-state solution of one or more solutes in a solvent. It keeps the same crystal structure of the solvent. Intermetallic is a phase formed at intermediate composition between the two constituent components. The crystal structure of the intermediate phase is different from those of both components [1].

Some intermediate phases have a fixed composition and are called stoichiometric intermetallic compounds; some have a range of compositions and are sometimes called intermediate solid solutions (or secondary solid solution). For most intermetallic phases, the bonding among various atomic species is a mixture of a predominantly metallic bond and lower fractions of other kinds of bonds (e.g. covalent bond, ionic bond and van der Waals' forces) [1]. The forming and crystal structure of intermetallic phases are affected by electronegativity, electron concentration and atomic size. According to this, intermetallic phases classified as normal valence compounds, electron (or Hume-Rothery) compounds, size factor related compounds and super structure (or ordered solid solution). The characteristic of intermetallic phases and their application are summarized as follows (for more details see Ref. 1).

1.1.1. Normal valence compounds

Normal valence compound is the compound forming among metals and some elements with high electronegativity in ⅣA, ⅤA or ⅥA groups. It follows the law of chemical valence and thus their ingredients can be expressed in molecular formulas.

The stability of normal valence compounds is related to the electronegativity difference between the constituent elements. The smaller the electronegativity difference is, the more unstable the compound is, and the larger tendency of forming metallic bond is; the larger the electronegativity difference is, the more stable the compound is, and the larger tendency of forming ionic bond is.

1.1.2. Electron compounds

Electron compounds or Hume-Rothery phases were firstly discovered by Hume-Rothery when he investigated alloys forming among noble metals (Ag, Au, Cu) in ⅠB

and main elements in ⅡA, ⅢA and ⅣA groups (e.g. Zn, Ga, Ge). Later on, it was also discovered in alloys of Fe-Al, Ni-Al, Co-Zn etc.

For electron compounds, the main factor determining the crystal structure is electron concentration (e/a, where e and a denote the number of valence electrons and the number of atoms in a unit cell, respectively) [1]. Compounds with the same electron concentration bear the same crystal structure. When electron concentration equals 21/12, electron compounds is termed as ε phase with hcp (hexagonal closed packed) structure; when electron concentration equals 21/13, electron compounds is termed as γ phase with complex cubic structure; when electron concentration equals 21/14, electron compounds is termed as β phase with bcc (body centered cubic) structure or sometimes complex cubic β-Mn or hcp structure. This is because besides being affected by electron concentration, the crystal structure is also affected by size factor and electrochemistry factor. [1]

Electron compounds can be expressed in molecular formulas, but do not match the law of chemical valence. Actually, electron compounds have a range of compositions and electron concentration. The bonding among atoms is predominantly metallic bond. Thus, electron compounds bear obvious metallic character.

1.1.3. Size factor related compounds

For some intermetallic compounds, the crystal structure is closely related to the size difference between constituent elements. When the size difference is large, the compound tends to form interstitial phase and interstitial compound; when the size difference is medium, the compound tends to form topologically close-packed (TCP) phases.

(a) Interstitial phase and interstitial compound

Non-metallic elements with small atomic radius (like C, H, N, B) and metallic elements (mainly transition elements) can form interstitial phase and interstitial compound, depending on the ratio of the atomic size between non-metallic element and metallic element (R_X/R_M). When $R_X/R_M < 0.59$, it forms the phase with simple crystal structure, called interstitial phase; when $R_X/R_M > 0.59$, it forms the phase with complex crystal structure, called interstitial compound.

1) Interstitial phase

Interstitial phase bears simple crystal structure, like fcc (face centered cubic), hcp; minority bcc or simple hexagonal structure. Interstitial phases bear different crystal structure of both components. In the crystal structure, metallic atoms occupy on normal crystal sites, while non-metallic atoms regularly distribute in interstitial sites. The type of occupied interstitial sites for non-metallic atoms is determined by the size factor. When $R_X/R_M < 0.414$, the atoms occupy tetrahedral interstices; when $R_X/R_M > 0.414$, the atoms occupy octahedral interstices.

Though interstitial phase can be expressed in molecular formulas, it bears a range of compositions. The bonding among atoms in interstitial phase is metallic bond and

covalent bond. Even though the mole fraction of non-metallic elements is larger than 50%, the interstitial phase still possesses obvious metallic character. Moreover, almost all interstitial phases bear high melting point and high hardness which are important precipitations in alloyed tool steels and hard alloy.

2) Interstitial compound

Interstitial compound bears complex crystal structure. Normally, carbides formed between transition elements (like Cr, Mn, Fe, Co, Ni) and carbon, are interstitial compounds.

The bonding among atoms in interstitial compound is metallic bond and covalent bond. Moreover, interstitial compounds bear relative high melting point and high hardness (though less than interstitial phase), and are the main strengthening phases in steels.

(b) Topologically close-packed (TCP) phases

The topologically close-packed (TCP) phases are one of the largest groups of intermetallic compounds, which are composed of metallic atoms with different atomic size. These atoms adapt each other forming a very complex crystal structure with high space utilization and high coordination number (CN). The first characteristic of the structure is that it is stacked by coordination polyhedron of CN 12, 14, 15 and 16 [1]. The second one is that small atoms compose close-packed plane within which are inserted large atoms. The close-packed planes stack regularly and compose the close-packed structure with high space utilization and only tetrahedral interstices.

TCP phases are common precipitates in Fe-, Ni-, Co- based superalloys and austenitic and duplex stainless steels [2–5]. The common members of TCP phases are sigma, chi, mu, laves, A15, R, P, delta and M phases [1,2]. A small amount of TCP precipitations can cause the effect of precipitation hardening and grain boundary strengthening [3,6]. However, in most cases, TCP phase is a detrimental phase in alloys. It is hard and brittle, which make alloys crack under the service conditions in tensile stress. Moreover, the TCP precipitation will lead to poor alloying elements in matrix, and thus decreases the mechanical properties and corrosion resistance of materials [2,3]. Therefore, accurate prediction and reasonable control of the precipitation of TCP phases is obviously the key to alloy design of iron-based, nickel-based, cobalt-based superalloys and stainless steels.

Besides, applications of TCP phases as high-temperature structural and superconducting materials have been highlighted. Also, their complex and often non-stoichiometric structure makes them good subjects for theoretical calculations.

1.1.4. Superstructure (ordered solid solution)

It has been found that the atoms of certain solid solutions, although distribute randomly among the crystal sites at high temperatures, tend to arrange themselves into an ordered state or superlattice at low temperatures [7]. Moreover, there exists a critical temperature below which the ordering process begins. The ordering process may occur only at certain fixed ratio of the solute and solvent atoms (e.g. AB or AB_3).

1.1.5. Properties of intermetallic phases and their application

Intermetallic phase bears variety of atomic bond and complex crystal structure conferring special physical and mechanical properties to this phase. Application of many intermetallic phases, especially superstructure as new functional materials and heat-resistant material is being developed and applied.

- Intermetallic compounds with superconductivity, e.g. Nb_3Ge, Nb_3Al, Nb_3Sn, V_3Si, NbN etc.
- Intermetallic compounds with special electrical properties, e.g. the application of InTe-PbSe, GaAs-ZnSe in semiconductor material.
- Intermetallic compounds with strong magnetism, e.g. compounds of rare earth element (Ce, La, Sm, Pr, Y etc.) and Co bear excellent permanent magnet performance.
- Intermetallic compounds with special properties of hydrogen uptake and release (usually called hydrogen storage material), e.g. $LaNi_5$, FeTi, R_2Mg_{17} and $R_2Ni_2Mg_{15}$, are promising energy storage and energy conversion materials.
- Intermetallic compounds with heat-resistant properties, e.g. Ni_3Al, NiAl, TiAl, Ti_3Al, FeAl, Fe_3Al, $MoSi_2$, $NbBe_{12}$, not only bear good high-temperature strength, but also good ductility at high temperature.
- Intermetallic compounds with corrosion resistance, e.g. some metallic carbides, borides, nitrides and oxides.
- Intermetallic compounds with shape memory effect, superelasticity and vibration damping, e.g. TiNi, CuZn, CuSi, MnCu, Cu_3Al, have been well applied in industry.

Besides, borides of rare earth elements, e.g. LaB_6, bear thermionic emission. Zr3Al possesses good neutron absorption. All these properties show broad prospects in application of new functional materials.

1.2. General features about the sigma phase

The sigma phase known as topologically close-packed (TCP) phase, is a non-stoichiometric intermetallic compound that crystallizes in a tetragonal structure with 30 atoms distributed on five nonequivalent sites [8–10]. It is a hard, brittle phase mostly formed between transition elements and deteriorates various properties of many technologically important materials, such as stainless and other high-alloy steels as well as Ni-based superalloys [8,9]. The sigma phase exists in 49 different binary alloy systems, five of which were reported but not confirmed in future works (i.e. Cr-Ni, Ta-V, Ti-Mn, Zr-Ir and Zr-Re). It has attracted great technological and theoretical study interests since the 1950s [11].

It should be mentioned that the sigma phase structure has also been observed in block copolymers [12,13], for which the unit cell volume is six orders of magnitude higher than that of the sigma phase in metal alloys [13]. Spherical aggregates formed by soft

macromolecules follow similar principle as metal alloys; the stability of the packing derives from large numbers of nearest neighbor interactions, which decrease free energy [13].

General features about the sigma phase are introduced hereafter (for more details see Ref. 9).

1.2.1. Crystal structure

The sigma phase crystallizes in a tetragonal structure with 30 atoms distributed on five nonequivalent sites, namely 2a, 4f, $8i_1$, $8i_2$ and 8j, as presented in Fig. 1.1, 1.2 and Table 1.1. The space group of the sigma phase is generally designated as $P4_2/mnm$, except for β-Ta and β-U.

Empirical rules exist for TCP phases indicating that atom A, with large size prefers the sites with high CN (CN16, 15 or 14). In most cases, atom A bears poor d-electrons and bcc structure. These high CN sites have more space to accommodate atomic size and their atomic environment is close to that found in a bcc structure. On the contrary, the smaller B atom tends to be accommodated in the site with low CN (CN 12), smaller in size and similar to the environment of B in fcc or hcp structure [9]. Thus the stoichiometric composition can be defined according to the size factor. For the sigma phase, it corresponds to the complete occupancy of sites 4f (CN 15), $8i_1$ (CN 14) and 8j (CN 14) by atom A and of sites 2a (CN12) and $8i_2$ (CN 12) by atom B. This ordered state yields the composition of $A_{20}B_{10}$ or A_2B [9]. Notably, the stoichiometric composition of the sigma phase cannot be observed from the homogeneity ranges.

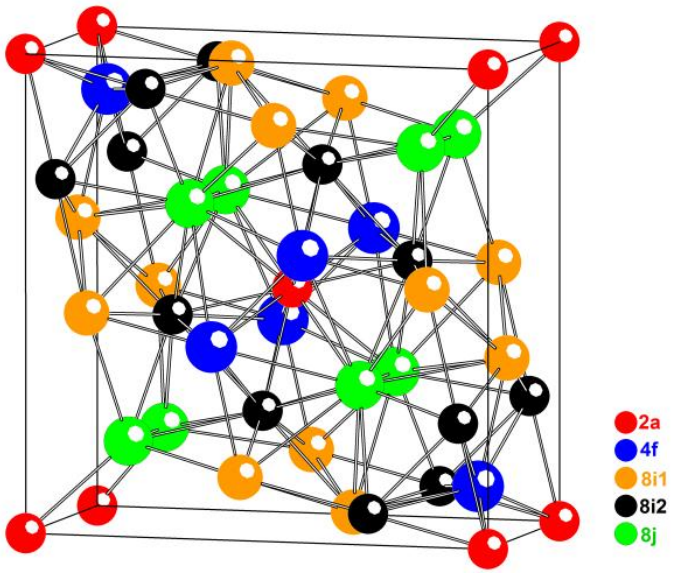

Figure 1.1 : Crystal structure of the sigma phase with different fillings indicating atoms occupying on different crystal sites, namely 2a, 4f, $8i_1$, $8i_2$ and 8j.

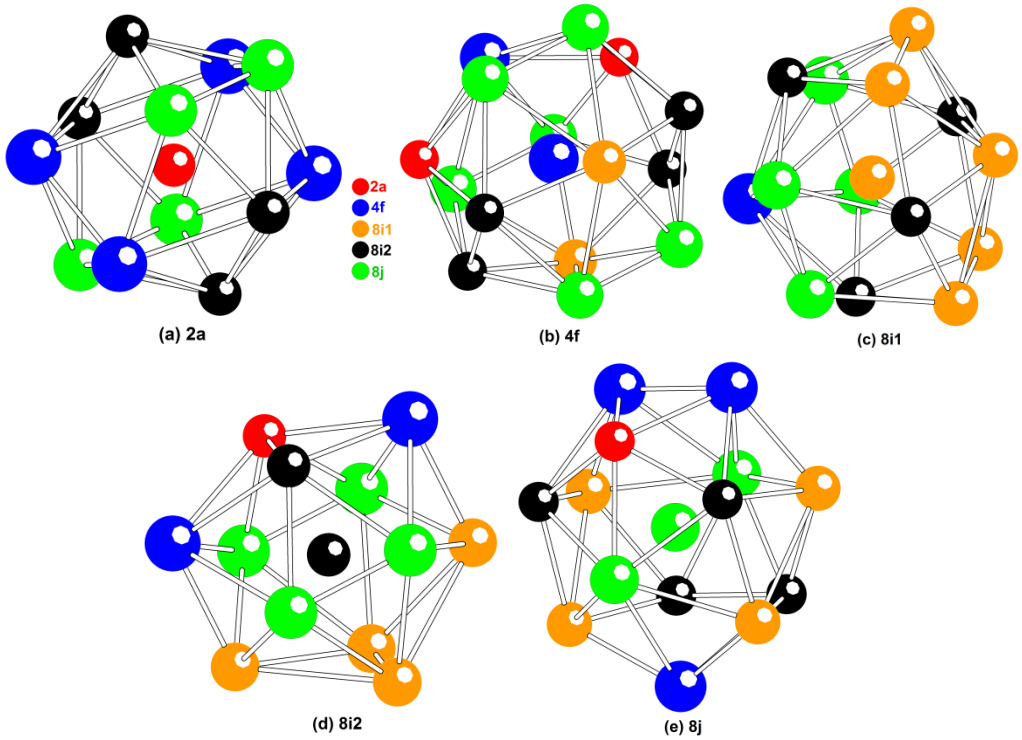

Figure 1.2 : Coordination polyhedron around five nonequivalent sites of the sigma phase structure with different fillings indicating atoms on different crystal sites, namely 2a, 4f, $8i_1$, $8i_2$ and 8j.

Table 1.1 : Crystal structure of the sigma phase [9].

Space group	$P4_2/mnm$ (no. 136)			
Pearson symbol	tP30			
lattice parameters	a: 8.785-10.060Å; c: 4.553-5.230Å.			
Wyckoff position	x	y	z	CN
2a	0	0	0	12
4f	≈0.399	x	0	15
$8i_1$	≈0.464	≈0.131	0	14
$8i_2$	≈0.741	≈0.066	0	12
8j	≈0.183	x	z≈0.251	14

1.2.2. Existence

The sigma phase is reported as existing in 49 different A-B (A bears a larger atomic size than B) binary alloy systems as shown in the following:

Cr-X (X=Co, Fe, Mn); Mo-X (X=Co, Fe, Ir, Mn, Os, Re, Ru, Tc); Nb-X (X=Ir, Os, Pd, Pt, Re, Rh); Os-Cr; Re-X (X=Cr, Fe, Mn, V); Ru-Cr; Ta-X (X=Au, Ir, Os, Pd, Pt, Re, Rh); Tc-X (X=Cr, Fe, Mn); V-X (X=Co, Fe, Mn, Ni); W-X (X=Ir, Os, Re, Ru, Tc); X-Al (X=Ta, Nb) and five not confirmed ones: Cr-Ni, Ta-V, Ti-Mn, Zr-Ir and Zr-Re.

The binary sigma phase is found to be formed between 20 different elements as presented in Table 1.2, among these containing Ti and Zr are not confirmed. It can be seen that element A mostly bears bcc structure and element B mostly fcc or hcp structure.

Among all the binary sigma phase systems, only two systems contain a main-gruop element; they are X-Al (X=Ta, Nb). It is reported [9] that Al behaves as if it had 9 or 10 valence electrons in the sigma phase structure. The isotypic sigma strucure has also been reported for pure uranium and tantalum, for more details see e.g. [9] and references therein.

Table 1.2 : Crystal structure of the sigma phase [9].

Al
fcc

Ti	V	Cr	Mn	Fe	Co	Ni		
hcp	bcc	bcc	complex	bcc	hcp	fcc		
Zr	Nb	Mo	Tc	Ru	Rh	Pd		
hcp	bcc	bcc	hcp	hcp	fcc	fcc		
	Ta	W	Re	Os	Ir	Pt	Au	
	bcc	bcc	hcp	hcp	fcc	fcc	fcc	

Element acts as A
Element acts as B
Element may act as either A or B

1.2.3. Homogeneity range

Fig. 1.3 shows the homogeneity ranges of the sigma phases according to Ref. 9. It shows that the sigma phase may exist almost at any composition. Thus it is quite difficult to define the stoichiometric composition from the evidenced range of compositions as mentioned in Section 1.2.1. As far as we know, sigma compound is the intermetallic compound that bears the broadest range of non-stoichiometry [9].

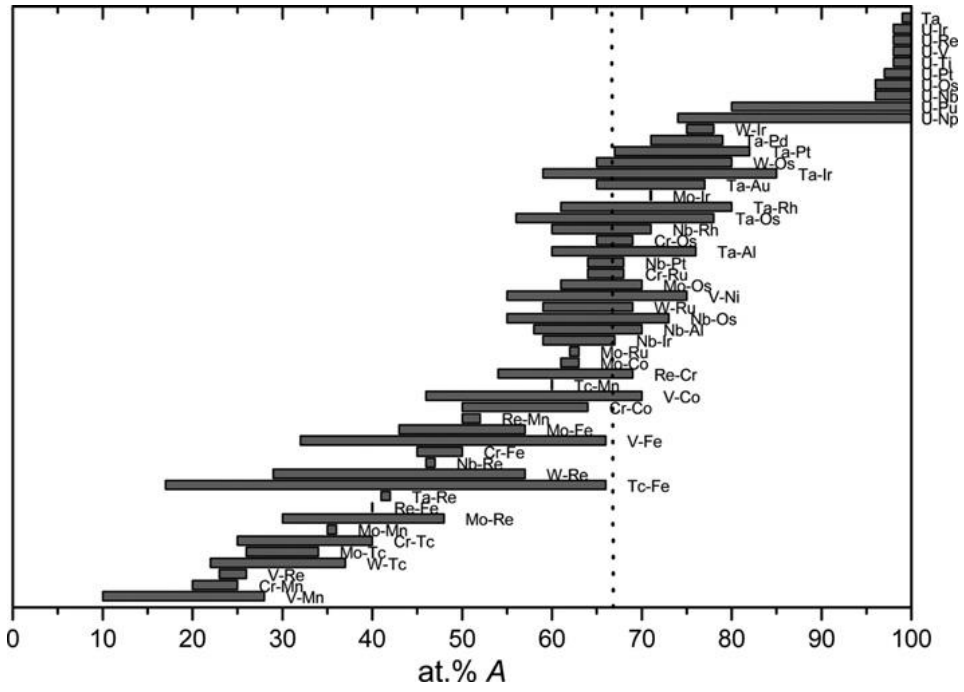

Figure 1.3 : Homogeneity ranges of the sigma phase with respect to mole fraction element A (from Ref. 9). The terminal solid solutions of sigma-U and metastable sigma-Ta is also indicated. The vertical dashed line indicates the stoichiometric composition A_2B.

1.3. Long-range order parameter (S)

For A-B binary ordered solid solution, the basic condition for ordering process is that the bonding among A-B atoms is larger than that among A-A/B-B atoms. This makes the ordered solid solution bearing a lower Gibbs energy than the disordered ones.

Normally, for A-B binary ordered phase, the degree of ordering process was quantitatively expressed by long-range order parameter S [1] :

$$S = \frac{P_A - X_A}{1 - X_A} \qquad (1.1)$$

where P_A is the probability of occurrence of atom A on the right crystal site for atom A (i.e. the crystal site occupied by atom A when in total ordered state); X_A is the mole fraction of atom A. When in ordered state, P_A =1 and thus S=1; When in disordered state, P_A =X_A and thus S=0.

However, the above equation is not able to describe the situation when all the right crystal sites for atom A are occupied by atom A, where P_A =1 but there are extra atom A occupying on the wrong site for atom A (i.e. the crystal site occupied by atom B when in total ordered state). In other words, according to the above equation, as long as P_A=1, S will equal to 1, no matter whether there are extra atom A occupying the wrong site or not. In order to overcome this issue, in the present work, the description is redefined which will be discussed in Section 4.3.1.

1.4. Electronegativity

Electronegativity scale was firstly proposed by Pauling [14]. He defined electronegativity as the power of an atom in a molecule to attract electrons to itself while the electrons are still attached to another atom [15,16]. The higher the value is, the stronger the ability of an atom to gain electrons from another one is. Since then, many other scales have been proposed [15–22]. Several typical scales are discussed as follows.

1.4.1. Pauling electronegativity

Linus Pauling [14] originally described the phenomena of electronegativity based on bond energies between atoms. For a hypothetical molecule AB, the electronegativity is defined as follows:

$$E_{AB(\,predicted\,)} = \left[E_{AA} + E_{BB}\right]/2 \qquad (1.2)$$

$$\left|\chi_A - \chi_B\right| = (eV)^{-1/2}\sqrt{E_{AB} - E_{AB(\,predicted\,)}} \qquad (1.3)$$

where E_{AA}, E_{BB} and $E_{AB(predicted)}$ are the A-A, B-B and A-B bond energies, respectively. χ_A and χ_B are the electronegativity of element A and B respectively; E_{AB} is the actual A-B bond energy; the factor $(eV)^{-1/2}$ is included to ensure a dimensionless result.

If the electronegativities of A and B are the same, then it is expected that the actual A-B bond energy equals the predicted A-B bond energy. If the electronegativities of these atoms are not the same, we would see a polar molecule. The greater the difference in electronegativity is, the greater the ionic character of the bond is. Moreover, by assigning an arbitrary reference point, Pauling was able to set up relative values for all of the elements. Afterwards, in 1961, Allred [23] updated Pauling's original electronegativity values considering newly available thermodynamic data. These values of the electronegativity are those that are most often used.

1.4.2. Mulliken electronegativity

In 1934, Mulliken [17] proposed the absolute electronegativity scale based on valence ionization potentials and electron affinities, as follows:

$$\chi = \frac{I + E}{2} \qquad (1.4)$$

where I and E are the valence-state ionization energy and the electron affinity, respectively; χ is the electronegativity of the corresponding element.

The Mulliken electronegativity can only be calculated for an element for which the electron affinity is known. It is more usual to use a linear transformation to transform these absolute values into values that resemble the more familiar Pauling scales [18,21].

1.4.3. Allred–Rochow electronegativity

Allred and Rochow [15] determined the electronegativity based on the force of attraction between the nucleus and an electron in a bonded atom. The electronegativity

should be related to the charge experienced by an electron on the 'surface' of an atom. The higher the charge per unit area of atomic surface the greater the tendency of that atom to attract electrons.

$$\chi = 0.359\frac{Z_{eff}}{r^2} + 0.744 \qquad (1.5)$$

where Z_{eff} is the effective nuclear charge, which can be estimated using Slater's rules; r is the distance between an electron and the nucleus (covalent radius); the magnitudes of Z_{eff}/r^2 represent 'absolute' electronegativity and the other parameters are used to resemble Pauling scales.

1.4.4. Allen electronegativity

Electronegativity of Allen scale [22], is considered as the average energy of the valence electrons in a free atom.

$$\chi = \frac{n_s\varepsilon_s + n_p\varepsilon_p}{n_s + n_p} \qquad (1.6)$$

where n_s, n_p are the number of p and s valence electrons respectively; ε_s, ε_p are the one-electron energies of *s*- and *p*-electrons in the free atom.

A scaling factor is usually applied to give values resembling Pauling scale. Besides, electronegativity for transition elements cannot be simply determined due to the nature of d-orbital radial distribution [22], which leads to an ambiguity for their electronegativities.

2. Methodology

2.1. First-principles calculations

First-principles calculations method is also called ab initio calculations. It is developed based on density function theory (DFT). The method does not rely on any empirical or experimental parameters. The only necessary information is the atomic species of the constituent elements. Afterwards, we can reasonably predict the total energy, stability, electron structure, various physical and chemical properties etc. by solving a Schrödinger-type equation [24]. Thus the method has been widely used in material calculations and design.

In the present work, two kinds of first-principles calculations were performed to calculate the properties of the sigma phase. EMTO-CPA (exact muffin-tin orbitals — coherent potential approximation) method is conducted mainly to deal with chemical disordered alloys. The plane wave method with projector augmented wave (PAW) pseudo-potentials [25] is conducted mainly to deal with chemical ordered alloys. It is implemented in the Vienna ab initio simulation package (VASP) [26]. Both these two methods as well as the based DFT theory are introduced in the present work (for more details see Ref. 27–31). Besides, the Bader charge analysis code [32] is also used to calculate the atomic volume and charge of the sigma phase combined with the VASP code.

2.1.1. DFT as a way to solve the quantum many-body problem

A solid is a collection of nuclei and electrons. Many-body problem indicates a problem dealing with several electromagnetically interacting particles (nuclei and electrons) [28]. From the point of view of quantum mechanics [33], almost all of the information of a system can be described by the wave function ψ of the multi-electron system. ψ can be obtained by solving the many-body Schrödinger equation:

$$\mathrm{H}\Psi = E\Psi \qquad (2.1)$$

where H is the Hamiltonian; E is the total energy.

For a many-body problem, the exact Hamiltonian is as following:

$$\hat{H} = -\frac{\hbar^2}{2}\sum_i \frac{\nabla^2_{\vec{R}_i}}{M_i} - \frac{\hbar^2}{2}\sum_i \frac{\nabla^2_{\vec{r}_i}}{m_e} - \frac{1}{4\pi\varepsilon_0}\sum_{i,j}\frac{e^2 Z_i}{\left|\vec{R}_i - \vec{r}_j\right|} + \frac{1}{8\pi\varepsilon_0}\sum_{i\neq j}\frac{e^2}{\left|\vec{r}_i - \vec{r}_j\right|} + \frac{1}{8\pi\varepsilon_0}\sum_{i\neq j}\frac{e^2 Z_i Z_j}{\left|\vec{R}_i - \vec{R}_j\right|} \qquad (2.2)$$

Where $\vec{R}_i$ and $\vec{r}_i$ are the coordinates of nuclei and electrons respectively; Z is the charge of nuclei; M_i is the mass of the nucleus at $\vec{R}_i$; m_e is the mass of the electron at $\vec{r}_i$. The first

term is the kinetic energy operator for the nuclei, the second for the electrons. The last three terms describe the electrostatic interaction between electrons and nuclei, electrons and other electrons, and nuclei and other nuclei.

The macroscopic observable solid bears about $N \approx 10^{23}$ electrons and nuclei [29]. Therefore, the Schrödinger equation for such a real system will be impossible to solve. In order to find acceptable eigenstates, approximations at 3 different levels are needed. The first is Born-Oppenheimer approximation; the second is density function theory (DFT); the third is the methods for solving the Kohn-Sham equations: the full-potential methods, the pseudopotential methods or the muffin-tin approximation to the effective potential and electron density. The third level approximations used in the present work will be discussed in Section 2.1.2 and 2.1.3.

2.1.1.1. Born-Oppenheimer approximation

To solve this thorny many-body problem, an important approximation is extensively used namely the Born-Oppenheimer approximation. This approximation decomposes the Hamiltonian for the entire system into two parts corresponding to electrons and nuclei, respectively. In this way, we can separately compute the motion of electrons and nuclei in the system, where electrons can be viewed as movements under the external forces generated by fixed nuclei. Thus, the first term on the right side of Eq. 2.2 becomes zero, and the last term is replaced by a constant potential.

2.1.1.2. Density functional theory (DFT)

The quantum many-body problem is much simpler than the original one after the Born-Oppenheimer approximation, but still far too difficult to solve. To furthermore simplify the equation, DFT theory was proposed. DFT theory is the most commonly used method of quantum mechanics. It has been successfully used to describe the properties of various materials. The main idea of the theory is using the charge density function to replace the complex multi-electron system wave function as a basic variable to achieve the calculation of electronic structure. By simplifying the Schrödinger equation of the multi-electron system as a Hartree single-electron equation, DFT provides us a powerful and efficient way to calculate the electronic properties of the ground-state interaction [29].

(a) Hohenberg-Kohn theory

In fact, we can reach large amount of information for the multi-electron system from the total energy E and the electron density n(r) of the system, which is the well-known Hohenberg-Kohn density-functional theory [34].

Hohenberg and Kohn suggested that E can be expressed as a universal functional of n(r), and E bears a minimum value in the ground state. In the frame of the Hohenberg-Kohn theory, we only need to consider the electron density n(r) in three dimensions, rather than the wave function of the multi-electron system in three dimensions when dealing with a many-body problem. Thus the theory greatly simplifies the many-body

problem. In general, given the external potential ν_{ext}, the total functional E[n] of the interacting electrons can be given as follows:

$$E[n] = F[n] + \int d\vec{r} v_{ext}(\vec{r}) n(\vec{r}) \qquad (2.3)$$

where $F[n]$ is a universal function independent on ν_{ext}.

(b) Kohn-Sham equation

Based on the Hohenberg-Kohn theory, Kohn and Sham simplify the resolution of the multi-electronic equation by solving a set of effective single-electron equations [35]:

$$\left(-\frac{1}{2}\nabla^2 + v_{eff}(\vec{r})\right)\Psi_i(\vec{r}) = \varepsilon_i \Psi_i(\vec{r}) \qquad (2.4)$$

where the effective potential ν_{eff} can be expressed as following:

$$v_{eff}(\vec{r}) = v_{ext}(\vec{r}) + \int d\vec{r} \frac{n(\vec{r})}{|\vec{r} - \vec{r}'|} + v_{xc}(\vec{r}) \qquad (2.5)$$

in which the first term on the right-hand is the external potential generated by the nucleus; the second term is derived from the coulombic interaction potential between electrons; the last term is the exchange-correlation from the many-body quantum effects.

The electron density n (r) can be obtained directly by the following equation using the electron orbital wave function:

$$n(\vec{r}) = \sum_{i=1}^{N} |\Psi_i(\vec{r})|^2 \qquad (2.6)$$

Eqs. 2.4-2.6 are the complete expressions of the so-called Kohn-Sham equation. Generally speaking, the Kohn-Sham scheme firstly considers the multi-electron system as a single electron system under an external potential (which is the effective potential ν_{eff} as expressed in Eq. 2.5), then solving the corresponding single electron Schrödinger equation. During the calculation, the Kohn-Sham equation needs to be solved by self-consistent method. The electron density n(r) is dependent on the single-electron state wave function.

In Eq. 2.3, the universal functional F[n] can be expressed as:

$$F[n] = T_s[n] + \iint d\vec{r} d\vec{r}' \frac{n(\vec{r}) n(\vec{r}')}{|\vec{r} - \vec{r}'|} + E_{xc}[n] \qquad (2.7)$$

where $T_s[n]$ is the kinetic energy of the non-interacting electrons. It can be expressed by the difference between the total energy of the electrons and the potential energy:

$$T_s[n] = \sum_i \varepsilon_i - \int d\vec{r} v_{eff}(\vec{r}') n(\vec{r}) \qquad (2.8)$$

Thus, the total energy functional E[n] can be re-specifically expressed as:

$$E[n] = \sum_i \varepsilon_i - \iint d\vec{r} d\vec{r}' \frac{n(\vec{r}) n(\vec{r}')}{|\vec{r} - \vec{r}'|} - \int d\vec{r} v_{xc}(\vec{r}) n(\vec{r}) + E_{xc}[n] \qquad (2.9)$$

The energy terms given on the right-hand of Eq. 2.9 describes almost all the many-body effects. Most of these terms can be calculated exactly as a functional of the electron density. Only the exchange-correlation potential ν_{xc} and its corresponding energy

functional $E_{xc}[n]$ are difficult to be given exactly, and further approximations need to be made.

(c) Exchange-correlation functional

1) Local density approximation (LDA)

On the basis of Kohn-Sham equation, we still need to make some approximations when dealing with the exchange-correlation functional for practical calculations. The widely used approximation is called the local density approximation (LDA) [36,37]. In this approximation method, the exchange- correlation energy density is approximately represented by the energy density of the isotropic electron gas at the same density. Thus, the exchange-correlation energy functional is expressed as:

$$E_{xc}^{LDA}[n] = \int d\vec{r} n(\vec{r}) \varepsilon_{xc}^{\text{hom}}(n(\vec{r})) \qquad (2.10)$$

where $\varepsilon_{xc}^{\text{hom}}(n(\vec{r}))$ is the sum of the exchange and correlation energies of the isotropic electron gas with electron density n(r). The exchange-correlation potential is the functional derivative of the energy functional w.r.t. the electron density:

$$v_{xc}^{LDA}(\vec{r}) = \varepsilon_{xc}^{\text{hom}}(n(\vec{r})) + n(\vec{r}) \frac{\delta \varepsilon_{xc}^{\text{hom}}([n], \vec{r})}{\delta n(\vec{r})} \qquad (2.11)$$

The commonly used expressions of LDA functionals are Vosko-Wilk-Nusair (VWN) [38] for correlation, Ceperley-Alder (CA) [39] and Von Barth and Hedin (VBH) [40] for exchange-correlation etc.

2) Generalized gradient approximation (GGA)

As compared to other approximations, LDA method is simple and can even be well applied to anisotropic materials. However, for many solid materials, LDA method usually models bond energies between atoms as too large, and as a consequence underestimates the lattice equilibrium volume (3%). It leads to deviations between the calculations for bulk modulus as well as some other mechanical properties and experimental measurements [29]. Trying to improve LDA method, a generalized gradient approximation (GGA) [41] has been therefore, proposed. In this method, not only the charge density itself, but also the local density gradient is treaded in the energy density functional factor. The exchange-correlation energy functional under the GGA method is expressed as:

$$E_{xc}^{GGA}[n] = \int d\vec{r} n(\vec{r}) \varepsilon_{xc}^{\text{hom}}(n(\vec{r}), |\nabla n|) \qquad (2.12)$$

The expression of the GGA exchange-correlation energy functional $E_{xc}^{GGA}[n]$ is not unique. The most popular one is the PW91 proposed by Perdew and Wang [42]. Its simplified form is PBE proposed by Perdew, Burke and Ernzerhof in 1996 [41]. GGA method in some content improves the calculation of the total energy. It corrects the excessive binding energy between atoms given the aforementioned LDA method. Thus GGA method usually provides lattice constants with more accuracy. However, in some cases, the lattice constants obtained by using GGA-PBE method may be slightly larger than the experimental values (1%) due to an over-correction w.r.t. the LDA method [29].

2.1.2. Exact muffin-tin orbitals (EMTO) method

Exact muffin-tin orbitals (EMTO) theory was proposed by Andersen and his colleagues in the 1990s [43]. It is an accurate and efficient method for solving the Kohn-Sham equation. Afterwards, Vitos and his colleagues developed their own EMTO method [27].

For the EMTO method developed by Vitos et al. [27], the single-electron Schrödinger equation is solved separately in each Wigner-Seitz unit cell. By means of spherical cell approximation (SCA), the effective potentials in Kohn-Sham equation are approximated as the best overlapping muffin-tin wells. Then the electron structure and charge density are obtained by self-consistent calculations; the total energy density is calculated by using the so-called full charge density (FCD) [27]. In addition, the coherent potential approximation (CPA) [44–46] is incorporated within the EMTO code, which facilitate the calculations dealing with chemical or magnetic disordered alloys. In the adopted EMTO-CPA calculation software, the total energies can be obtained by using LDA, PBE, PBEsol, AM05 and LAG exchange-correlation functionals.

The two main advantages of EMTO approach are: i) by using the approximation of the overlapping spherical potentials, one can more accurately describe the crystal potential, which is not possible with other conventional non-overlapping spherical potentials; ii) EMTO self-consistent calculation can be combined with the CPA method maintaining the accuracy and efficiency. As compared to the traditional first-principle full potential (FP) and pseudopotential (PP) methods, EMTO method is obviously more favorable to calculation in disordered alloys [29]. The main mechanisms for the EMTO approach will be described in the following (for more details see Ref. 27,29).

2.1.2.1. EMTO potential

In EMTO theory, the effective single electron potential is approximated by the sum of the spherical potential well $\nu_R(r_R)$- ν_0 centered on lattice sites R and a constant potential ν_0:

$$v(\vec{r}) \approx v_{mt}(\vec{r}) \equiv v_0 + \sum_R [v_R(r_R) - v_0] \qquad (2.13)$$

Out of the spherical potential radius s_R, $\nu_R(r_R)$ is defined as equal to the constant potential ν_0. For simplicity, the density dependence of the potential is suppressed. For the vector coordinate, the notation $\vec{r}_R \equiv r_R \hat{r}_R = \vec{r} - \vec{R}$ is used, where r_R is the modulus of $\vec{r}_R$, and omit the vector notation for index R.

For a given potential, the spherical potentials $\nu_R(r_R)$ and ν_0 on the right side of the Eq. 2.13 can be obtained by minimizing the average functional of the square of the difference between the muffin-tin potential $v_{mt}(\vec{r})$ and the total effective potential $v(\vec{r})$ $\nu(r)$:

$$F_v\left[\{v_R\}, v_0\right] \equiv \int_\Omega \left\{ v(\vec{r}) - v_0 - \sum_R [v_R(r_R) - v_0] \right\}^2 d\vec{r} \qquad (2.14)$$

where Ω is the volume of the unit cell. Thus, the minimization condition can be expressed as:

$$\int_{\Omega} \delta v_R(\vec{r}) \frac{\delta F_v\left[\{v_R\}, v_0\right]}{\delta v_R(\vec{r})} d\vec{r} = 0 \text{ for any R, and } \frac{\partial F_v\left[\{v_R\}, v_0\right]}{\partial v_0} = 0 \qquad (2.15)$$

where $\frac{\delta}{\delta v_R(\vec{r})}$ stands for the functional derivative. From the solution of Eq. 2.15, we can get the optimal $v_R(r_R)$ and v_0 and thus construct the so-called best mutual overlapping muffin-tin well. Notably, both the best spherical potential $v_R(r_R)$ and the constant potential v_0 are functionals of the total effective single electron potential of the spherical part.

In fact, during EMTO calculation, the effective single electron potential is built including two steps: i) from the total charge density to calculate the total potential function; ii) constructing the best mutual overlapping muffin-tin well as described in Eq. 2.14 and 2.15.

The first step, constructing the total potential function, is fairly complex. Firstly, the potential function at the apex of the cell usually cannot be considered very accurate. In addition, we need to evaluate an integral over the whole real space to solve the Hartree potential. Thus in order to avoid these two problems, we adopt the so-called spherical cell approximation (SCA) method. The main idea is that during the self-consistent iterative calculations, the spherical cell is used to replace the equal-volume Wigner-Seitz cell to simplify the solution for Hartree potential.

Based on the mutual overlapping muffin-tin potential approximation combined with SCA, for the ordered system, the single-electron potential of the spherical part $v_R(r_R)$ can be divided into four parts. Firstly, we divide the total electrostatic potential generated by the nuclei charges and other electrons into two parts: the potential functions in the sphere and the potential out of the sphere. The potential out of the sphere is expressed by the so-called Madelung potential. Secondly, the spherical symmetry part of the exchange-correlation potential also needs to be considered. Finally, due to SCA, the total number of electrons in the muffin-tin potential is not equal to the actual number of electrons in the Wigner-Seitz cell. The missing charges are considered to be evenly distributed over the adjacent unit cells, which contribute a constant potential. Thus, the spherical part of the total effective potential is expressed as:

$$v_R(r_R) = v_R^I(r_R) + v_R^M + \Delta v_R^{SCA} + \mu_{xcR}(r_R) \qquad (2.16)$$

where $v_R^I(r_R)$ and v_R^M are the Coulomb potential in the sphere and the Madelung potential, respectively; v_R^{SCA} is the constant potential; $\mu_{xcR}(r_R)$ is the exchange-correlation potential.

2.1.2.2. EMTO wave function

In EMTO method, the orbital wave function in the Kohn-Sham equation is developed with the exact muffin-tin orbital wave function:

$$\Psi_j(\vec{r}) = \sum_{RL} \overline{\Psi}^{\alpha}_{RL}(\varepsilon_j, r_R) \nu^{\alpha}_{RL,j} \qquad (2.17)$$

where $\sum_{RL} \overline{\Psi}^{\alpha}_{RL}(\varepsilon_j, r_R)$ is the electron orbit basis function defined by the lattice position R and the total angular momentum L≡(l, m) (l and m are the orbital and magnetic quantum number); the expansion coefficient $\nu^{\alpha}_{RL,j}$ can be determined by the so-called kink-cancellation equation. That is, the expansion of the Kohn-Sham orbital wave function Eq. 2.17 satisfies the solution of the Eq. 2.4 in all spaces.

The exact muffin-tin orbital wave function $\sum_{RL} \overline{\Psi}^{\alpha}_{RL}(\varepsilon_j, r_R)$ consists of three different basis functions. In the gap of the potential sphere, the effective potential is approximated as the constant potential ν_0; the basis function is expressed as the solution of the wave equation:

$$\left\{\nabla^2 + \kappa^2\right\} \psi^a_{RL}(\kappa^2, \mathrm{r}_R) = 0 \qquad (2.18)$$

i.e. the screened spherical waves $\Psi^{\alpha}_{RL}(\kappa^2, r_R)$, where $\kappa^2 = \varepsilon - \nu_0$; ε represents energy.

Inside the potential sphere, at R, the basis function is expressed as partial waves, that is, the product of the conventional solution (Eq. 2.20) for the radial Schrödinger equation (Eq. 2.19) under the effective potential $\nu_R(\mathrm{r}_R)$:

$$\frac{\partial^2 \left[r_R \phi_{Rl}(\varepsilon, r_R)\right]}{\partial r_R^2} = \left[\frac{l(l+1)}{r_R^2} + \nu_R(r_R) - \varepsilon\right] r_R \phi_{Rl}(\varepsilon, r_R) \qquad (2.19)$$

$$\phi^a_{RL}(\varepsilon, \mathrm{r}_R) = N^a_{Rl}(\varepsilon) \phi_{Rl}(\varepsilon, r_R) Y_L(\hat{r}_R) \qquad (2.20)$$

where $N^a_{Rl}(\varepsilon)$ is a normalized function.

In order to match the wave functions $\Psi^{\alpha}_{RL}(\kappa^2, r_R)$ and $\phi^{\alpha}_{RL}(\varepsilon, r_R)$ at the boundary of the potential sphere, an additional free electron wave solution $\varphi^{\alpha}_{RL}(\varepsilon, r_R) Y_L(\hat{r}_R)$ is introduced.

Thus, the exact muffin-tin orbital wave function can be seen as a wave function composed of a screened spherical waves $\Psi^{\alpha}_{RL}(\kappa^2, r_R)$, a partial wave function $\phi^{\alpha}_{RL}(\varepsilon, r_R)$ and a free electron wave solution $\varphi^{\alpha}_{RL}(\varepsilon, r_R) Y_L(\hat{r}_R)$:

$$\overline{\Psi}^a_{RL}(\varepsilon_j, \mathrm{r}_R) = \psi^a_{RL}(\kappa^2, \mathrm{r}_R) + \phi^a_{RL}(\varepsilon, \mathrm{r}_R) - \varphi^a_{RL}(\varepsilon, r_R) Y_L(\hat{r}_R) \qquad (2.21)$$

2.1.2.3. Total energy of full charge density (FCD)

The full charge density (FCD) technique is designed to maintain high efficiency and in the mean while to give total energies as accurate as that of the full-potential methods. It adopts the assumed spherically symmetric part of the potential but at the same time uses the full non-spherically symmetric charge density [27].

The principal idea of the FCD technique is to use the total charge density to compute the total energy functional. The total density can be obtained from a self-consistent calculation by employing certain approximations. The shape function technique is used to calculate the space integrals over the Wigner-Seitz cells. The interaction energy

between remote Wigner-Seitz cells is described by the Madelung term. The so-called displaced cell technique is used to deal with the energy, which arises from the overlapping bounding spheres. Thus the total energy becomes:

$$E_{tot} = T_s[n] + \sum_R \left(F_{\text{intraR}}[n_R] + E_{xcR}[n_R]\right) + F_{\text{inter}}[n] \qquad (2.22)$$

where $T_s[n]$ is the kinetic energy of the non-interacting electrons; $F_{intraR}[n_R]$ and $F_{inter}[n]$ are the Coulomb interaction energies in and out of the Wigner-Seitz cells, respectively; $E_{xcR}[n_R]$ is the exchange-correlation energy; $F_{intraR}[n_R]$ and $E_{xcR}[n_R]$ depend only on the charge density in the actual unit cell; $F_{inter}[n]$ is derived from the Coulomb charge energy distributed over the different unit cells; $T_s[n]$ is the non-local functional of the charge density.

2.1.2.4. Coherent potential approximation (CPA)

Coherent potential approximation (CPA) is one of the most effective methods to deal with the disorder problem in multi-component alloy system. For EMTO method combined with CPA calculation, the principle idea is to introduce two approximations: i) it is assumed that the local potentials P_i, around a certain type of atom i from the alloy are the same, i.e. the effect of local environments is ignored; ii) the alloy system is treated as a monoatomic system described by the site independent coherent potential $\tilde{P}$.

Based on these two approximations, Green's function for describing the whole system is treated as a coherent Green function $\tilde{g}$. For each alloy component i, a single-site Green function g_i is introduced. There are certain relationship among the four quantities P_i, $\tilde{P}$, g_i and $\tilde{g}$. First of all,

$$\tilde{g} = \left[S - \tilde{P}\right]^{-1} \qquad (2.23)$$

where S denotes the structural constant matrix of the lattice; second, from the mathematical point of view, g_i can be expressed by the real-space Dyson equation:

$$g_i = \tilde{g} + \tilde{g}(P_i - \tilde{P})g_i,\ i = A, B, C... \qquad (2.24)$$

Finally, the coherent Green function $\tilde{g}$ can be expressed as the sum of the average of the individual Green's function g_i:

$$\tilde{g} = ag_A + bg_B + cg_C + ... \qquad (2.25)$$

Eqs. 2.23-2.25 are solved iteratively. The output $\tilde{g}$ and g_i are used to determine the electronic structure, charge density and total energy for the random alloy.

Due to the coherent potential approximation (CPA), for a particular component of the disordered alloy, a non-zero electrostatic charge may be introduced. Depending on the screened impurity model (SIM) [47,48], due to this part of the electrostatic charge, the total spherical potential will lead to an additional potential shift and the total energy will lead to an additional Coulomb energy.

2.1.3. Pseudopotentials

Developing both accurate and efficient numerical methods for solving the Kohn-Sham equations has been among the biggest challenges within computational materials

science. In principle, the full-potential methods have been designed as techniques with high accuracy. However, they are generally very cumbersome and cause expensive computational efforts. The reason is that atomic potential becomes very strong inside the core and it needs an excessively large number of plane waves to reach reasonable results. Nevertheless, the core electrons do not contribute to atomic bonding, but only their absolute energy is affected by the average electrostatic potential in the vicinity of the core [31]. Thus, the pseudopotential methods were born, for which the pseudopotential and pseudo wave-functions differ from the one for all electrons only inside a region around the nucleus and are constructed to be smooth as presented in Fig. 2.1 and 2.2. In practice, the physical and chemical properties calculated by using pseudopotential methods, in most cases, are almost identical with those obtained by using all-electron full-potential methods [27].

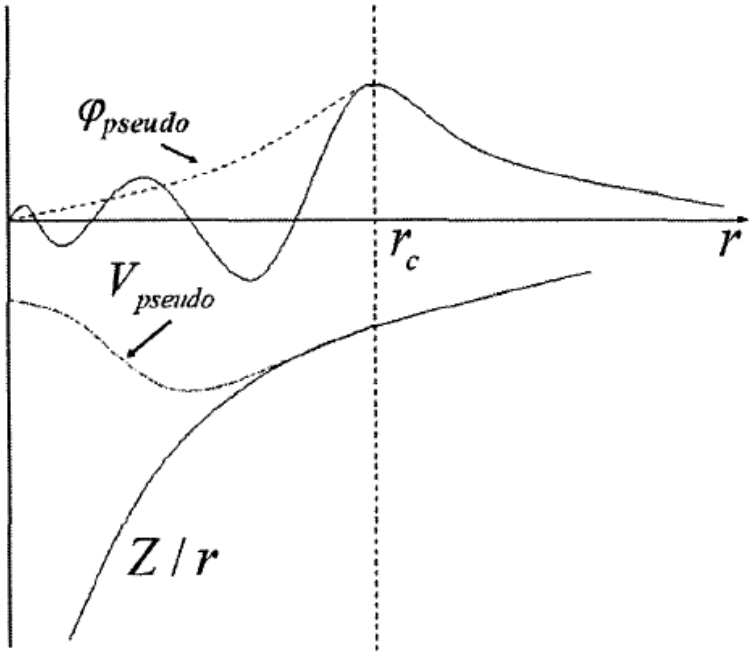

Figure 2.1 : All-electron (solid lines) and pseudo-electron (dashed lines) potentials and their corresponding wave functions (from Ref. 30).

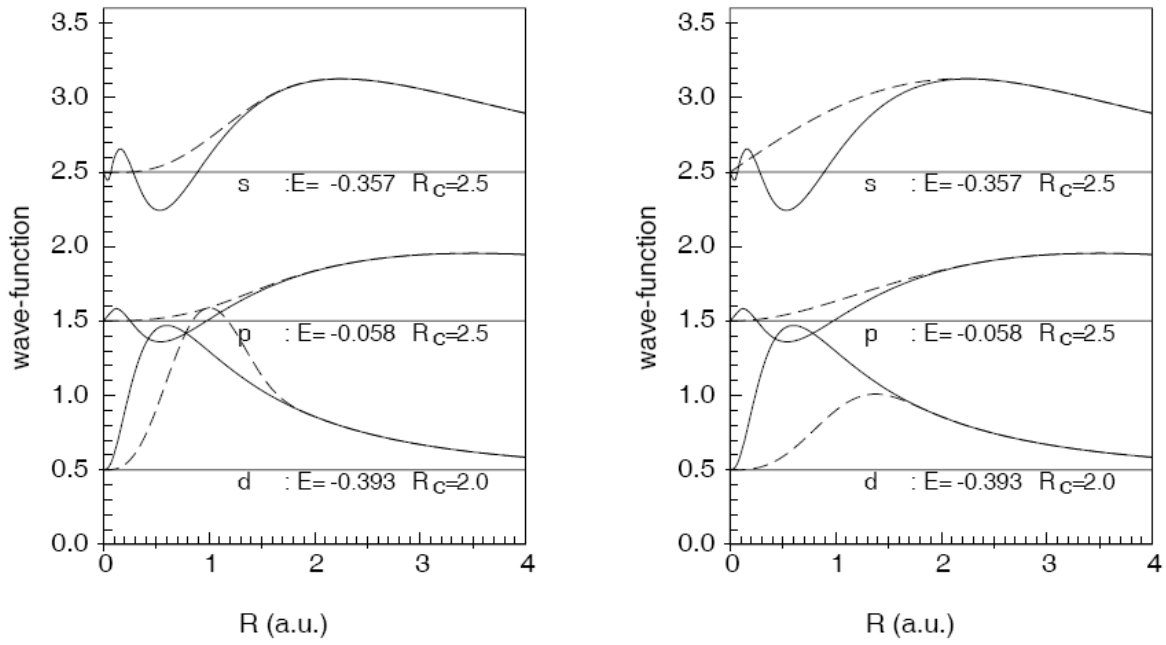

Figure 2.2 : All –electron (full line) and pseudo (dashed line) wave function for a norm-conserving (left panel) and ultrasoft pseudopotential (right panel) of Cu. Kohn-Sham eigen-energies and cutoff raddi are specified in atomic units (a.u.) (from Ref. 31).

2.1.4. PAW (projector augmented-wave) method

The PAW method [49,50] was developed by combining ideas from ultrasoft-pseudo-potential [51,52] and the linearized augmented-plane-wave (LAPW) method [53]. It was first proposed and implemented by Blöchl [49]. The close connection between the ultrasoft pseudopotentials and the PAW method has been derived by Kresse and Joubert [25]. The PAW method, in practice, uses the frozen-core approximation, and is in principle an all-electron method, not because all electrons are treated explicitly, but because the valence electronic wave functions are kept orthogonal to the core states [54].

In the PAW method the one electron wave functions Ψ are derived from the pseudo functions $\tilde{\Psi}$ by means of a linear transformation:

$$|\psi\rangle = |\tilde{\psi}\rangle - \sum_{N,i} |\tilde{\phi}_{N,i}\rangle \langle \tilde{p}_{N,i} | \tilde{\psi}\rangle + \sum_{N,i} |\phi_{N,i}\rangle \langle \tilde{p}_{N,i} | \tilde{\psi}\rangle \qquad (2.26)$$

where all quantities related to pseudo are indicated by a tilde; Ø are the local wave functions; the index N goes over all sites; i runs over the quantum numbers n, l and m; $\tilde{p}_i$ are localized projector functions.

The pseudo- and all-electron wave functions can be easily constructed from the plane-wave expanded pseudo wave functions [31]. The decomposition of all-electron wave function in the PAW method is presented in Fig. 2.3. This general scheme is applicable to all operators (like wave functions, Charge density, kinetic energy, exchange correlation energy and Hartree energy). Sometimes one may choose to include only parts of the PAW expressions [54].

The PAW method is implemented in the VASP software package. The corresponding calculation results can match the most accurate DFT ones presently available [31].

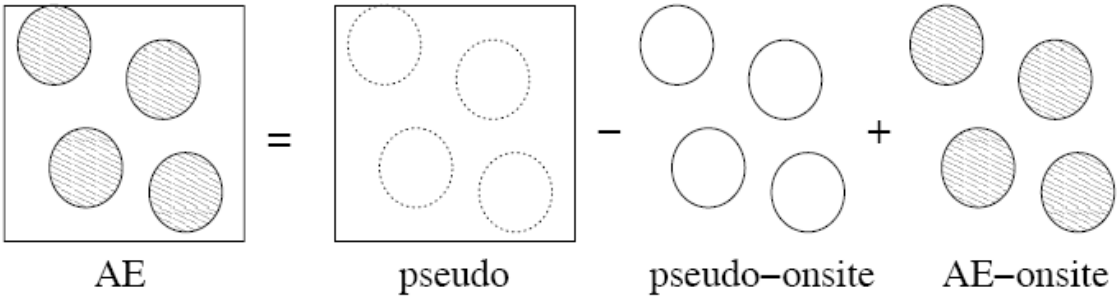

Figure 2.3 : Decomposition of the all-electron wave function in the PAW method (from Ref. 31).

2.1.5. The Vienna Ab initio Simulation Package (VASP)

The Vienna Ab initio Simulation Package (VASP) is developed by Kresse and Furthmüller [26,55]. It is a plane wave based density functional theory code. The interaction between ions and electrons is described by ultra-soft Vanderbilt pseudopotentials (US-PP) or by the projector-augmented wave (PAW) method [56]. The first parts of the code were written in the early 1990's. Currently, it contains more than 80000 lines written in Fortran90 [31]. The package is still developing.

VASP solves the Kohn-Sham equations of local density or spin-density functional theory iteratively within a plane-wave basis set. The electronic ground state is determined either by a conjugate gradient algorithm [57], a blocked Davidson scheme [58], or via an unconstrained band-by-band matrix-diagonalization scheme based on a residual minimization method (RMM) [55,59].

After every iteration, the charge density has to be recalculated. The new density is mixed with the input charge density of the previous cycle by use of an improved Pulay mixing [60] to guarantee numerical stability.

With respect to the exchange-correlation functional, besides the pure local density approximation (LDA), the gradient corrected functionals are implemented in VASP to account for the nonlocality in exchange and correlation, e.g. GGA-LM, GGA-BP, GGA-PW91, GGA-PBE and GGA-RPBE. For more details about these functionals see Ref. 31. The most common used ones are GGA-PW91 and GGA-PBE.

For the energy band dispersion in the Brillouin-zone, the k-point meshes sampling in the reciprocal space is constructed using Monkhorst-Pack special grids [61]. For the integration over the Brillouin zone, the tetrahedron method with Blöchl corrections [62] and a generalized Gaussian smearing [63] can be adopted as well as other less involved methods. A brief flow chart of a single self-consistency cycle in VASP is presented in Fig. 2.4.

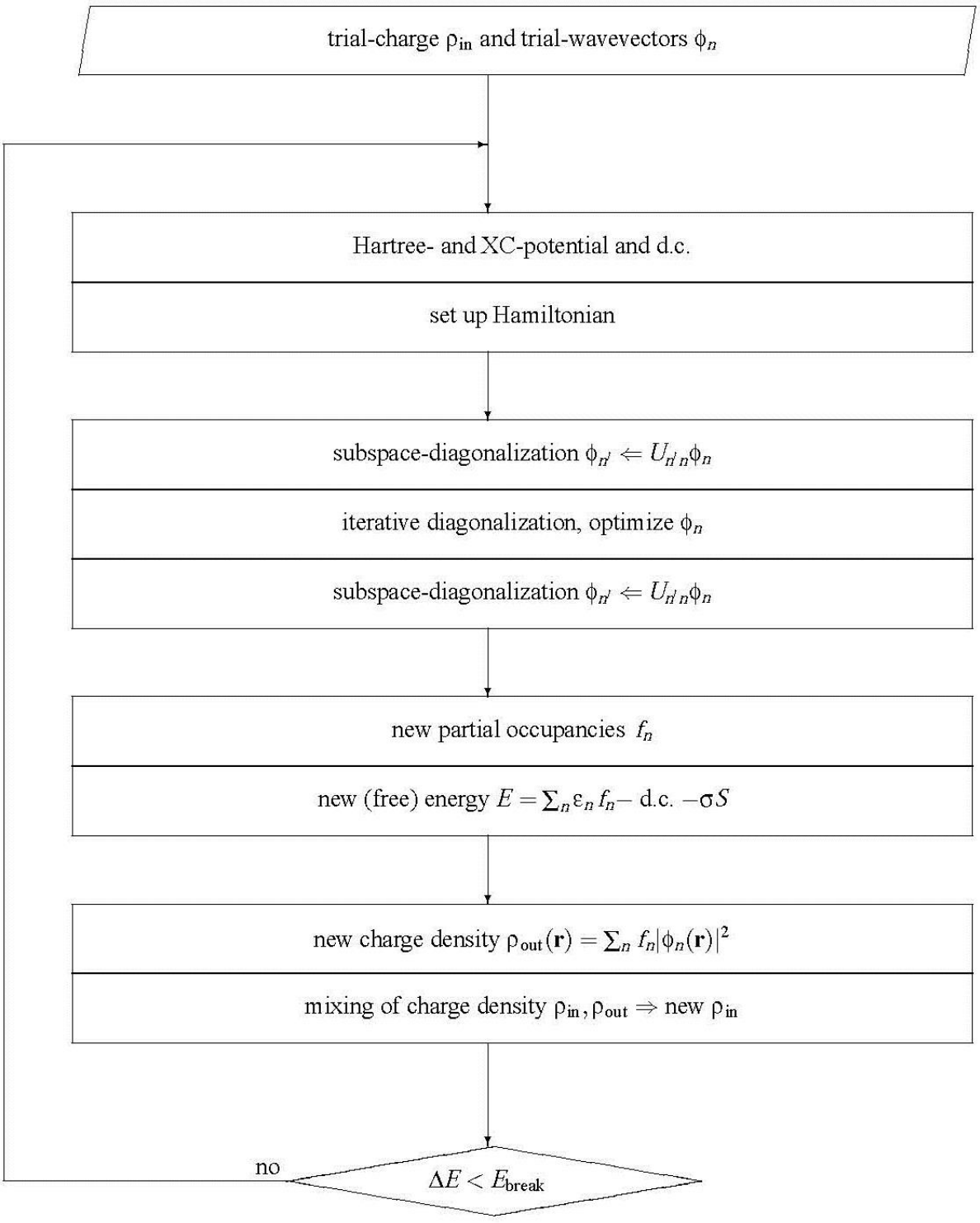

Figure 2.4 : A single self-consistency cycle calculation of Kohn-Sham ground-state in VASP (from Ref. 56).

2.1.6. Bader Charge Analysis

2.1.6.1. Atoms in Molecules (AIM)

Atomic charges do not correspond to any physical observable quantity and thus are not uniquely defined by quantum mechanical theory. Many different definitions have been proposed in the literature, some based on electronic orbitals and others based on the electrostatic potential or the electron density (for more details see Ref. 64).

Richard Bader's theory of Atoms in Molecules (AIM) [65] provides an intuitive way of dividing molecules into atoms with definition of an atom based purely on the electronic charge density. Typically in molecular systems, the charge density reaches a minimum between atoms, which is a natural place to separate atoms from each other [32]. Thus zero flux surfaces in the gradient vector field of the electron density are used to separate atoms [65]. The schematic illustration of electronic charge density around atoms is presented in Fig. 2.5 and 2.6. The physical properties of atoms, including atomic charge and dipole moment, can be obtained by integrating the appropriate operator in the atomic region [65].

Bader partitioning method has an advantage over other partitioning schemes (e.g. Mulliken population analysis [66]) as it is based upon the observable quantity of charge density, which can be measured or calculated [67]. Furthermore, in a converged electronic structure calculation, the charge density is insensitive to the basis set used. In this regard, the Bader analysis is more robust than orbital-based methods for which the analysis is sensitive to the choice of basis set [67].

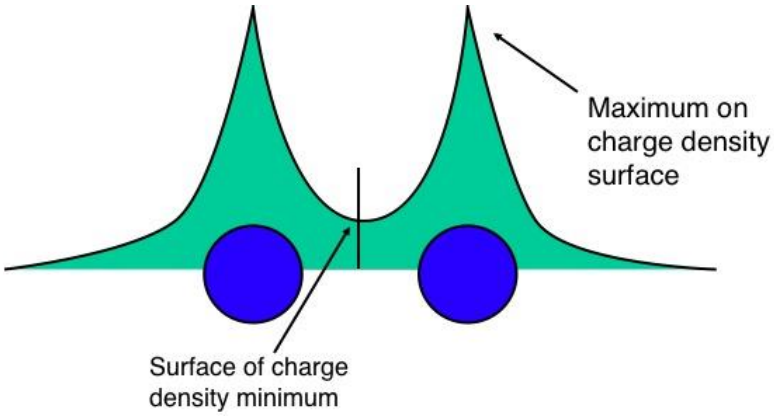

Figure 2.5 : Schematic illustration of electronic charge density around atoms in two dimensions (from Ref. 32). The surface of charge density minimum is the place where the gradient of the electron density is zero along the surface normal.

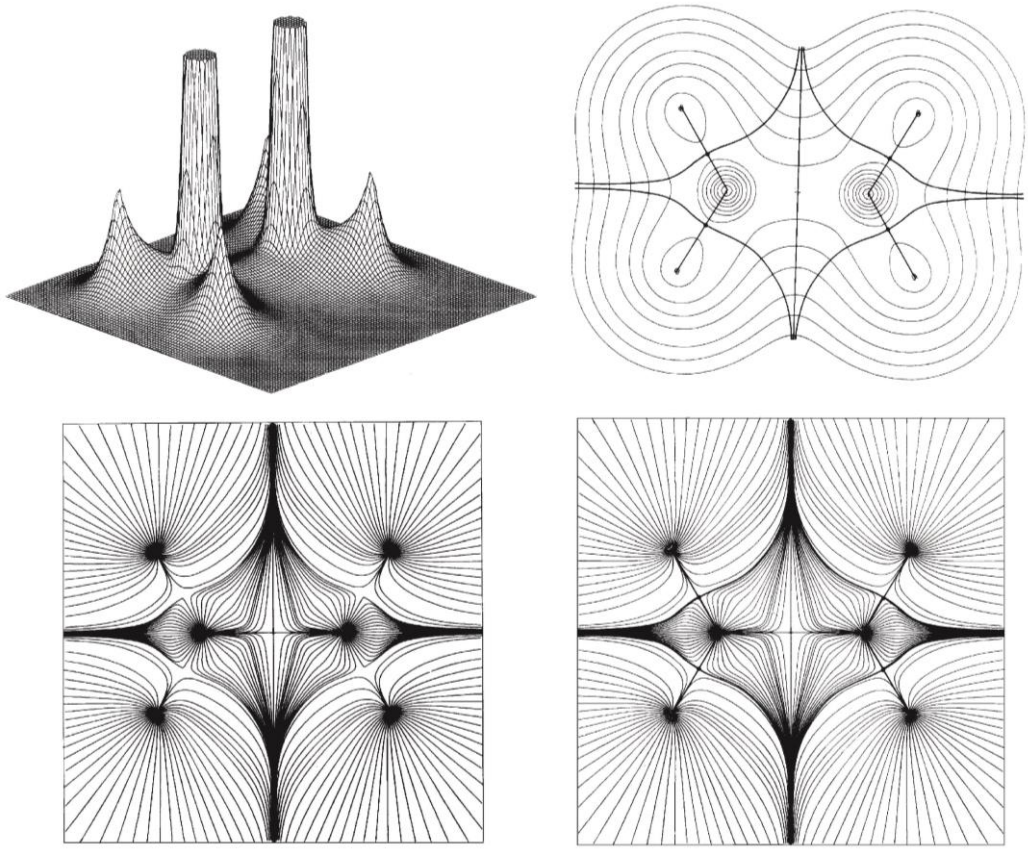

Figure 2.6 : Schematic illustration of electronic charge density around atoms in three dimensions: relief and contour maps of the electron density for diborane in the plane of the terminal hydrogen atoms. The lower maps illustrate the gradient vectors of the density (from Ref. 65,68).

2.1.6.2. Code: Bader Charge Analysis

There are several methods to calculate Bader volumes. Early algorithms were employed for quantum chemistry calculations of small molecules. These methods first find stationary points in the charge density and then follow trajectories along the density gradient from these points to map out their connectivity and the zero-flux dividing surfaces [67]. However, the methods need expensive computational effort for large systems.

Most current implementations of Bader's analysis are based upon a grid of charge density values. Henkelman et al. [69] proposed a simple and fast grid based method for carrying out Bader decomposition of electron density, which can be implemented for DFT calculation of large molecules or materials. It is different from the previous methods. With this method, the zero-flux dividing surfaces and critical points do not need to be found explicitly, which makes the algorithm more robust. The algorithm was introduced in which ascent paths on the charge density were followed between grid points to determine the Bader volumes as indicated in Fig. 2.7. The method is highly efficient, scales linearly with the number of grid points, and is robust and insensitive to

the complex bonding topology [69]. However, this algorithm introduces a lattice bias due to the fact that ascent paths are constrained to the grid points. Thus, improved grid-based methods based on this algorithm were proposed by these authors [67,70].

Based on the above theory and algorithm, the Henkelman group developed the Bader charge analysis code [32], which was adopted in the present work. The program can read in charge density files from the VASP code and then output the total charge associated with each atom, and the zero flux surfaces defining the Bader volumes. For more information about the code see Ref. 32.

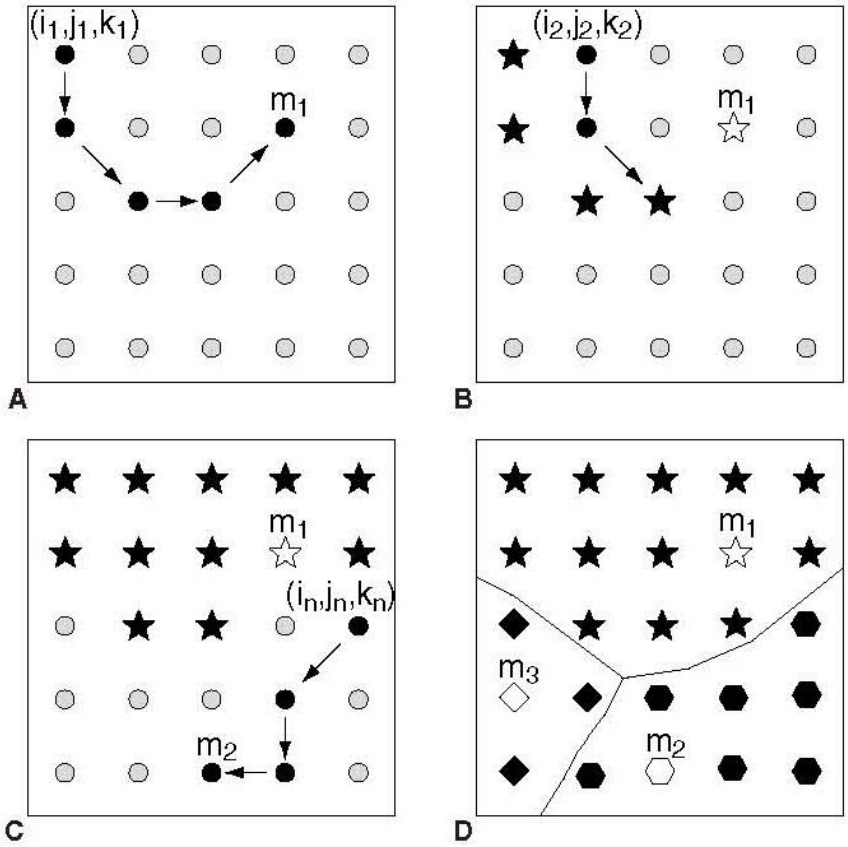

Figure 2.7 : An illustration of the steepest ascent paths on the charge density grid that are used to find Bader regions (from Ref. 69). (A) The first path starts from point (i_1, j_1, k_1) and after four steepest ascent moves ends at point m_1, a point of maximum charge density. Each point along the path is assigned to the region associated with m_1. (B) The second path starts from (i_2, j_2, k_2) and is terminated after two moves when it reaches a point which has already been assigned to m_1 (stars indicate points assigned to region 1). This process is repeated from each unassigned grid point. (C) Starting from the point (i_n, j_n, k_n), a new maximum m_2 is found and all grid points which lead to this maximum are assigned to m_1. (D) After all grid points have been assigned, three maxima have emerged and the three groups of grid points are shown with m_1, m_2 and m_3.

2.2. CALPHAD approach

In 1956, Kaufman and Cohen firstly calculated the Fe-Ni phase diagram by using the regular solution model [71], which indicates the birth of the CALPHAD method. CALPHAD [72–74] is short for calculation of phase diagram or computer coupling of phase diagram and thermochemistry. It is now widely used to develop thermodynamic databases for multi-component and multi-phase material systems. The thermodynamic models should be firstly established. The model parameters are evaluated and fit the data from experimental measurements, first-principles calculations, statistical methods and empirical or semi-empirical estimations. There are numerous reviews on the CALPHAD methods [72–74] and thus we just briefly introduce the method here (for more details see Ref. 74,24,75).

2.2.1. Thermodynamic modelling

In CALPHAD method, the Gibbs energy is selected as the modelled thermodynamic parameters, since the Gibbs energy is a function of temperature and pressure, which are convenient to control in experiments. For each phase in a specific system, the Gibbs energy can be expressed as two parts, the one in atmospheric pressure and the pressure contribution.

$$G(T,P,n_i) = G(T,P_0,n_i) + G(T,P>P_0,n_i) \qquad (2.27)$$

Most CALPHAD databases include data under atmospheric pressure with ignoring the pressure contribution, namely the second term. For a solid solution phase α, the Gibbs energy is expressed by:

$$G_m^{\alpha} = \sum_i x_i {}^0G_i^{\alpha} + RT\sum_i x_i \ln x_i + {}^{phys}G_m + \sum_i \sum_{j>i} x_i x_j \left[\sum_{r=0}^{m} {}^rL_{i,j}^{\alpha}(x_i - x_j)^r \right] \qquad (2.28)$$

where G_m^{α} is the mole Gibbs energy of phase α; ${}^0G_i^{\alpha}$ is the Gibbs energy of component i; x_i and x_j are the constituent fractions; R is the gas constant; T is the temperature; $L_{i,j}^{\alpha}$ is the binary interaction parameter; the first term is the Gibbs "surface of reference" and represents the Gibbs energy of an unreacted mixture of the constituents of the phase; the second term is ideal configurational entropy; the third term ${}^{phys}G_m$ represents the physical effect contribution, like magnetic transition; the last term is the so called excess Gibbs energy that represent the deviation from the ideal behavior. To simplify only binary interaction parameter is considered here. Actually, the excess term could contain even higher order interactions. Different thermodynamic models [74] have been proposed according to different phases to describe the excess Gibbs energy.

2.2.2. Compound energy formalism (CEF)

The compound energy formalism (CEF) [76–78] is widely used in the CALPHAD assessments for binary or higher order system. It was constructed to describe models of the nonstoichiometric phases with two or more sublattices, e.g. $(A, B)_m(C, D, E)_n$. A and B mix on the first sublattice; C, D and E mix on the second one; m and n are the

stoichiometric coefficient. The definition of the sublattices is in principle based on the crystal structure of the phase, namely the nonequivalent crystal sites [9].

In the CEF model the reference Gibbs energy is defined as a linear combination of the Gibbs energy of the end-members compounds, namely the ordered configurations. The substitutional solutions model [74] is applied on each sublattice to compute the end-member and excess Gibbs energy. The Gibbs energy of the phase consists of the reference free Gibbs energy, the configurational entropy and the excess Gibbs energy. For more details see Ref. 9,77,78.

2.2.3. Volume modelling

Based on the same concept and method as thermodynamic modelling, databases of kinetic and physical properties can also be developed. CALPHAD modeling of molar volume has cost great investigation interests in recent years [79].

Molar volume (or density) is an important physical property of materials. It varies with the chemical composition, temperature and pressure. In many cases, the volume with respect to composition does not follow linear relationship, presenting negative or positive deviation from Vegard's law. Even for a fixed composition, alloys with different atomic order or crystal structure may bear different volumes. CALPHAD approach provides a modeling framework which can account for the relations among chemical composition, temperature, pressure and materials properties [79]. It can build a complex database from unary, binary, ternary upwards to multi-component systems. He et al. [79] have discussed the different molar volume models in details, as shown in the following.

2.2.3.1. Volume model for pure substances at atmospheric pressure

For non-magnetic materials, at atmospheric pressure, the molar volume can be expressed as:

$$V_m^{nonmagn}(T) = V_0 \exp(\int_{T_0}^{T} 3\alpha dT) \qquad (2.29)$$

where V_0 is the molar volume at the reference temperature T_0, α represents the coefficient of linear thermal expansion (CLE) in the non-magnetic state.

For magnetic materials, the magnetic contribution to molar volume is added as an extra term:

$$V_m(T) = V_m^{nonmagn}(T) + \Delta V_m^{magn}(T) \qquad (2.30)$$

where ΔV_m^{magn} is the magnetic term.

$$\Delta V_m^{magn}(T) = \Delta H_m^{magn} \frac{d\ln(T_c)}{dP} \qquad (2.31)$$

where ΔH_m^{magn} is the magnetic contribution to the enthalpy of formation. The model was proposed by Inden [80] and later simplified by Hillert and Jarl [81]. In Hillert and Jarl's model, the Gibbs free energy is formulated as a function of Tc and the magnetic moment β, allowing the calculation of ΔH_m^{magn}.

2.2.3.2. Volume model for solution phases at atmospheric pressure

In a binary system, the molar volume can be expressed as:

$$V_m = (1-x)V_A^\beta + xV_B^\beta + V_m^E = (1-x)V_A^\beta + xV_B^\beta + x(1-x)L \qquad (2.32)$$

where V_A^β and V_B^β are the molar volume of the constituent elements A and B, respectively, in β phase structure; x is the mole fraction of B; V_m^E is the excess molar volume. As with thermodynamic model, L can be regarded as the interaction parameter for volume of solution phases, and expressed by Redlich-Kister polynomial as a function of temperature.

2.2.3.3. Pressure model

In the CALPHAD method, the models are formulated as Gibbs energy functions with temperature, pressure and composition as variables. The pressure contribution is considered separately as an additional term and the total Gibbs energy is described as following:

$$G(T,P,n_i) = G(T,P_0,n_i) + G(T,P>P_0,n_i) \qquad (2.33)$$

where P_0 is the atmospheric pressure; n_i is the number of moles of element i.

Most CALPHAD databases include data under atmospheric pressure with ignoring the pressure contribution, namely the second term. The pressure contribution is constructed by using the equation of state (EOS) in the framework of the CALPHAD method. As one of the most commonly used EOS, Murnaghan EOS assumes that the isothermal bulk modulus B is a linear function of pressure [82]:

$$B = B(T,P_0) + nP \qquad (2.34)$$

where $B(T,P_0)$ is the bulk modulus at atmospheric pressure; n is a constant. However, large deviation from Murnaghan's linear relation is caused at high pressures.

Grover et al. [83] proposed an empirical equation in which the pressure model is valid in a wider range than that of the Murnaghan EOS, as shown in the following:

$$V_m(T,P) = a + b\ln(B/P_{ref}) \qquad (2.35)$$

where a and b are the parameters characterizing material properties as a function of temperature but independently of volume or pressure.

More recently, Lu et al. [84] transformed the Grover EOS into the Gibbs free energy expression by adopting Eq. 2.36 and Eq. 2.37. It has been integrated into the Thermo-Calc software and used to assess the temperature-pressure phase diagram of pure Fe below 100GPa [84].

$$V_m(T,P) = c(T)Ei^{-1}[Ei(\frac{V_m(T,P_0)}{c(T)}) + (P-P_0)\kappa(T,P_0)\exp(-\frac{V_m(T,P_0)}{c(T)})] \qquad (2.36)$$

$$G(T,P) = \int V_m(T,P)dP \qquad (2.37)$$

$V_m(T,P_0)$ denotes the molar volume at 1 bar; $\kappa(T,P_0)$ is the isothermal compressibility at 1 bar which is the reciprocal of the isothermal bulk modulus; $Ei(z)=\int_z^{\infty}\frac{e^{-x}}{x}dx$, Ei^{-1} is the reciprocal of Ei(z); $c(T)$ is a parameter to be assessed.

In the above model, the molar volume and the isothermal compressibility at atmospheric pressure should be assessed individually before assessing the high pressures model parameters.

2.2.3.4. Helmholtz energy model

The mentioned pressure model in Section 2.2.3.3 can describe most experimental data in a wide range of temperature and pressure. However, abnormal behaviors are often observed beyond a certain temperature or pressure range, such as negative values of entropy / heat capacity or extremum values of thermodynamic properties. Thus the reliability of model prediction is greatly reduced when extrapolated to high temperatures or pressures.

In practical applications, temperature and pressure are the two conditions that are most convenient to control. Thus, in the CALPHAD method, Gibbs free energy is used to describe the energy states of materials. However, for theoretical investigation, Helmholtz free energy is more often used since the calculations are usually performed at certain temperature and volume. Helmholtz free energy is usually described as the total contributions of various physical phenomena or processes as indicated in Eq. 2.38. For a non-magnetic system, the total Helmholtz free energy F is mainly composed of three parts, namely the total energy at 0K (i.e. static lattice energy， E_{tot}), the lattice vibrational energy (F_D) and the energy due to the electronic thermal excitations (F_{el}):

$$F(T,V)=E_{tot}(V)+F_D(T,V)+F_{el}(T,V)=E_{tot}(V)+E_D(T,V)-TS_D(T,V)+E_{el}(T,V)-TS_{el}(T,V) \quad (2.38)$$

where E_{el} and S_{el} are the energy and entropy due to the electronic thermal excitations, respectively; E_D and S_D are the lattice vibrational energy and entropy respectively.

The lattice vibrational energy (F_D) can be formulated by Debye model and the quasi-harmonic approximation. The Debye temperature is calculated by the EOS at a reference temperature (e.g. 0K or room temperature) and Grüneisen model, which is termed as Debye-Grüneisen model [85–87]:

$$\theta_D(V)=DV^{2/3}\left[-\frac{\partial P(V)}{\partial V}-\frac{2(\lambda+1)}{3}\frac{P(V)}{V}\right]^{1/2} \quad (2.39)$$

where D is a material-related constant; λ is the Grüneisen parameter; P(V) is the relation between pressure and volume at a reference temperature.

According to Eq. 2.38, the physical properties of a simple metal can be described accurately [87]. For transition metals, it requires a more suitable model due to the influence of the phonon-phonon interactions as well as magnetism, vacancies and other factors.

Once the free energy model is established, the various thermodynamic and physical properties can be calculated without individually evaluating each property. Thus the inherent constrains relations between various material properties are maintained.

2.2.4. Thermo-Calc software package

Thermo-Calc software package [88,89] is a thermodynamics software that was developed in 1981. It is a sophisticated software and database package used to perform all kinds of phase equilibrium, phase diagram and phase transformation calculations and thermodynamic assessments. The calculations consider a wide range of temperature, pressure and compositions conditions. It can calculate complex homogeneous and heterogeneous phase equilibria, and then plot the results as property diagrams or phase diagrams. Thermo-Calc software fully supports liquid, stoichiometric and non-ideal solution models and databases, which can be applied to make calculations on a large variety of materials such as steels, alloys, slags, salts, ceramics, solders, polymers, subcritical aqueous solutions, supercritical electrolyte solutions, non-ideal gases and hydrothermal fluids or organic substances [90].

Thermo-Calc contains 8 basic modules with different functions [90]. GES module is used to list system information, thermodynamic data and kinetic data, and one can modify and input new data in this model; POLY-3 is used for the calculations of phase equilibrium, phase diagram and thermodynamic properties etc. for binary, ternary or higher order systems; POST module is for drawing phase diagram and property diagram; PARROT module can be used to evaluate phase diagram by using experimental, semi-empirical information or first-principles calculations; TAB module can be used to list the different properties of pure substances, mixtures or chemical reactions; SCHDEIL module can be used to simulate solidification processes; BIN module is used to calculate phase diagram and thermodynamic properties for binary systems; TERN is used to calculate the phase diagram and thermodynamic properties for ternary systems. All modules are interrelated and can perform specific functions. Moreover, all modules can be converted into each other during runtime.

3. Influencing factors of atomic order in the binary sigma phase

The present work brings new insights into the influencing factors of atomic order (i.e. atomic constituent distribution or site occupancy preference on nonequivalent sites of a crystal structure) in the binary sigma phase. We have calculated the atomic volumes and atomic charges of the constituent elements of 32 stoichiometric end-member compounds (i.e. the complete set of ordered configurations) in the binary sigma phase systems by using first-principles calculations. The calculation results show that the size factor, the number of valence electrons and the total number of electron shells are the three factors influencing the atomic order of the sigma phase. Moreover, the calculation results indicate that between the two constituent elements, the one with larger atomic size, smaller number of valence electrons or smaller total number of electron shells prefers occupying large coordination number (CN) sites namely 4f, $8i_1$ and 8j; the other one prefers occupying small CN sites, namely 2a and $8i_2$. Furthermore, we have dissociated the effect of individual influencing factor on atomic order of the sigma phase combining with the measured site occupancies from the literature.

3.1. Introduction

The atomic order indicates atomic constituent distribution or site occupancy preference on nonequivalent sites of a crystal structure. There have been extensive studies of atomic order in intermetallic and solid state compounds, e.g. Mu phase [91], sigma phase [9], chi phase [92], $L1_2$ phase [93] and B2 phase [94]. As an important crystallographic property, the atomic order is closely related to thermodynamic and thermo-physical properties of materials, such as formation enthalpy, volume and elastic modulus.

The sigma phase is a typical topologically close-packed (TCP) phase that crystallizes in a tetragonal structure with 30 atoms distributed on five nonequivalent sites, namely 2a, 4f, $8i_1$, $8i_2$ and 8j [8–10]. It can serve as a prototype of TCP phases when investigating the atomic order, as the sigma phase bears a broad homogeneity range and there are abundant experimental site occupancy data available for the sigma phase. Even though numerous investigations on the atomic order of the sigma phase have been conducted, e.g. Ref. 8,9,95–107, by using XRD (X-ray diffraction), ND (neutron diffraction), mathematical methods or first-principles calculations, the atomic order of the sigma phase and its influencing factors are still not clear.

At first, Kasper and Waterstrat [96] tried to explain the atomic order phenomenon of the sigma phase by treating Mn as a dividing point for the sigma phase: 2a and $8i_2$ sites should be occupied by elements to the right of Mn in the periodic table, 4f site by elements to the left of Mn and $8i_1$ and 8j sites by a mixture of both. Then, Spooner and Wilson [98] considered the size and valence electron influencing factors and stated that the size of the constituent atoms of the sigma phase was a major factor in governing the filling of 2a, 4f, and $8i_2$ sites. However, in addition some valence electron factor governs the filling of $8i_1$ and 8j sites. Later on, a more thorough statement of the atomic order of the sigma phase and the effect of its influencing factors have been proposed by Hall and Algie [8] and then by Joubert [9]. They pointed that atoms with large size or small number of valence electrons preferentially occupy sites with large coordination number (CN), namely 4f, $8i_1$ and 8j; atoms with small size or large number of valence electrons preferentially occupy sites with small CN, namely 2a and $8i_2$.

However, all the above arguments cannot explain the atomic order of the sigma phase satisfactorily. The main reason is that the size factor and the number of valence electrons are not sufficient to clarify the atomic order. For example, with regard to Re-Mn system, as Re ($5d^5 6s^2$) and Mn ($3d^5 4s^2$) bears the same numbers of valence electrons, the size factor should be the prominent influencing factor on the atomic order according to the statement by Hall and Algie [8] and Joubert [9]. However, we can observe large differences in the measured site occupancies for the same CN sites ($8i_1$ vs 8j, CN=14) which bear similar site size, as discussed in the following Section 3.3.2. In fact, the measured site occupancies indicate that the atomic order among the large CN sites (i.e. 4f, $8i_1$ and 8j) or between the small CN sites (i.e. 2a and $8i_2$) can be very large, more examples being Nb-Re (4f vs $8i_1$/8j) [9], Re-Fe ($8i_1$ vs 8j) [9]. The early conclusions [8,9] about the atomic order cannot interpret the site occupancy preference among the large or small CN sites.

In addition, the site occupancies of the sigma compounds in Cr-Fe [104], Os-Cr [107], Re-Ta [105], Re-W [105,106] and Ru-Cr [107] systems were calculated by Sluiter et al. using a first-principle statistical thermodynamic approach. Due to simplified assumptions, the calculation results do not fit the experimental data satisfactorily, especially for Cr-Fe [104] and Os-Cr [107] systems. They sought and considered the influencing factors of atomic order for Ru-Cr and Os-Cr systems from the perspective of the crystal structure [107]. They considered (1) the size factor (the size difference among the five nonequivalent sites), (2) the electronic degeneracy arguments and (3) the pairwise interaction (A-A, A-B or B-B) within a unit cell. It was clarified that their conclusion has no predictive value [107]. In fact, their statement about the pairwise interaction was based on the deduction that all five crystal sites were equivalent based on the experimental evidence that Cr and Ru/Os do not have much overwhelming preference for any of the sites [107]. However, the deduction is suspicious, which will be illustrated in Section 3.3.2.3.

Besides, Crivello et al. [95] investigated the atomic order of the sigma phase in binary Re-X (X= Co, Cr, Fe, Hf, Mn, Mo, Nb, Ni, Os, Ru, Ta, Tc, Ti, V, W and Zr) systems by using the compound energy formalism (CEF) combining with first-principles calculations. The

studied systems include stable sigma phase (Re-V, Re-Cr, Re-Mn, Re-Fe, Nb-Re, Mo-Re, Ta-Re and W-Re) and some hypothetically unstable ones (Ti-Re, Zr-Re, Hf-Re, Re-Co, Re-Ni, Re-Tc, Re-Ru and Re-Os). Crivello et al. [95] pointed that the atomic order of the binary sigma phase is related to whether Re bears a larger size between the two constituent elements or not. If Re bears a larger size (e.g. for Re-V, Re-Cr, Re-Mn, Re-Fe, Re-Co, Re-Ni, Re-Tc, Re-Ru and Re-Os systems), the site occupancy preference for Re follows $4f > 8i_1 > 8j > 8i_2 > 2a$ and if Re bears a smaller size (e.g. for Nb-Re, Mo-Re, Ta-Re, W-Re, Ti-Re, Zr-Re and Hf-Re systems), the corresponding site occupancy preference follows $8i_2/2a > 8i_1/8j > 4f$. However, for Re-Os, Re-Ru and Re-V systems where Re bears a larger size, their calculation results indicated that the site occupancy preference for Re follows $8j > 8i_1$ (for Re-Os and Re-Ru systems) and $8i_2 > 8j$ (for Re-V system) which is inconsistent with their above conclusion. On the other hand, from the experimental perspective, with respect to Re-V system, the site occupancy preference follows for Re $8i_2 > 2a > 8i_1 > 4f > 8j$ (see Section 3.3.2) which is almost opposite as the one proposed by Crivello et al. [95]. Moreover, the site occupancy behavior between the same CN (i.e. CN12: 2a vs $8i_2$; CN14: $8i_1$ vs 8j) sites was unclarified in that work.

At present, numerous site occupancy measurements have been conducted on the binary sigma phase systems with high accuracy. However, the influencing factors on the atomic order of the sigma compounds are still not clarified. Apparently, the size and the number of valence electrons influencing factors are not enough to explain the atomic order. Another obstacle to sort out the connections is that the experimental site occupancies are results of competition and cooperation of the influencing factors on atomic order, and that it is difficult to dissociate the effect of individual influencing factor, as sometimes, for a specific system different influencing factors have similar effects [104] (e.g. for Cr-Fe system, larger size and smaller number of valence electrons of Cr comparing to Fe both cause Cr to preferentially occupy sites with large CN, namely 4f, $8i_1$ and 8j).

In the present work, besides the size factor and the number of valence electrons, the total number of electron shells was also considered as an influencing factor affecting the atomic order of the sigma phase. Furthermore, we dissociated the effect of individual influencing factor on atomic order. To facilitate explanation, all the binary sigma phases investigated were designated as A-B binary system where atom A always bears a larger size than atom B. The sizes of the constituent elements (A and B) are determined by the molar volumes of their pure elements in the sigma phase structure from the CALPHAD assessments as will be presented in Section 5. Besides, the site occupancy of atom A is given in the present work. Atom B complements atom A on each sites. We use $Y_S(A)$ to denote the site occupancy of atom A on site S. The site occupancy of atom B on site S is equal to 1- $Y_S(A)$. The sequence of atomic order of atom A was given in the present work. For example, the sequence of atomic order, $4f_{(A)} > 8i_{1(A)} > 8j_{(A)} > 8i_{2(A)} > 2a_{(A)}$, denotes a descending site occupancy preference of atom A from the site 4f to 2a. The sequence of atomic order of atom B is opposite.

3.2. Methodology and calculation details

3.2.1. First-principles calculations

First-principles calculations were performed using the plane wave method with projector augmented wave (PAW) pseudo-potentials [25], as implemented in the Vienna ab initio simulation package (VASP) [26]. We used the exchange-correlation functional within the generalized gradient approximation (GGA) as parameterized by Perdew and Wang (i.e. GGA-PW91) [108]. The magnetic parameter for ferromagnetism was set and spin-polarized calculations were conducted. The structure was fully relaxed and after the relaxation, a final static calculation was performed by adopting tetrahedron method with Blöchl corrections. A large plane-wave cutoff energy of 400 eV was used. The k-point meshes (8×8×15) for Brillouin zone sampling were constructed using the Monkhorst–Pack scheme [61]. The convergence criteria for electronic self-consistency and ionic relaxation were 10^{-5} eV/ unit cell and 10^{-4} eV/ unit cell, respectively. These settings ensure that the energy converges to at least 1 meV/ unit cell. To facilitate the calculations, ZenGen script-tool was used to automatically generate input files for VASP calculations [109].

3.2.2. Bader Charge Analysis

The Bader charge analysis code [32] developed by the Henkelman Group was used in this work, which is an efficient and robust algorithm for the Bader decomposition of charge density [67,69,70,110]. The program can read in charge density files from the VASP code and then output the total charge associated with each atom, and the zero flux surfaces defining the Bader volumes [32].

As the Bader analysis assumes that charge density maxima are located at the center of an atom, in the present calculations, the total charge was obtained by summing the core charge and the valence charge from the VASP code and the Bader analysis was done on this total charge density file.

After the calculation, we can obtain the electronic charges and atomic volumes of 30 atoms for each compound. To get the atomic charge for each atom, we use the valence electrons (for which the valence states were set by VASP calculation) minus the calculated electronic charge. The negative value of atomic charge indicates that an atom tends to gain electrons and the positive one indicates that an atom tends to lose electrons.

3.3. Results and discussion

In the present work, besides the size factor and the number of valence electrons (e), we also considered the total number of electron shells (s) to clarify the regularity of the atomic order for the binary sigma phase. We classify the A-B binary sigma phase systems involving transition elements according to the electron configuration of the

constituent elements as presented in Fig. 3.1. The A-Al (A= Nb and Ta) systems, for which the main element Al is concerned, are classified into a separate category. The systems with the measured site occupancies available are as follows:

1) ***SMe*** *(atom A bears smaller number of valence electrons than atom B)*

V-Mn ($3d^3 4s^2$, $3d^5 4s^2$), V-Fe ($3d^3 4s^2$, $3d^6 4s^2$), V-Co ($3d^3 4s^2$, $3d^7 4s^2$), V-Ni ($3d^3 4s^2$, $3d^8 4s^2$), Cr-Mn ($3d^5 4s^1$, $3d^5 4s^2$), Cr-Fe ($3d^5 4s^1$, $3d^6 4s^2$), Cr-Co ($3d^5 4s^1$, $3d^7 4s^2$) W-Re ($5d^4 6s^2$, $5d^5 6s^2$);

2) LAs *(atom A bears larger total number of electron shells than atom B)*

Re-Mn ($5d^5 6s^2$, $3d^5 4s^2$);

3) LAs-LAe *(atom A bears larger total number of electron shells and larger number of valence electrons than atom B)*

Ru-Cr ($4d^7 5s^1$, $3d^5 4s^1$), Re-Cr ($5d^5 6s^2$, $3d^5 4s^1$), Re-V ($5d^5 6s^2$, $3d^3 4s^2$), Os-Cr ($5d^6 6s^2$, $3d^5 4s^1$);

4) LAs-SMe *(atom A bears larger total number of electron shells and smaller number of valence electrons than atom B)*

Mo-Mn ($4d^5 5s^1$, $3d^5 4s^2$), Mo-Fe ($4d^5 5s^1$, $3d^6 4s^2$), Mo-Co ($4d^5 5s^1$, $3d^7 4s^2$), Ta-Rh ($5d^3 6s^2$, $4d^8 5s^1$), Ta-Pd ($5d^3 6s^2$, $4d^{10}$), W-Ru ($5d^4 6s^2$, $4d^7 5s^1$), Re-Fe ($5d^5 6s^2$, $3d^6 4s^2$);

5) SMs-SMe *(atom A bears smaller total number of electron shells and smaller number of valence electrons than atom B)*

Nb-Re ($4d^4 5s^1$, $5d^5 6s^2$), Nb-Os ($4d^4 5s^1$, $5d^6 6s^2$), Nb-Ir ($4d^4 5s^1$, $5d^7 6s^2$), Nb-Pt ($4d^4 5s^1$, $5d^9 6s^1$), Mo-Re ($4d^5 5s^1$, $5d^5 6s^2$), Mo-Os ($4d^5 5s^1$, $5d^6 6s^2$), Mo-Ir ($4d^5 5s^1$, $5d^7 6s^2$);

6) A-Al (A= Nb and Ta)

Nb-Al ($4d^4 5s^1$, $3s^2 3p^1$), Ta-Al ($5d^3 6s^2$, $3s^2 3p^1$).

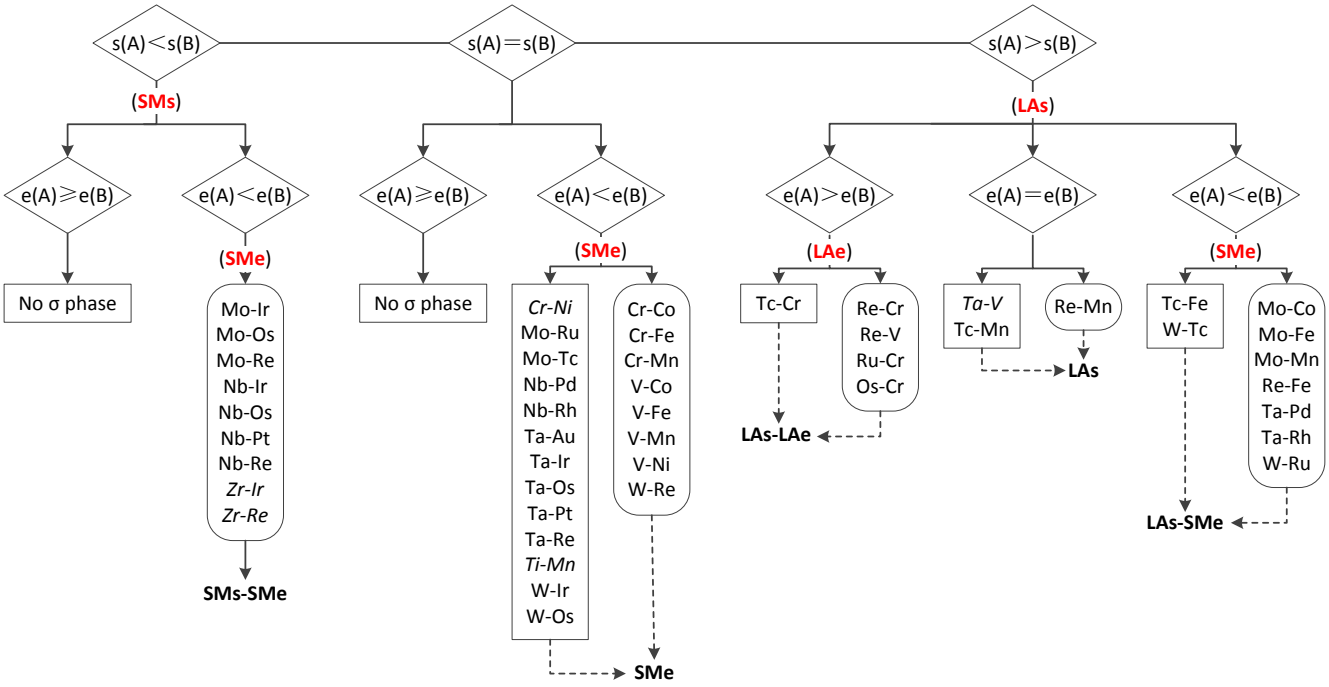

Figure 3.1 : A-B (V(A)>V(B), where V(A) and V(B) are the molar volumes of element A and B, respectively, in their hypothetic sigma phase structure from the CALPHAD assessments as

presented in Section 5) binary sigma systems divided into different categories according to the electron configuration of the constituent elements. The right angled rectangles indicate no existing sigma phase or no available experimental site occupancies for the included systems; the rounded rectangles indicate experimental data for site occupancies are available for the included systems. Note that the existence of the sigma phase in Cr-Ni, Ta-V, Ti-Mn, Zr-Ir and Zr-Re systems is not confirmed and these systems are labelled with italic in the figure. (LAs: Atom A bears larger total number of electron shells than atom B; LAe: Atom A bears larger number of valence electrons than atom B; SMs: Atom A bears smaller total number of electron shells than atom B; SMe: Atom A bears smaller number of valence electrons than atom B.)

3.3.1. Size and electronic factors affecting atomic order

3.3.1.1. Size factor

The size factor has twofold meanings. The first is the size difference among crystal sites. Both CN and nearest neighbor (NN) sites affect the size of sites, which will be discussed in Section 3.3.1.1 (a). The second is the atomic size difference between the constituent elements, which was discussed in Section 3.1. If only the size factor affecting atomic order is considered, it is obvious that among the two constituent elements, the one with a large atomic size preferentially occupies sites with large size.

In the sigma phase structure, for a specific element, the atomic size varies with the change of occupying sites. Normally, the atomic size sequence follows the occupied site size sequence. However, it may not be always true owing to the influences of NN atoms and coordination polyhedron (CP) on atomic volume, which will be discussed in the following 3.3.1.1(b).

In the following discussion, as shown in Fig. 3.2, 3.3, 3.5 and 3.6, the atomic charge indicates the tendency of electron loss or gain. When the value is negative, it means that the atom tends to gain the corresponding number of electrons; when the value is positive, the atom tends to lose the corresponding number of electrons.

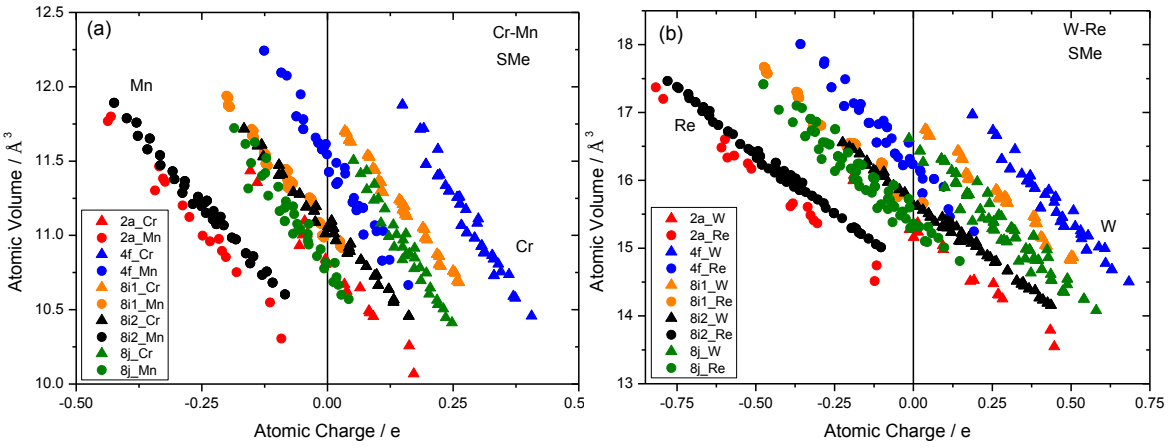

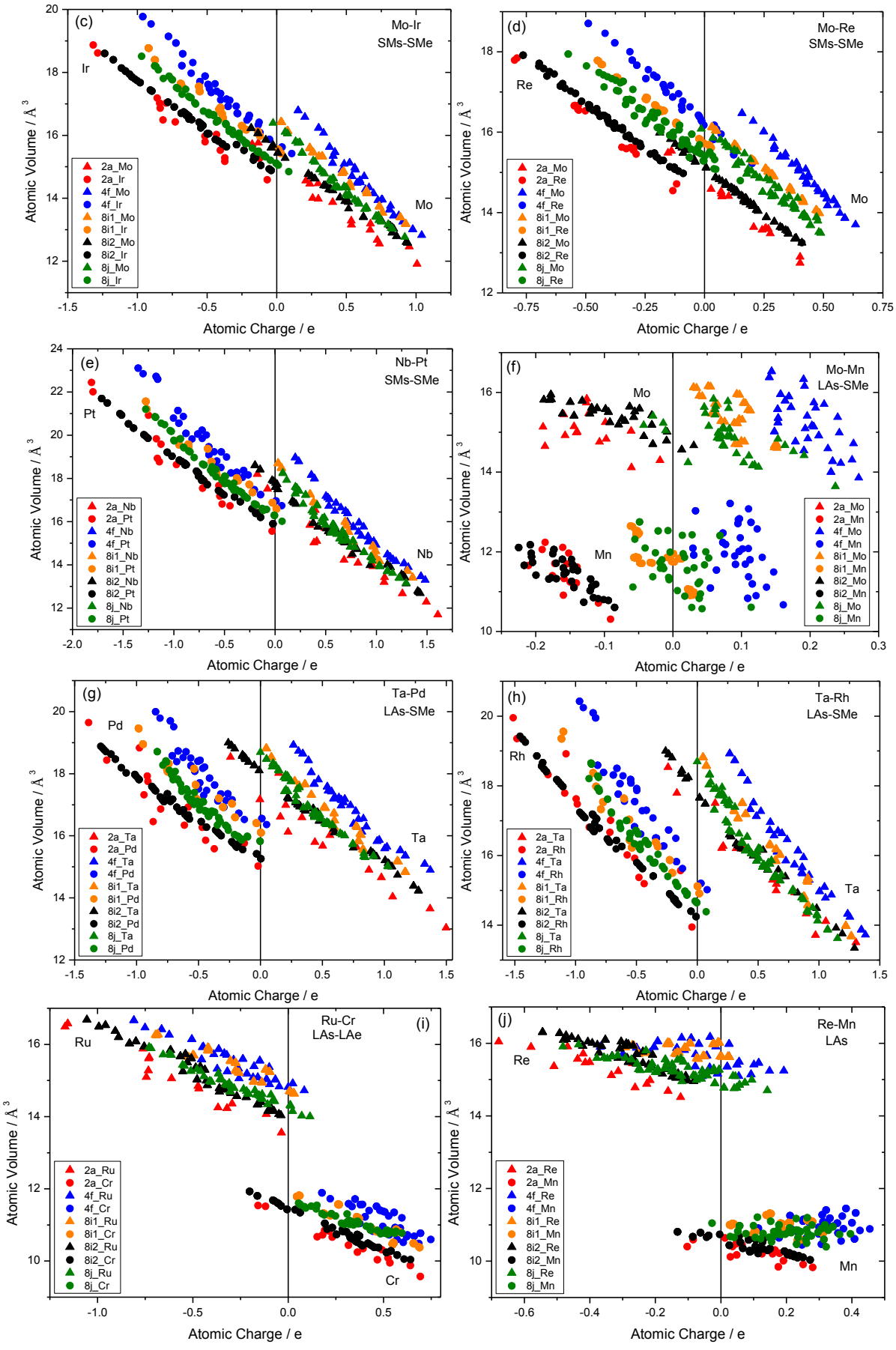
(c)
Mo-Ir
SMs-SMe
Ir
Mo
2a_Mo
2a_Ir
4f_Mo
4f_Ir
8i1_Mo
8i1_Ir
8i2_Mo
8i2_Ir
8j_Mo
8j_Ir
Atomic Volume / Å 3
Atomic Charge / e
(d)
Mo-Re
SMs-SMe
Re
Mo
2a_Mo
2a_Re
4f_Mo
4f_Re
8i1_Mo
8i1_Re
8i2_Mo
8i2_Re
8j_Mo
8j_Re
Atomic Volume / Å 3
Atomic Charge / e
(e)
Nb-Pt
SMs-SMe
Pt
Nb
2a_Nb
2a_Pt
4f_Nb
4f_Pt
8i1_Nb
8i1_Pt
8i2_Nb
8i2_Pt
8j_Nb
8j_Pt
Atomic Volume / Å 3
Atomic Charge / e
(f)
Mo-Mn
LAs-SMe
Mo
Mn
2a_Mo
2a_Mn
4f_Mo
4f_Mn
8i1_Mo
8i1_Mn
8i2_Mo
8i2_Mn
8j_Mo
8j_Mn
Atomic Volume / Å 3
Atomic Charge / e
(g)
Ta-Pd
LAs-SMe
Pd
Ta
2a_Ta
2a_Pd
4f_Ta
4f_Pd
8i1_Ta
8i1_Pd
8i2_Ta
8i2_Pd
8j_Ta
8j_Pd
Atomic Volume / Å 3
Atomic Charge / e
(h)
Ta-Rh
LAs-SMe
Rh
Ta
2a_Ta
2a_Rh
4f_Ta
4f_Rh
8i1_Ta
8i1_Rh
8i2_Ta
8i2_Rh
8j_Ta
8j_Rh
Atomic Volume / Å 3
Atomic Charge / e
(i)
Ru-Cr
LAs-LAe
Ru
Cr
2a_Ru
2a_Cr
4f_Ru
4f_Cr
8i1_Ru
8i1_Cr
8i2_Ru
8i2_Cr
8j_Ru
8j_Cr
Atomic Volume / Å 3
Atomic Charge / e
(j)
Re-Mn
LAs
Re
Mn
2a_Re
2a_Mn
4f_Re
4f_Mn
8i1_Re
8i1_Mn
8i2_Re
8i2_Mn
8j_Re
8j_Mn
Atomic Volume / Å 3
Atomic Charge / e

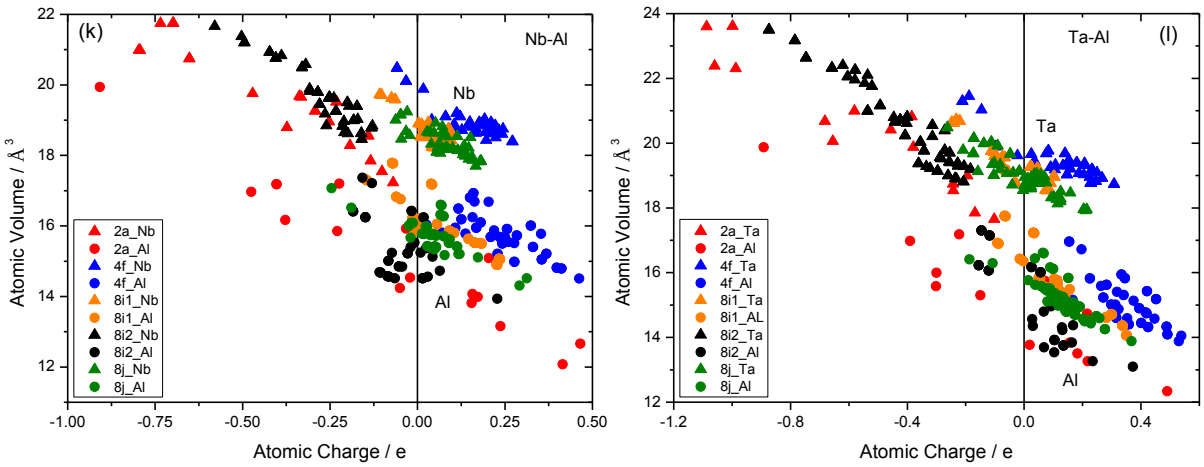

Figure 3.2 : Atomic volume with respect to atomic charge of the constituent elements in 32 (2^5=32) stoichiometric sigma end-member compounds ($Mo_2Mo_4Mo_8Mo_8Mo_8$, $Re_2Mo_4Mo_8Mo_8Mo_8$ etc.) for binary systems calculated using VASP and Bader's AIM approach. (Every figure contains the results of 32 stoichiometric sigma end-member compounds for a specific system and every compound contains 30 atoms. Thus, every figure contains 30×32 points but some of them are overlapped).

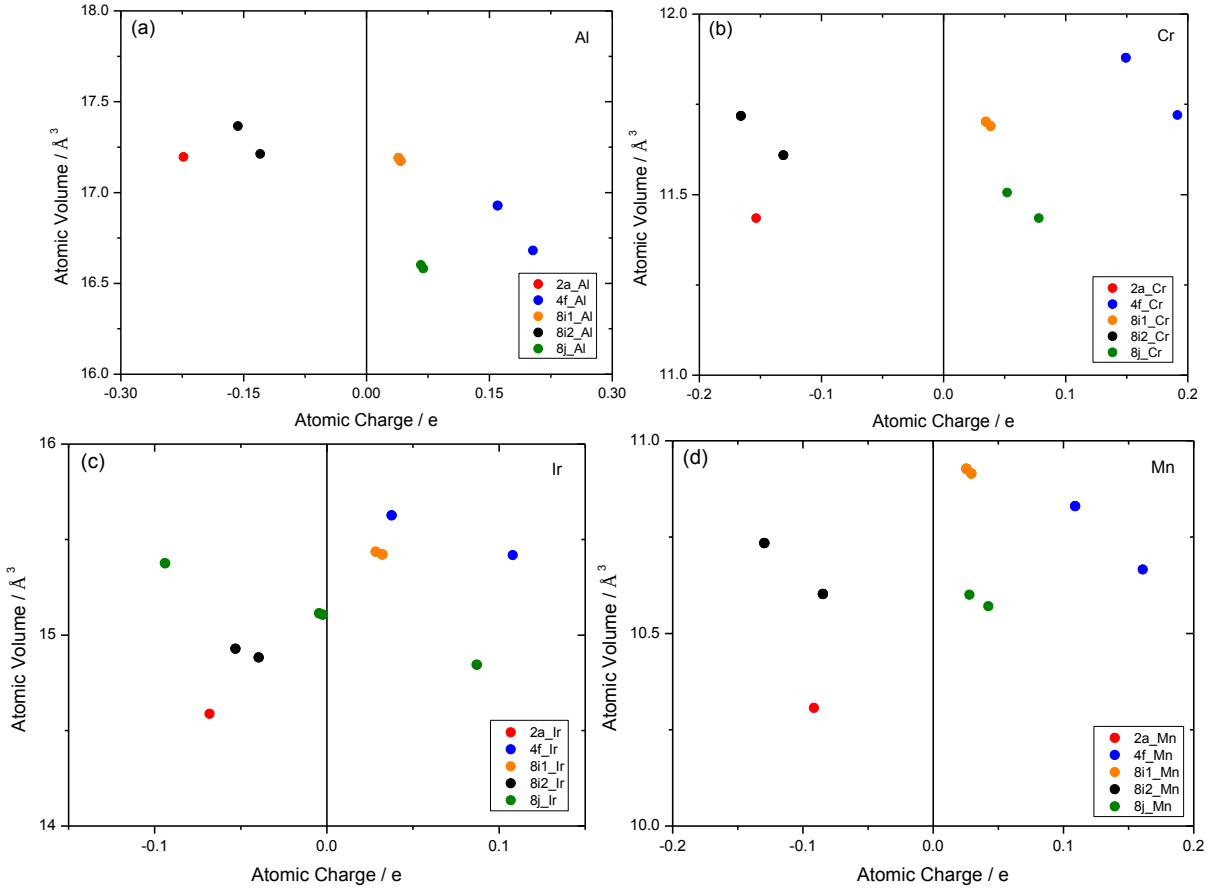

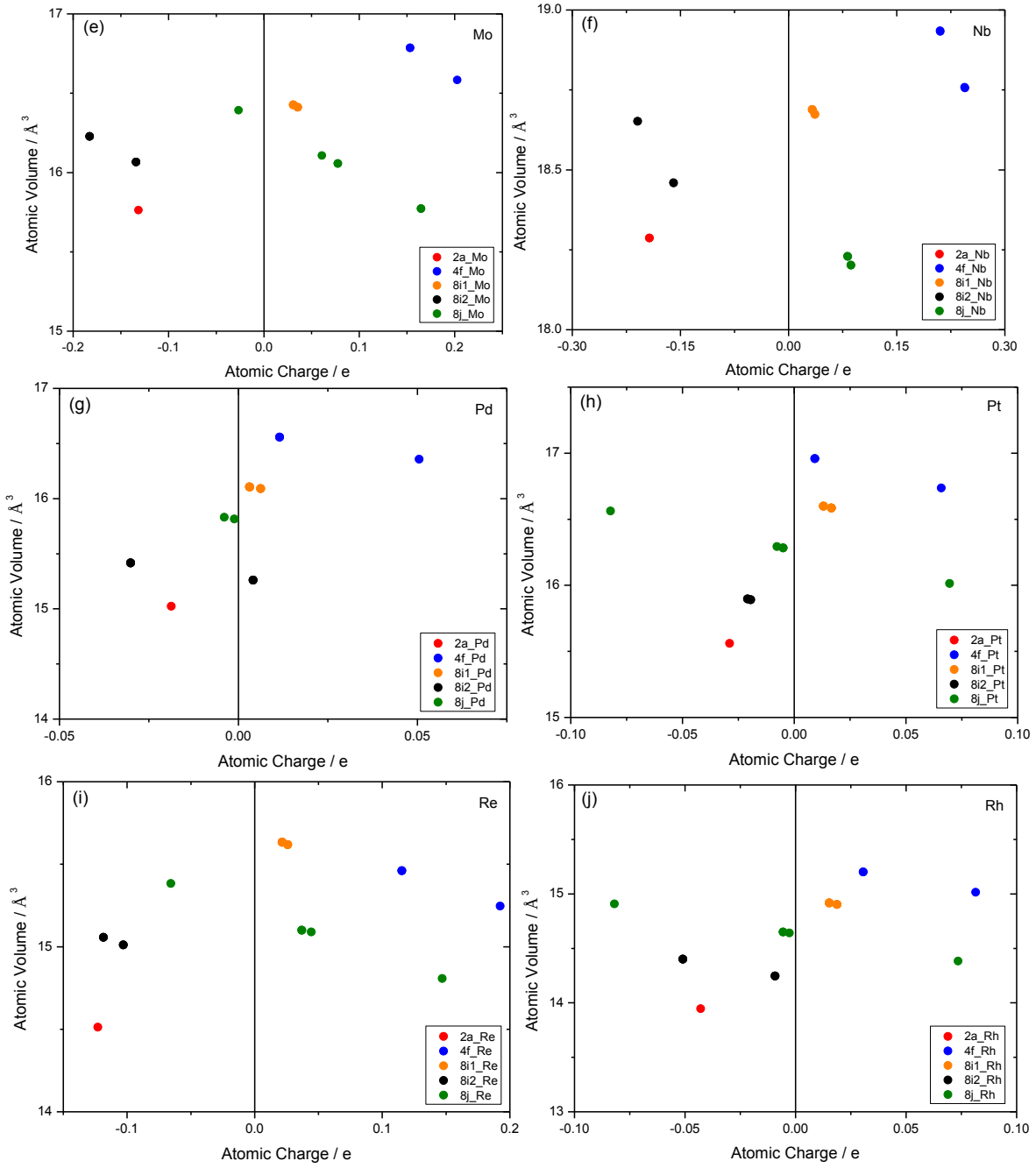
(e)
Mo
2a_Mo
4f_Mo
8i1_Mo
8i2_Mo
8j_Mo
Atomic Volume / Å^3
Atomic Charge / e
(f)
Nb
2a_Nb
4f_Nb
8i1_Nb
8i2_Nb
8j_Nb
Atomic Volume / Å^3
Atomic Charge / e
(g)
Pd
2a_Pd
4f_Pd
8i1_Pd
8i2_Pd
8j_Pd
Atomic Volume / Å^3
Atomic Charge / e
(h)
Pt
2a_Pt
4f_Pt
8i1_Pt
8i2_Pt
8j_Pt
Atomic Volume / Å^3
Atomic Charge / e
(i)
Re
2a_Re
4f_Re
8i1_Re
8i2_Re
8j_Re
Atomic Volume / Å^3
Atomic Charge / e
(j)
Rh
2a_Rh
4f_Rh
8i1_Rh
8i2_Rh
8j_Rh
Atomic Volume / Å^3
Atomic Charge / e

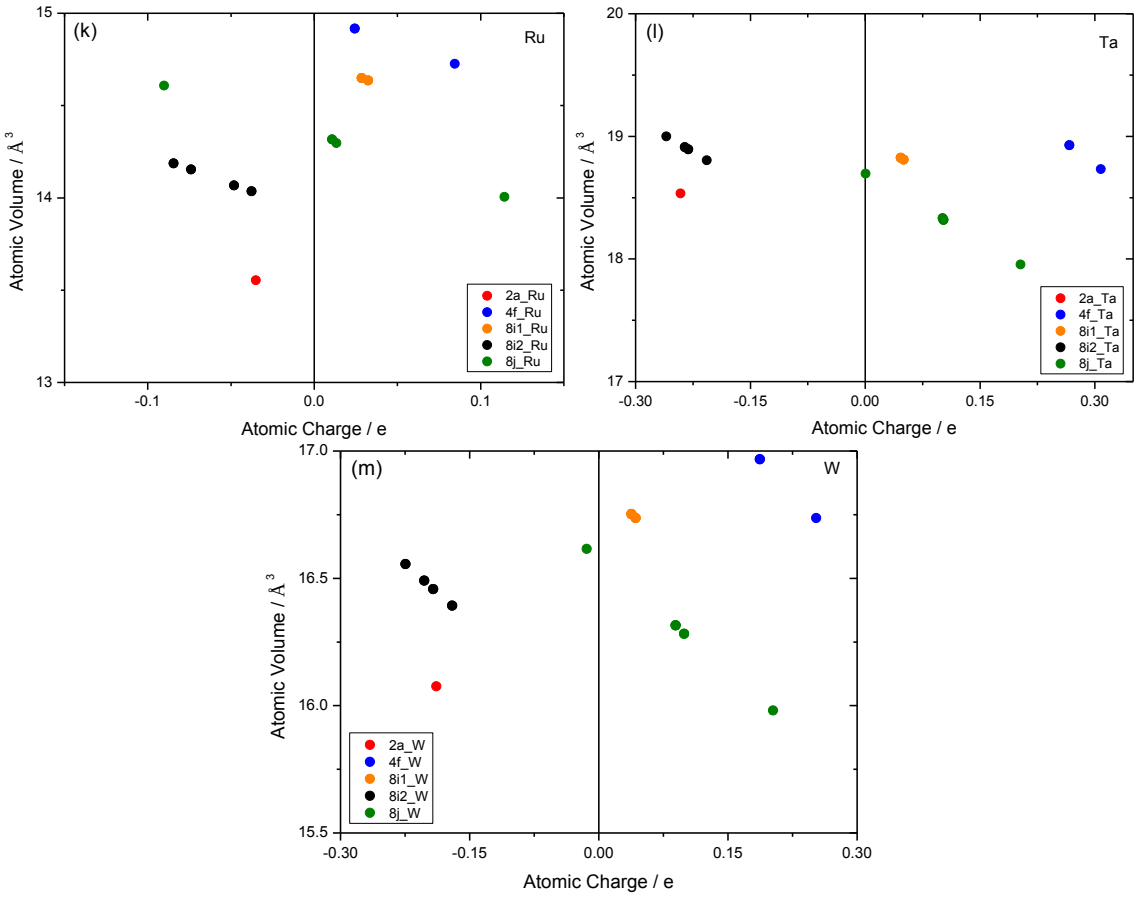

Figure 3.3 : Atomic volume with respect to atomic charge of the pure elements in the hypothetic sigma phase structure calculated using VASP and Bader's AIM approach. Every figure contains 30 points but some of them are overlapped.

a) Size difference among the five nonequivalent sites

To clarify the size difference among the five nonequivalent sites of the sigma phase, we calculated the atomic volume and the corresponding atomic charge of the two constituent elements in the complete set (2^5=32) of ordered configurations (i.e. the stoichiometric end-member compounds in the following discussions) of the sigma phase for different binary systems. Fig. 3.2 presents the atomic volume with respect to the atomic charge of the constituent elements in the 32 stoichiometric end-member compounds for 12 typical sigma phase systems. For systems in SMe, SMs-SMe categories and some systems (i.e. Ta-Pd and Ta-Rh systems) in LAs-SMe category, a nearly linear relationship can be observed between atomic volume and atomic charge for a specific element on a specific site and the linear slopes for different sites are very close to each other; for systems in LAs, LAs-LAe, A-Al (A= Nb and Ta) categories and a system (i.e. Mo-Mn system) in LAs-SMe category, no evident linear relationship can be observed as the atomic volume difference for a specific element on a specific site can be very large, even when the atomic charge is constant. The large difference is due to the influence of NN atoms and coordination polyhedron (CP), which will be discussed in Section 3.3.1.1 (b).

Fig. 3.3 shows the atomic volume versus atomic charge of the pure elements in the hypothetic sigma structure. In this respect, we can observe the size difference among the five nonequivalent sites without the effect of unlike NN atoms. If we consider the linear relationship between atomic volume and atomic charge as observed in Fig. 3.2, and extrapolate this evolution to a specific atomic charge (e.g. the vertical line in Fig. 3.3), we can obtain the corresponding atomic volumes for all five sites. Then we can propose from Fig. 3.3 that the site size sequence follows: $4f_{(CN15)} > 8i_{1(CN14)} > 8j_{(CN14)} > 8i_{2(CN12)} > 2a_{(CN12)}$. This result agrees with the weighted average of the interatomic distances reported for Cr-Fe sigma by Hall and Algie [8], i.e. 2.701 Å (4f) > 2.652 Å ($8i_1$) > 2.638 Å (8j) > 2.526 Å ($8i_2$) > 2.508 Å (2a).

The above results agree with the analysis by considering crystal structure. Firstly, sites with large CN (i.e. CN=14 or 15) are expected to bear a large size, as with more surrounding atoms the space of a site is larger. Thus the size difference among different CN sites are expected to be $4f_{(CN15)} > 8i_{1(CN14)}/8j_{(CN14)} > 8i_{2(CN12)}/2a_{(CN12)}$. Secondly, regarding the sites with the same CN, namely CN14 (i.e. $8i_1$ and 8j) and CN12 (i.e. $8i_2$ and 2a), we should consider the effect of the NN sites. The size of the site is expected to be larger when the surrounding small CN sites (i.e. CN=12) are fewer, which implies that the surrounding large CN sites are more. Fig. 3.4 and Table 3.1 show the number of the NN sites for the five nonequivalent sites of the sigma phase. The $8i_1$ site is surrounded by 4 CN12 sites and the 8j site is surrounded by 5 CN12 sites, so the size of the $8i_1$ site is expected to be larger than that of the 8j site. The $8i_2$ site is surrounded by 2 CN12 sites and the 2a site is surrounded by 4 CN12 sites, so the size of the $8i_2$ site is expected to be larger than that of the 2a site. The above analysis is well consistent with the calculation results based on Fig. 3.2 and 3.3, i.e. the site size sequence follows $4f_{(CN15)} > 8i_{1(CN14)} > 8j_{(CN14)} > 8i_{2(CN12)} > 2a_{(CN12)}$.

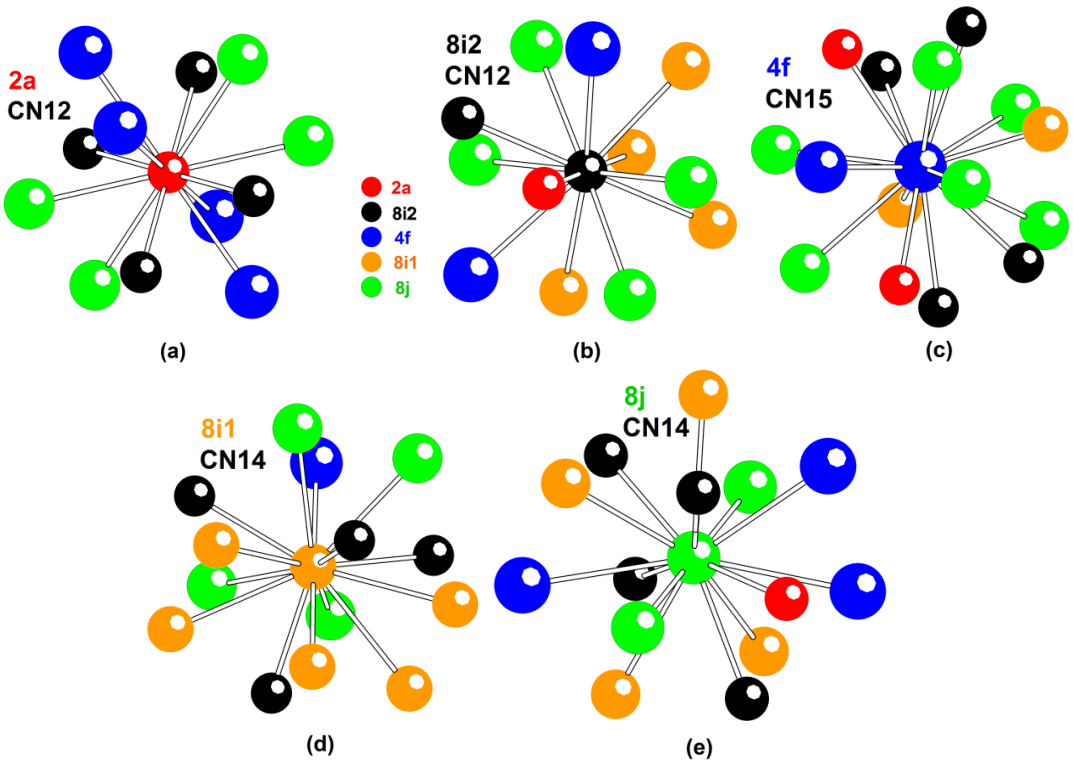

Figure 3.4 : Coordination polyhedron around five nonequivalent sites of the sigma phase structure. Atoms occupying different Wyckoff positions, namely 2a, 4f, $8i_1$, $8i_2$ and 8j, are indicated by different fillings.

Table 3.1 : Number of nearest neighbor (NN) sites for the five nonequivalent sites of the sigma phase.

Site	NN sites					Total
	2a	4f	8i$_1$	8i$_2$	8j	
2a	-	4	-	**4**	4	12
4f	**2**	1	2	**4**	6	15
$8i_1$	-	1	5	**4**	4	14
$8i_2$	**1**	2	4	**1**	4	12
8j	**1**	3	4	**4**	2	14

b) Influence of nearest neighbor atoms and coordination polyhedron on atomic volume

For a specific atom in the sigma phase structure, two factors determine its atomic volume. The first one is its occupying crystal site (i.e. one among 2a, 4f, $8i_1$, $8i_2$ and 8j) and the corresponding CP symmetry. The second concerns the NN atoms around the atom. The effect of the next NN atoms is assumed small that can be neglected.

1) Influence of nearest neighbor (NN) atoms on atomic volume

The NN atoms mainly affect the atomic charge and the space to accommodate the specific atom, and thus affect its atomic volume. In the following, we respectively discussed how the atomic charge and the accommodation space affect the atomic volume of the sigma phase.

Atomic charge

Fig. 3.2 shows the calculated atomic volume with respect to atomic charge of the constituent elements in the complete set (2^5=32) of ordered configurations of the A-B (V(A) ＞V(B)) binary sigma phase. It indicates that for systems belonging to SMe, SMs-SMe and some systems (e.g. Ta-Pd and Ta-Rh systems) belonging to LAs-SMe categories, the atomic size and site size follow the same sequence. It can be obviously seen that for a specific element, on a specific site, atoms with more negative atomic charge bear a larger volume.

For systems belonging to LAs, LAs-LAe, A-Al (A=Nb, Ta) and some systems (e.g. Mo-Mn system) belonging to LAs-SMe categories, for the same or a small variation of the atomic charge, the atomic volume difference for a specific element on a specific site can be very large. This is due to the fact that for these systems, the atomic volume is more sensitive to the accommodation space. For LAs, LAs-LAe, A-Al (A-Nb, Ta) categories and some systems in LAs-SMe category, large atom A tend to gain electrons and the atomic size further increases; small atom B tend to lose electrons and the atomic size further decreases as indicated in Fig. 3.2. Thus the size difference between the two constituent elements becomes very large, which makes the factor of accommodation space crucial.

Accommodation space

As mentioned in the last section, for LAs, LAs-LAe categories, the atomic volume is more sensitive to accommodation space. Thus we selected Re-Mn and Ru-Cr systems, and analyzed the atomic volume among the 32 stoichiometric end-member compounds, compound-by-compound. Fig. 3.5 and Fig. 3.6 show the atomic volume with respect to atomic charge of the constituent elements in several stoichiometric sigma end-member compounds for Re-Mn and Ru-Cr system, respectively. Table 3.2 shows the number of NN atom A around the $8i_1$, 8j and $8i_2$ sites of the corresponding compounds in Fig. 3.5 and Fig. 3.6, which can be conveniently achieved from Fig. 3.4 and Table 3.1. It was found that when large atom A (V(A)>V(B)) occupy $8i_1$ and 8j sites, and in the meanwhile the number of the NN atom A surrounding 8j site is large enough as indicated in Table 3.2, the atomic sizes of B on $8i_1$ and 8j follows 8j＞ $8i_1$ (normally the atomic size sequence for a specific element follows the occupied site size sequence, i.e. $8i_{1(CN14)}$＞$8j_{(CN14)}$ [111]) as seen in Fig. 3.5 (e-h) and Fig. 3.6 (e-h). Hence we can conclude that the more the NN large atoms, the larger the space to accommodate the specific atom.

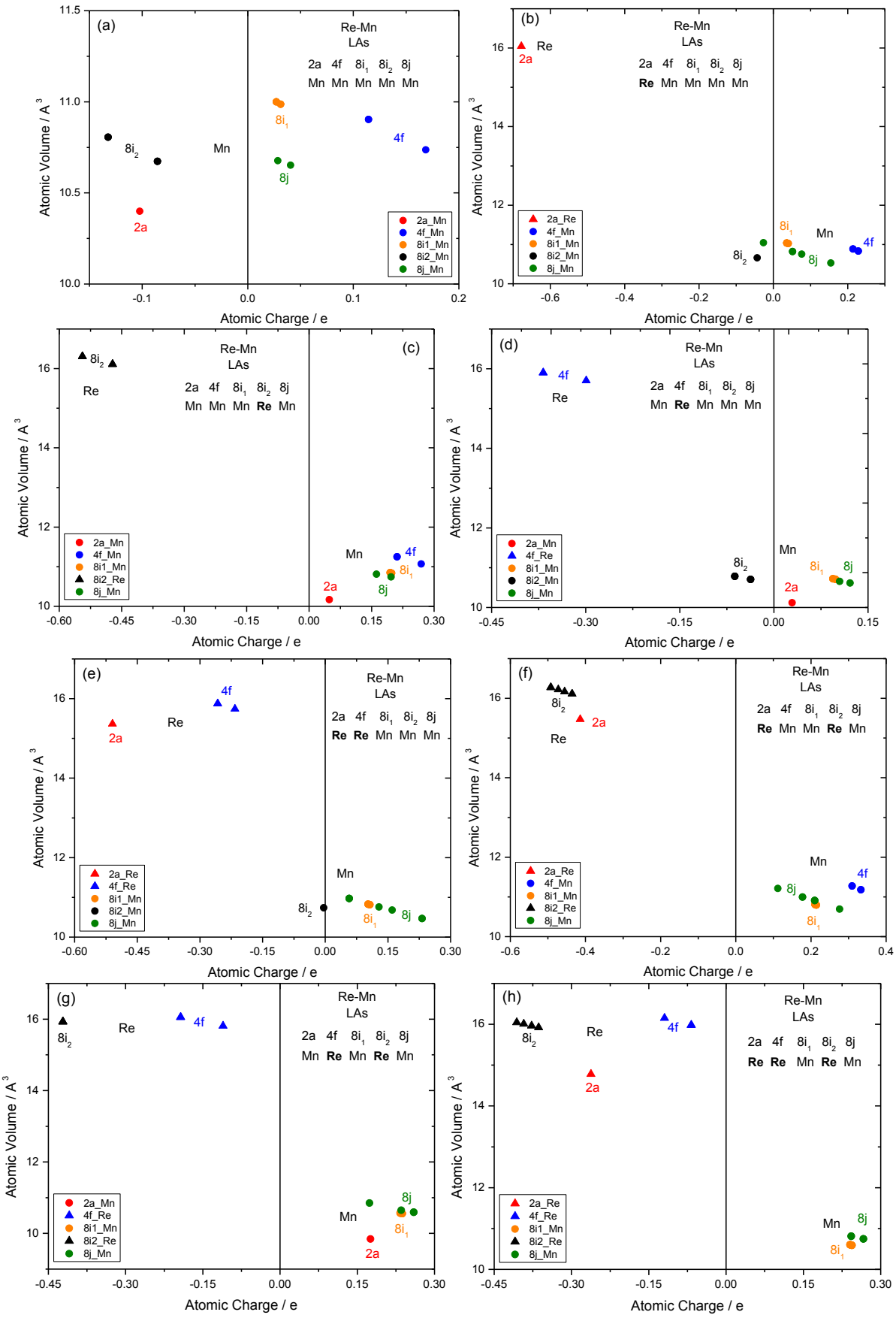
(a)
Re-Mn
LAs
2a 4f 8i1 8i2 8j
Mn Mn Mn Mn Mn
2a_Mn
4f_Mn
8i1_Mn
8i2_Mn
8j_Mn
(b)
Re-Mn
LAs
2a 4f 8i1 8i2 8j
Re Mn Mn Mn Mn
2a_Re
4f_Mn
8i1_Mn
8i2_Mn
8j_Mn
(c)
Re-Mn
LAs
2a 4f 8i1 8i2 8j
Mn Mn Mn Re Mn
2a_Mn
4f_Mn
8i1_Mn
8i2_Re
8j_Mn
(d)
Re-Mn
LAs
2a 4f 8i1 8i2 8j
Mn Re Mn Mn Mn
2a_Mn
4f_Re
8i1_Mn
8i2_Mn
8j_Mn
(e)
Re-Mn
LAs
2a 4f 8i1 8i2 8j
Re Re Mn Mn Mn
2a_Re
4f_Re
8i1_Mn
8i2_Mn
8j_Mn
(f)
Re-Mn
LAs
2a 4f 8i1 8i2 8j
Re Mn Mn Re Mn
2a_Re
4f_Mn
8i1_Mn
8i2_Re
8j_Mn
(g)
Re-Mn
LAs
2a 4f 8i1 8i2 8j
Mn Re Mn Re Mn
2a_Mn
4f_Re
8i1_Mn
8i2_Re
8j_Mn
(h)
Re-Mn
LAs
2a 4f 8i1 8i2 8j
Re Re Mn Re Mn
2a_Re
4f_Re
8i1_Mn
8i2_Re
8j_Mn
Atomic Volume / A3
Atomic Charge / e

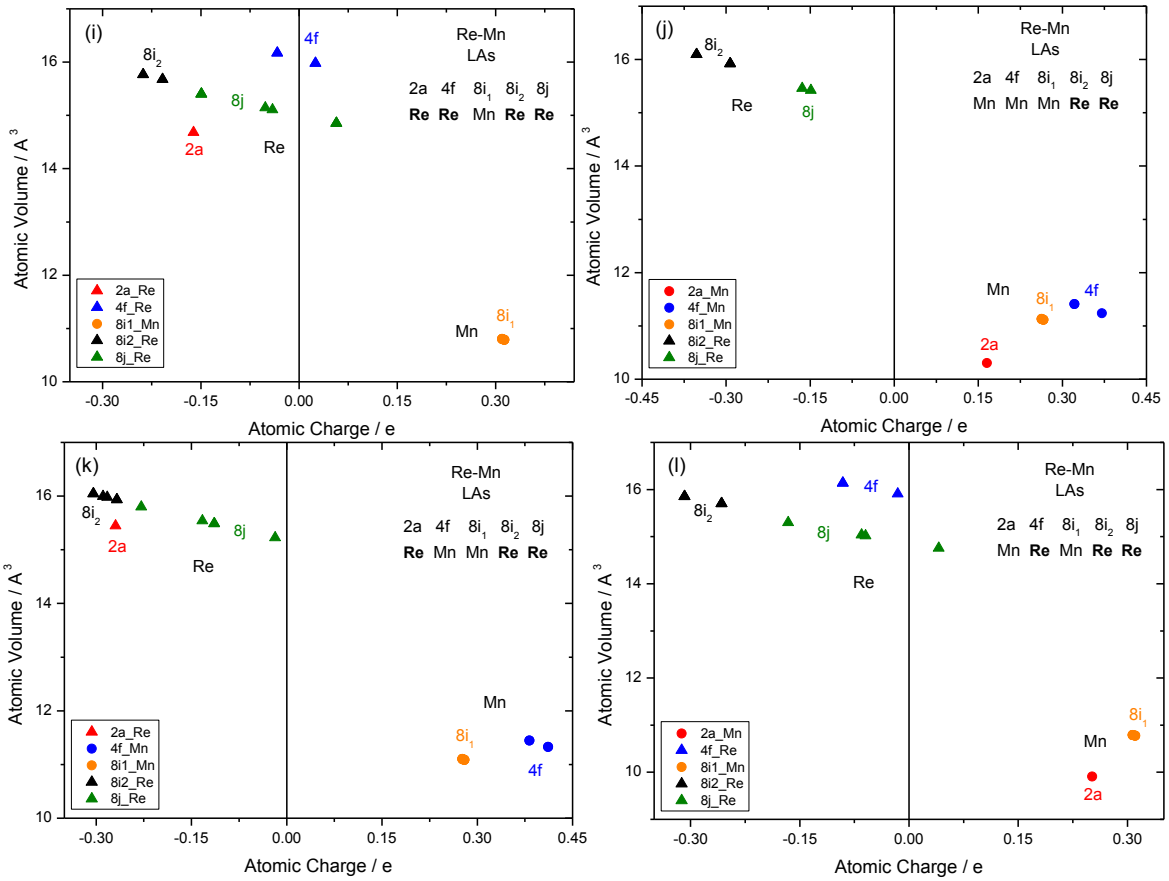

Fig. 3.5. Atomic volume with respect to atomic charge of the constituent elements in stoichiometric sigma end-member compounds for Re-Mn system calculated using VASP and Bader's AIM approach. (a-h): $X_2X_4Mn_8X_8Mn_8$; (i-l) $X_2X_4Mn_8Re_8Re_8$ (X=Re or Mn). Every figure contains 30 points but some of them are overlapped.

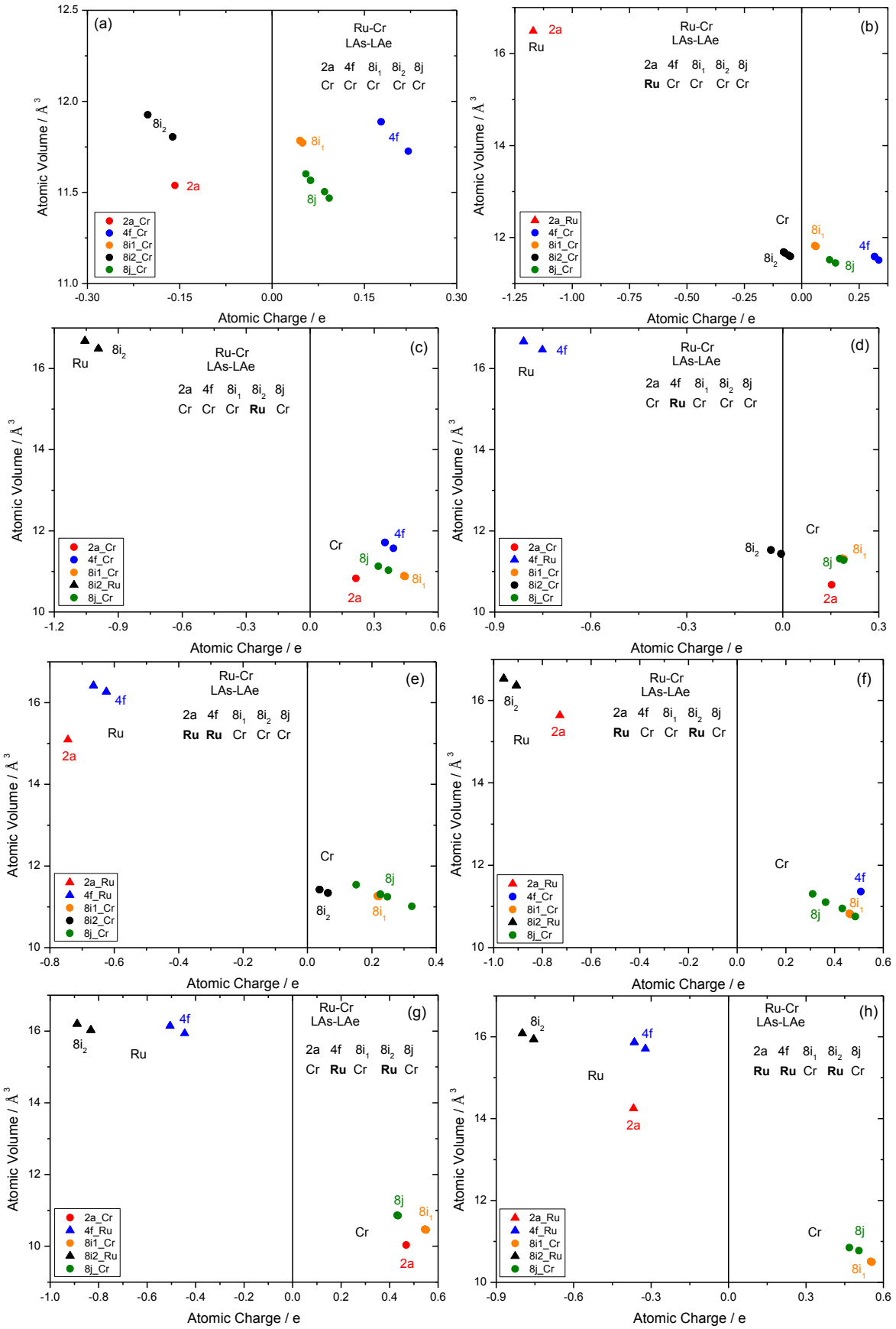
(a)
Ru-Cr
LAs-LAe
2a 4f 8i1 8i2 8j
Cr Cr Cr Cr Cr
2a_Cr
4f_Cr
8i1_Cr
8i2_Cr
8j_Cr
Atomic Volume / Å3
Atomic Charge / e
(b)
Ru-Cr
LAs-LAe
2a 4f 8i1 8i2 8j
Ru Cr Cr Cr Cr
2a_Ru
4f_Cr
8i1_Cr
8i2_Cr
8j_Cr
(c)
Ru-Cr
LAs-LAe
2a 4f 8i1 8i2 8j
Cr Cr Cr Ru Cr
2a_Cr
4f_Cr
8i1_Cr
8i2_Ru
8j_Cr
(d)
Ru-Cr
LAs-LAe
2a 4f 8i1 8i2 8j
Cr Ru Cr Cr Cr
2a_Cr
4f_Ru
8i1_Cr
8i2_Cr
8j_Cr
(e)
Ru-Cr
LAs-LAe
2a 4f 8i1 8i2 8j
Ru Ru Cr Cr Cr
2a_Ru
4f_Ru
8i1_Cr
8i2_Cr
8j_Cr
(f)
Ru-Cr
LAs-LAe
2a 4f 8i1 8i2 8j
Ru Cr Cr Ru Cr
2a_Ru
4f_Cr
8i1_Cr
8i2_Ru
8j_Cr
(g)
Ru-Cr
LAs-LAe
2a 4f 8i1 8i2 8j
Cr Ru Cr Ru Cr
2a_Cr
4f_Ru
8i1_Cr
8i2_Ru
8j_Cr
(h)
Ru-Cr
LAs-LAe
2a 4f 8i1 8i2 8j
Ru Ru Cr Ru Cr
2a_Ru
4f_Ru
8i1_Cr
8i2_Ru
8j_Cr

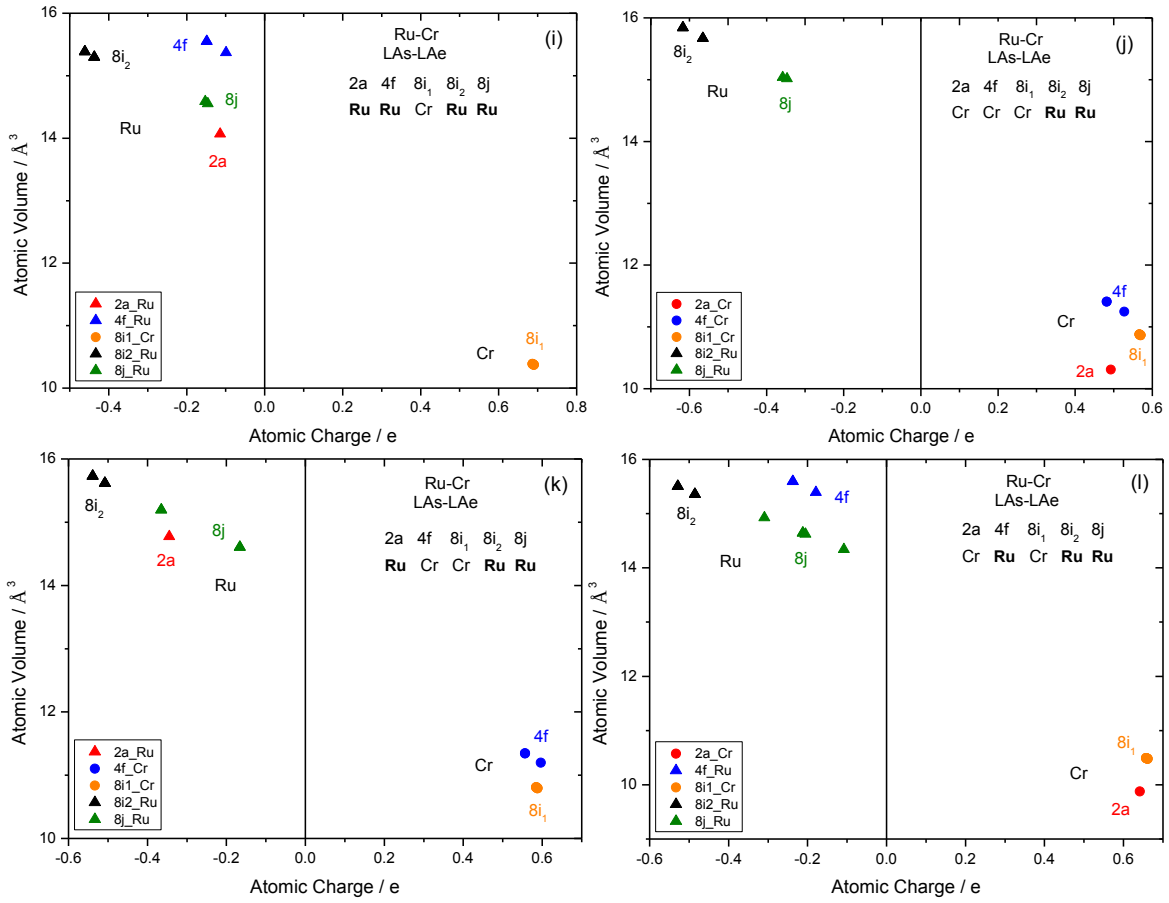

Fig. 3.6. Atomic volume with respect to atomic charge of the constituent elements in stoichiometric sigma end-member compounds for Ru-Cr system calculated using VASP and Bader's AIM approach. (a-h): $X_2X_4Cr_8X_8Cr_8$; (i-l) $X_2X_4Cr_8Ru_8Ru_8$ (X=Ru or Cr). Every figure contains 30 points but some of them are overlapped.

Table 3.2 : Number of nearest neighbor (NN) atom A around the $8i_1$, 8j and $8i_2$ sites of the corresponding A-B (V(A)>V(B)) binary sigma compounds in Fig. 3.5 and Fig. 3.6.

Site	2a	4f	$8i_1$	$8i_2$	8j	NN atom A around the site		
						$8i_1$(CN14)	8j(CN14)	$8i_2$(CN12)
(a)	B	B	B	B	B	0	0	
(b)	A	B	B	B	B	0	1	
(c)	B	B	B	A	B	4	4	
(d)	B	A	B	B	B	1	3	
(e)	A	A	B	B	B	1	4	
(f)	A	B	B	A	B	4	5	
(g)	B	A	B	A	B	5	7	
(h)	A	A	B	A	B	5	8	

(i)	A	A	B	A	A	10	8
(j)	B	B	B	A	A	6	5
(k)	A	B	B	A	A	7	6
(l)	B	A	B	A	A	9	7

Some interesting phenomena found in Fig. 3.2 can also be explained by considering the effect of the NN atoms on accommodation space, which further validate our arguments. Fig. 3.7 (a-f) shows the calculated atomic volume with respect to the atomic charge of W and Re in 6 stoichiometric sigma end-member compounds for W-Re system. By replacing site by site W atom by Re atom, one obtains 6 compounds in succession going from pure W sigma to pure Re sigma. By following the path W→2a→4f→$8i_1$→$8i_2$→8j→Re, the atomic charge changes in a way that i) the pure sigma compounds show a smaller range of atomic charge around zero in comparison with binary ones; ii) when the content of Re increases, in general the atomic charge of both W and Re increases. As a corollary for a specific atom with larger atomic charge, with regard to the corresponding compound the atom belongs to, the content of atom Re (which tends to gain electrons as compared to atom W) must be higher. The above conclusions are universal and valid for all the binary sigma systems.

With the above argument based on W-Re system, we can explain the following phenomenon presented in Fig. 3.2 (a-e): for SMe and SMs-SMe category, when the atomic charge increases, the size difference of atoms occupying different CN sites (CN12, CN14 and CN15) decreases. Notably, as can be seen from Fig. 3.2 that for SMe and SMs-SMe categories, atom B tends to gain electrons. Thus the reason is that when the atomic charge increases, the content of atom B increases, and thus irrespective of the atom, the number of NN atom B (smaller than atom A) increases.

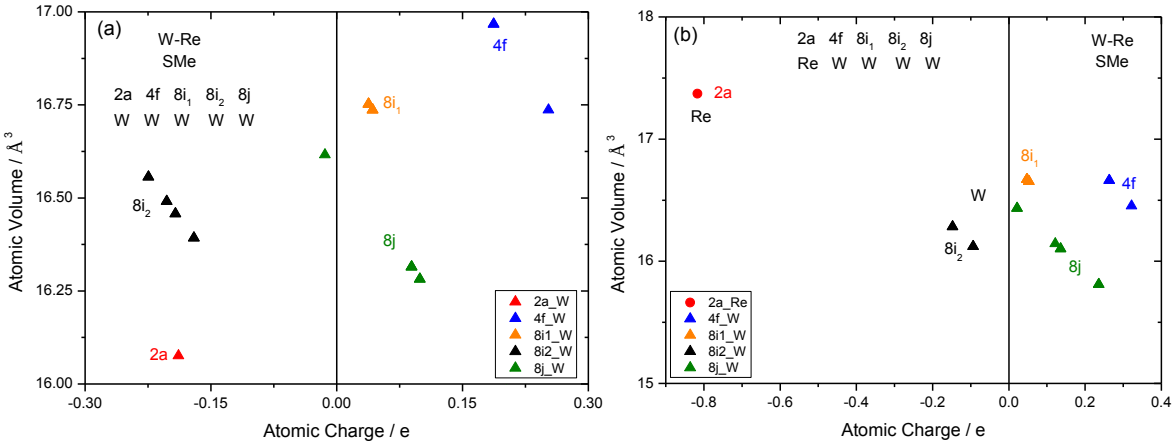

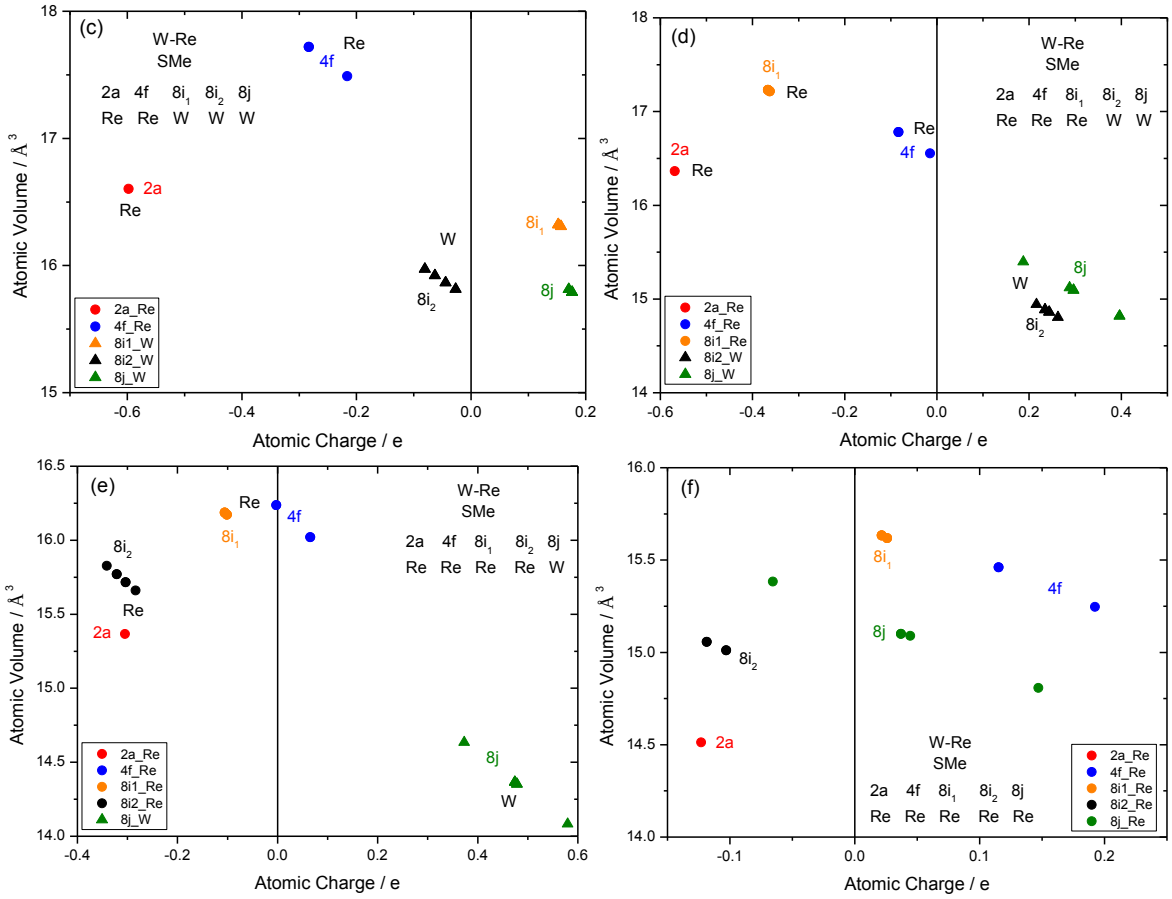

Figure 3.7 : Atomic volume with respect to atomic charge of the constituent elements in stoichiometric sigma end-member compounds for W-Re system calculated using VASP and Bader's AIM approach. Every figure contains 30 points but some of them are overlapped.

2) Influence of coordination polyhedron (CP) on atomic volume

The CP mainly affects the space to accommodate a specific atom, and thus affect its atomic volume. According to the above discussion on the influence of NN atoms on accommodation space, it should follow $8j_{(CN14)} > 8i_{2(CN12)}$, as 8j site has larger CN and more large NN atom A as indicated in Table 3.2 (i-l). However, Fig. 3.5 (i-l) and Fig. 3.6 (i-l) show that when the large atom A occupy $8i_2$ and 8j sites, the smaller atom B occupy $8i_1$ site, and 4f and 2a sites are occupied by either A or B, then the atomic sizes of A on $8i_2$ and 8j sites are close (normally it follows $8j_{(CN14)} > 8i_{2(CN12)}$). This is related to the CP symmetry and the location of the NN sites around 8j sites. The symmetry of CN12 sites is higher than that of CN14 sites [112] as can be clearly observed in Fig. 1.2. Besides, when the NN $8i_1$ site around 8j is occupied by small atom B rather than large atom A, the CP symmetry of 8j site further decreases due to the location of $8i_1$ site on the CP as can be referenced to Fig. 1.2 (e).

3.3.1.2. Electronic factors

The influencing factors of the number of valence electrons and the total number of electron shells as well as their general effects on atomic order are clearly clarified in Section 3.3.1.2 (b). It indicates that the electronic factors affect the tendency of electron

loss or gain (or electronegativity) of the constituent elements and thus affect the atomic order. Hence, in Section 3.3.1.2 (a), we generally discuss the electronegativity of constituent elements in the binary sigma phase according to different electronegativity scales as well as our calculation results in Fig. 3.2

a) Electronegativity of constituent elements in the binary sigma phase

Electronegativity scale was firstly proposed by Pauling [14] based on bond energies (A-A, B-B and A-B bond energies) and he defined electronegativity as the power of an atom in a molecule to attract electrons to itself while the electrons are still attached to another atom [15,16]. The higher the value, the stronger the ability of an atom to gain electrons from another one. Since then, many other scales have been proposed [15–22]. In the present work, several typical electronegativity scales, Pauling scale [14,23], Allred-Rochow scale [15] and Allen scale [22], for which values for transition elements are available, were selected to compare the electronegativity of the constituent elements in the sigma phase.

Electronegativity values of the constituent elements in the sigma phase by using Pauling scale [14], Allred-Rochow scale [15] and Allen scale [22] are listed in Table 3.3. Table 3.4 shows the binary sigma phase systems belonging to SMe, SMs-SMe, LAs and LAs-LAe categories.

For SMe and SMs-SMe categories, both Allred-Rochow scale [15] and Allen scale [22] indicate that for all the A-B binary sigma systems, atom A bears smaller electronegativity than atom B. Pauling scale [14] indicates that for systems with no color filled as presented in Table 3.4, atom A bears smaller electronegativity than atom B, while for Cr-Mn, V-Mn, Mo-Tc and Mo-Re systems (filled in blue color as presented in Table 3.4), atom A bears larger electronegativity than atom B, which disagrees with Allred-Rochow scale [15] and Allen scale [22]. However, the atomic charge calculations for both Cr-Mn and Mo-Re systems as presented in Fig. 3.2 (a, d) show that atom A tends to lose electrons and thus bears smaller electronegativity than atom B which agrees with Allred-Rochow scale [15] and Allen scale [22]. Besides, for V-Mn system, Pauling scale [14] indicates that V bears smaller electronegativity than Cr and the atomic charge calculations indicate that Cr bears smaller electronegativity than Mn, thus it can be expected that V bears smaller electronegativity than Mn which agrees with Allred-Rochow scale [15] and Allen scale [22]. For Mo-Tc system, Pauling scale [14] indicates that Re bears smaller electronegativity than Tc and the atomic charge calculations indicate that Mo bears smaller electronegativity than Re, thus it can be expected that Mo bears smaller electronegativity than Tc which agrees with Allred-Rochow scale [15] and Allen scale [22]. Hence, for the binary sigma compounds belonging to SMe and SMs-SMe categories, atom A bears smaller electronegativity than atom B.

On the other hand, for LAs and LAs-LAe categories, Pauling scale [14] indicates that for all the A-B binary sigma systems, except Ta-V system (filled in red color as presented in Table 3.4) which is the system with few information supporting the existence of the sigma phase [113] and was not considered, atom A bears larger electronegativity than atom B. Allred-Rochow scale [15] and Allen scale [22] indicate that for Re-V system, atom A bears

larger electronegativity than atom B, while for Re-Mn, Tc-Mn, Re-Cr, Ru-Cr, Os-Cr and Tc-Cr systems (filled in orange color as presented in Table 3.4), atom A bears smaller electronegativity than atom B, which disagrees with Pauling scale [14]. However, the atomic charge calculations for both Re-Mn and Ru-Cr systems as presented in Fig. 3.2 (i, j) show that atom A tends to gain electrons and thus bears larger electronegativity than atom B which agrees with Pauling scale [14]. Besides, for Re-Cr system, Rochow scale [15] and Allen scale [22] indicate that Cr bears smaller electronegativity than Mn and the atomic charge calculations indicate that Re bears larger electronegativity than Mn, thus it can be expected that Re bears larger electronegativity than Cr which agrees with Pauling scale [14]. For Os-Cr system, Rochow scale [15] and Allen scale [22] indicate that Ru bears smaller electronegativity than Os and the atomic charge calculations indicate that Ru bears larger electronegativity than Cr, thus it can be expected that Os bears larger electronegativity than Cr which agrees with Pauling scale [14]. For Tc-Mn and Tc-Cr systems, there is not enough evidence to confirm the electronegativity difference between the two constituent elements for each system. In general, for the most binary sigma compounds belonging to LAs and LAs-LAe categories, atom A bears larger electronegativity than atom B.

In summary, for the binary sigma compounds belonging to SMe and SMs-SMe categories, atom A bears smaller electronegativity than atom B; for the binary sigma compounds belonging to LAs and LAs-LAe categories, atom A bears larger electronegativity than atom B. Only for Tc-Mn and Tc-Cr systems (belonging to LAs and LAs-LAe categories respectively), more evidence is needed to confirm the electronegativity difference between the two constituent elements for each system.

Table 3.3 : Electronegativity values of the constituent elements in the sigma phase by using Pauling scale [14], Allred-Rochow scale [15] and Allen scale [22].

							Al
							1.61
							1.47
							1.613
Ti	**V**	**Cr**	**Mn**	**Fe**	**Co**	**Ni**	
1.54	1.63	1.66	1.55	1.83	1.88	1.91	
1.32	1.45	1.56	1.6	1.64	1.7	1.75	
1.38	1.53	1.65	1.75	1.8	1.84	1.88	
Zr	**Nb**	**Mo**	**Tc**	**Ru**	**Rh**	**Pd**	
1.33	1.6	2.16	2.1	2.2	2.28	2.2	
1.22	1.23	1.3	1.36	1.42	1.45	1.35	
1.32	1.41	1.47	1.51	1.54	1.56	1.59	
	Ta	**W**	**Re**	**Os**	**Ir**	**Pt**	**Au**
	1.5	1.7	1.9	2.2	2.2	2.2	2.4
	1.33	1.4	1.46	1.52	1.55	1.44	1.42
	1.34	1.47	1.6	1.65	1.68	1.72	1.92

Pauling electronegativity values

Allred-Rochow electronegativity values

Allen electronegativity values

Table 3.4 : Binary sigma phase systems belonging to SMe, SMs-SMe, LAs and LAs-LAe categories with filling colors to facilitate explanation. Since the existence of the sigma phase in Cr-Ni, Ta-V, Ti-Mn, Zr-Ir and Zr-Re systems is not confirmed, these systems are labelled in italic; when atomic charge calculations have been performed in the present work, the systems are labelled in bold.

SMe	Cr-Co	Cr-Fe	**Cr-Mn**	V-Co	V-Fe	V-Mn	V-Ni	**W-Re**	
	Cr-Ni	Mo-Ru	Mo-Tc	Nb-Pd	Nb-Rh	Ta-Au	Ta-Ir	Ta-Os	
	Ta-Pt	Ta-Re	*Ti-Mn*	W-Ir	W-Os				
SMs-SMe	Mo-Ir	Mo-Os	**Mo-Re**	Nb-Ir	Nb-Os	**Nb-Pt**	Nb-Re	*Zr-Ir*	*Zr-Re*
LAs	**Re-Mn**	*Ta-V*	Tc-Mn						
LAs-LAe	Re-Cr	Re-V	**Ru-Cr**	Os-Cr	Tc-Cr				

b) Electronic factors: valence electrons and electron shells

Fig. 3.2 indicates that between the two constituent elements of the sigma phase, the one with smaller total number of electron shells or smaller number of valence electrons tends to lose electrons; the one with larger total number of electron shells or larger number of valence electrons tends to gain electrons. On the other hand, Fig. 3.3 indicates that generally, atoms on 2a and $8i_2$ sites tend to gain electrons and atoms on 4f, $8i_1$ and 8j sites tend to lose electrons. It is worth mentioning that the atoms on 8j site bear a relatively larger atomic charge range as compared to the atoms on the other sites. In some cases, atoms on 8j site can either gain or lose electrons. Thus in general, between the two constituent elements, the one with smaller total number of electron shells or smaller number of valence electrons prefers occupying large CN sites (4f, $8i_1$ and 8j) and the one with larger total number of electron shells or larger number of valence electrons prefers occupying small CN sites (2a and $8i_2$).

The above argument about the valence electron factor is consistent with the previous investigations [8,9,112] that atoms poor in *d*-electrons preferentially occupy large CN sites (4f, $8i_1$ and 8j) and atoms rich in *d*-electrons preferentially occupy small CN sites (2a and $8i_2$). However, the authors in Ref. 8,9,112 did not consider the effect of the total number of electron shells on atomic order, which makes it unable to well explain the experimental site occupancies. Besides, Berne [112] indicates that CN12 sites show predominance for atoms with filled or nearly filled or else empty d shells. The reason is that the CN12 sites have approximate icosahedral symmetry causing high degeneracy of electronic d-like levels [107,112]. Atoms with half-filled d shells would have high density of states when occupying the CN12 site and thus consequently occupy high CN sites, which allows a better separation of bonding and antibonding d bands [95].

For A-Al (A= Nb and Ta) category shown in Fig. 3.2 (k, l), the characteristics of atomic charge seem a little different, i.e. the tendency of electron loss or gain for the two constituent elements is similar. Hence for this category, the atomic order is mainly determined by the size factor, i.e. large atoms (atom A) occupy large CN sites (4f, $8i_1$ and

8j) and small atoms (atom B) occupy small CN sites (2a and $8i_2$). This is consistent with the measured occupancies presented in Section 3.3.2.

A-Al (A= Nb and Ta) systems could be wrongly classified into the LAs-LAe category as Nb and Ta bear both a larger number of valence electrons and larger total number of electron shells than Al. However, the behavior of A-Al category as mentioned above is similar to that of LAs-SMe category. This is consistent with the discovery by Joubert [9], who indicates that Al behaves as if it had 9 or 10 valence electrons in the sigma phase structure. On some level, it is like that the compromise of LAs and SMe factors cause the tendency of electron loss or gain for the two constituent elements to be similar. Actually, as can be seen in Fig. 3.2 (f, k, l), the behavior of A-Al (A= Nb and Ta) systems is similar to that of Mo-Mn system (which belongs to LAs-SMe category).

On the other hand, as discussed in 3.3.1.2 (a), in general, for the binary sigma compounds belonging to SMe and SMs-SMe categories, atom A bears smaller electronegativity than atom B; for the binary sigma compounds belonging to LAs and LAs-LAe categories, atom A bears larger electronegativity than atom B. The above support the deduction based on the calculation in Fig. 3.2 that between the two constituent elements of the sigma phase, the one with smaller total number of electron shells or smaller number of valence electrons tends to lose electrons; the other one tends to gain electrons. As concerned to LAs-SMe category, when electronegativity of the two constituent elements is similar due to the competition of LAs and SMe factors, the tendency of electron loss or gain of the constituent atoms in 32 end-member compounds is mainly determined by the occupied crystal sites, such as Mo-Mn system as shown in Fig. 3.2 (f).

3.3.2. Effects of electronic factors on atomic order

Section 3.3.1.2 indicates that between the two constituent elements, the one with smaller total number of electron shells or smaller number of valence electrons prefers occupying large CN sites (i.e. 4f, $8i_1$ and 8j) and the one with larger total number of electron shells or larger number of valence electrons prefers occupying small CN sites (i.e. 2a and $8i_2$). Thus, SMs and SMe factors affect the sequence of atomic order to be $4f_{(A)}/8i_{1(A)}/8j_{(A)} > 8i_{2(A)}/2a_{(A)}$; LAs and LAe factors affect the sequence of atomic order to be $8i_{2(A)}/2a_{(A)} > 4f_{(A)}/8i_{1(A)}/8j_{(A)}$. To reveal the atomic order among the large CN sites (i.e. 4f, $8i_1$ and 8j) and between the small CN sites (i.e. 2a and $8i_2$) of the sigma phase, we present in Fig. 3.8 the measured site occupancies from the literature category by category for which, only recent data were collected in order to ensure their accuracy. Fig. 3.9 shows the size differences of the constituent elements of the binary sigma phase with respect to their differences both in the number of valence electrons and the total number of electron shells. For a specific system, when the size difference is smaller and in the meantime, the differences in both the number of valence electrons and the total number of electron shells are larger as compared to other systems, the electronic factors affect the atomic order more remarkably.

In this section, we aim in dissociating the effect of individual influencing factor on atomic order based on first-principles calculation results reported in Section 3.3.1 and experimental data obtained from the literature in order to further analyze and explain the atomic order. It is worth mentioning that the discussion in this section is based on the assumption that the atomic order of the binary sigma phase is only influenced by the size factor, the number of valence electrons and the total number of the electron shells of the constituent elements. The experimental site occupancies results from the competition and cooperation of these factors.

3.3.2.1. Effect of the number of valence electrons on atomic order

Fig. 3.8 (a) shows that in most cases for the SMe category, the site occupancies follow $Y_{2a}(A) > Y_{8i2}(A)$ and $Y_{4f(A)} > Y_{8j(A)} > Y_{8i1(A)}$. We showed above in Section 3.3.1.1 that the size sequence of the crystal site is $4f > 8i_1 > 8j > 8i_2 > 2a$. It is thus clear that it is the electronic factor (SMe) that affects the sequence of atomic order to be $2a_{(A)} > 8i_{2(A)}$ and $8j_{(A)} > 8i_{1(A)}$.

Besides, for all the measurements in Fig. 3.8 (a), among the measurements of Cr-Co, Cr-Mn and V-Ni systems, there are experimental data indicating that 4f site is not the most favorable site for atom A, which exhibits $Y_{8i1(A)} > Y_{4f(A)}$ and $Y_{8j(A)} > Y_{4f(A)}$ for Cr-Co system, $Y_{8j(A)} > Y_{4f(A)}$ for Cr-Mn and V-Ni systems. It is expected to be due to the effect of the electronic factor (SMe) since in terms of the size factor, 4f site should be the most favorable one for atom A. It can also be seen from Fig. 3.9 (a) that the electronic factor can be more remarkable for these systems than for the other ones in SMe category, as for Cr-Mn system, the two constituent atoms bear the smallest size difference; for V-Ni system, the two constituent atoms bear the largest difference of valence electrons; Cr-Co system is in between.

Therefore, we can expect that SMe factor affects the atomic order along the sequence $8j_{(A)} > 8i_{1(A)} > 4f_{(A)} > 2a_{(A)} > 8i_{2(A)}$. Vice versa, LAe factor affects the atomic order along the sequence $8i_{2(A)} > 2a_{(A)} > 4f_{(A)} > 8i_{1(A)} > 8j_{(A)}$.

3.3.2.2. Effect of the total number of electron shells on atomic order

For LAs category presented in Fig. 3.8 (b), measured site occupancies for Re-Mn system are available only. The figure shows $Y_{8i2(A)} > Y_{2a(A)}$ and $Y_{8i1(A)} > Y_{8j(A)}$. Moreover, the difference in A occupancies on $8i_2$ and 2a sites, and on $8i_1$ and 8j sites for LAs category, is too large to be explained only with the size factor. It is expected that LAs factor affects the atomic order in the sequence $8i_{2(A)} > 2a_{(A)}$ and $8i_{1(A)} > 8j_{(A)}$; taking into account the discovery in Section 3.3.1.2 as mentioned in the beginning of Section 3.3.2, we can conclude $8i_{2(A)} > 2a_{(A)} > 8i_{1(A)} > 8j_{(A)}$.

On the other hand, both LAs-LAe and LAe categories need to be considered to extrapolate the occupying sequence of 4f site affected by LAs factor, as there is no experimental information available. For LAs-LAe category, Fig. 3.9 (b) indicates that the electronic factors affect the atomic order most remarkably for Re-V system. Fig. 3.8 (d)

shows that for Re-V system, the site occupancies follow $Y_{8i2(A)}>Y_{2a(A)}>Y_{8i1(A)}>Y_{4f(A)}>Y_{8j(A)}$ and the difference in A occupancies on $8i_1$ and 8j sites is dramatically large. Besides, the first-principles calculation results from Crivello et al. [95] also indicate the sequence of site occupancies $Y_{8i1(A)}>Y_{4f(A)}>Y_{8j(A)}$ among large CN sites for Re-V system with high content of Re (see Fig. 9 in Ref. 95). Thus we can expect that the electronic factors (both LAs and LAe) affect the atomic order in a sequence $8i_{2(A)}>2a_{(A)}>8i_{1(A)}>4f_{(A)}/8j_{(A)}$ for LAs-LAe category. As discussed above, for LAe and LAs-LAe categories the electronic factors affect the atomic order in a sequence $8i_{2(A)}>2a_{(A)}>4f_{(A)}>8i_{1(A)}>8j_{(A)}$ and $8i_{2(A)}>2a_{(A)}>8i_{1(A)}>4f_{(A)}/8j_{(A)}$, respectively. In this regard, LAs factor must affect the atomic order in a sequence of $8i_{1(A)}>4f_{(A)}$.

Thus LAs factor affects the atomic order in a sequence $8i_{2(A)}>2a_{(A)}>8i_{1(A)}>4f_{(A)}/8j_{(A)}$. Vice versa, SMs factor affects the atomic order in a sequence $4f_{(A)}/8j_{(A)}>8i_{1(A)}>2a_{(A)}>8i_{2(A)}$.

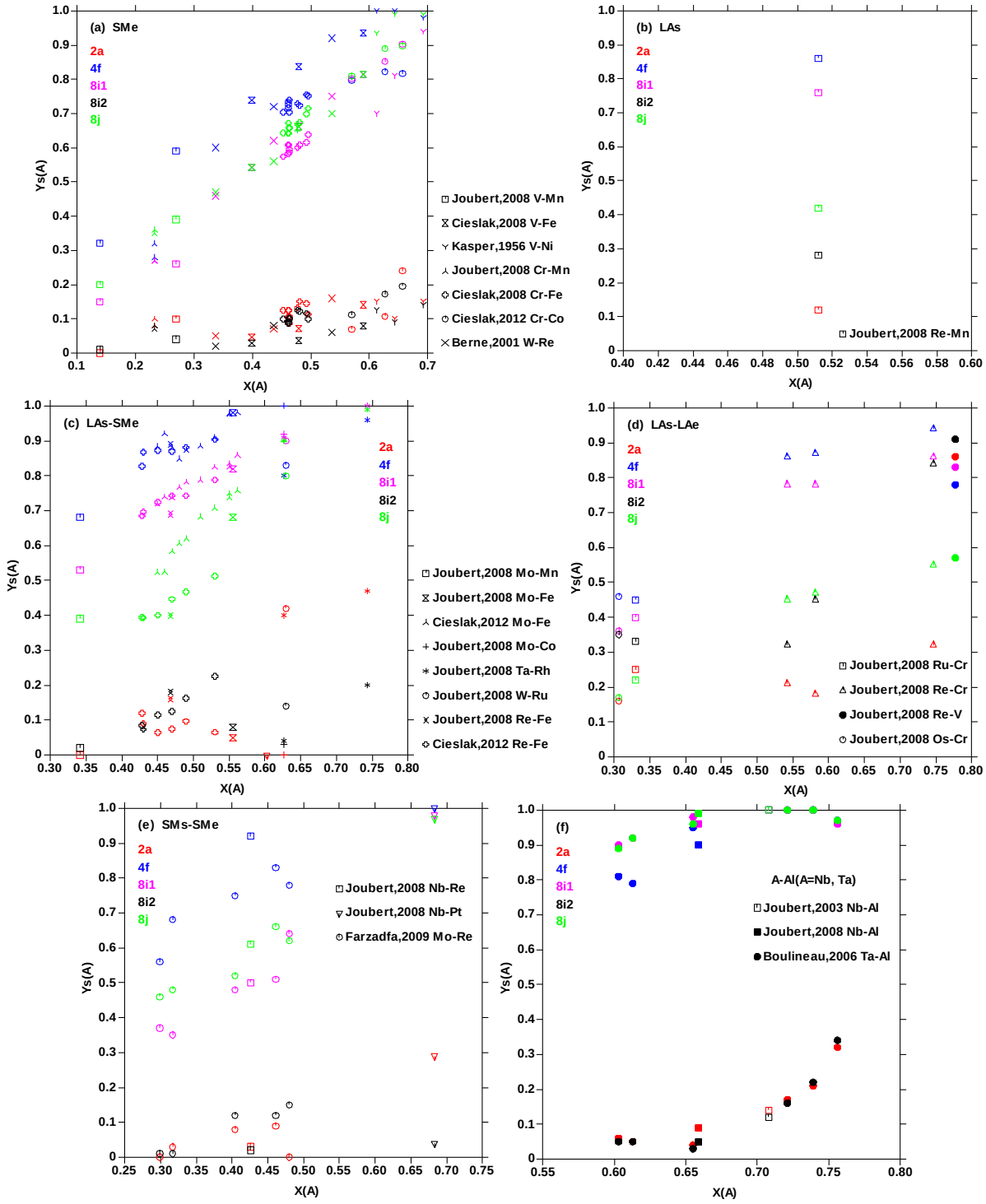

Figure 3.7 : Site occupancy, Ys(A), w.r.t. mole fraction of A, X(A). Measured data are from Ref. 9,10,96–103,114–119.

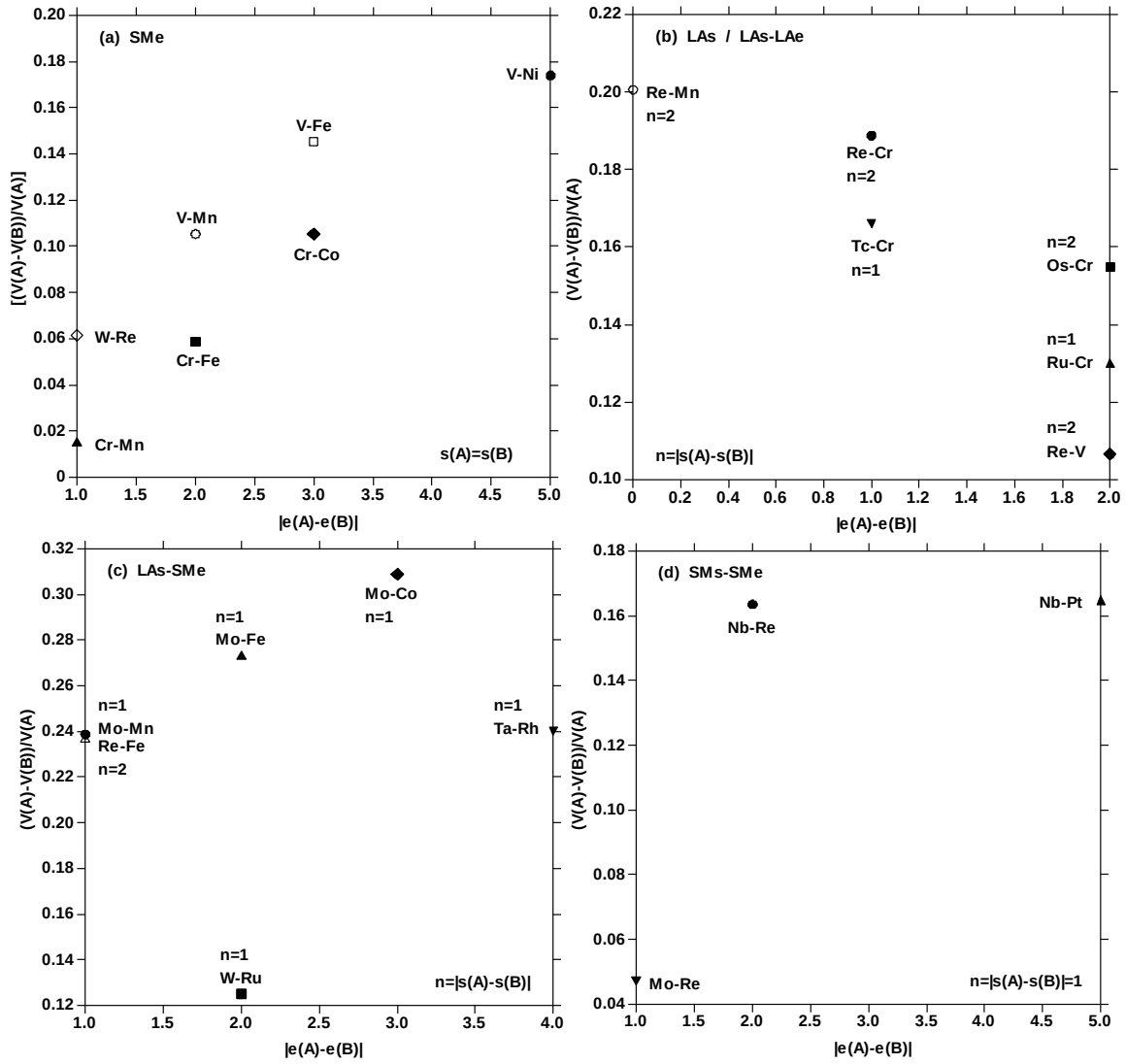

Figure 3.8 : Molar volume difference with respect to differences between the number of valence electrons of the constituent elements (A and B) of the binary sigma compounds. The assessed molar volume data are from the CALPHAD assessments as presented in Section 5. The differences between the total number of electron shells of the elements are indicated. s(A) and s(B): number of valence electrons of atom A and B, respectively; e(A) and e(B): number of valence electrons of atom A and B, respectively ; V(A) and V(B): molar volume of atom A and B, respectively.

3.3.2.3. Experimental site occupancies

The dissociation of influencing factors on atomic order as discovered in Section 3.3.2.1 and 3.3.2.2 can well explain all the accurate experimental data and first-principles calculations as will be discussed in the following section and Section 3.3.3, respectively.

(a) SMe category (Fig. 3.8 (a))

The influencing factors on atomic order for this category are the size and SMe factors that lead to a sequence $4f_{(A)} > 8i_{1(A)} > 8j_{(A)} > 8i_{2(A)} > 2a_{(A)}$ and $8j_{(A)} > 8i_{1(A)} > 4f_{(A)} > 2a_{(A)} >$

$8i_{2(A)}$, respectively. In this category, the site occupancy data on sites with the same CN (CN12: $8i_2$ vs 2a, CN14: $8i_1$ vs 8j) are close. Most data show $Y_{2a(A)}>Y_{8i2(A)}$ and $Y_{8j(A)}>Y_{8i1(A)}$. This is because SMe factor affects the atomic order more remarkably than the size factor.

For Cr-Mn, Cr-Co and V-Ni systems, as mentioned in Section 3.3.2.1, the effect of SMe factor on atomic order is particularly notable which leads to $Y_{8j(A)}/Y_{8i1(A)}>Y_{4f(A)}$ or $Y_{8j(A)}>Y_{4f(A)}$. For the other systems, the size factor determines the site occupancy on 4f site. It is worth mentioning that data for Cr-Co system from Cieślak [114] and data for W-Re system from [106] show that site occupancies are inverted among sites with the same CN (2a vs $8i_2$; $8i_1$vs 8j). This is due to a competition between electronic and size factors.

For V-Ni system, Joubert [9] also measured the site occupancies by using the XRD method, but the data are not accurate due to the weak XRD contrast between the two constituent elements, as a consequence these data were not considered in the present work. On the contrary, the early data measured by Kasper [96] are more accurate since they conducted neutron diffraction (ND) experiments yielding a better resolution for site occupancy measurements.

(b) LAs category (Fig. 3.8 (b))

The influencing factors on the atomic order for this category are the size and LAs factors that lead to a sequence $4f_{(A)}>8i_{1(A)}>8j_{(A)}>8i_{2(A)}>2a_{(A)}$ and $8i_{2(A)}>2a_{(A)}>8i_{1(A)}>4f_{(A)}/8j_{(A)}$, respectively.

For the LAs category, experimental data are available for Re-Mn system only. Both size and electronic factors affect the atomic order in a sequence $8i_{2(A)}>2a_{(A)}$ and $8i_{1(A)}>8j_{(A)}$. The size factor determines the site occupancy of 4f site.

(c) LAs-SMe category (Fig. 3.8 (c))

The influencing factors on the site occupancies for this category are the size, LAs and SMe factors that lead to a sequence $4f_{(A)}>8i_{1(A)}>8j_{(A)}>8i_{2(A)}>2a_{(A)}$, $8i_{2(A)}>2a_{(A)}>8i_{1(A)}>4f_{(A)}/8j_{(A)}$ and $8j_{(A)}>8i_{1(A)}>4f_{(A)}>2a_{(A)}>8i_{2(A)}$, respectively. The atomic order results from a competition among the three factors above. Atom A prefers occupying large CN sites (i.e. 4f, $8i_1$ and 8j) rather than small CN sites (i.e. 2a and $8i_2$), because of both the size and SMe factors.

For Mo-Fe, Mo-Mn and Re-Fe systems, Fig. 3.8 (c) presents $Y_{8i1(A)}>Y_{8j(A)}$ and $Y_{8i2(A)}>Y_{2a(A)}$, because the effect of SMe factor on atomic order is less significant than the combined effects of LAs and size factors. Besides, the difference of site occupancies between $8i_1$ and 8j sites for Re-Fe system is the largest among the three systems. It is because of the effect of LAs factor, as for Re-Fe system the size difference between the two constituent elements is the smallest and n (n=s(A)-s(B)=2) is the largest among the three systems as shown in Fig. 3.9 (c).

From Mo-Co to Ta-Rh systems, SMe factor increasingly affects the atomic order as indicated in Fig. 3.9 (c). For Mo-Co system, Fig. 3.8 (c) shows $Y_{4f(A)}>Y_{8i1(A)}\approx Y_{8j(A)}$ and $Y_{8i2(A)}>Y_{2a(A)}$. It is because that SMe factor affects the atomic order almost equivalently

as the combined effects of LAs and size factors. For Ta-Rh system that presents $Y_{8i1(A)} \approx Y_{8j(A)} > Y_{4f(A)}$ and $Y_{2a(A)} > Y_{8i2(A)}$, SMe factor affects the atomic order more dramatically. Notably, both SMe and LAs factors tend to decrease occupancy of atom A on 4f site. Joubert [9] also conducted the measurements for Ta-Pd compound, but the measured compositions describe a tie-line in disagreement with the published phase diagram. Hence the data were not considered.

For W-Ru system, the data from Joubert [9] show that $Y_{2a(A)} > Y_{8i2(A)}$ (due to SMe factor), $Y_{8i1(A)} > Y_{8j(A)}$ (due to LAs and size factors) and $Y_{8i1(A)} > Y_{4f(A)}$ (due to SMe and LAs factors). In addition, it can be seen from Fig. 3.9 (c) that the values of n (n=s(A)-s(B)) and e(A)-e(B) for W-Ru system are the same as those for Mo-Fe system, but the site occupancy orderings for these two systems are different as presented in Fig. 3.8 (c). The reason is that the size difference between W and Ru atoms is far smaller than that for Mo-Fe system (see Fig. 3.9 (c)), thus effect of size factor on the atomic order of W-Ru system is less remarkable that of Mo-Fe system.

(d) LAs-LAe category (Fig. 3.8 (d))

The influencing factors on the atomic order for this category are the size, LAs and LAe factors leading to a sequence $4f_{(A)} > 8i_{1(A)} > 8j_{(A)} > 8i_{2(A)} > 2a_{(A)}$, $8i_{2(A)} > 2a_{(A)} > 8i_{1(A)} > 4f_{(A)}/8j_{(A)}$ and $8i_{2(A)} > 2a_{(A)} > 4f_{(A)} > 8i_{1(A)} > 8j_{(A)}$, respectively. The atomic order results from a competition among the three factors above.

The site occupancy of Os-Cr, Re-V and Ru-Cr systems is almost completely disordered [9]. This is because the almost opposite effects of the size and electron factors are evenly matched. A less disordered state for Re-Cr system as compared to Os-Cr, Re-V and Ru-Cr systems as shown in Fig. 3.8 (d) is due to a larger effect of the size factor as presented in Fig. 3.9 (b).

For Re-V system, the size difference between the two constituent elements is the smallest and the values of n (n=s(A)-s(B)) and e(A)-e(B) are the largest (see Fig. 3.9 (c)), which indicates that the effects of electron factors are stronger for Re-V system as compared to other systems. The experimental site occupancies of Re-V system shows $Y_{8i2(A)} > Y_{2a(A)} > Y_{8i1(A)} > Y_{4f(A)} > Y_{8j(A)}$, which is an evidence that the electronic factors affect more dramatically the atomic order than the size factor.

It is worth noting that as mentioned in Section 3.1, Sluiter and Pasturel [107] clarified that for Ru-Cr and Os-Cr systems, all five crystal sites were equivalent as there is no overwhelming ordering preference of constituent elements. However, as discussed above, we can conclude that the reason for no overwhelming ordering preference is because of a competition among the effects of size and electronic factors rather than an equivalence of five crystal sites. Actually, the five crystal sites are not equivalent for these systems as well as the other existing sigma systems with difference either in CN or NN sites.

(e) SMs-SMe category (Fig. 3.8 (e))

The influencing factors on the atomic order for this category are the size, SMs and SMe factors, which lead to a sequence $4f_{(A)}>8i_{1(A)}>8j_{(A)}>8i_{2(A)}>2a_{(A)}$, $4f_{(A)}/8j_{(A)}>8i_{1(A)}>2a_{(A)}>8i_{2(A)}$ and $8j_{(A)}>8i_{1(A)}>4f_{(A)}>2a_{(A)}>8i_{2(A)}$, respectively.

For Mo-Re system, in general, Farzadfar's [117] measurements show $Y_{8i2(A)}>Y_{2a(A)}$. This is caused by the size factor. Even though the size difference between Mo and Re atoms is the smallest among all systems in SMs-SMe category, it is the small values of n (n=s(A)-s(B)) and e(A)-e(B) that cause the size factor to be more prominent (see Fig. 3.9 (d)).

(f) A-Al (A= Nb and Ta) category (Fig. 3.8 (f))

As mentioned in Section 3.3.1.2, A-Al category behaves like LAs-SMe category with regard to the electron loss or gain. Thus the influencing factors on atomic order for this category are expected to be the size, LAs and SMe factors that lead to a sequence $4f_{(A)}>8i_{1(A)}>8j_{(A)}>8i_{2(A)}>2a_{(A)}$, $8i_{2(A)}>2a_{(A)}>8i_{1(A)}>4f_{(A)}/8j_{(A)}$ and $8j_{(A)}>8i_{1(A)}>4f_{(A)}>2a_{(A)}>8i_{2(A)}$, respectively.

Fig. 3.8 (f) shows that generally atom A and Al occupy large CN sites (i.e. 4f, $8i_1$ and 8j) and small CN sites (2a and $8i_2$), respectively. In addition, the site occupancies are inverted between sites with the same CN (2a and $8i_2$; $8i_1$ and 8j). The above observations can be explained by a compromise among the three influencing factors. Besides, the measurements show that $Y_{8i1(A)}/Y_{8j(A)}>Y_{4f(A)}$, which is caused by the effects of both LAs and SMe factors.

3.3.3. Discussion

In view of the size and electron configuration of the constituent elements, we have classified all the binary sigma phase systems into different categories. With this classification approach, it is possible to study the tendency of electrons loss or gain of the constituent elements and obtain the regularity of atomic order as investigated in this chapter.

The present findings cannot only explain various results for stable sigma phase but also the calculation results for hypothetically unstable sigma phase. As mentioned in Section 3.1, Crivello et al. [95] calculated the site occupancies of the sigma phase in binary Re-X (X= Co, Cr, Fe, Hf, Mn, Mo, Nb, Ni, Os, Ru, Ta, Tc, Ti, V, W and Zr) systems including stable sigma compounds (Re-V, Re-Cr, Re-Mn, Re-Fe, Nb-Re, Mo-Re, Ta-Re and W-Re) as well as some hypothetically unstable ones (Ti-Re, Zr-Re, Hf-Re, Re-Co, Re-Ni, Re-Tc, Re-Ru and Re-Os). Some calculation results cannot be well explained in that work as already mentioned in Section 3.1 but are interpretable by using the analysis method of the present chapter as follows.

Among the sigma phase studied by Crivello et al. [95] Hf-Re, Ta-Re, W-Re and Re-Os systems belong to SMe category and Ti-Re, Zr-Re, Nb-Re and Mo-Re systems belong to SMs-SMe category. For SMe and SMs-SMe categories, both the size and electronic factors cause the atomic order to follow $4f_{(A)}/8i_{1(A)}/8j_{(A)}>8i_{2(A)}/2a_{(A)}$, that is why the site occupancies of Nb-Re, Mo-Re, Ta-Re, W-Re, Ti-Re, Zr-Re and Hf-Re systems behave in a more ordered way [95]. With regard to Re-Os system, the site occupancies present relative

less order at the finite temperature of 2000K (see Fig. 9 in Ref. 95), which is because the effects of the size and electronic factors are both small for this system.

Re-Mn and Re-Tc systems belong to LAs category, while Re-V and Re-Cr systems belong to LAs-LAe category and Re-Fe, Re-Co, Re-Ni and Re-Ru systems belong to LAs-SMe category. A competition of the influencing factors makes a less ordered state in these categories. Besides, Crivello et al. [95] indicated that site occupancy behavior for the sites with the same CN (i.e. 2a vs $8i_2$; $8i_1$ vs 8j) is different. Taking Re-Os vs Re-Tc and Re-V systems as examples, for Re-Os (belonging to SMe category) system, the site occupancies present the order $8j_{(A)} > 8i_{1(A)}$ which is due to the effect of SMe factor. For Re-Tc (belonging to LAs) and Re-V (belonging to LAs-LAe) systems, the site occupancies present the order $8i_{1(A)} > 8j_{(A)}$ which is due to the effects of size, LAs and LAe factors.

In addition, we are also expecting to use the present method to investigate the atomic order for other non-stoichiometric intermetallic compounds, like Chi phase and Mu phase, etc.

3.4. Summary

In this chapter, influencing factors of atomic order in the binary sigma phase have been investigated by using VASP calculations and Bader charge analysis. The main conclusion can be drawn as follows:

1. Both the coordination number (CN) and nearest neighbor (NN) crystal sites affect the size of the five crystal sites of the sigma phase. The size of the five nonequivalent crystal sites of the sigma phase follows $4f_{(CN15)} > 8i_{1(CN14)} > 8j_{(CN14)} > 8i_{2(CN12)} > 2a_{(CN12)}$.

2. Both the nearest neighbor (NN) atoms and coordination polyhedron (CP) affect the atomic volume of the sigma phase. The CP mainly affects the accommodate space, the NN atoms mainly affect the atomic charge and the accommodate space, and thus affect the atomic volume.

3. In the binary sigma compounds, between the two constituent elements, the one with smaller total number of electron shells or smaller number of valence electrons tends to lose electrons; the one with larger total number of electron shells or larger number of valence electrons tends to gain electrons. On the other hand, atoms on 2a and $8i_2$ sites tend to gain electrons and those on 4f, $8i_1$ and 8j sites tend to lose electrons. Hence between the two constituent elements, the one with a larger size, smaller total number of electron shells or smaller number of valence electrons prefers occupying large CN sites (i.e. 4f, $8i_1$ and 8j) and the one with a smaller size, larger total number of electron shells or larger number of valence electrons prefers occupying small CN sites (i.e. 2a and $8i_2$). The site occupancies for a specific system are a compromise of the size and electronic influencing factors.

4. The dissociated effect of the electronic factors leads to the following atomic order:

LAs: $8i_{2(A)} > 2a_{(A)} > 8i_{1(A)} > 4f_{(A)}/8j_{(A)}$; SMs: $4f_{(A)}/8j_{(A)} > 8i_{1(A)} > 2a_{(A)} > 8i_{2(A)}$; LAe: $8i_{2(A)} > 2a_{(A)} > 4f_{(A)} > 8i_{1(A)} > 8j_{(A)}$; SMe: $8j_{(A)} > 8i_{1(A)} > 4f_{(A)} > 2a_{(A)} > 8i_{2(A)}$.

4. Influence of atomic order on physical properties of the binary sigma phase focusing on molar volume

The present chapter systematically clarifies the influence of atomic order (i.e. atomic constituent distribution or site occupancy preference on nonequivalent sites of a crystal structure) on the enthalpy of formation, bulk modulus and molar volume of the binary sigma phase. First-principles calculations of these properties have been conducted for 19 binary sigma phase systems with different atomic order based on the experimental site occupancy as well as the hypothetically ordered and disordered states by using EMTO-CPA method. The calculation results of enthalpy of formation and bulk modulus show that at 0K, the sigma phase in ordered state bears a lower enthalpy of formation and a larger bulk modulus than the ones in less ordered state. On the other hand, the investigation of the molar volume for the sigma phase is from two aspects. Firstly, the calculated molar volumes with respect to the composition of the sigma phase show that the sigma compounds do not comply with linear volume-composition relationship. The deviation can be either negative or positive depending on the tendency of electron loss or gain of the two constituent elements. Secondly, we have compared the calculated molar volume of the binary sigma compounds of hypothetically ordered and disordered states. The results show that the effect of the atomic order on the molar volume of the sigma phase depends on electron configuration of the two constituent elements.

4.1. Introduction

As a typical example of the TCP phase, the physical properties of the sigma phase have attracted great interests of study, e.g. enthalpy of formation [120], bulk modulus [3,121], site occupancy [9,122] and molar volume (or lattice parameters) [8–10,95] by using either XRD (X-ray diffraction), ND (neutron diffraction), CALPHAD or first-principles calculation methods. The present chapter is mainly focusing on the investigation of the molar volume in the sigma phase.

From the 1950s to 2010s, there are numerous measurements (see e.g. [113] and references therein) on the molar volume (or lattice parameters) of the binary sigma compounds by using XRD or ND methods. The measured data from 2000s to 2010s are with more accuracy and most measured volume data with respect to composition present linear relationship within the homogeneity range. Even though, the plentiful

experimental measurements of the sigma phase are available, the influencing factors and their effects on molar volume are still not clear.

Beside experimental measurements, there are also some investigations on the molar volume of the sigma phase by using first-principles calculations. For example, Crivello et al. [95] have calculated the cell volume of the stoichiometric end-member compounds (i.e. the complete set of ordered configurations) of the Re-X (X= Co, Cr, Fe, Hf, Mn, Mo, Nb, Ni, Os, Ru, Ta, Tc, Ti, V, W and Zr) systems by using first-principles calculations. They indicated that for most systems, there is an approximately linear relationship existing between the cell volume and the composition (see Fig.5 in Ref. 95). For Hf-Re, Nb-Re, Ta-Re, Ti-Re and Zr-Re systems, a negative deviation from linearity was observed. However, the behavior of the deviation from linearity was not clearly clarified.

Actually, for a nonstoichiometric intermetallic compound, the molar volume of the sigma phase is affected by both the atomic mixing and the atomic order (or site occupancy). The main purpose of the present chapter is to find out how the atomic mixing and the atomic order affect the molar volume of the sigma phase.

In the present chapter, the enthalpy of formation, bulk modulus and molar volume of the sigma compounds have been calculated by using EMTO-CPA approach. The atomic order for the corresponding compounds has been modeled using the ordered and disordered states as defined in Table 4.1 as well as the experimental site occupancy. The effect of atomic order on enthalpy of formation, bulk modulus and molar volume is described by the corresponding calculation difference between the A_2B sigma compound with the ordered and disordered states as referenced in Table 4.1. On the other hand, the effect of atomic mixing on molar volume is described by the deviation from the linear relationship between the molar volume and the composition of the sigma phase in disordered states, which automatically eliminates the influence of atomic order on molar volume.

To facilitate explanation, all the binary sigma compounds investigated were designated as A-B where atom A always bears a larger size than atom B. The size of the constituent elements (A and B) is determined by the molar volume of their pure elements in the sigma phase structure from the CALPHAD assessments as presented in Section 5.

Table 4.1 : Crystal structure of the sigma phase with assignment of the site occupancy of atom A corresponding to the ordered and disordered compounds A_2B and $A_xB_{(1-x)}$ (V(A)>V(B), where V(A) and V(B) are the molar volumes of element A and B in their hypothetic sigma phase structure from the CALPHAD assessments as presented in Section 5).

Space group	$P4_2/mnm$ (no. 136)				
Wyckoff position	2a	4f	$8i_1$	$8i_2$	8j
Coordination number (CN)	12	15	14	12	14
Completely ordered state (A_2B)	0	1	1	0	1
Disordered state ($A_xB_{(1-x)}$)	x	x	x	x	x

4.2. Methodology and calculation details

First-principles calculations were performed using the exact muffin-tin orbitals (EMTO) method [27,123] based on the density-functional theory (DFT) [124]. With this method, Green's function technique has been used to solve the one electron Kohn-Sham equation. The effective potential in the one-electron equation is treated with the optimized overlapping muffin-tin approximation. Besides, the total energy is corrected with the full charge density (FCD) method [27]. The basis sets of the exact muffin-tin orbitals [27,123] are used to expand the wave function. The coherent potential approximation (CPA) [44–46] is incorporated within the EMTO code, which facilitates the calculations dealing with chemical disordered alloys. With these techniques, the EMTO-CPA method bears a great higher accuracy than the linear muffin-tin orbital (LMTO) method [53] and ensures the reliability of calculations dealing with atomic and magnetic disordered systems [125].

In the present chapter, Green's function has been calculated for 16 complex energy points distributed exponentially on a semicircular contour. The scalar-relativistic and soft-core approximations are employed. We have used the electronic exchange-correlation functional within the generalized-gradient approximation (GGA) parameterized by Perdew et al.[41]. The Brillouin zone is sampled by a uniform k-point mesh without any smearing technique. The k-point mesh is set as $3\times3\times6$.

4.3. Results and discussion

The binary sigma phase systems chosen in this work to perform EMTO-CPA calculations are Cr-Co, Cr-Fe, Cr-Mn, Mo-Co, Mo-Mn, Mo-Os, Mo-Re, Nb-Al, Nb-Ir, Os-Cr, Re-Cr, Re-Mn, Re-V, Ru-Cr, Ta-Al, V-Co, V-Fe, V-Mn and V-Ni systems. The molar volumes of the pure elements in a hypothetic sigma phase structure obtained from first-principle calculations are compared in Fig. 4.1 with those obtained from CALPHAD assessments. This figure shows that the volumes calculated by EMTO-CPA and VASP method follow a similar trend and that for most elements, the differences between the EMTO-CPA results and the CALPHAD assessment ones are within 10%. Such small deviations validate our methodology.

The calculation results of enthalpy of formation and molar volume of the sigma compounds have been presented in Fig. 4.2 and 4.3. The calculated molar volume data with respect to the composition follow similar changing trend as compared with the measured ones as shown in Fig. 4.3, especially for Cr-Co, Mo-Re, Re-Cr and Ta-Al systems. In addition, the changing trend of the calculated volume results is less remarkable than the experimental ones. Obvious examples are Cr-Co and Re-Cr systems, as can be seen in Fig. 4.3 (a, o). It should be noted that for Re-Cr system, the composition of the compound with the highest Re content examined by Joubert [9] by EPMA measurement (69% Re) is inconsistent with that from XRD-determined site occupancy (74.4% Re). The value adopted in the present work is the latter one.

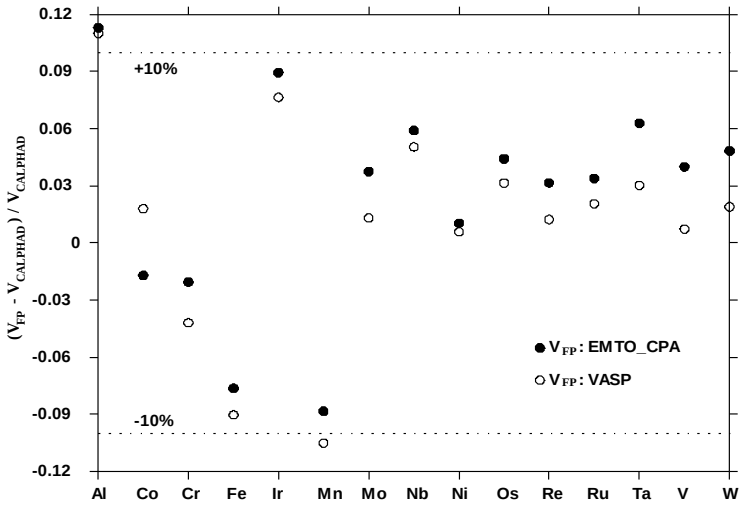

Figure 4.1 : Molar volumes of pure elements in a hypothetic sigma phase structure obtained by first-principles (EMTO-CPA and VASP) calculations compared with CALPHAD assessment results (for more details see Section 5) (VASP calculation results are from Crivello et al. [95]; the dashed line is a guide to the eye).

In the present chapter, the calculations accounting for magnetism were conducted on several sigma compounds of A-Fe (A=Cr, V) systems to determine the enthalpy of formation and molar volume (see Fig. 4.2 and 4.3 (b, e)). The experimental magnetic moment for $V_{39.9}Fe_{60.1}$ compound is 0.63 μ_B [126] and the calculated magnetic moment for the same compound with the corresponding experimental occupancy taken from Ref. 10 is 0.56 μ_B. The good agreement between these results further validates our calculations. For the other systems in Fig. 4.2 and 4.3, magnetism was not considered, as there is no experimental evidence.

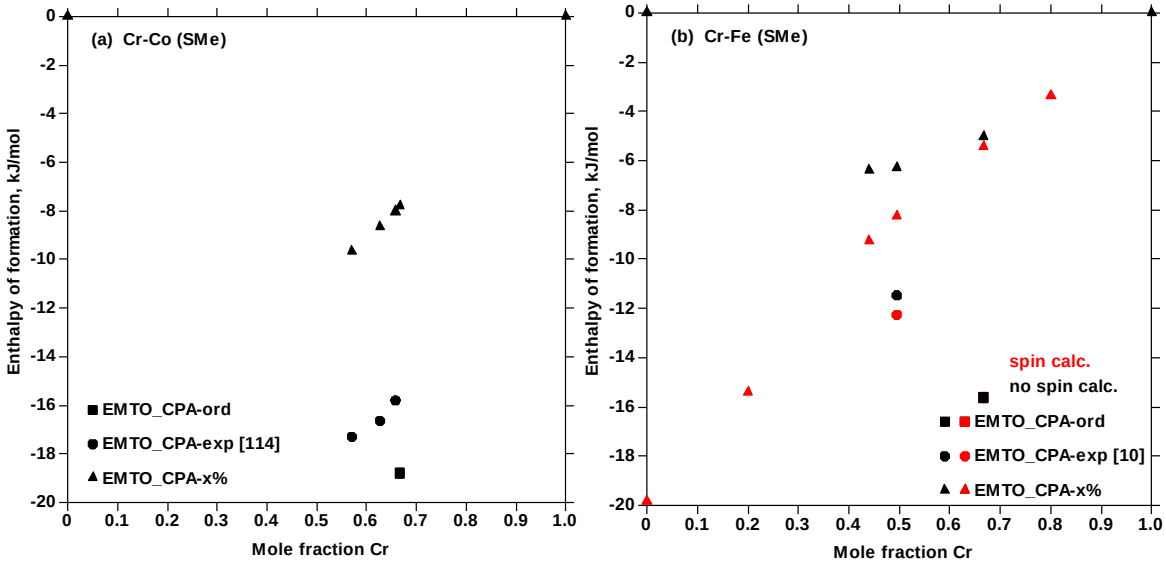

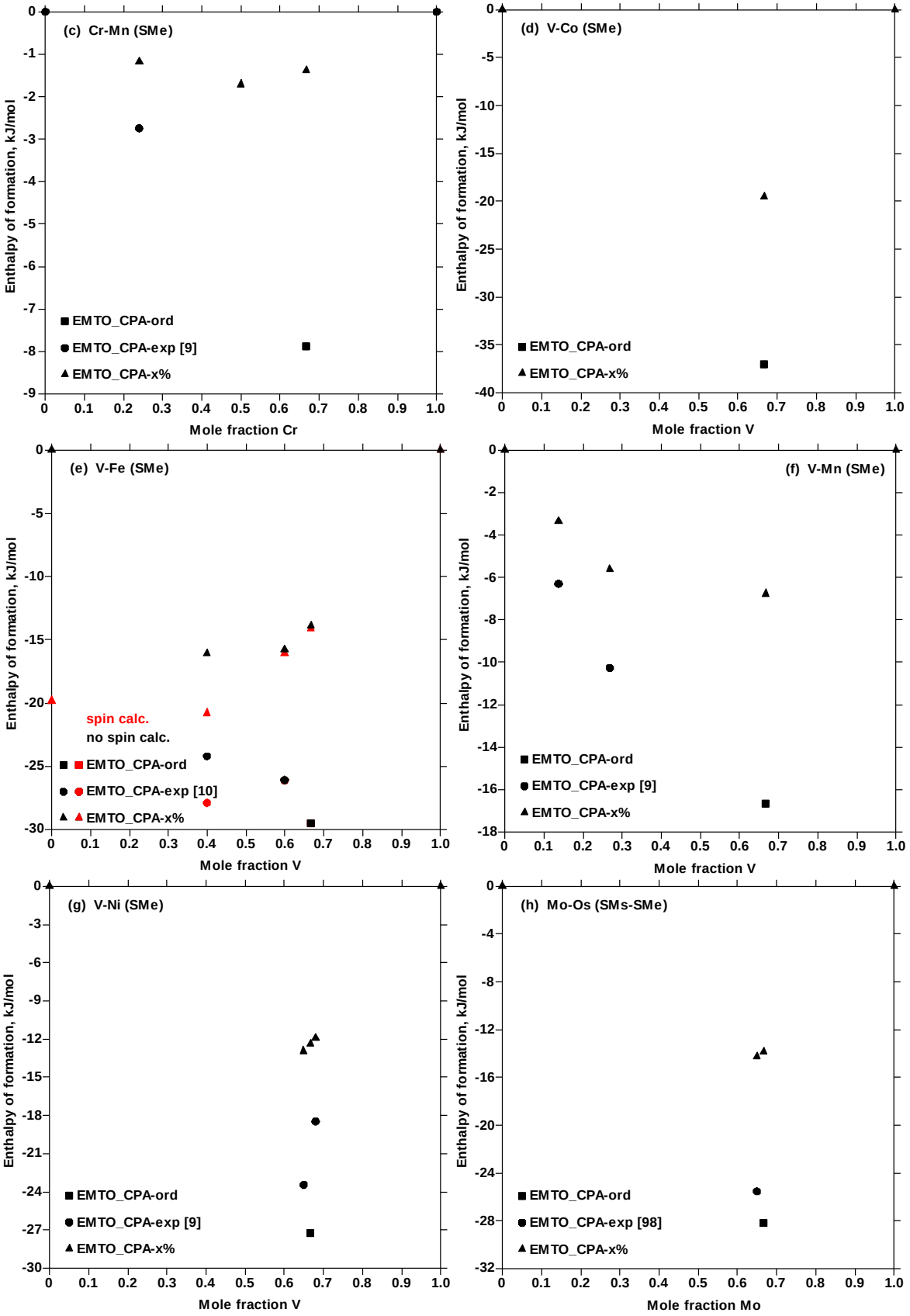
(c) Cr-Mn (SMe)
Enthalpy of formation, kJ/mol
Mole fraction Cr
EMTO_CPA-ord
EMTO_CPA-exp [9]
EMTO_CPA-x%
(d) V-Co (SMe)
Enthalpy of formation, kJ/mol
Mole fraction V
EMTO_CPA-ord
EMTO_CPA-x%
(e) V-Fe (SMe)
Enthalpy of formation, kJ/mol
Mole fraction V
spin calc.
no spin calc.
EMTO_CPA-ord
EMTO_CPA-exp [10]
EMTO_CPA-x%
(f) V-Mn (SMe)
Enthalpy of formation, kJ/mol
Mole fraction V
EMTO_CPA-ord
EMTO_CPA-exp [9]
EMTO_CPA-x%
(g) V-Ni (SMe)
Enthalpy of formation, kJ/mol
Mole fraction V
EMTO_CPA-ord
EMTO_CPA-exp [9]
EMTO_CPA-x%
(h) Mo-Os (SMs-SMe)
Enthalpy of formation, kJ/mol
Mole fraction Mo
EMTO_CPA-ord
EMTO_CPA-exp [98]
EMTO_CPA-x%

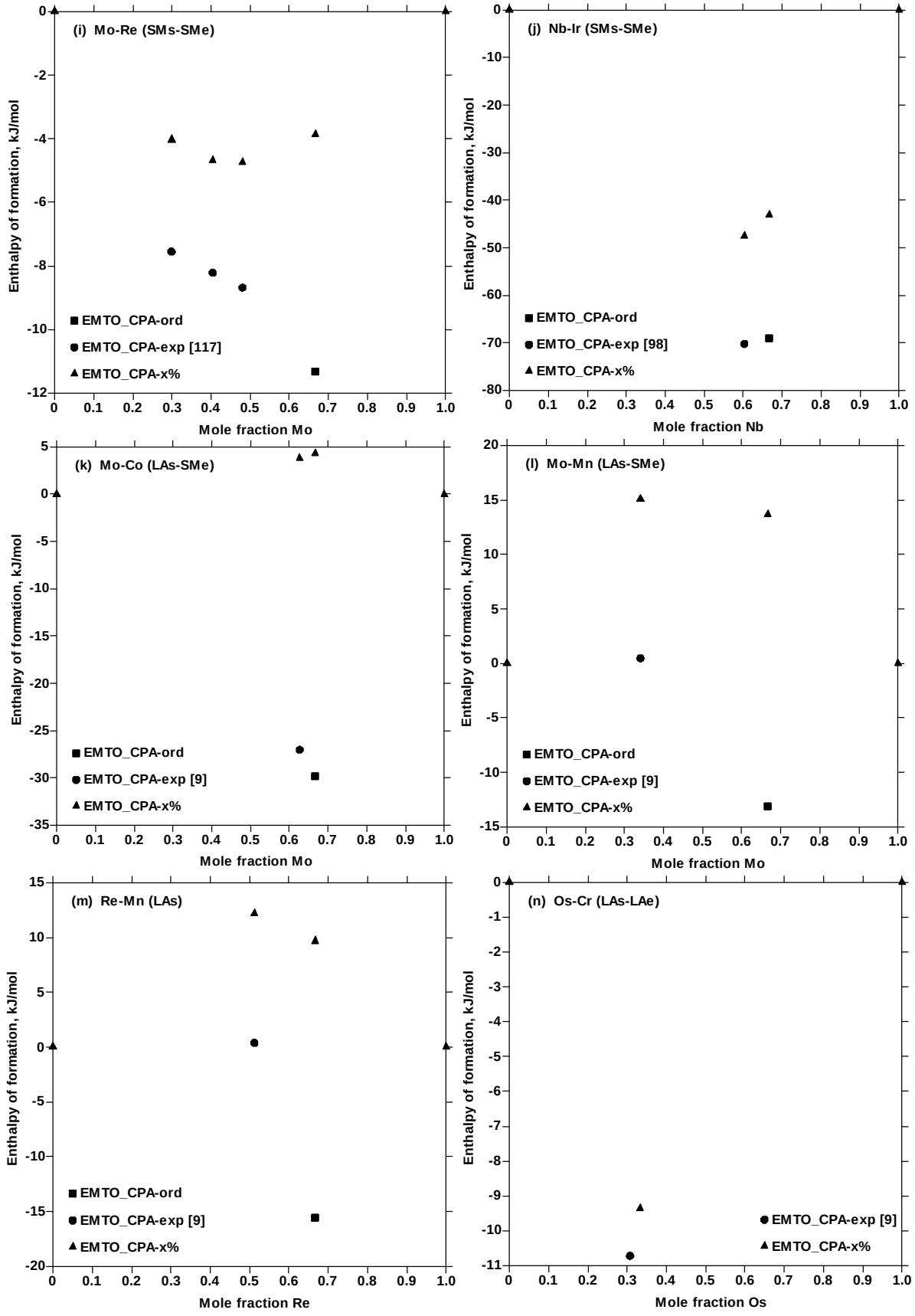
(i) Mo-Re (SMs-SMe)
Enthalpy of formation, kJ/mol
Mole fraction Mo
EMTO_CPA-ord
EMTO_CPA-exp [117]
EMTO_CPA-x%
(j) Nb-Ir (SMs-SMe)
Enthalpy of formation, kJ/mol
Mole fraction Nb
EMTO_CPA-ord
EMTO_CPA-exp [98]
EMTO_CPA-x%
(k) Mo-Co (LAs-SMe)
Enthalpy of formation, kJ/mol
Mole fraction Mo
EMTO_CPA-ord
EMTO_CPA-exp [9]
EMTO_CPA-x%
(l) Mo-Mn (LAs-SMe)
Enthalpy of formation, kJ/mol
Mole fraction Mo
EMTO_CPA-ord
EMTO_CPA-exp [9]
EMTO_CPA-x%
(m) Re-Mn (LAs)
Enthalpy of formation, kJ/mol
Mole fraction Re
EMTO_CPA-ord
EMTO_CPA-exp [9]
EMTO_CPA-x%
(n) Os-Cr (LAs-LAe)
Enthalpy of formation, kJ/mol
Mole fraction Os
EMTO_CPA-exp [9]
EMTO_CPA-x%

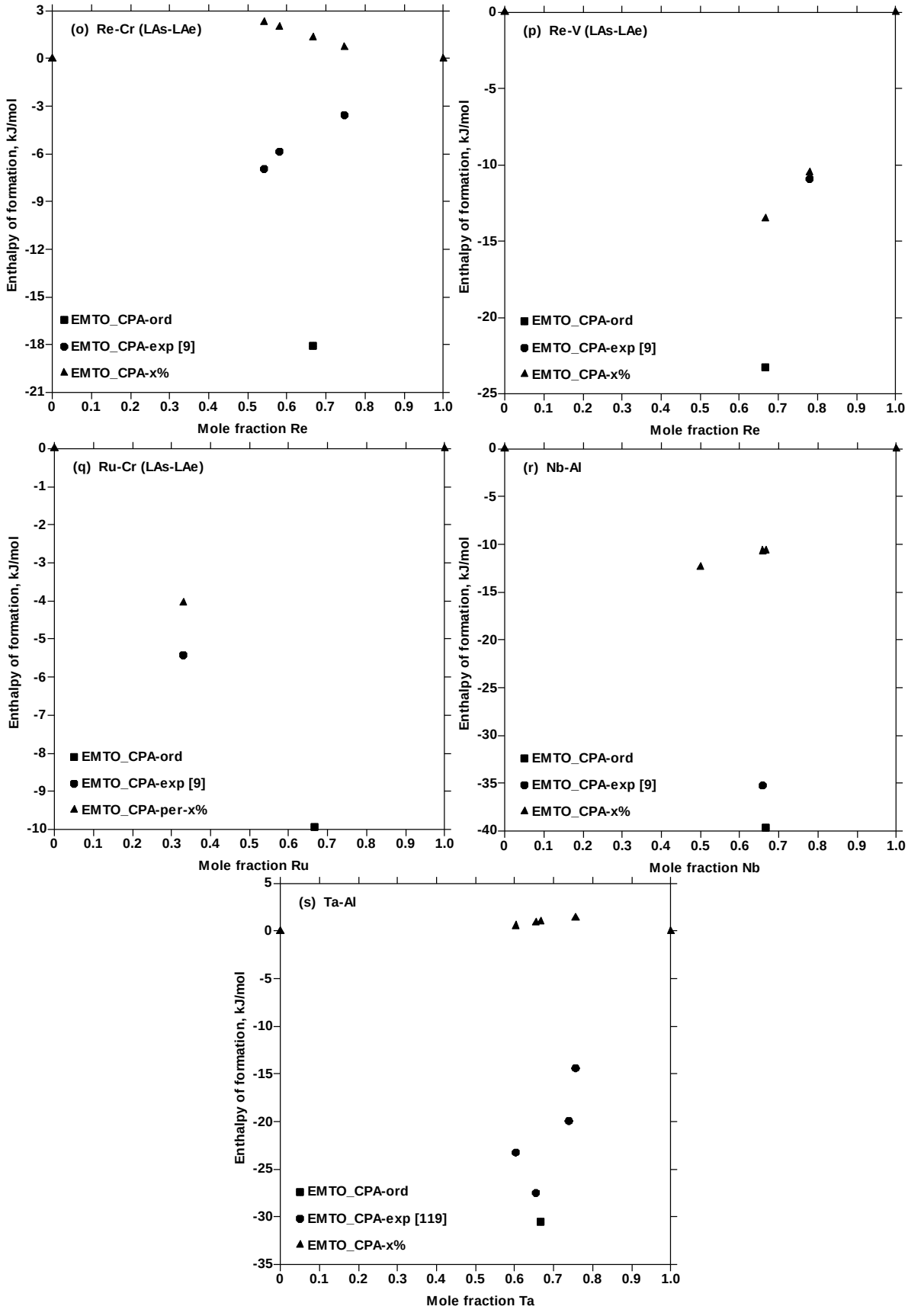
(o) Re-Cr (LAs-LAe)
Enthalpy of formation, kJ/mol
Mole fraction Re
EMTO_CPA-ord
EMTO_CPA-exp [9]
EMTO_CPA-x%
(p) Re-V (LAs-LAe)
Enthalpy of formation, kJ/mol
Mole fraction Re
EMTO_CPA-ord
EMTO_CPA-exp [9]
EMTO_CPA-x%
(q) Ru-Cr (LAs-LAe)
Enthalpy of formation, kJ/mol
Mole fraction Ru
EMTO_CPA-ord
EMTO_CPA-exp [9]
EMTO_CPA-per-x%
(r) Nb-Al
Enthalpy of formation, kJ/mol
Mole fraction Nb
EMTO_CPA-ord
EMTO_CPA-exp [9]
EMTO_CPA-x%
(s) Ta-Al
Enthalpy of formation, kJ/mol
Mole fraction Ta
EMTO_CPA-ord
EMTO_CPA-exp [119]
EMTO_CPA-x%

Figure 4.2 : Enthalpy of formation of A-B (V_A>V_B, where V_A and V_B are the molar volumes of element A and B in their hypothetic sigma phase structure from the CALPHAD assessments as presented in Section 5) binary sigma phase systems referred to the enthalpy of the pure elements in a hypothetic sigma phase structure calculated by EMTO-CPA method at 0 K. EMTO-CPA-ord, EMTO-CPA-exp and EMTO-CPA-x% represent results for volumes calculated with site occupancies corresponding to that of completely ordered state, experimental measurements [9,10,98,114,117,119] and completely disordered state, respectively.

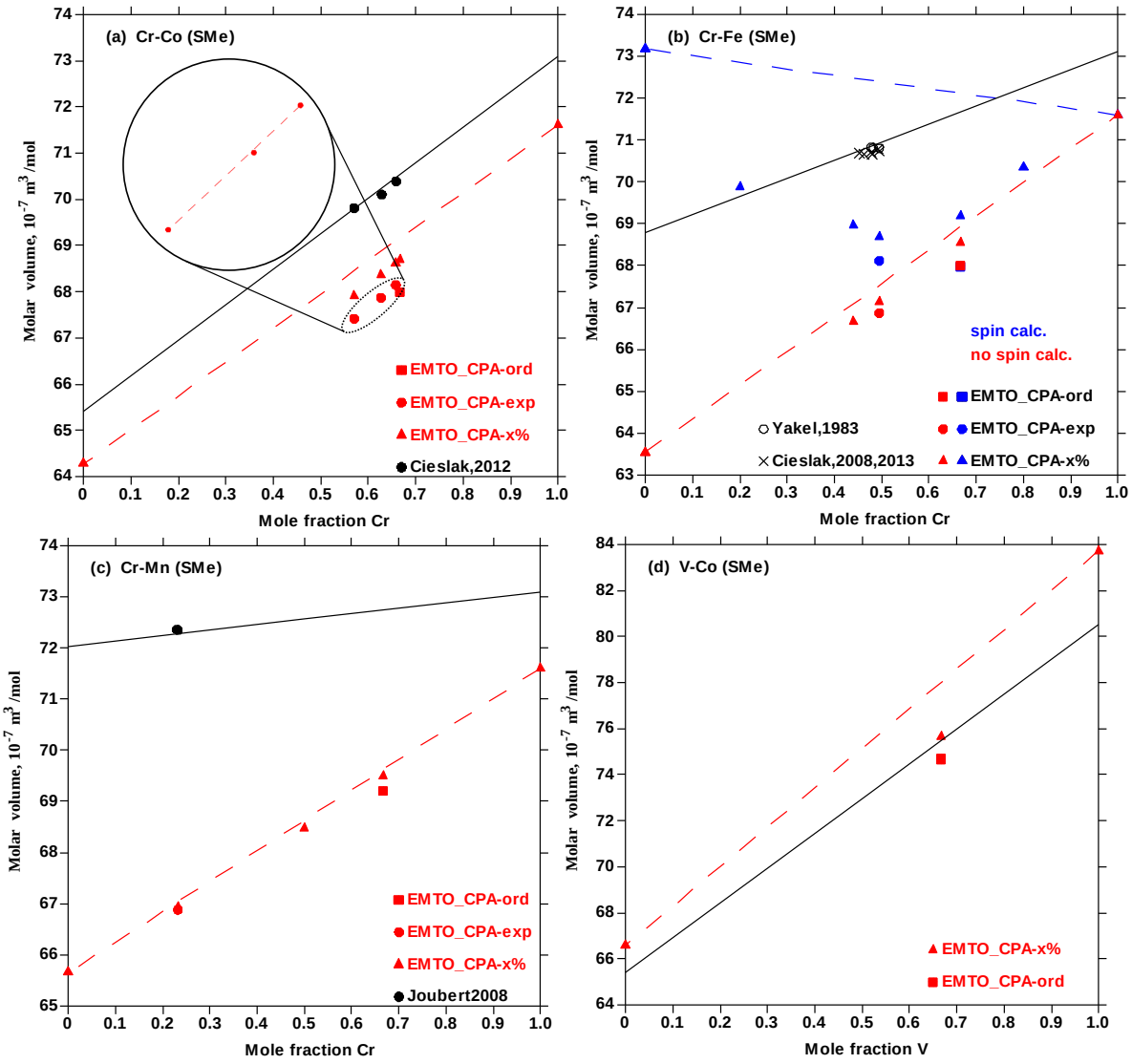

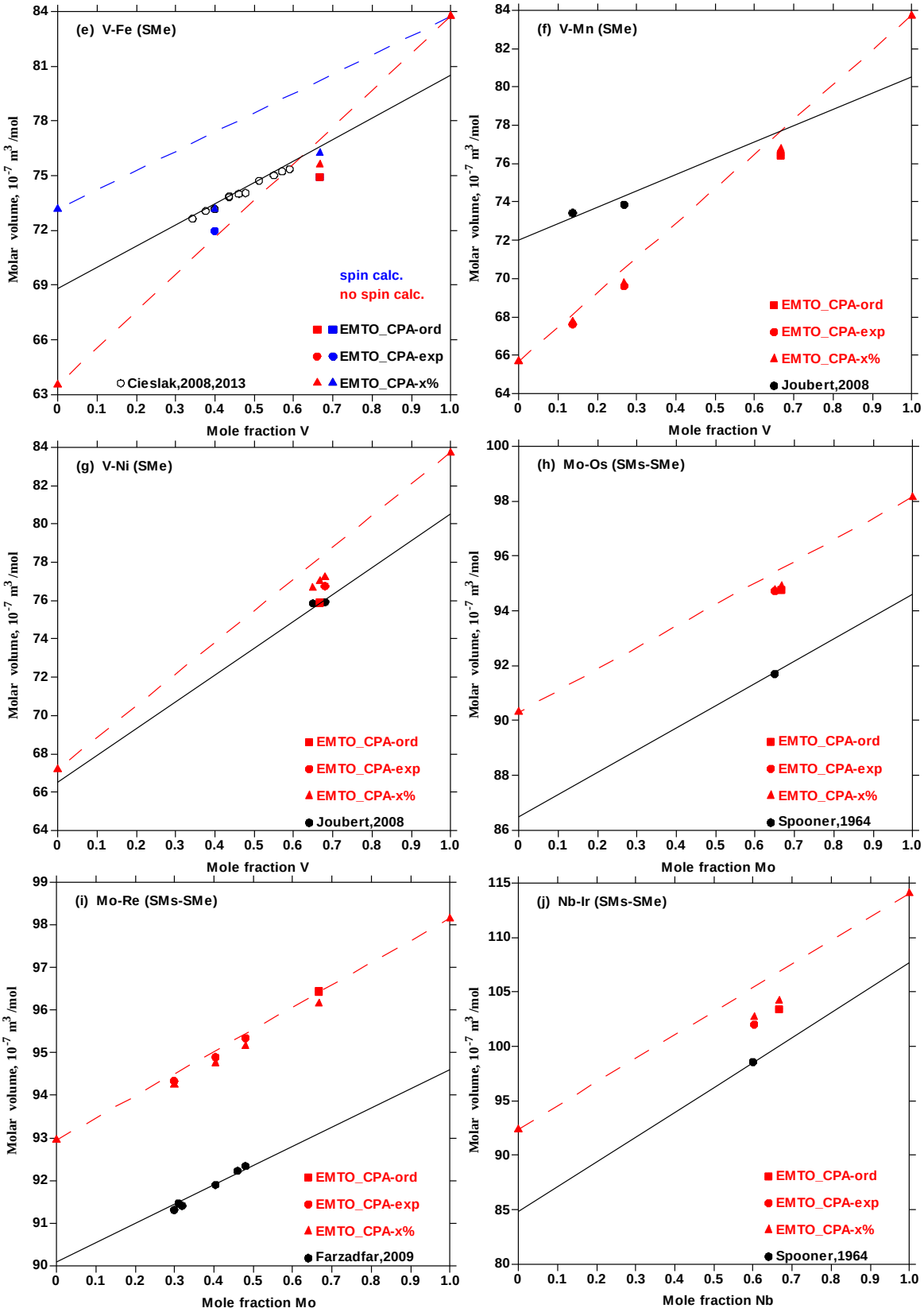
(e) V-Fe (SMe)
spin calc.
no spin calc.
EMTO_CPA-ord
EMTO_CPA-exp
EMTO_CPA-x%
Cieslak,2008,2013
Molar volume, 10^-7 m^3 /mol
Mole fraction V
(f) V-Mn (SMe)
EMTO_CPA-ord
EMTO_CPA-exp
EMTO_CPA-x%
Joubert,2008
Molar volume, 10^-7 m^3 /mol
Mole fraction V
(g) V-Ni (SMe)
EMTO_CPA-ord
EMTO_CPA-exp
EMTO_CPA-x%
Joubert,2008
Molar volume, 10^-7 m^3 /mol
Mole fraction V
(h) Mo-Os (SMs-SMe)
EMTO_CPA-ord
EMTO_CPA-exp
EMTO_CPA-x%
Spooner,1964
Molar volume, 10^-7 m^3 /mol
Mole fraction Mo
(i) Mo-Re (SMs-SMe)
EMTO_CPA-ord
EMTO_CPA-exp
EMTO_CPA-x%
Farzadfar,2009
Molar volume, 10^-7 m^3 /mol
Mole fraction Mo
(j) Nb-Ir (SMs-SMe)
EMTO_CPA-ord
EMTO_CPA-exp
EMTO_CPA-x%
Spooner,1964
Molar volume, 10^-7 m^3 /mol
Mole fraction Nb

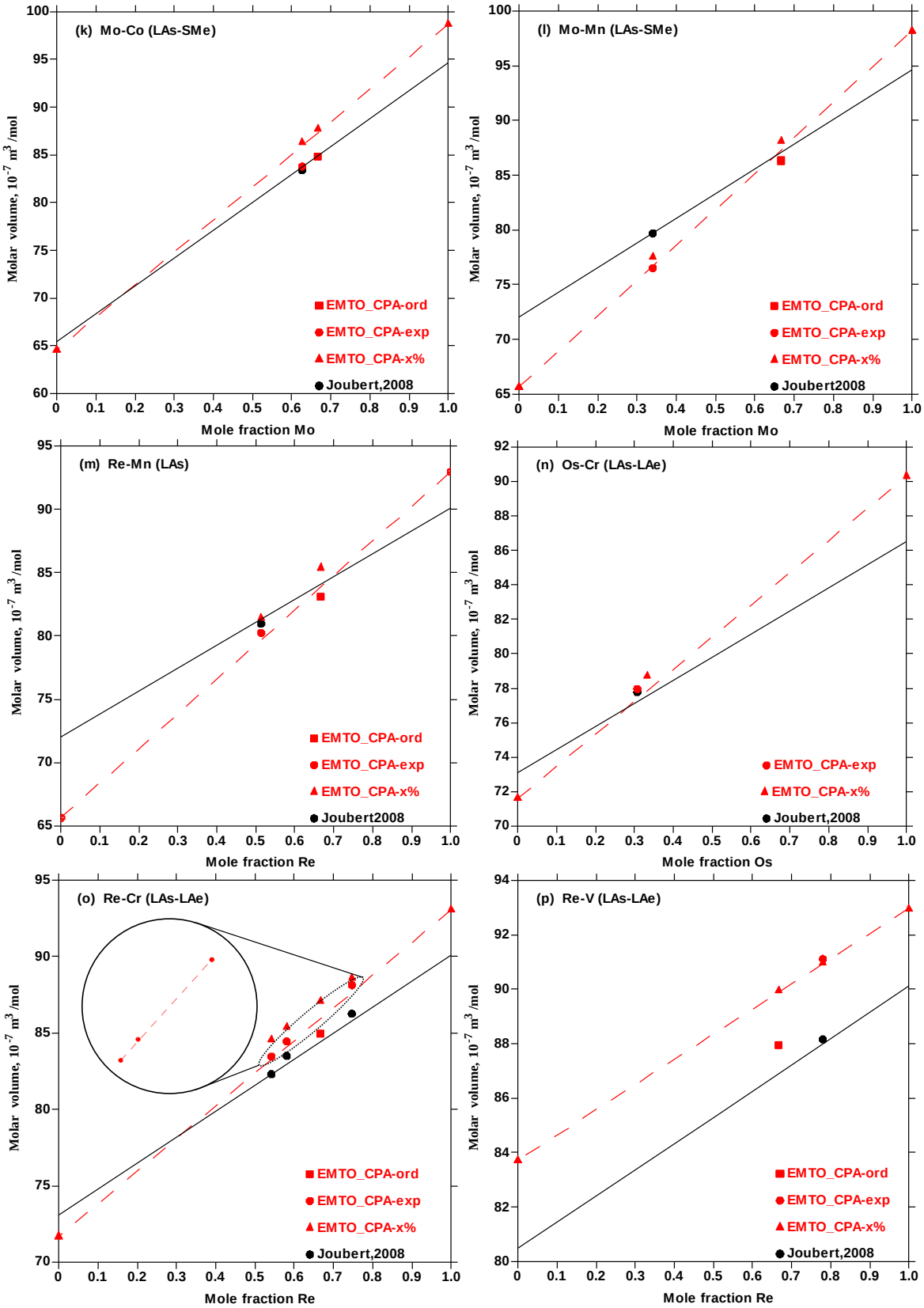
(k) Mo-Co (LAs-SMe)
Molar volume, 10^-7 m^3 /mol
Mole fraction Mo
EMTO_CPA-ord
EMTO_CPA-exp
EMTO_CPA-x%
Joubert,2008
(l) Mo-Mn (LAs-SMe)
Molar volume, 10^-7 m^3 /mol
Mole fraction Mo
EMTO_CPA-ord
EMTO_CPA-exp
EMTO_CPA-x%
Joubert2008
(m) Re-Mn (LAs)
Molar volume, 10^-7 m^3 /mol
Mole fraction Re
EMTO_CPA-ord
EMTO_CPA-exp
EMTO_CPA-x%
Joubert2008
(n) Os-Cr (LAs-LAe)
Molar volume, 10^-7 m^3 /mol
Mole fraction Os
EMTO_CPA-exp
EMTO_CPA-x%
Joubert,2008
(o) Re-Cr (LAs-LAe)
Molar volume, 10^-7 m^3 /mol
Mole fraction Re
EMTO_CPA-ord
EMTO_CPA-exp
EMTO_CPA-x%
Joubert,2008
(p) Re-V (LAs-LAe)
Molar volume, 10^-7 m^3 /mol
Mole fraction Re
EMTO_CPA-ord
EMTO_CPA-exp
EMTO_CPA-x%
Joubert,2008

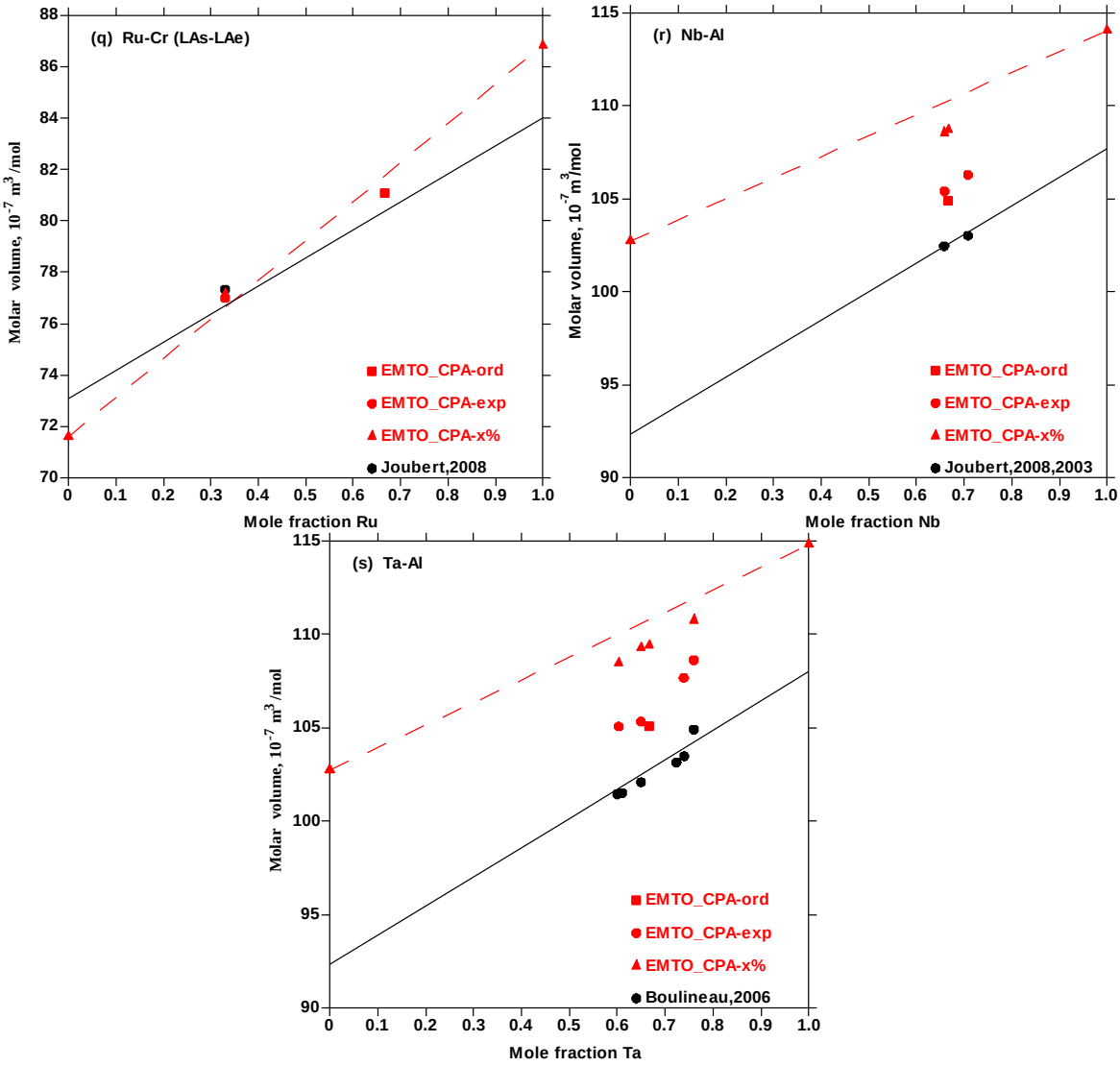

Figure 4.3 : EMTO-CPA-calculated and CALPHAD assessed molar volume of A-B (V(A)>V(B)) (Cr-Co, Cr-Fe, Cr-Mn, Mo-Co, Mo-Mn, Mo-Os, Mo-Re, Nb-Al, Nb-Ir, Os-Cr, Re-Cr, Re-Mn, Re-V, Ru-Cr, Ta-Al, V-Co, V-Fe, V-Mn and V-Ni) sigma-containing binary systems compared with the experimental data [9,10,98,103,114,117–119,127], where EMTO-CPA-ord, EMTO-CPA-exp and EMTO-CPA-x% represent volume calculated results with site occupancy of ordered state, experimental measurements and disordered state, respectively (the full line represents the CALPHAD assessment results as presented in Section 5 and the dashed line is a guide to the eye)

4.3.1. Definition of order degree

For A-B binary ordered phase, the order degree was quantitatively expressed by long-range order parameter S [1] :

$$S = \frac{P_A - X_A}{1 - X_A} \qquad (4.1)$$

where P_A is the probability of occurrence of atom A on the right crystal site for atom A (i.e. the crystal site occupied by atom A when the crystal is in total ordered state); X_A is

the mole fraction of atom A. When in ordered state, P_A =1 and thus S=1; When in disordered state, P_A =X_A and thus S=0.

However, the above Eq. 4.1 is not able to describe the situation when all the right crystal sites for atom A are occupied by atom A, where P_A =1 but there are extra atom A occupying its wrong site (i.e. the crystal site occupied by atom B when the crystal is in total ordered state). In other words, the defect of the above equation is that as long as P_A=1, S will equal to 1, no matter whether there are extra atom A occupying its wrong site or not. In order to overcome this issue, we introduce the following description for long-range order parameter S:

$$S = \frac{n_A}{n} \cdot \frac{P_A - X_A}{1 - X_A} + \frac{n_B}{n} \cdot \frac{P_B - X_B}{1 - X_B} \qquad (4.2)$$

where P_A and P_B are the probability of occurrence of atoms A and B (i.e. the site occupancy), respectively on their right crystal sites; X_A and X_B are the mole fraction of atom A and B, respectively; n, n_A and n_B are the total number of atoms, the number of atom A and B, in a unit cell respectively, when the crystal is in total ordered state. When S=1, the compound is totally ordered; when the probabilities P_A and P_B equal the mole fractions X_A and X_B, respectively, the compound is totally disordered with S=0.

As regard to TCP phases, there are several nonequivalent sites in the crystal structure. Thus, we can extend Eq. 4.2 to several terms based on the number of nonequivalent sites. The case for the sigma phase is as follows:

$$S = \frac{2}{30} \cdot \frac{P_{B_{2a}} - X_B}{1 - X_B} + \frac{4}{30} \cdot \frac{P_{A_{4f}} - X_A}{1 - X_A} + \frac{8}{30} \cdot \frac{P_{A_{8i1}} - X_A}{1 - X_A} + \frac{8}{30} \cdot \frac{P_{B_{8i2}} - X_B}{1 - X_B} + \frac{8}{30} \cdot \frac{P_{A_{8j}} - X_A}{1 - X_A} \qquad (4.3)$$

where atom A bears a larger size than atom B; P_A and P_B are the probability of occurrence (i.e. the site occupancy) on 2a, 4f, $8i_1$, $8i_2$ and 8j sites of atoms A and B, respectively; X_A and X_B are the mole fraction of atom A and B, respectively. The five terms on the right hand side of Eq. 4.3 represent the order degree of the five nonequivalent sites respectively, designated as S_{2a}, S_{4f}, S_{8i1}, S_{8i2} and S_{8j}. The long-range order parameter S is hereafter mentioned as order degree. Actually, Eq. 4.3 can be simplified to Eq. 4.2.

When S=1, the compound is totally ordered; when the probabilities P_A or P_B on the five nonequivalent sites equal the mole fractions X_A or X_B, respectively, the compound is totally disordered with S=0. When the order degree on the five nonequivalent sites (i.e. S_{2a}, S_{4f}, S_{8i1}, S_{8i2}, S_{8j}) is negative with $P_{B2a}<X_B$, $P_{A4f}<X_A$, $P_{A8i1}<X_A$, $P_{B8i2}<X_B$, or $P_{A8j}<X_A$, one deals with an anti-order degree. It should be noted that for a specific value of S, there could be many possible values of site occupancies, but in the present work, for a specific sigma compound, the site occupancy on every site changes within a certain range, which makes the above phenomenon unimportant. The calculated order degree is listed in Appendix A.

4.3.2. Influence of atomic order on enthalpy of formation

The calculation results of enthalpy of formation in Fig. 4.2 indicate that the sigma compound in a more ordered state holds a lower enthalpy of formation (more negative), i.e. the ordered structure is more stable than the less ordered ones at 0K.

Besides, it has been found out that the formation enthalpy of the sigma phase depends on both the volume difference and the electron configuration of its constitutive elements. Table 4.2 presents the volume difference between the two constitutive elements (A and B) and the enthalpy of formation of the $A_{66.7}B_{33.3}$ sigma phase in ordered and disordered states calculated by EMTO-CPA method at 0 K.

It indicates that for SMe and SMs-SMe categories, generally, the enthalpy of formation for compounds in both ordered and disordered states decreases with increasing the size difference between the two constitutive elements (except for V-Fe and V-Ni systems between which inversion is observed).

For LAs and LAs-LAe categories, the enthalpy of formation in disordered state for systems with large size difference (Re-Mn and Re-Cr systems), is positive, which indicates a less stable state. This behavior is related to the tendency of electron loss and gain of the two constituent elements. For LAs and LAs-LAe categories, atom A (atom A bears a larger size than atom B) tends to gain electrons (the obtained electrons will be termed as transferred electrons later) and generally, its atomic size in the crystal structure further increases [111]. The transferred electrons are expected to be less strongly bound to the nucleus of atom A as compared to the situation when they are bound to atom B, as normally the larger the atomic size is the weaker the bond between the nucleus and the valence electrons is. Thus for these categories, the larger the size difference between the constituent elements is the less stable the system is.

For Mo-Co and Mo-Mn systems belonging to LAs-SMe category, the enthalpy of formation in disordered state is also positive due to the influence of LAs factor and the size factor. Moreover, the enthalpy of formation for Mo-Co system is smaller than that for Mo-Mn system, due to the large effect of SMe factor (i.e. Atom A is with smaller number of valence electrons than atom B, which makes atom A tending to lose electrons [111]), which for Mo-Co system partially counteracts the effect of LAs factor on the tendency of electron loss or gain of the two constituent elements. For X-Al (X= Nb, Ta) category, by considering electron loss and gain, it behaves similarly as LAs-SMe category [111]. The strong effect of LAs factor and a relatively large size difference for Ta-Al system cause the enthalpy of formation in disordered state to be positive.

In addition, the calculation results for Cr-Fe and V-Fe systems as presented in Fig. 4.2 (b, e) show that at 0K when magnetism is accounted for compounds are more stable than those for which magnetism is not accounted for, especially for compounds with high content in Fe, which agrees with the experimental measurements [126,128].

Table 4.2 : Size difference between the constitutive elements (A and B) and enthalpy of formation (Hf) of the $A_{66.7}B_{33.3}$ sigma phase in both ordered and disordered states calculated

by EMTO-CPA method at 0 K. V_A and V_B are the molar volumes of element A and B in their hypothetic sigma phase structure from the CALPHAD assessments as presented in Section 5.

category	A-B	$(V_A-V_B)/V_A$	Hf, kJ/mol		category	A-B	$(V_A-V_B)/V_A$	Hf, kJ/mol	
			ordered	disordered				ordered	disordered
SMe	Cr-Mn	0.0147	-7.88	-1.37	SMs-SMe	Nb-Ir	0.2126	-69.05	-43.13
SMe	Cr-Fe	0.0588	-15.62	-5.04	LAs-SMe	Mo-Mn	0.2386	-13.08	13.68
SMe	V-Mn	0.1052	-16.67	-6.77	LAs-SMe	Mo-Co	0.3087	-29.83	4.27
SMe	Cr-Co	0.1053	-18.79	-7.79	LAs	Re-Mn	0.2006	-15.53	9.68
SMe	V-Fe	0.1453	-29.54	-13.90	LAs-LAe	Re-V	0.1065	-23.29	-13.54
SMe	V-Ni	0.1739	-27.26	-12.35	LAs-LAe	Ru-Cr	0.1298	-9.94	
SMe	V-Co	0.1876	-37.06	-19.56	LAs-LAe	Re-Cr	0.1887	-18.09	1.32
SMs-SMe	Mo-Re	0.0476	-11.33	-3.87	X-Al	Nb-Al	0.143	-39.69	-10.63
SMs-SMe	Mo-Os	0.0856	-28.18	-13.85	X-Al	Ta-Al	0.1454	-30.54	0.97

4.3.3. Influence of atomic order on bulk modulus

The bulk modulus of the sigma phase in the Cr-Co, Cr-Fe, Cr-Mn, Mo-Co, Mo-Fe, Mo-Mn, Mo-Os, Mo-Re, Nb-Al, Nb-Ir, Re-Cr, Re-Mn, Ta-Al, V-Co, V-Fe, V-Mn and V-Ni systems has been evaluated by fitting the Birch-Murnaghan equation of state [82,129]. The corresponding results are listed in Table 3. For most systems, sigma phase in ordered state has a large bulk modulus and a small molar volume, which indicates a strong binding between atoms and a compact structure, respectively. Only for Mo-Re system, sigma phase in ordered state has a large bulk modulus but a large molar volume, which indicates a strong binding between atoms but a loose structure, respectively.

Table 4.3 : EMTO_CPA calculated bulk modulus (B_0) and corresponding molar volume (Vm) of the $A_{66.7}B_{33.3}$ sigma phase in both ordered and disordered states at 0 K.

A_xB_y	B_0, Gpa		Vm, 10^{-6} m^3/mol	
	ordered	disordered	ordered	disordered
$Cr_{66.7}Co_{33.3}$	251.345	242.347	6.799	6.869
$Cr_{66.7}Fe_{33.3}$	257.813	249.913	6.801	6.855
$Cr_{66.7}Mn_{33.3}$	255.737	250.914	6.921	6.950
$V_{66.7}Co_{33.3}$	206.275	195.199	7.467	7.566
$V_{66.7}Fe_{33.3}$	212.796	203.138	7.491	7.562
$V_{66.7}Mn_{33.3}$	209.324	203.167	7.643	7.675
$V_{66.7}Ni_{33.3}$	195.071	183.190	7.588	7.700
$Mo_{66.7}Os_{33.3}$	283.269	274.343	9.478	9.491
$Mo_{66.7}Re_{33.3}$	273.023	268.617	9.644	9.614
$Nb_{66.7}Ir_{33.3}$	222.794	207.189	10.345	10.417
$Mo_{66.7}Co_{33.3}$	246.252	225.691	8.482	8.771
$Mo_{66.7}Mn_{33.3}$	250.635	232.845	8.633	8.808

$Re_{66.7}Mn_{33.3}$	330.679	311.432	8.310	8.539
$Re_{66.7}Cr_{33.3}$	319.851	306.083	8.493	8.706
$Re_{66.7}V_{33.3}$	296.475	288.341	8.794	8.994
$Nb_{66.7}Al_{33.3}$	151.447	136.561	10.493	10.870
$Ta_{66.7}Al_{33.3}$	169.286	152.224	10.505	10.944

4.3.4. Influence of atomic mixing on molar volume

Actually, for an ideal solid solution, the thermodynamic excess properties of mixing are zero and thus, the molar volume or the unit cell volume varies linearly with respect to the composition [130]. Sometimes, Retger's law [130–132] is used to describe this linearity for solid solution as well as Vegard's law [130], although Vegard's law is originally used to describe the linear relationship between lattice parameters and composition for solid solution. In the present work, we introduce linear volume-composition relationship for compound to describe the linear relationship between molar volume and composition.

It can be seen from the calculated volume results in Fig. 4.3 that the sigma compounds do not comply with linear volume-composition relationship and present positive or negative deviations, which is summarized in Table 4.4. For X-Al, SMe and SMs-SMe categories, the calculations in disordered state (i.e EMTO-CPA-x% in Fig. 4.3) present a negative deviation from linear volume-composition relationship. For LAs, LAs-LAe and LAs-SMe categories, a positive deviation is observed. Noteworthy, with respect to the sigma binary systems, the common characteristic for SMe and SMs-SMe categories is that atom A tends to lose electrons and for LAs and LAs-LAe categories it is that atom A tends to gain electrons. Thus it is expected that the deviation from LVCC law is related to the tendency of electron loss or gain between the two constituent elements. The tentative discussion is as follows.

For SMe and SMs-SMe categories, atom A tends to lose electrons (the number of lost electrons will be termed as transferred electrons hereafter) and generally, its atomic size in the crystal structure decreases (see Fig. 3.2 in Section 3). The transferred electrons are expected to be more strongly bound to the nucleus of atom B (which bears a smaller size than atom A) as compared to the situation when they are bound to atom A, as atom A bears a larger size than atom B and normally, the larger the atomic size, the weaker the bond between the nucleus and the valence electrons [133]. Hence the volume shrinks and therefore, for SMe and SMs-SMe categories, the calculations present a negative deviation from LVCC law.

Vice versa, for LAs and LAs-LAe categories, atom A tends to gain electrons (the number of obtained electrons will be termed as transferred electrons hereafter) and generally, its atomic size in the crystal structure increases (see Fig. 3.2 in Section 3). The transferred electrons are expected to be less strongly bound to the nucleus of atom B as compared to the situation when they are bound to atom A. Hence the volume swells and therefore, for LAs and LAs-LAe categories, the calculations present a positive deviation from LVCC law.

With regard to LAs-SMe category, the tendency of electron loss or gain between the two constituent elements is due to a competition of LAs (i.e. atom A bears larger total number of electron shells than atom B) and SMe (i.e. atom A bears smaller number of valence electrons than atom B) factors and the one for X-Al category behaves similarly as LAs-SMe category. Thus, for LAs-SMe category, the deviation from linear volume-composition relationship depends on the competition effect of LAs and SMe factors on electronegativity.

Table 4.4 : Deviation from linear volume-composition relationship of the binary sigma phase systems based on the EMTO-CPA volume calculations by using the experimental site occupancy and the hypothetical site occupancy of disordered states.

Categories	Systems				Deviation (exp.)		Deviation (x %)	
					Negative	Positive	Negative	Positive
X-Al	Nb-Al	Ta-Al			✔		✘	
SMe	Cr-Co	Cr-Fe	Cr-Mn		✔		✘	
	V-Co	V-Fe	V-Mn	V-Ni				
SMs-SMe	Nb-Ir	Mo-Re	Mo-Os		✔		✘	
LAs-SMe	Mo-Co	Mo-Mn			✔			✘
LAs	Re-Mn					✔		✘
LAs-LAe	Os-Cr	Re-Cr	Re-V	Ru-Cr		✔		✘

✔ results based on the volume calculations by using the experimental site occupancy (exp.)

✘ results based on the volume calculations by using the hypothetical site occupancy of disordered states (x %), which were mentioned as the deviation from LVCC law in the present work.

From the above, it is understandable why among all the systems studied by Crivello et al. [95] as mentioned in Section 4.1, for Hf-Re and Ta-Re (both belonging to the SMe category), and Nb-Re, Ti-Re and Zr-Re (all belonging to the SMs-SMe category) systems, the cell volumes of 32 stoichiometric end-member compounds present a negative deviation with respect to the composition, although the conducted calculations involve all stoichiometric end-member compounds even compounds in an anti-ordered state, for which the cell volume can be very large due to the size mismatch. The negative deviation is due to a significant effect of SMs (i.e. atom A bears smaller total number of electron shells than atom B) or SMe factors. As concerned to the studied W-Re (SMe category), Re-Os (SMe category), Mo-Re (SMs-SMe category) systems, no obvious negative deviation is observed since for these systems the effect of SMs or SMe factors is less remarkable.

It is worth mentioning that Fig. 4.3 and Table 4.4 show that for systems in LAs and LAs-LAe categories the calculation results based on the experimental site occupancy present positive deviation from linearity. The reason is that for these systems the atomic order presents a far away ordered state, which is close to disordered state or even an anti-order state (e.g. for Re-V systems, the order degree is -0.236, as referenced in Appendix A). This relatively disordered state for these systems is due to the competition between the size and electronic factors, i.e. considering the size factor, atom A prefers

occupying large CN sites (4f, $8i_1$, 8j), while considering LAs or LAe (i.e. Atom A is with larger number of valence electrons than atom B) factors, atom A prefers occupying small CN sites (2a, $8i_2$).

4.3.5. Influence of atomic order on molar volume

4.3.5.1. Influence of atomic order on molar volume based on experimental evidence

Besides, atomic mixing, the molar volume of the sigma phase is also influenced by the atomic order. Fig. 4.3 shows that for the calculation results in disordered state, a nearly linear relationship exists between the molar volume and the composition within the homogeneity range. Furthermore, we can expect that the nearly linear relationship exists when the order degree for the compounds is the same. Hence the prominent deviation from linearity among the experimental data presented in Fig. 4.3 is due to the effect of atomic order.

Fig. 4.4 (a, b) present the experimental results of the composition with respect to the order degree and the corresponding molar volume of the sigma phase. As the measured site occupancy is sensitive to alloy processing and instrumental factor, for a specific system, only the data measured by the same authors were selected to conduct the comparison. Noteworthy, for Cr-Fe and Mo-Re systems, the experimental results [10,103,117] indicate that the influence of atomic order on molar volume is very weak, less than the range of error and thus are not presented.

Fig. 4.4 (a) shows that with increasing the mole fraction of atom A, x(A), for Cr-Co, Ta-Al and V-Ni systems, the rate of change for order degree with respect to the composition (x(A)) decreases; for Re-Cr system, the rate of change increases; for V-Fe system, the rate of change is almost constant, where a linear relationship between order degree (S) and composition (x(A)) is presented

Fig. 4.4 (b) indicates that for all the systems, the molar volume increases with increasing mole fraction of atom A, x(A). This is due to the fact that A bears a larger size than B and thus with the content of atom A increasing, the molar volume naturally increases. On the other hand, we can see that the rate of change for molar volume with respect to composition (x(A)) is opposite to the one for order degree. With increasing the mole fraction of atom A, x(A), for Cr-Co, Ta-Al and V-Ni systems, the rate of change for molar volume with respect to the composition (x(A)) increases; for Re-Cr system, the rate of change decreases; for V-Fe system, the rate of change is almost constant.

Hence, we can expect that when a nearly linear relationship exists between the order degree and the composition, a nearly linear relationship exists between the molar volume and the composition as well, which is the case for V-Fe system as shown in Fig. 4.4. Besides, when the rate of change for order degree with respect to composition increases, the rate of change for molar volume with respect to composition decreases as

presented in Fig. 4.5. Above all, it can further indicate that with the order degree (S) increasing, the molar volume decreases.

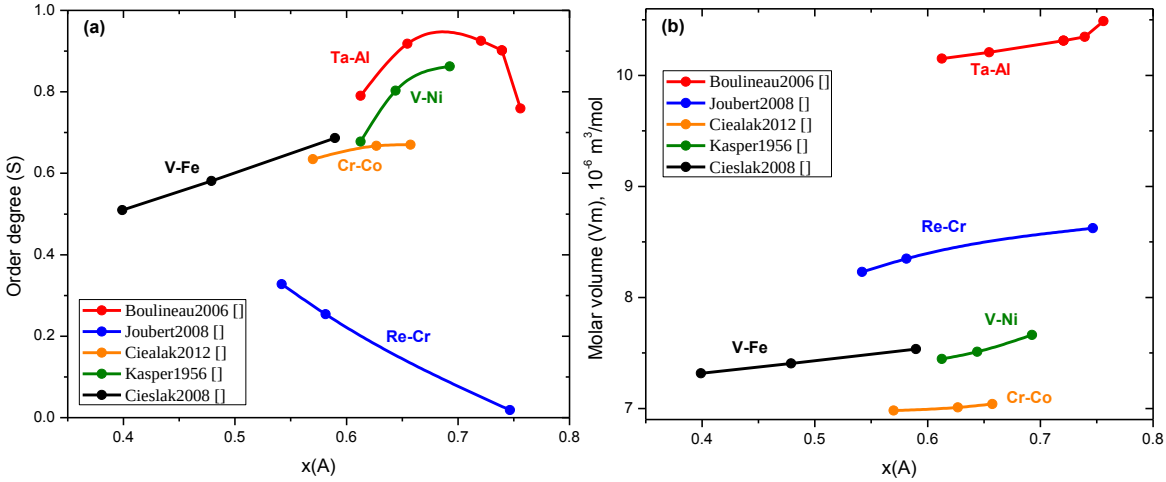

Figure 4.4 : Order degree (S) calculated from the experimental site occupancy and corresponding measured molar volume (Vm) of the sigma phase from the literature [9,10,96,114,119] with respect to composition.

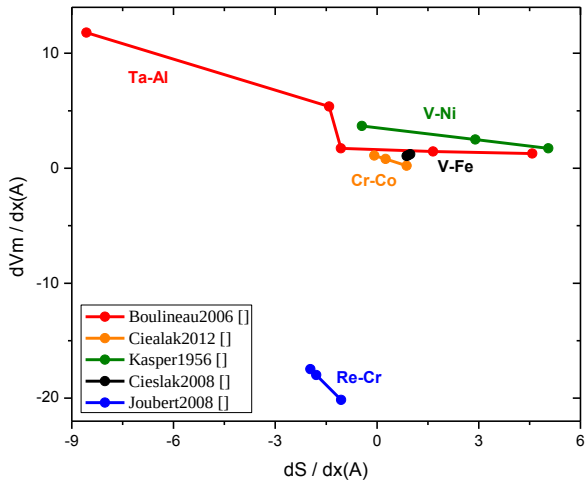

Figure 4.5 : Rate of change for molar volume with respect to composition, dVm/dx(A) based on experimental measurements from the literature [9,10,96,114,119] versus rate of change for order degree with respect to composition, dS/dx(A).

Notably, for V-Ni system, the ND measurements performed by Kasper et al. [96] make the measured volume less accurate, but the site occupancy more accurate as compared to the XRD determination method. For Ta-Al system, Boulineau et al. [119] also conducted the measurement on the compound with 60.3 at. % Ta as listed in Appendix A, but the measurement seems less accurate due to high amount of coexisting β phase (65 wt. %) in alloys [119] and was not presented in Fig. 4.4.

On the other hand, the calculation results in Fig. 4.3 show that for most binary systems, the compound with smaller order degree bears a larger molar volume, which agrees well with the experimental evidence as discussed above. Only for Mo-Re system, the calculated result is opposite, which will be discussed later in Section 4.3.5.2. It is

worth mentioning that for Re-V system, as the atomic order bears an anti-order degree (where S=-0.236 as shown in Appendix A) and causes a large size mismatch, the calculated molar volume with the atomic order based on experimental site occupancy is even larger than the one based on disordered state as presented in Fig. 4.3 (p).

4.3.5.2. Influence of atomic order on molar volume based on first-principles calculations

The calculation results in Fig. 4.3 indicate that the influence of atomic order on the molar volume of the sigma phase depends on systems. For Ta-Al system, the volume difference between the compound in ordered state and the one in disordered state is the largest among all the systems in Fig. 4.3, which indicates a large influence of atomic order on the molar volume.

To clarify why for different systems, the atomic order affects the molar volume differently, the volume difference ($\Delta Vm=V_{disorder}-V_{order}$) between disordered and ordered states of the A-B (V(A)>V(B)) binary sigma phase calculated by EMTO-CPA method is presented in Table 4.5. By comparing the volume difference among different systems as shown in Fig. 4.6, we can conclude that for A-B (V(A)>V(B)) binary sigma systems, with increasing (decreasing) the total number of electron shells of atom A (atom B) or decreasing (increasing) the number of valence electrons of atom A (atom B), the volume difference of the sigma compound increases. Thus we can deduce that SMe and LAs factors cause the volume difference to be large; LAe and SMs factors cause the volume difference to be small.

Table 4.5 : Molar volume difference ($\Delta Vm=V_{disorder}-V_{order}$) between disordered and ordered states of the A-B (V(A)>V(B)) binary sigma phase calculated by EMTO-CPA method.

X-Al	Nb-Al ($4d^4 5s^1$-$3s^2 3p^1$)	Ta-Al ($5d^3 6s^2$-)		
$\Delta Vm, 10^{-7}$ m^3/mol	3.80	4.37		
LAs	Re-Mn ($5d^5 6s^2$-$3d^5 4s^2$)			
$\Delta Vm, 10^{-7}$ m^3/mol	2.26			
SMe	V-Mn ($3d^3 4s^2$-$3d^5 4s^2$)	V-Fe (-$3d^6 4s^2$)	V-Co (-$3d^7 4s^2$)	V-Ni (-$3d^8 4s^2$)
$\Delta Vm, 10^{-7}$ m^3/mol	0.31	0.71	0.99	1.12
	Cr-Mn ($3d^5 4s^1$-$3d^5 4s^2$)	Cr-Fe (-$3d^6 4s^2$)	Cr-Co (-$3d^7 4s^2$)	
	0.28	0.55	0.70	
SMs-SMe	Nb-Ir ($4d^4 5s^1$-$5d^7 6s^2$)			
$\Delta Vm, 10^{-7}$ m^3/mol	0.73			
	Mo-Re ($4d^5 5s^1$-$5d^5 6s^2$)	Mo-Os (-$5d^6 6s^2$)		
	-0.30	0.12		
LAs-SMe	Mo-Mn ($4d^5 5s^1$-$3d^5 4s^2$)	Mo-Co (-$3d^7 4s^2$)		
$\Delta Vm, 10^{-7}$ m^3/mol	1.76	2.88		
LAs-LAe	Re-V ($5d^5 6s^2$-$3d^3 4s^2$)	Re-Cr (-$3d^5 4s^1$)		
$\Delta Vm, 10^{-7}$ m^3/mol	2.01	2.13		

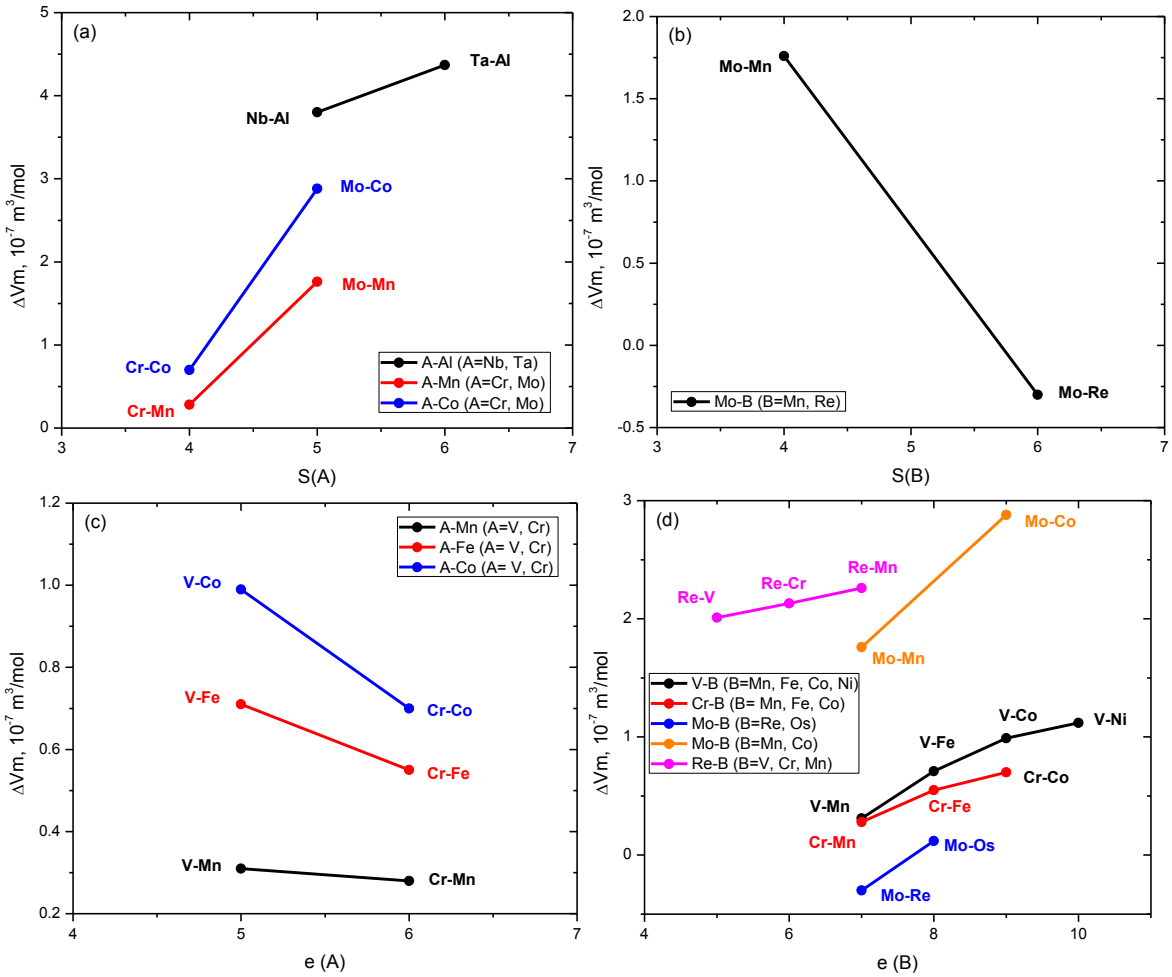

Figure 4.6 : Molar volume difference ($\Delta Vm=V_{disorder}-V_{order}$) between disordered and ordered states of the A-B (V(A)>V(B)) binary sigma phase calculated by EMTO-CPA method with respect to: (a) the total number of electron shells of element A, S (A); (b) the total number of electron shells of element B, S (B); (c) the number of valence electrons of element A, e (A); (d) the number of valence electrons of element B, e (B).

Table 4.5 and Fig. 4.6 show that for Mo-Re system (belonging to SMs-SMe category), the volume difference is negative. The reason should be that SMs factor plays a more important role than SMe factor and thus causes the volume difference to be small. Actually, Mo-Re system is the only case among all the stable sigma compounds for which the volume in ordered state is larger than the one in disordered state.

To support our arguments, the calculations for hypothetic Nb-W ($4d^45s^1$, $5d^46s^2$) and Au-W ($5d^{10}6s^1$, $5d^46s^2$) (belonging to SMs-SMe and LAe categories, respectively) sigma compounds were conducted. The volume difference for Nb-W compound is -0.496×10^{-7} m^3/mol ($\Delta Vm=V_{disorder}-V_{order}=10.959e^{-6}$ m^3/mol - $11.008e^{-6}$ m^3/mol) and for Au-W compound is -0.779×10^{-7} m^3/mol ($\Delta Vm= 10.726e^{-6}$ m^3/mol - $10.804e^{-6}$ m^3/mol), which all present negative value due to the effect of SMs or LAe factors.

4.4. Summary

In this chapter, the influence of atomic order on the enthalpy of formation, bulk modulus and molar volume of the binary sigma phase have been investigated by using EMTO-CPA calculations. The main conclusion can be drawn as follows:

1) At 0K, when in the ordered state, the sigma phase bears a low enthalpy of formation and a large bulk modulus. It indicates that at 0K, the ordered structure is more stable than the less ordered ones and also bears a strong binding between atoms. The formation enthalpy of the sigma phase depends on the size difference and the electron configuration between the two constitutive elements.

2) The A-B (V(A)>V(B)) binary sigma phase systems do not comply with linear volume-composition relationship and present negative or positive deviation. For SMe and SMs-SMe categories, atom A (which bears a larger size than atom B) tends to lose electrons and the compounds in disordered state present a negative deviation from linear volume-composition relationship; for LAs and LAs-LAe categories, atom A tends to gain electrons and the compounds in disordered state present a positive deviation. For LAs-SMe category, the tendency of electron loss or gain of the constituent elements and furthermore the deviation from linear volume-composition relationship are due to a competition between LAs (i.e. atom A bears larger total number of electron shells than atom B) and SMe (i.e. atom A bears smaller number of valence electrons than atom B) factors.

3) The influence of atomic order on the volume of the sigma phase depends on the electron configuration of the two constituent elements. That is SMe and LAs factors increase volume difference ($\Delta V=V_{disorder}-V_{order}$); LAe and SMs factors decrease volume difference.

5. CALPHAD modeling of molar volume of the sigma phase

The molar volume of the sigma phase has been modeled and evaluated at room temperature and atmospheric pressure for binary systems concerning 21 transition elements Au, Co, Cr, Fe, Ir, Mn, Mo, Nb, Ni, Os, Pd, Pt, Re, Rh, Ru, Ta, Tc, Ti, V, W and Zr as well as one main element Al by using the CALPHAD approach. The volume model proposed in this work expresses the molar volume of a non-stoichiometric sigma phase as a linear average of volumes of the constituting elements in their hypothetic sigma structure. Reasonable model parameters have been obtained and yield reasonable description of most experimental data. For comparison, volumes of the 21 transition elements in the sigma structure have been calculated by using first-principles calculations. The results illustrate a reasonable consistency with the assessed values.

5.1. Introduction

The sigma phase exists in 49 different binary alloy systems, five of which are not confirmed (i.e. Cr-Ni, Ta-V, Ti-Mn, Zr-Ir and Zr-Re). It has attracted great technological and theoretical study interests since the 1950s [11]. It deteriorates various properties of many technologically important materials, such as stainless and other high-alloy steels as well as Ni-based superalloys [8,9]. In this connection there are plenty of investigations on how to avoid or control the precipitation of the sigma phase, as well as its crystallographic property, physical properties, thermodynamic properties and phase stability (see e.g. [9] and references therein). In addition, multi-component phase diagrams involving the sigma phase have been measured experimentally and critically evaluated to build the corresponding thermodynamic databases by using the CALPHAD method [72–74].

As an important crystallographic property, molar volume has also been modeled and evaluated by the CALPHAD approach mostly for solution phases [134–138]. The evaluated volume databases act as an indispensable complement to the growing CALPHAD databases. Various CALPHAD models of molar volume have been recently reviewed by He et al. [79] for pure substances or solution phases including atmospheric pressure model, pressure model and Helmholtz energy model etc. At present, there are numerous measurements on the molar volume (or lattice parameters) of the sigma phase available by using XRD (X-ray diffraction) or ND (neutron diffraction) methods, which makes it capable of modelling the molar volume for the sigma phase.

At certain temperature and pressure, the molar volume of a disordered solution phase is dependent on the composition of this phase. For an intermetallic compound that is ordered or partially ordered, the volume is dependent on both the composition and the atomic order (i.e. atomic constituent distribution or site occupancy preference on nonequivalent sites of a crystal structure). For more details see Section 4.3.4 and 4.3.5. In order to obtain molar volumes of involved phases in a multi-component and multi-phase material system, phase equilibrium calculations based on thermodynamic databases should be performed first to determine the amounts and compositions or site occupancies of all constituting phases of the system. One can then calculate the molar volumes of individual phases as well as the overall volume of the system by taking a linear average of volumes of all phases with the phase amounts as the linear coefficients.

Databases for thermodynamics, diffusional mobility and molar volume are developed and integrated within the framework of the CALPHAD approach. This integration greatly facilitates the practice of materials design. However, a problem may arise that any updates of thermodynamic databases may predict different site occupancies for ordered or partially ordered compounds and thus it necessitates modifications of model parameters for volume data.

In the present chapter, a method to conveniently model molar volume of the sigma phase is proposed with the introduction of approximations that neglect the influence of atomic mixing (or composition) and atomic order on molar volume. With this method, the molar volumes of sigma phases at room temperature and atmospheric pressure involving 22 elements were systematically assessed by using the CALPHAD approach based on experimental data from the literature. The volumes of sigma phases in real alloy systems can be calculated conveniently by using our established volume database, which is independent of the thermodynamic data for the sigma phases.

5.2. Methodology

5.2.1. CALPHAD modeling

On the basis of the compound energy formalism (CEF) [76,139] in the CALPHAD approach, to facilitate modeling, the sigma phase is modeled using 3 sublattices (SL) with a stoichiometric ratio of 10:4:16, although the atoms in the unit cell occupy 5 nonequivalent sites and other SL models are proposed in the literature [9,120,139–142]. Noteworthy, with the linear model proposed in the present work, the SL model can be changed conveniently without modifying any assessed parameters (e.g. from 3SL to 5SL), as the assessed parameters represent the molar volume of pure elements in their hypothetic sigma phase structure.

For a binary non-stoichiometric sigma phase concerning elements A and B, the SL model adopted in the present work is $(A, B)_x(A, B)_y(A, B)_z$, with x, y and z equaling 10, 4 and 16, respectively. In CEF, the Gibbs free energies for all eight (2^3=8) stoichiometric end-member compounds (e.g. $A_xA_yA_z$, $A_xB_yA_z$) and the possible interaction energy have

to be assessed to represent the total Gibbs energy of the sigma phase. Similar to CEF, molar volumes of the stoichiometric end-member compounds, denoted V_{ijk}, are assessed to model the molar volume of the non-stoichiometric sigma phase as follows:

$$V_m = \sum y_i' y_j'' y_k''' V_{ijk} + V_m^E, \qquad (5.1)$$

where y', y'' and y''' are the site occupancies in the first, second and third SL, respectively. The subscripts i, j and k represent the constituent elements A or B. V_m^E is the excess molar volume. In the present work, molar volume means volume per mole of atoms instead of per mole of formula units containing 30 atoms in the unit cell.

It is difficult to evaluate all eight values for V_{ijk} as some of the compounds are metastable or non-stable. The number of the end-member compounds increases sharply as n^3 when describing a n-component sigma phase. In the following we propose a convenient way to avoid the difficulty:

$$V_{ijk} = \frac{x}{x+y+z} V_i + \frac{y}{x+y+z} V_j + \frac{z}{x+y+z} V_k + V_{ijk}^E, \qquad (5.2)$$

where V_i, V_j and V_k represent molar volumes of pure elements in the hypothetic sigma structure, either V_A or V_B. V_{ijk}^E is the deviation from the linear combination for pure elements. When there is no experimental evidence, V_{ijk}^E is set to zero. It is then possible to calculate all values for V_{ijk} by using only V_A and V_B.

As shown in Appendix B, when both V_m^E and V_{ijk}^E equal zero, meaning that a linear relation exists among components or compounds, the molar volume of the non-stoichiometric sigma phase is:

$$V_{\mathrm{m}} = x_A V_A + x_B V_B, \qquad (5.3)$$

which means that V_m is a function of mole fraction (x_A and x_B) of the constituting elements (A or B) and independent of site fractions in each SL. This method can be extended beyond binary systems and reduces the n^3 unknowns for end-member compounds to n values for n elements for a n-component sigma phase. Another practical significance is that the development of volume database can be separated from thermodynamic databases since the volume is dependent only on mole fraction instead of site occupancy.

For the binary sigma phases concerning transition elements Au, Co, Cr, Fe, Ir, Mn, Mo, Nb, Ni, Os, Pd, Pt, Re, Rh, Ru, Ta, Tc, Ti, V, W and Zr, we performed a systematic evaluation of the volume data and found that V_m^E and V_{ijk}^E are indeed negligible which indicate that the linearity between the molar volume and composition of the constituting elements exists.

5.2.2. First-principles calculations

In Eqs. 5.2 and 5.3, molar volumes of pure elements in the hypothetic sigma structure are used. These data can be evaluated from the experimental data as fitting model parameters. On the other hand, it is not difficult to obtain these values from first-principles calculations. In the present chapter, we compare data from both methods and

try to reveal the physical significance of the evaluated parameters in order to make reliable predictions for multi-component systems.

First-principles calculations were performed using the plane wave method with projector augmented wave (PAW) pseudo-potentials [25], as implemented in the Vienna ab initio simulation package (VASP) [26]. We used the exchange-correlation functional within the generalized gradient approximation (GGA) as parameterized by Perdew and Wang [108]. The k-point meshes (8×8×15) for Brillouin zone sampling were constructed using the Monkhorst–Pack scheme [61]. A large plane-wave cutoff energy of 400 eV was used. Spin-polarized calculations were conducted. To facilitate the calculations, ZenGen script-tool was used to automatically generate input files for VASP calculations [109].

5.3. Results and discussion

Parameters were optimized by using the PARROT module [143] in the Thermo-Calc software package [88,89]. Every end-member was supplied with a volume corresponding with the composition average of the element volumes in the sigma phase structure. All the element volumes in the sigma phase structure served as assessing parameters and were optimized simultaneously considering all the systems. By considering experimental conditions and sample quality, different weights were assigned to experimental data from the literature during the assessment. Experimental data were mostly lattice parameters measured by X-ray or neutron diffraction and were converted to molar volumes in the present work. Some experimental data measured by X-ray diffraction in the 1950-1960s with unit of kX were converted to absolute length [136,144,145]. Parameters that can best represent the experimental data were obtained and listed in Table 5.1.

Table 5.1 : Assessed molar volumes of pure elements in the sigma phase structure compared with the first-principles calculation results.

	V_m, 10^{-6} m^3/mol			V_m, 10^{-6} m^3/mol			V_m, 10^{-6} m^3/mol	
Element	CALPHAD	First-principles	Element	CALPHAD	First-principles	Element	CALPHAD	First-principles
Au	10.100	11.248	Nb	10.770	11.313*	Ru	8.400	8.573*
Co	6.540	6.658*	Ni	6.650	6.689*	Ta	10.800	11.127*
Cr	7.310	7.003*	Os	8.650	8.922*	Tc	8.770	8.842*
Fe	6.880	7.137*	Pd	9.100	9.514	Ti	--	10.298*
Ir	8.480	9.128	Pt	9.000	9.808	V	8.050	8.109*
Mn	7.203	6.446*	Re	9.010	9.121*	W	9.600	9.782*
Mo	9.460	9.585*	Rh	8.200	8.808	Zr	--	13.775*

* Data from Crivello et al.[95] and confirmed in the present work.

Assessed molar volumes of the 21 transition elements in the sigma phase structure compared with the first-principles calculations are shown in Fig. 5.1. It is obvious that the molar volumes of 4d and 5d transition elements decrease and then increase with increasing atomic number. It should be mentioned that Cu-, and Hf- related systems are not evaluated in the present work since the experimental data are mostly for ternaries

(e.g. Al-Cu-Nb, Cu-Ga-Nb and Hf-Mo-Ru). The assessment results are discussed below. For the convenience of comparison and discussion, all assessed binary systems are grouped 11 categories (Section 5.3.2 to 5.3.12).

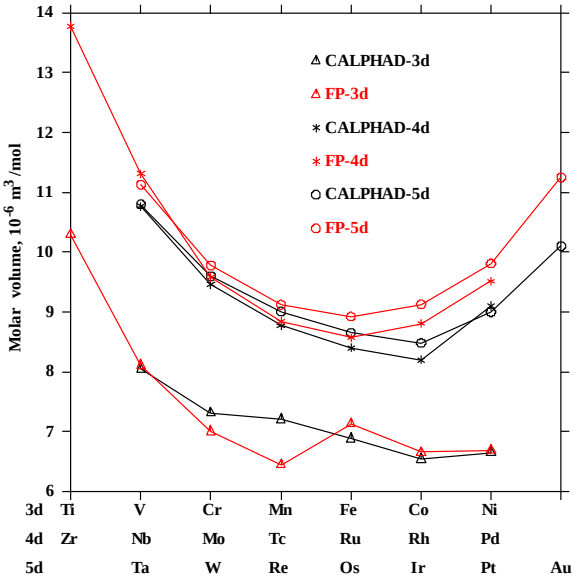

Figure 5.1 : Assessed molar volumes of transition elements in the sigma phase structure compared with the first-principles calculation (FP) results.

5.3.1. General discussion

Greenfield and Beck [146] measured the lattice parameters of sigma phases in many binary systems, i.e. Cr-Re, Cr-Ru, Mo-Re, Mo-Ru, Nb-Pd, Nb-Pt, Nb-Re, Nb-Rh, Pt-Ta, Re-Ta, Re-W and Rh-Ta. They mentioned that the analyzed compositions were not accurate. Moreover, alloys with different compositions were prepared for each binary system but it is not clear which alloys were used for X-ray diffraction measurements. For systems (Mo-Ru, Nb-Pd, Nb-Pt, Nb-Re, Re-Ta and Rh-Ta) for which sigma phases coexisted with other phases, the compositions of the sigma phases were estimated by Greenfield and Beck. For systems (Mo-Re, Pt-Ta and Re-W) with several alloys consisting of single sigma phase, among the compositions of alloys determined by X-ray diffraction those that best fit the assessment were chosen. The measured data were mostly accepted in the present work except for those Re-related systems (Cr-Re, Mo-Re, Nb-Re, Re-Ta and Re-W) that are lower than the assessed values. It should be noted that data with unknown units in Greenfield and Beck's work were assumed to be in kX unit, although both kX and Å were used by Greenfield and Beck.

Knapton [147] measured the lattice parameters of several transition-metal sigma phases, namely Cr-Os, Ir-Mo, Ir-Nb, Ir-Ta, Ir-W, Mo-Os, Nb-Os, Nb-Re, Os-Ta, Os-W and Re-Ta. Most of the data had a relatively large error bar. All the examined samples were as-melted alloys except that the samples of the W-related systems (Ir-W and Os-W) that were annealed at 1000 ℃. The data of the W-related systems are rather higher than the assessed values. According to the Ir-W phase diagram, the temperature range for the

precipitation of the sigma phase if from 1802 to 2535 ℃ [148]. However the sigma phase was detected by Knapton after annealing at 1000 ℃ for 7 days. It may not reach equilibrium due to the short annealing time at such a relatively low temperature. For Os-W system, the composition of the sigma phase far exceeded its homogeneity range that span from 63.41 to 79.73 at.% W according to the phase diagram [149]. The data from these two systems were not considered in the present assessment. For the as-melted alloys, most of the data are in good agreement with the assessment except for the Cr-Os, Os-Ta and Re-Ta systems. For Cr-Os system, the sigma phase coexisted with the Cr solution phase and the composition of the sigma phase was tentatively given according to the homogeneity range of the sigma phase spanning from 64.98 to 69.18 at.% Cr based on the phase diagram [150]. However, the value is rather lower than the assessed one. For Os-Ta and Re-Ta systems, the experimental data with the compositions far beyond the homogeneity range of the sigma phase of 55.27-77.90 at.% Ta [151] and 58.00-59.08 at.% Re [152,153], respectively based on the phase diagrams, were not used in the assessment either. For Ir-Mo and Nb-Re systems, the sigma phases coexisted with other phases. The compositions of the sigma phases were determined in the present work based on the phase diagrams (homogeneity range of the sigma phase in Ir-Mo system: 28.17 at.% Ir [154]; Nb-Re system: 42.86-43.81 at.% Nb [155]). The data for those two systems are in good agreement with the assessment.

Bucher et al. [156] determined lattice parameters of sigma phases in the following systems: Ir-Mo, Ir-Nb, Ir-Ta, Ir-W, Mo-Os, Mo-Re, Mo-Ru, Nb-Os, Nb-Pt, Nb-Re, Nb-Rh, Os-Ta, Os-W, Pt-Ta, Re-Ta, Re-W, Rh-Ta and Ru-W. Most of these data are in good agreement with the assessment and except for Ir the purity of the elements was listed: Mo: 99.6 wt.%, Nb: 98.6 wt.%, Os: 99.9 wt.%, Pd: 99.9 wt.%, Pt: 99.99 wt.%, Re: 99.9 wt.%, Rh: 99.8 wt.%, Ru: 99.95 wt.%, Ta: 98.6 wt.%, W: 99.6 wt.%. Exceptions are the data for Ir-Nb, Ir-W and Nb-Os sigma phases. For Nb-Re and Re-Ta systems, the compositions of the sigma phases coexisting with other phases were not given. Fortunately, the homogeneity ranges of the sigma phases in these two systems were narrow and in the present work the compositions were given based on the phase diagrams, i.e. homogeneity range of the sigma phase in Nb-Re: 45.68-46.77 at.% Nb [157], Re-Ta: 58.00-59.08 at.% Re [152,153].

Recently, Joubert [9] performed the lattice parameter determination for Al-Nb, Co-Mo, Cr-Os, Cr-Re, Cr-Ru, Fe-Mo, Fe-Re, Nb-Pt, Nb-Re, Pd-Ta, Re-V, Rh-Ta and Ru-W sigma phases. In general, these measurements are accurate and data agree well with the assessment.

5.3.2. Cr-X (X= Co, Ni, Os, Re, Ru, Tc) (Fig. 5.2)

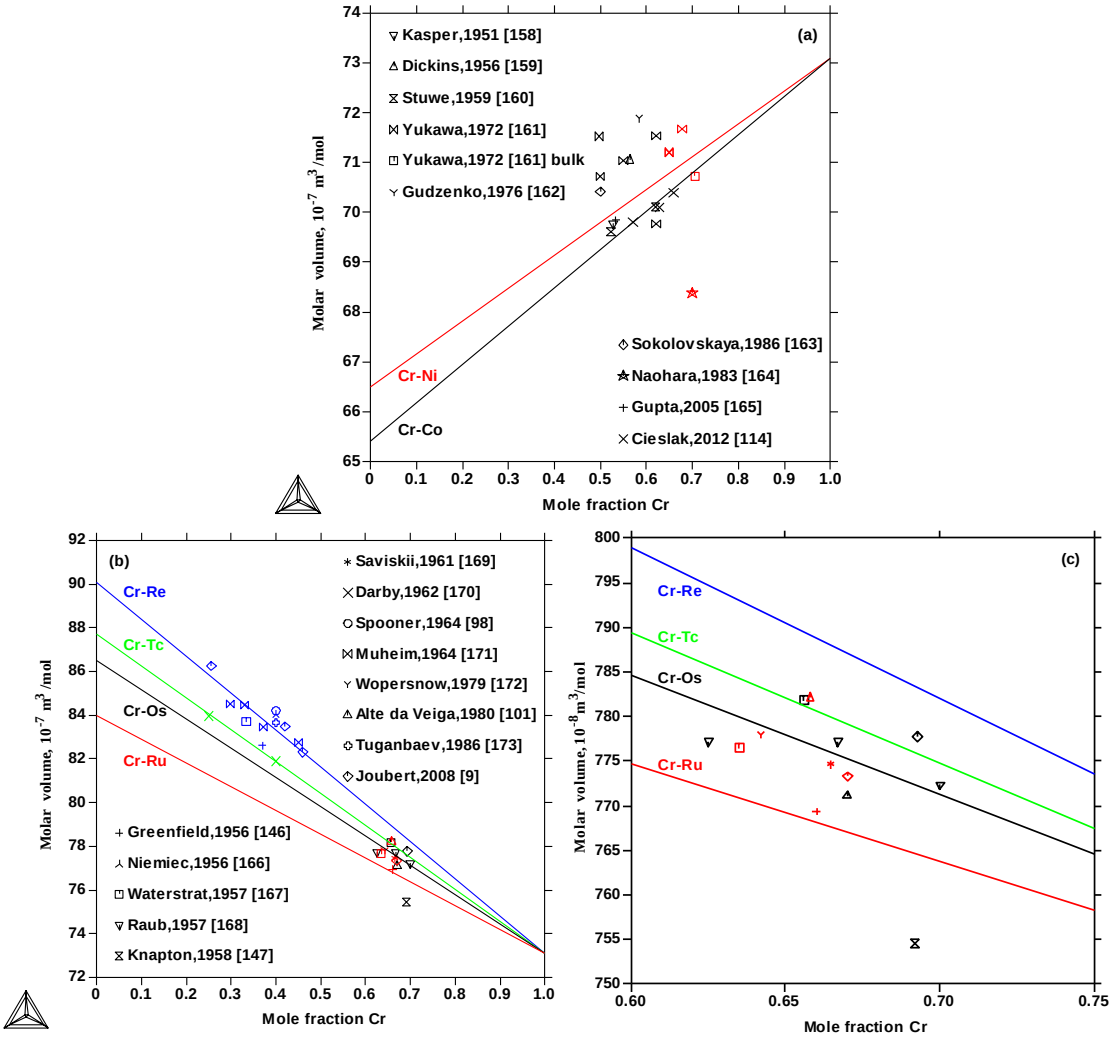

Figure 5.2 : The calculated molar volumes of Cr-X (X=Co, Ni, Os, Re, Ru, Tc) sigma phases compared with the experimental data [9,98,101,114,146,147,158–173]. (c) is the enlarged part of (b). Note that for one sigma phase, the same color is assigned to both the calculated line and the experimental data.

For Cr-Co system, in the work by Dickins et al. [159], the experiment detail was not presented. Data from Yukawa et al. [161] were scattered which will be discussed together with Cr-Ni system in the following. The lattice parameter of the sigma phase for sample rapidly cooled from the liquid state was determined by Gudzenko and Polesya [162], but the measured value was far higher than the assessed one. Sokolovskaya et al. [163] determined the lattice parameter of the sigma phase CrCo (i.e. 50 at.% Cr). However, the composition is doubtful as the phase diagram given by Sokolovskaya et al. showed that the actual composition of the examined sigma phase was about 57 or 60 at.% Cr. The present assessment did not use the aforementioned data, but based on the most recent measurements by Gupta [165], Cieślak et al. [114] and agrees with earlier data by Kasper et al. [158] and Stüwe [160].

For Cr-Ni system, the existence of the sigma phase was indicated in only a few reports due to the difficulty in the sigma phase formation and only a few experimental data were available. Yukawa et al. [161] investigated the formation of particulate sigma phases in Cr-Co, Cr-Fe and Cr-Ni systems by vaporizing fine alloy particles and determined the lattice parameters of the sigma phases. Most of these data are scattered or inconsistent with the assessment especially in Cr-Co and Cr-Ni systems. The Cr-Fe system will be discussed together with Fe-X systems. For Cr-Co and Cr-Ni systems, the compositions of the particulate sigma phases were given according to the phase diagrams constructed by Yukawa et al. Only the Cr-Ni alloy with content of 70.0 at.% Cr examined at 1250 ℃ by using the high-temperature X-ray diffraction technique was a bulk alloy. For comparison the high-temperature value is plotted together with the room temperature data in Fig. 5.2 (a) and it is doubtable that the high-temperature value is lower than the data examined at room temperature. All the data determined by Yukawa et al. were not considered in the assessment. Naohara and Shinohara [164] studied the effect of the surface layer on the sigma phase formation in Cr-Ni system. The X-ray diffraction was conducted on the same sample in three conditions, i.e. as-cast, as-quenched (aged at 923 K for 165 h followed by water quenching) and slightly polished successively. An oxidation layer of Cr_2O_3 was found after water quenching. The sigma phase was only formed at the interface between Cr_2O_3 and the matrix phases (ferrite and austenite). The lattice parameter was not calculated in Naohara and Shinohara's investigation. Based on the X-ray diffraction data in their study, the lattice parameter was calculated afterwards and quoted in the Power Diffraction File (PDF). However the calculated result is far lower than the assessed one.

For Cr-Ru system, the value determined by Alte da Veiga et al. [101] is too high. The majority of data for Cr-Os, Cr-Ru and Cr-Tc agree reasonably with a margin of error of about 1% and were adopted in the assessment.

For Cr-Re system, the value determined by Joubert [9] at 31 at.% Cr is higher than the assessed one, which might be due to the influence of the relatively high amount of coexisting hcp phase (10 wt.%). The other two data from Joubert are consistent with data reported by Muheim and Müller [171] and Tuganbaev et al. [173], which were used in the assessment.

5.3.3. Fe-X (X= Cr, Mo, Re, Tc) (Fig. 5.3)

For Fe-X systems, the agreement between different data is fairly good except for some data in Fe-Cr and Fe-Re systems.

For Fe-Cr system, the lattice parameters were measured by Yukawa et al. [161]. The compositions of the particulate sigma phase were given according to the phase diagram constructed by Yukawa et al. with the homogeneity range of the sigma phase 50.00-56.84 at.% Fe. Only the alloy with content of 50.0 at.% Cr was a bulk alloy. As can be seen from Fig 5.3, all the measured values by Yukawa et al. especially that for the bulk alloy are higher than both the assessed values and other experimental ones.

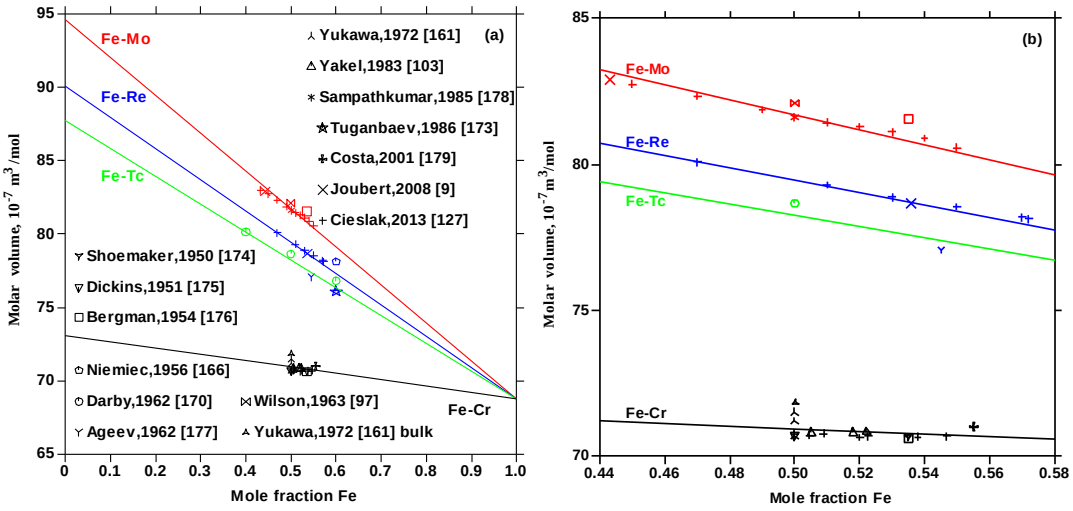

Figure 5.3 : The calculated molar volumes of Fe-X (X=Cr, Mo, Re, Tc) sigma phases compared with the experimental data [9,97,103,127,161,166,170,173–179]. (b) is the enlarged part of (a). Note that for one sigma phase, the same color is assigned to both the calculated line and the experimental data.

For Fe-Re system, the determined lattice parameter by Tuganbaev et al. [173] was not accurate with relatively large error bar (+0.0452 Å and -0.0387 Å in a, ±0.0414 Å in c). As for the work by Ageev and Schekhtman [177], the sample purity and error bar of the lattice parameter were not specified. These two sets of data are much lower than other data and were not adopted in the assessment.

5.3.4. Ir-X (X= Mo, Nb, Ta, W) (Fig. 5.4)

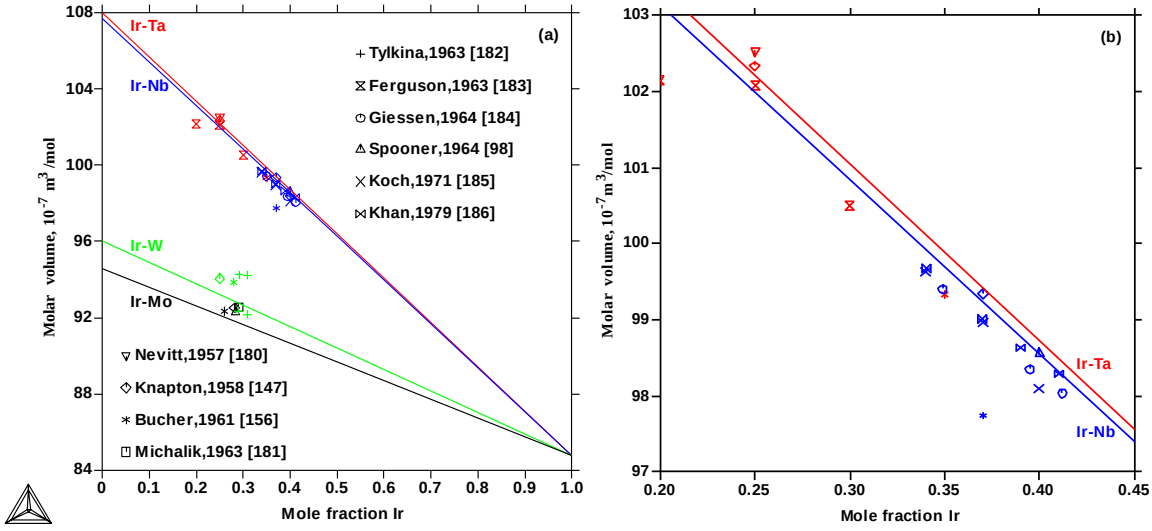

Figure 5.4 : The calculated molar volumes of Ir-X (X=Mo, Nb, Ta, W) sigma phases compared with the experimental data [98,147,156,180–186]. (b) is the enlarged part of (a). Note that for one sigma phase, the same color is assigned to both the calculated line and the experimental data.

Tylkina et al. [182] determined the lattice parameters of the sigma phase in Ir-W system. Among the four tested alloys annealed at 2000 ℃, only the alloy with a composition of 29.08 at.% Ir was single sigma phase. For other three alloys, due to the existence of another coexisting phase, the compositions of the sigma phase were not certain. According to the phase diagram of Ir-W system constructed by Tylkina et al., the homogeneity range of the sigma phase at 2000 ℃ was about 28.98-30.88 at.% Ir. The compositions of the sigma phase in those three alloys presented in Fig. 5.4 were given according to the phase diagram.

5.3.5. Mn-X (X=Cr, Mo, Re, Tc, Ti and V) (Fig. 5.5)

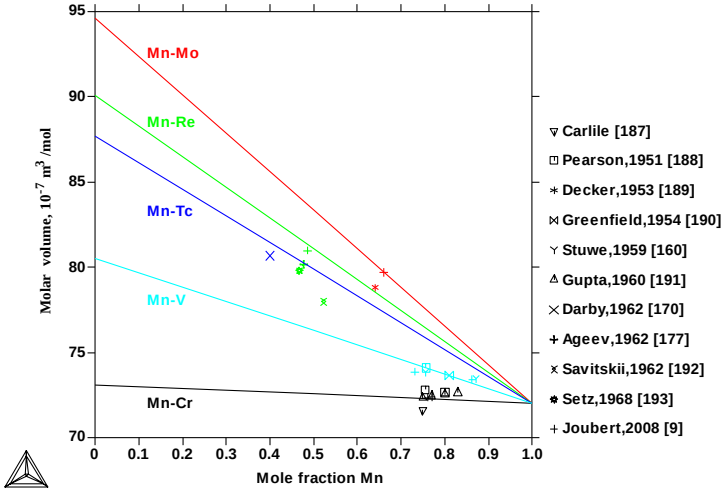

Figure 5.5 : The calculated molar volumes of Mn-X (X=Cr, Mo, Re, Tc, Ti and V) sigma phase compared with the experimental data [9,160,170,177,187–193]. Note that for one sigma phase, the same color is assigned to both the calculated line and the experimental data.

During the assessments, recent data from Joubert [9] are given more considerations. The agreement between the different data is fairly good. For Ti-Mn system, the sigma phase was reported (Vm=7.19×10^{-6} m^3/mol at around 48.6 at.% Mn) [194] but not confirmed. The present work does not attempt to assess the volume of Mn-Ti system, but present the first-principles values with other elements in Fig. 5.1 and Table 5.1.

5.3.6. Mo-X (X= Co, Os, Ru, Tc) (Fig. 5.6)

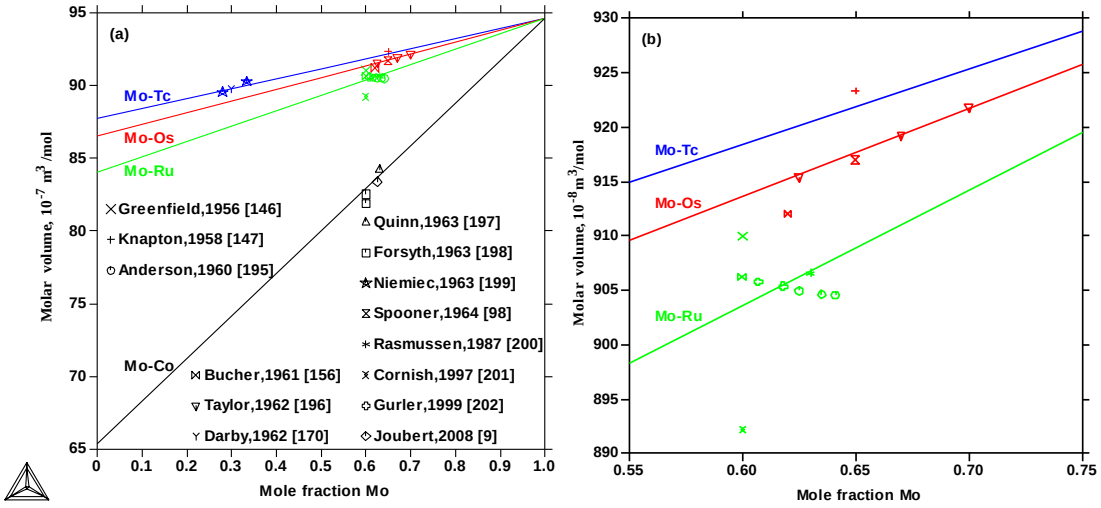

Figure 5.6 : The calculated molar volumes of Mo-X (X= Co, Os, Ru, Tc) sigma phases compared with the experimental data [9,98,146,147,156,170,195–202]. (b) is the enlarged part of (a). Note that for one sigma phase, the same color is assigned to both the calculated line and the experimental data.

For Mo-Ru system, among the three alloys examined by Anderson and Hume-Rothery [195], the one with the highest Mo content was a two-phase structure. The composition of the sigma phase was given based on the phase diagram constructed by Anderson and Hume-Rothery, i.e. the homogeneity range of the sigma phase in Mo-Ru system is 62.28-64.11 at.% Mo. Cornish and Pratt [201] determined the lattice parameter of the sigma phase. As mentioned in their investigation, the morphology of the sigma phase detected by X-ray diffraction was too fine and the examined result was inaccurate. For other Mo-X systems, the assessment is in accordance with the experimental data.

5.3.7. Nb-X (X=Al, Os, Pd, Pt, Re, Rh) (Fig. 5.7)

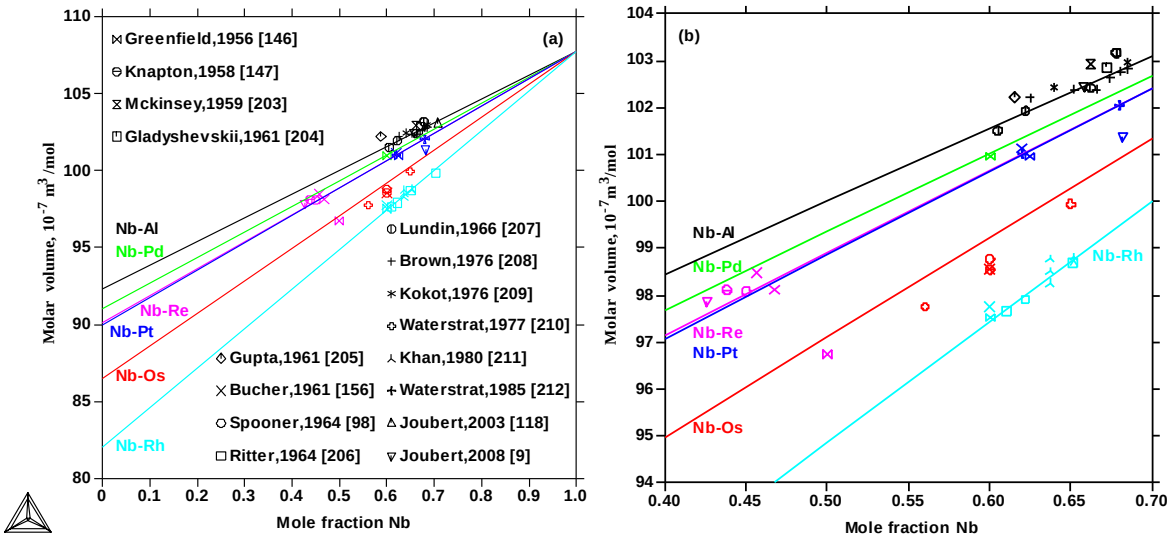

Figure 5.7 : The calculated molar volumes of Nb-X (X= Al, Os, Pd, Pt, Re, Rh) sigma phases compared with the experimental data [9,98,118,146,147,156,203–212]. (b) is the enlarged part of (a). Note that for one sigma phase, the same color is assigned to both the calculated line and the experimental data.

Although Al is not a transition element and not in the scope of this work, the successful assessment for Nb-Al system gives a value of 9.230×10^{-6} m^3/mol for Al in comparison with the corresponding first-principles result of 10.245×10^{-6} m^3/mol.

For Nb-Re system, the experimental values from Greenfield and Beck [146] and Tylkina et al. [213] (6.240×10^{-6} m^3/mol) are too low comparing with other data and was not considered in the assessment. For the majority of the experimental data for Nb-X systems, the agreement with the assessment is acceptable.

5.3.8. Re-X (X= Mo, Ta, W) (Fig. 5.8)

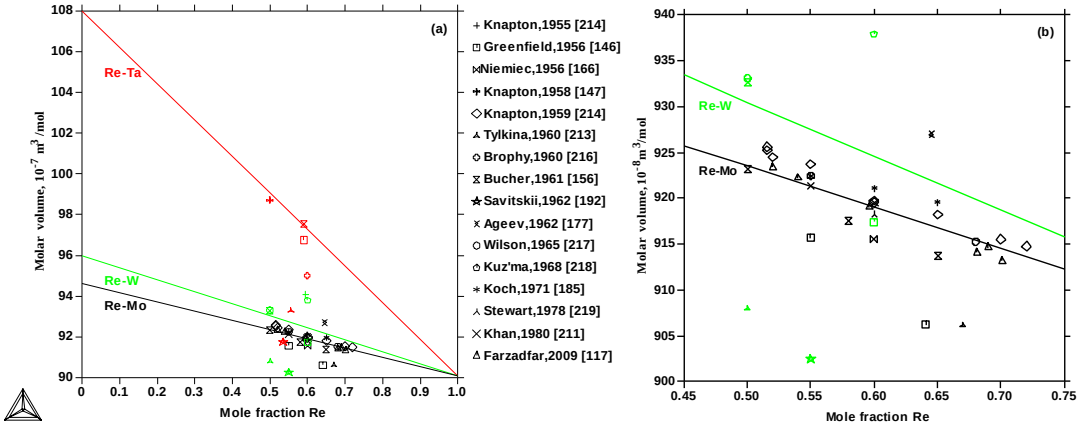

Figure 5.8 : The calculated molar volumes of Re-X (X=Mo, Ta, W) sigma phases compared with the experimental data [117,146,147,156,166,177,185,192,211,213–219]. (b) is the enlarged part of (a). Note that for one sigma phase, the same color is assigned to both the calculated line and the experimental data.

For Re-Ta system, the sigma phase examined using X-ray diffraction by Brophy et al. [216] coexisted with a small quantity of tantalum solid solution or χ phase, which is the possible reason for large deviation from the assessed one.

For Re-W system, the experimental condition was not clear in the work by Knapton [215] and Kuz'ma et al. [218] and their data were not used in the assessment. The composition of the sample examined by Tylkina et al. [213] was quoted in the PDF and that by Savitskii and Tylkina [192] was designated in the present work in agreement with the phase diagram [192]. It is worth mentioning that most data determined by Tylkina et al. and Savitskii and Tylkina for this group of Re-X systems are far lower than other measurements, therefore their data were not considered in the assessment.

5.3.9. Ta-X (X= Al, Au, Os, Pd, Pt, Rh) (Fig. 5.9)

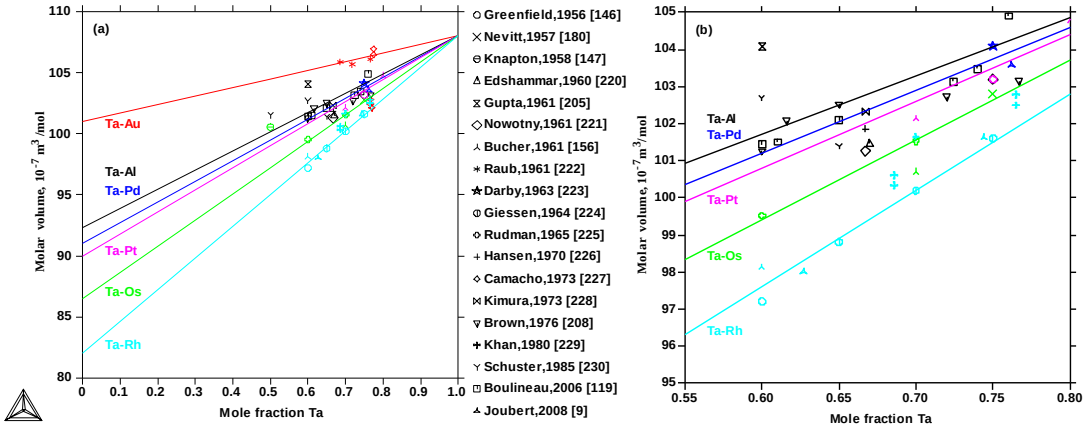

Figure 5.9 : The calculated molar volumes of Ta-X (X=Al, Au, Os, Pd, Pt, Rh) sigma phases compared with the experimental data [9,119,146,147,156,180,205,208,220–230]. (b) is the enlarged part of (a). Note that for one sigma phase, the same color is assigned to both the calculated line and the experimental data.

For Ta-Al system, the measured value from Gupta [205] is higher than other experimental data probably due to a suspicious composition. After heat treatment of the sample with composition of 60 at.% Ta at 1250 ℃ for 10 days, the sigma phase is formed accompanied with 25% of unknown phase [205], whereas the homogeneity range of the sigma phase at 1250 ℃ in Ta-Al system is 59.48-79.45 at.% Ta [231]. The sample $Ta_{40}Al_{60}$ used by Schuster [230] was regarded to be wrong in composition according to the phase diagram presented in Schuster's work with a homogeneity range of about 50-75 at.% Ta for the sigma phase. It was thus assigned to the sigma phase with a composition of 60 at.% Ta. However, the data (including the value with composition of $Ta_{50}Al_{50}$) are still higher than the assessed results. In addition, the source of value for $Ta_{65}Al_{35}$ is unclear as it may not be determined by Schuster.

For Ta-Au system, the samples from Raub et al. [222] with the overall composition of 71.8 and 76.6 at.% Ta were of double-phase structure and only that with the composition of 68.6 at.% Ta was single sigma phase, which was set a high weight in the assessment. Data determined by Camacho [227] were too scattered and were not used in the assessment.

For Ta-Rh system, the data examined by Khan et al. [229] were not considered in the present work due to coexisting phases in the samples.

Several researchers [232–234] studied the structure of β-Ta, one of the two unary sigma phases, the other one being β-U. Arakcheeva et al. [233] pointed out that the crystal structure of β-Ta exhibits all the main features of the sigma phase but with a symmetry reduced from $P4_2/mnm$ to $P\bar{4}2_1m$. The molar volume of the β-Ta calculated from their measured lattice parameter (a=10.211 Å, c=5.3064 Å [233]) is 11.106×10^{-6} m^3/mol, which is slightly higher than that of the present assessment but close to the first-principles result (see Table 5.1).

5.3.10. V-X (X= Co, Fe, Ni, Re, Ta) (Fig. 5.10)

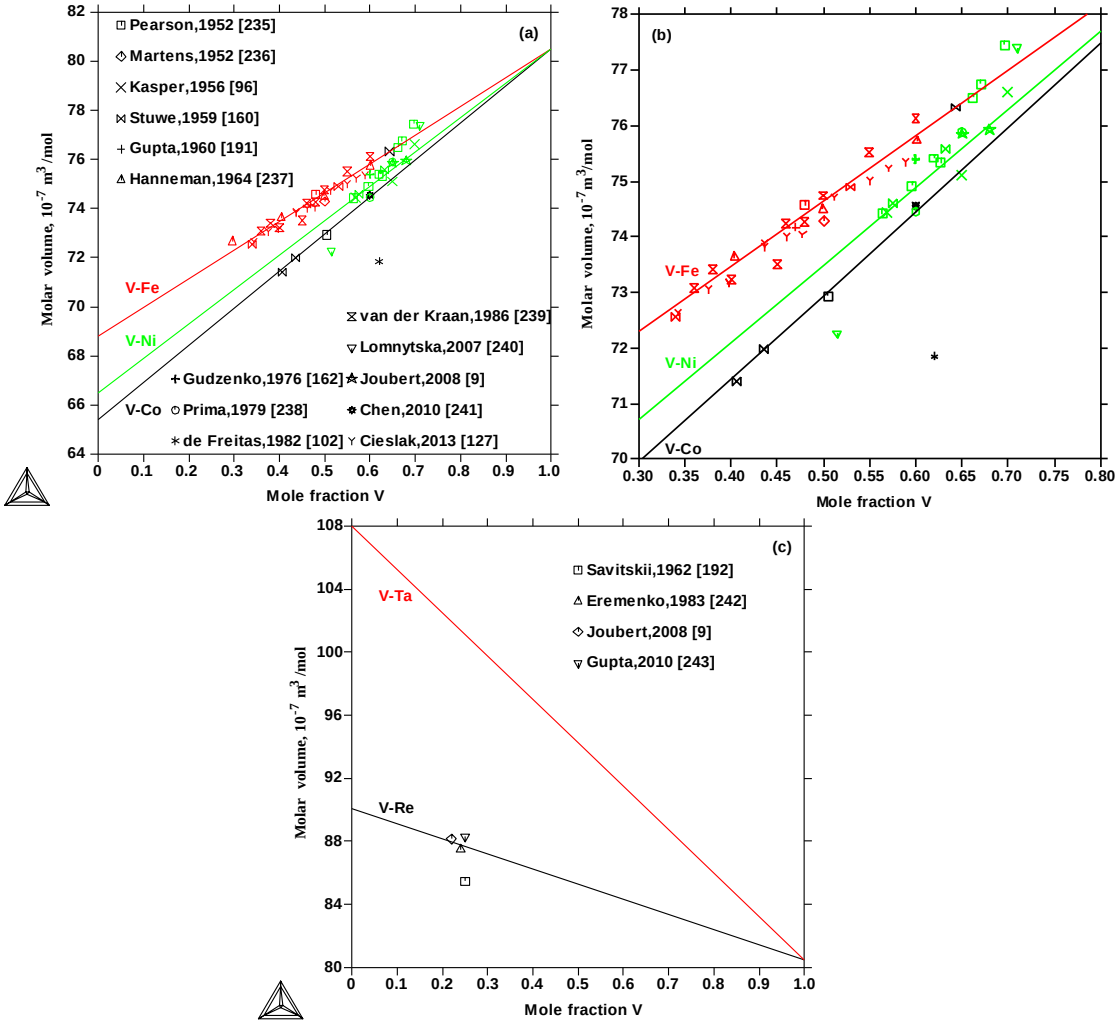

Figure 5.10 : The calculated molar volumes of V-X (X=Co, Fe, Ni, Re, Ta) sigma phases compared with the experimental data [9,96,102,127,160,162,191,192,235–243]. (b) is the enlarged part of (a). Note that for one sigma phase, the same color is assigned to both the calculated line and the experimental data.

For V-Co system, the measured value for the highest V content from Stüwe [160] is higher than the assessed data, which agree well with Stüwe's low composition values, data from Pearson and Christian [235] and the most recent data by Chen et al. [241] except one value by de Freitas et al. [102]

For V-Fe system illustrated in Fig. 5.10 (a) and (b), all experimental data and the assessment show a good agreement.

For V-Ni system, the experimental data from Pearson and Christian [235] and Lomnytska and Pavliv [240] show different trend from the present assessment that fits well with other measurements especially recent data by Joubert [9].

For V-Re system, the value obtained by Savitskii and Tylkina [192] is lower than other data and was not used in the present assessment.

For V-Ta system, Rostoker and Yamamoto [244] and Eremenko et al. [245] both detected a tetragonal phase as a member of the sigma phase family with molar volume of 6.65×10^{-6} m^3/mol (a=6.117 Å, c=8.851 Å) at about 50 at.% V and 6.886×10^{-6} m^3/mol (a= 6.163 Å, c= 8.868 Å) at about 68 at.% V, respectively (both fall outside Fig. 5.10 (c)). However, in the discussion part following Rostoker and Yamamoto's paper, Greenfield among many other researchers pointed out that the X-ray diffraction data obtained by Rostoker and Yamamoto in no way could support that the detected phase was isomorphous with the sigma phase. Eremenko et al. stated that in V-Ta system, the sigma phase precipitated at 1420 ℃ from solid solution with the content of about 67 at.% V. The homogeneity ranges of the sigma phase and coexisting solution phase were 57-67 and 35-95 at.% V respectively. However, according to the established phase diagram of Ta-V [246–248], no sigma phase is present and the phase detected as sigma phase by Eremenko et al. may be α-TaV_2 (Cu_2Mg structure with the space group of $Fd\bar{3}m$ [246–248]) or β-TaV_2 ($MgZn_2$ structure with the space group of $P6_3/mmc$ [246–248]). The predicted molar volume of the V-Ta sigma phase is much higher than both measurements and that presented in Fig. 5.10 (c).

5.3.11. W-X (X= Os, Ru, Tc) (Fig. 5.11)

For W-X systems, the present assessment is in a good agreement with most experimental data. There are a few exceptions. Raub's [168] measured molar volume of 10.07×10^{-6} m^3/mol at the composition of W_3Os, as well as data from Nevitt and Downey [180] and Knapton [147], are rather high and were not used in the assessment. It should be noted that the stoichiometric composition of WOs_2, at which the experiment by Spooner and Wilson [98] was conducted, was regarded as a typo considering the homogeneity range of about 63.41-79.73 at.% W for the sigma phase based on the phase diagram of W-Os system [149], and converted to the stoichiometric composition of W_2Os in the present work. For W-Tc system, the value determined by Darby et al. [170] is also too high.

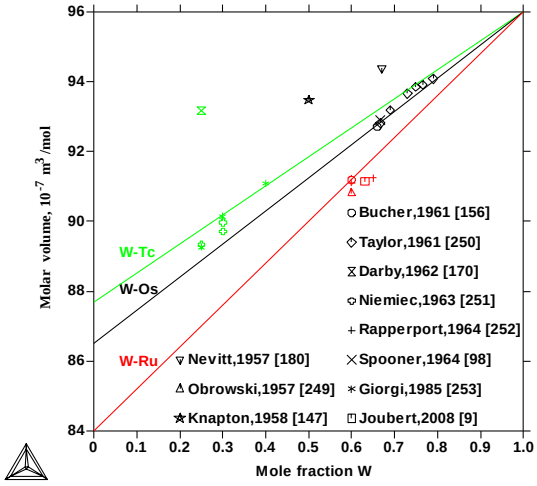

Figure 5.11 : The calculated molar volumes of W-X (X=Os, Ru, Tc) sigma phases compared with the experimental data [9,98,147,156,170,180,249–253]. Note that for one sigma phase, the same color is assigned to both the calculated line and the experimental data.

5.3.12. Zr-X (X= Ir, Re)

For Zr-Ir system, Raman and Schubert [254] and Eremenko [255] considered the phase Zr_3Ir as sigma phase with β-U structure. However, the contention may be doubtful because of the different electron concentration value of Zr_3Ir compared with that of sigma phases as mentioned by Cenzual and Parthé [256]. Therefore Cenzual and Parthé [256] redetermined the phase structure of Zr_3Ir as tetragonal α-V_3S structure. Actually no experimental data are available in this system at present.

For Zr-Re system, the $ReZr_2$ phase was designated as isotypic with sigma phase structure by Savitskii et al. [257]. Though Kuz'ma et al. [218] also detected the $ReZr_2$ phase with lattice parameter in accordance with Savitskii et al.'s study, the phase structure was not confirmed. Considering the fact that few information are available, these data were not considered in the assessment.

The present work does not attempt to assess the volumes of Zr-X systems, but compares the first-principles values with those of other elements in Fig 5.1 and Table 5.1.

5.4. Summary

In the present chapter, a linear volume model has been proposed to describe the molar volume of the non-stoichiometric sigma phase as a linear average of volumes of its constituting elements in their hypothetic sigma structure. After systematically assessing the molar volumes of binary sigma phases at room temperature and atmospheric pressure involving 21 transition elements (among which Ti and Zr were not assessed) by using the CALPHAD approach, we show that the proposed linear model can satisfactorily reproduce most experimental data from the literature. The assessed data for volume of 21 transition elements in the sigma phase structure are comparable to the first principle calculation results, and show a similar trend along the periodic table.

6. Site occupancy prediction of the binary sigma phase systems

Site preference of the binary sigma phase was computed by using the CALPHAD approach combined with first-principles calculations. The sigma phase was described by the compound energy formalism with 5 sublattices (SL) model using the formation energy of the complete set of ordered configurations directly from first-principles calculations. For some systems, the calculated site occupancies agree well with the experimental data from the literature while some others disagree.

6.1. Introduction

Traditionally, the PHACOMP [258] and the newPHACOMP [259,260] method are used to predict the precipitation of the TCP phases in alloys. However, the prediction for the new generation alloys is not very accurate [2]. Seiser et al. [2] compared the accuracy of the CALPHAD method and the newPHACOMP method. It turns out that the CALPHAD method is more successful when predicting the precipitation of the TCP phases. However, the prerequisite is to have reliable databases.

Until now, multi-component phase diagrams involving the sigma phase have been experimentally measured and assessed to build comprehensive thermodynamic databases. However, the thermodynamic descriptions of the sigma phase in these databases are not consistent, which makes it impossible to extend the databases involving the sigma phase from bianry to multi-component systems. Besides, the site occupancy data were usually neglected in the thermodynamic assessments. Taking the assessment of Cr-Fe system by Xiong et al. [141] as an example, two sublattices model, namely $(A,B)_{10}(A,B)_{20}$ was selected and the calculated site preferences are totally reversed as compared to the experimental data. Besides, without considering the site occupancies, it will cause a problem when thermodynamic databases are integrated with other databases (e.g. volume databases). Any updates of thermodynamic databases may predict different site occupancies and other databases have to change correspondingly. Thus it is necessary to take the site occupancy data into account during thermodynamic assessments.

There exist several sublattices (SL) models for the sigma phase. According to CEF (compound energy formalism) [76,139], the following SL models were proposed: $(A)_4(A,B)_{16}(B)_{10}$ [139], $(A,B)_{18}(A)_4(B)_8$ [140], $(A)_4(A,B)_{16}(A,B)_{10}$ [9,120], $(A,B)_4(A,B)_{16}(A,B)_{10}$ [142], $(A,B)_{20}(A,B)_{10}$ [9] and $(A,B)_2(A,B)_4(A,B)_8(A,B)_8(A,B)_8$ [9,120]. 5 SL model is the one that can best reflect the crystal information of the sigma phase. However, it also means more

endmember parameters (n^5) have to be assessed. With this consideration, Mathieu et al. [120] modeled the sigma phase in Mo-Re system with 2, 3, 4 and 5 SL respectively, by using the CALPHAD method combined with first-principles calculations. The enthalpies of formation for the complete set of ordering configurations (2^5=32) were input to for the databases directly. For the full SL description (i.e. 5 SL), they assumed that all the inter-atomic interactions characterizing the sigma phase were considered by first-principles calculations. Thus no extra interaction parameters were added to obtain the thermodynamic self-consistent databases. The calculated site occupancies of the sigma phase agree well with the experimental data. Besides first-principles methods, other methods such as cluster expansion method can also be used to predict site preference, which could be more time-consuming. For more details see Ref. 261.

In the present work, first-principles calculations were conducted on several binary sigma phase systems. The thermodynamic databases of the sigma phase were built with 5 SL based on the compound energy formalism combined with first-principles calculations. No assessed parameters were added. Site occupancies of the sigma phase were calculated by using the established databases. The results show that for some systems, extra interaction parameters may be needed to fit the site occupancies.

6.2. Methodology

6.2.1. Thermodynamic modeling

In the present work, we adopted the 5 SL model on the basis of the compound energy formalism (CEF) [76,139] in the CALPHAD approach proposed by Mathieu et al. [120]:

$(A, B)_2(A, B)_4(A, B)_8(A, B)_8(A, B)_8$.

It can best reflect the crystal structure information. The corresponding Gibbs energy is expressed as:

$$G^{\sigma} = \sum_{ABCDE} y_A^{2a} y_B^{4f} y_C^{8i_1} y_D^{8i_2} y_E^{8j} G^{\sigma}_{ABCDE} + RT \sum_s a^s \sum_i y_i^s \ln y_i^s$$

$$G^{\sigma}_{ABCDE} - \sum_s a^s G_i^{SER} = E^{\sigma}_{ABCDE} - \sum_s a^s E_i^{SER} - T \sum_s a^s \Delta S_i^{\sigma}$$

where y_i^s denotes the site fraction of element i in sublattice s; G^{σ}_{ABCDE} represents the Gibbs energy of ordering configuration ABCDE; R is the gas constant; a^s denotes the number of sites corresponding to sublattice s; G_i^{SER} represents the Gibbs energy of the element i in its SER (standard element reference) state; E^{σ}_{ABCDE} represents the DFT energy of the compound ABCDE in the sigma structure; E_i^{SER} represents the DFT energy of the element i in its SER structure; ΔS_i^{σ} is the entropy difference of the element i in the sigma structure and in its stable structure, namely $\Delta S_i^{\sigma}=S_i^{\sigma}-S_i^{SER}$. For more details see Ref. 95,120.

6.2.2. First-principles calculations

First-principles calculations were performed using the plane wave method with projector augmented wave (PAW) pseudo-potentials [25] implemented in VASP [26]. The

exchange-correlation functional within the generalized gradient approximation (GGA) as parameterized by Perdew and Wang [108] was adopted. The k-point mesh for Brillouin zone sampling was constructed using the Monkhorst–Pack scheme [61], which was set to 8×8×15. Spin-polarized calculations were conducted. A large plane-wave cutoff energy of 400 eV was employed. To facilitate the calculations, ZenGen script-tool was used to generate input files [109].

6.3. Results and discussion

Fig. 1 and Fig. 2 show the calculated enthalpy of formation and site occupancy of the binary sigma phase, respectively. The calculated site occupancies show that for W-Re, Mo-Re, Re-Fe, Nb-Al and Ta-Al systems, the calculation results can well fit the experimental data. However for the other systems, a relatively large deviation exits.

One possible reason is that the measured samples may not reach equilibrium at the corresponding annealing temperature, which may happen for Cr-Fe, Mo-Mn, Re-Mn and Re-Cr systems. The other possible reason may be the impropriate first-principles calculated enthalpy of formations, which could be the case for Cr-Mn, V-Mn, Nb-Re, Re-V and Ru-Cr systems, as for these systems, we can obviously see the opposite results between the calculations and experiments regarding the site preference. According to the effect of the influencing factors (size and electronic factors) on atomic order (i.e. atomic constituent distribution or site occupancy preference on nonequivalent sites of a crystal structure) as discussed in Section 3, we can expect that the first-principles calculations for these systems cannot realistically reflect the contributions of the size or electronic factors. This can be corrected by adding assessed parameters.

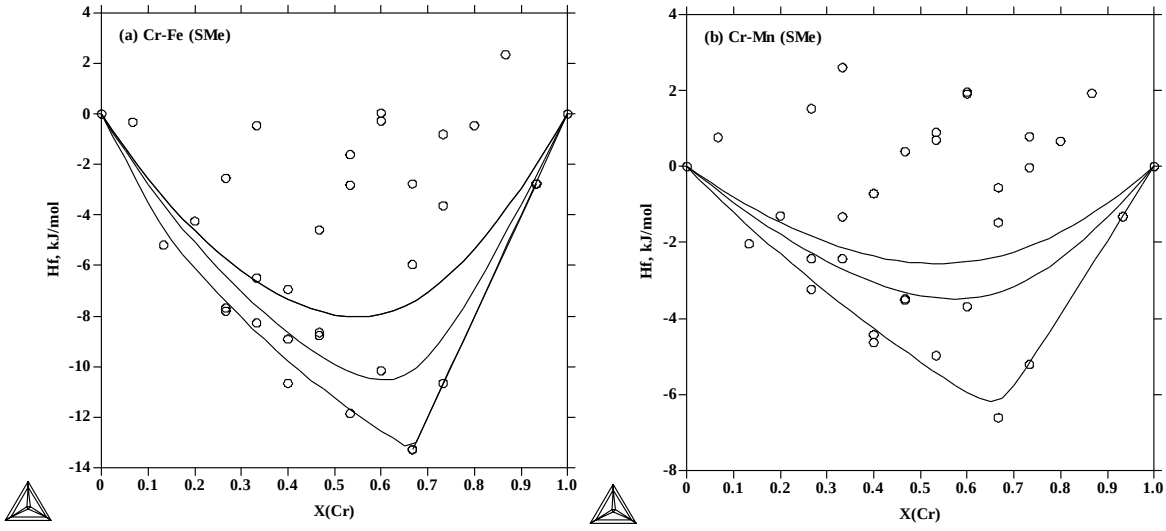

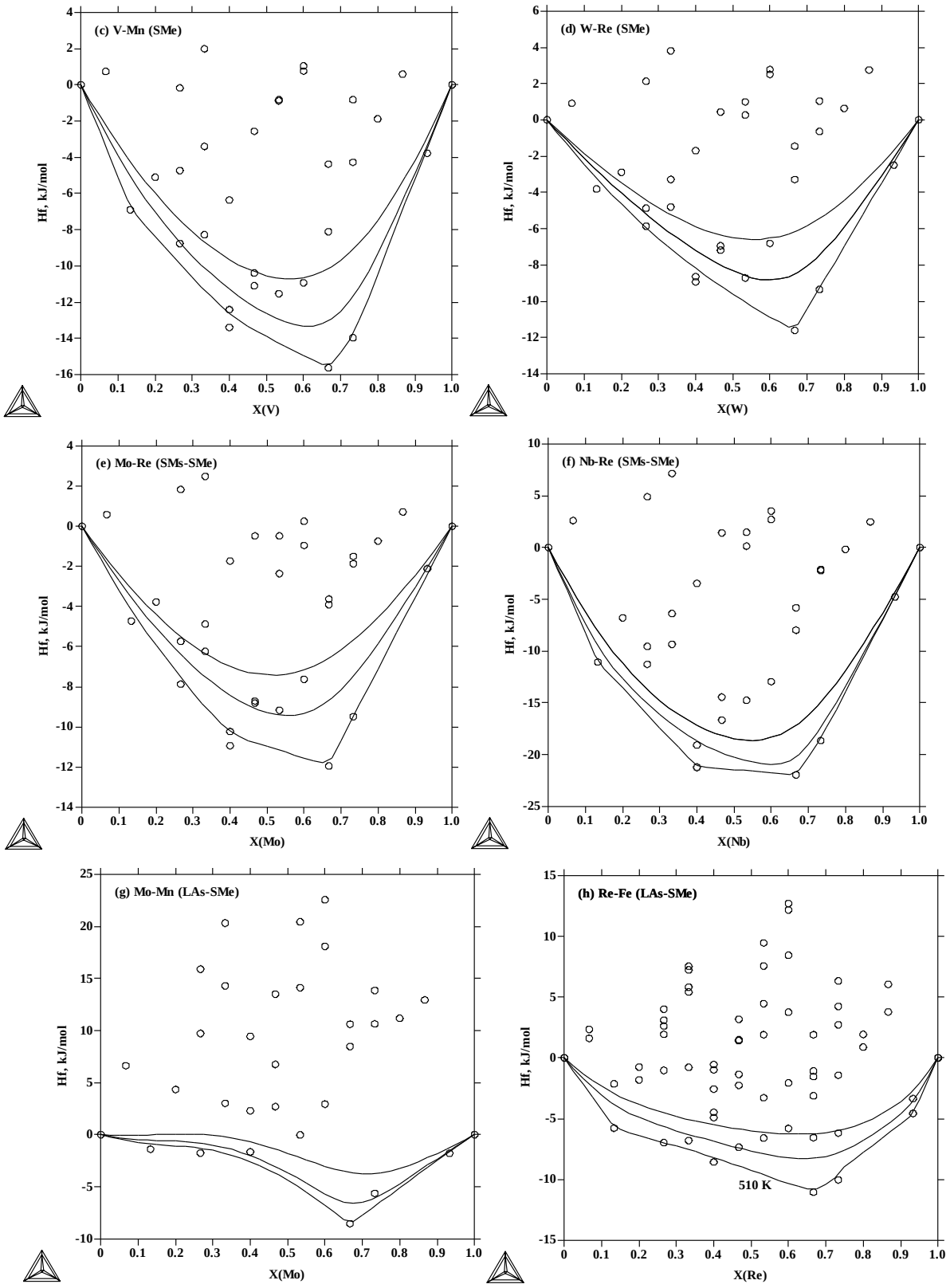
(c) V-Mn (SMe)
Hf, kJ/mol
X(V)
(d) W-Re (SMe)
Hf, kJ/mol
X(W)
(e) Mo-Re (SMs-SMe)
Hf, kJ/mol
X(Mo)
(f) Nb-Re (SMs-SMe)
Hf, kJ/mol
X(Nb)
(g) Mo-Mn (LAs-SMe)
Hf, kJ/mol
X(Mo)
(h) Re-Fe (LAs-SMe)
Hf, kJ/mol
510 K
X(Re)

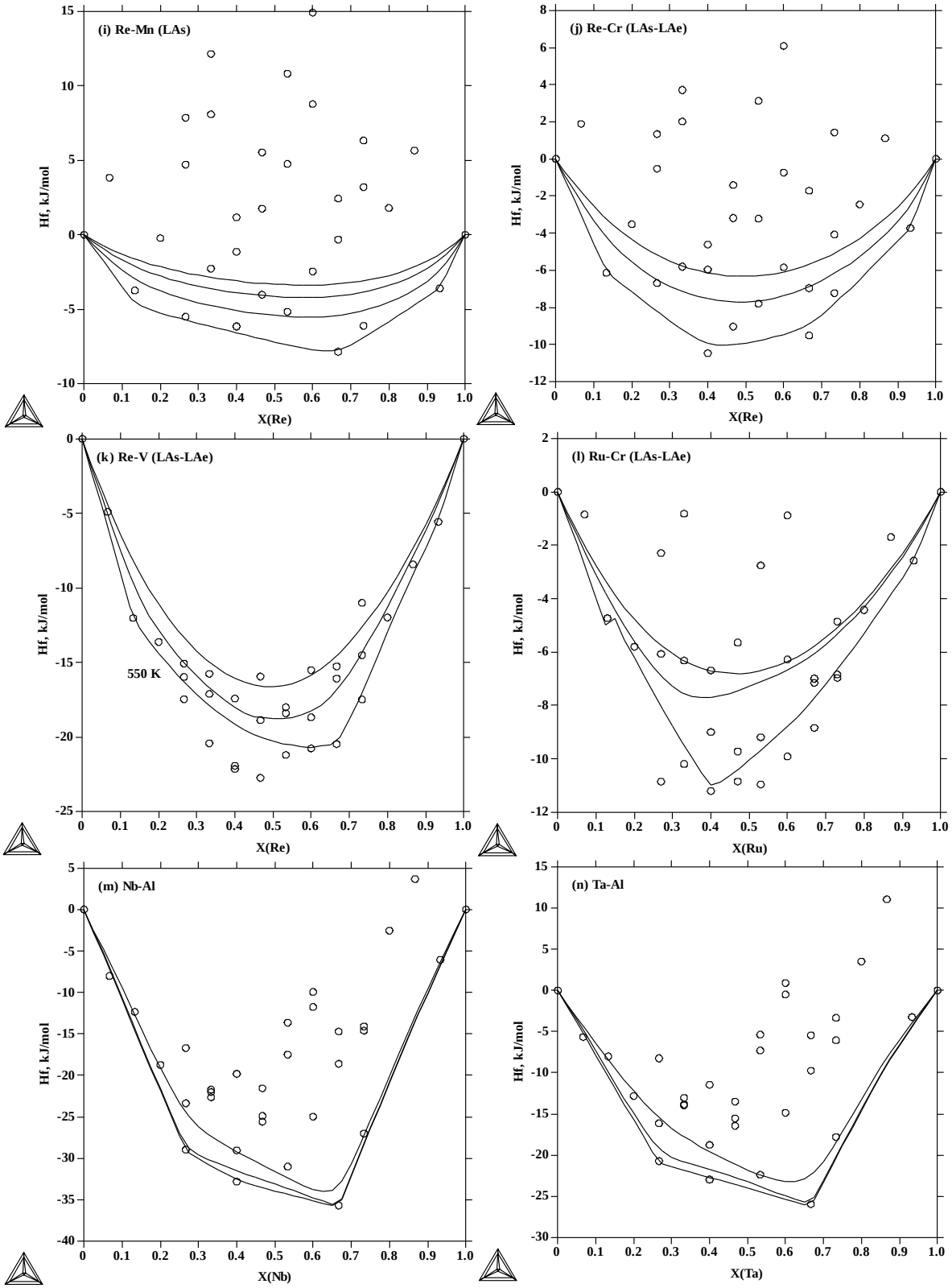

Figure 6.1 : Enthalpy of formation of the binary sigma phase at 500, 1500 and 2500 K calculated by using the CALPHAD method combined with first-principles calculations. The open circles correspond to the first-principles calculations of the 32 stoichiometric endmember compounds referred to the values of the pure Re and Mo configurations. The

calculation results of Re-related systems are from Crivello et al. [95] except for Mo-Re system, for which our own calculation results are employed.

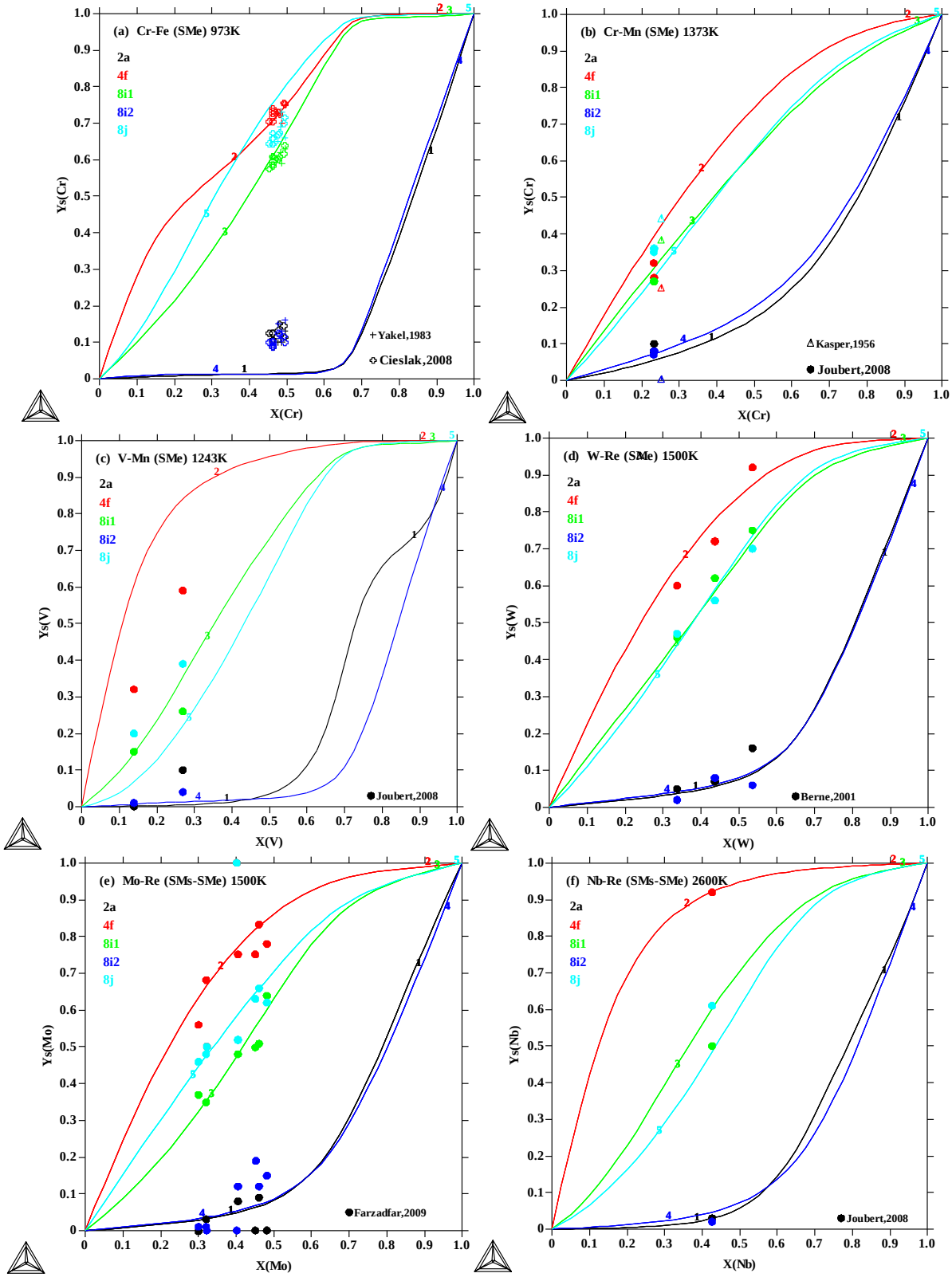

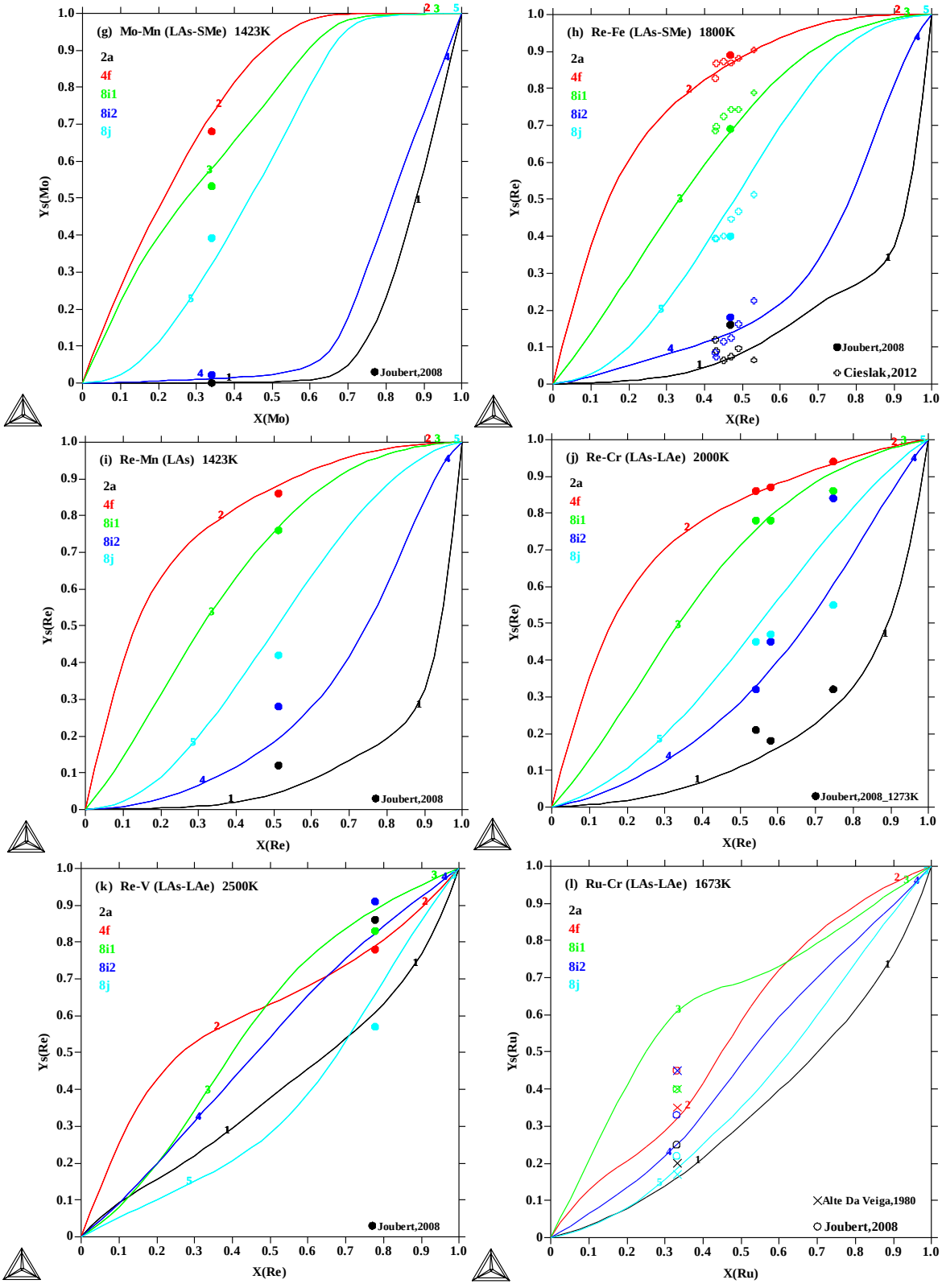
(g) Mo-Mn (LAs-SMe) 1423K
2a
4f
8i1
8i2
8j
Ys(Mo)
X(Mo)
Joubert,2008
(h) Re-Fe (LAs-SMe) 1800K
Ys(Re)
X(Re)
Joubert,2008
Cieslak,2012
(i) Re-Mn (LAs) 1423K
Joubert,2008
(j) Re-Cr (LAs-LAe) 2000K
Joubert,2008_1273K
(k) Re-V (LAs-LAe) 2500K
Joubert,2008
(l) Ru-Cr (LAs-LAe) 1673K
Ys(Ru)
X(Ru)
Alte Da Veiga,1980
Joubert,2008

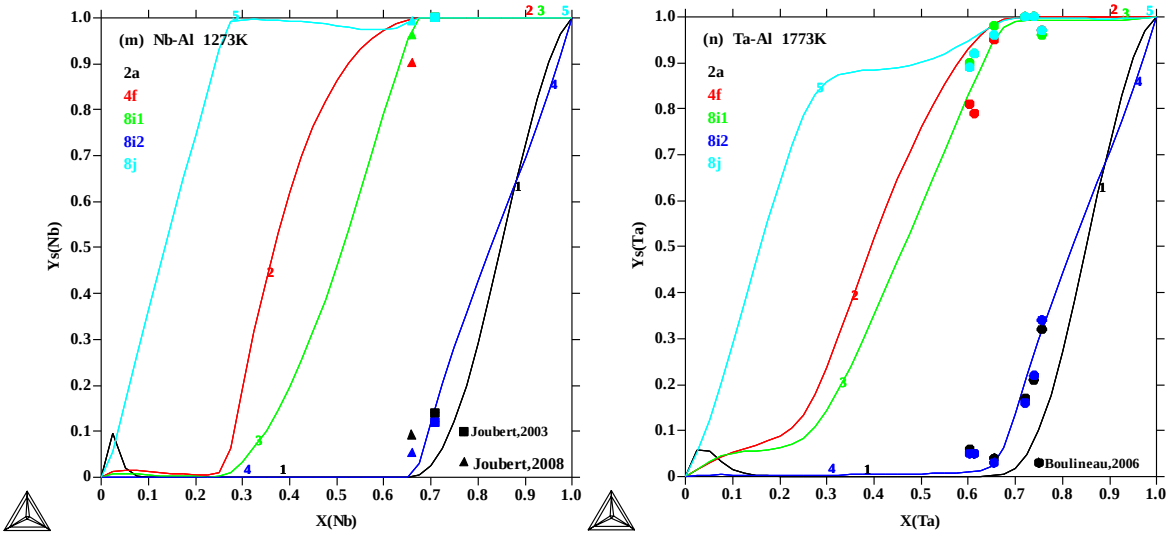

Figure 6.2 : Site occupancy, Ys (A), with respect to mole fraction of atom A, X(A), calculated by using the CALPHAD method combined with first-principles calculations compared with experimental data from the literature [9,10,96,101,103,106,116–119]. The calculation results of Re-related systems are from Crivello et al. [95] except for Mo-Re system, for which our own calculation results are employed.

6.4. Summary

The site occupancy of the sigma phase can be predicted by using CALPHAD method combined with first-principles calculations. For some systems, one can obtain self-consistent databases without any interaction parameters when useing full sublattice description. For some other systems, assessed parameters are necessary even to fit the site occupancies.

Conclusion

In the present work, physical properties of the sigma phase focusing on atomic order and molar volume have been systematically investigated by using first principles calculations and CALPHAD method combining with the experimental data from the literature.

Firstly, we conducted VASP calculations combining with Bader analysis on totally 12 typical sigma phase systems. Thus we obtained the atomic volume and the corresponding atomic charge of the constituent atoms for each system in the complete set of ordered configurations of the sigma phase, from which it is obvious to discover the tendency of electron gain or loss of the two constituent elements and the size difference among the five nonequivalent crystal sites It was found out that besides size factor and the number of valence electrons, the total number of electron shells is the third factor that affects the atomic order of the sigma phase. The experimental site occupancies are results of competition and cooperation of the three influencing factors. In addition, we dissociated the effect of individual influencing factor on the atomic order for the binary sigma phase. All accurately measured site occupancies can be well explained by using our discoveries.

Secondly, we investigated the influence of atomic order on the enthalpy of formation, bulk modulus and molar volume of the binary sigma phase. During the investigation, the long-range order parameter S is redefined to state the influence of atomic order on the above-mentioned properties. It has been found out that in the ordered state at 0K, the sigma phase bears a low enthalpy of formation and a large bulk modulus; the influence of atomic mixing on the molar volume of the sigma phase depends on the tendency of electron loss or gain of the two constituent elements; the influence of atomic order on the molar volume of the sigma phase depends on the electron configuration of the two constituent elements.

Thirdly, we propose a model to describe the molar volume of the non-stoichiometric sigma phase as a linear average of volumes of its constituting elements in their hypothetic sigma structure. The proposed linear model can satisfactorily reproduce most experimental data from the literature. After having systematically evaluated the literature data, the molar volume database of binary sigma phases at room temperature and atmospheric pressure involving 20 elements (Al, Au, Co, Cr, Fe, Ir, Mn, Mo, Nb, Ni, Os, Pd, Pt, Re, Rh, Ru, Ta, Tc, V, and W) has been obtained by using the CALPHAD approach. The adopted method can be extended to multi-component systems and reduces the n^3 unknowns for end-member compounds to n values for n elements in a n-component sigma phase. Another practical advantage is that the development of volume database for these sigma phases can be separated from the thermodynamic databases.

Finally, we tentatively discussed the site occupancy prediction of the sigma phase. The CALPHAD method combined with first-principles calculations is a good way to predict site preference of the sigma phase but for some systems assessed parameters are needed.

Bibliographie

1. Hu, G.-X., Cai, X. & Rong, Y.-H. *Fundamentals of materials science, third ed.* (Shanghai Jiao Tong University Press, Shanghai, 2010).
2. Seiser, B., Drautz, R. & Pettifor, D. G. TCP phase predictions in Ni-based superalloys: Structure maps revisited. *Acta Mater.* **59,** 749–763 (2011).
3. Ladines, A. N., Hammerschmidt, T. & Drautz, R. Structural stability of Fe-based topologically close-packed phases. *Intermetallics* **59,** 59–67 (2015).
4. Rettig, R. & Singer, R. F. Numerical modelling of precipitation of topologically close-packed phases in nickel-base superalloys. *Acta Mater.* **59,** 317–327 (2011).
5. Palumbo, M. *et al.* First-principles-based phase diagrams and thermodynamic properties of TCP phases in Re–X systems (X=Ta, V, W). *Comput. Mater. Sci.* **81,** 433–445 (2014).
6. Zhao, J.-Y., Liu, W. & Lu, X.-G. Assessments of molar volume of the binary C14 Laves phase. *Calphad* **50,** 82–91 (2015).
7. Kirkwood, J. G. Order and Disorder in Binary Solid Solutions. *J. Chem. Phys.* **6,** 70–75 (1938).
8. Hall, E. O. & Algie, S. H. The sigma phase. *Metall. Rev.* **11,** 61–88 (1966).
9. Joubert, J.-M. Crystal chemistry and Calphad modeling of the σ phase. *Prog. Mater. Sci.* **53,** 528–583 (2008).
10. Cieślak, J., Reissner, M., Dubiel, S. M., Wernisch, J. & Steiner, W. Influence of composition and annealing conditions on the site-occupation in the σ-phase of Fe–Cr and Fe–V systems. *J. Alloys Compd.* **460,** 20–25 (2008).

11. Dickins, G. J., Douglas, A. M. B. & Taylor, W. H. Structure of the sigma-phase in the iron-chromium and cobalt-chromium systems. *Nature* **176,** 192 (1951).
12. Lee, S., Bluemle, M. J. & Bates, F. S. Discovery of a Frank-Kasper σ Phase in Sphere-Forming Block Copolymer Melts. *Science* **330,** 349–353 (2010).
13. Peterca, M. & Percec, V. Recasting Metal Alloy Phases with Block Copolymers. *Science* **330,** 333–334 (2010).
14. Pauling, L. The nature of the chemical bond . IV. The energy of single bonds and the relative electronegativity of atoms. *J. Am. Chem. Soc.* **54,** 3570–3582 (1932).
15. Allred, A. L. & Rochow, E. G. A scale of electronegativity based on electrostatic force. *J. Inorg. Nucl. Chem.* **5,** 264–268 (1958).
16. Pearson, R. G. Electronegativity scales. *Acc Chem Res* **23,** 1–2 (1990).
17. Mulliken, R. S. A New Electroaffinity Scale; Together with Data on Valence States and on Valence Ionization Potentials and Electron Affinities. *J. Chem. Phys.* **2,** 782–793 (1934).
18. Pritchard, H. O. & Skinner, H. A. The Concept Of Electronegativity. *Chem. Rev.* **55,** 745–786 (1955).
19. Parr, R. G., Donnelly, R. A., Levy, M. & Palke, W. E. Electronegativity: The density functional viewpoint. *J. Chem. Phys.* (1978). doi:10.1063/1.436185
20. Sanderson, R. T. Electronegativity and bond energy. *J. Am. Chem. Soc.* **105,** 2259–2261 (1983).
21. Bratsch, S. G. Revised Mulliken electronegativities: I. Calculation and conversion to Pauling units. *J. Chem. Educ.* **65,** 34 (1988).
22. Allen, L. C. Electronegativity is the average one-electron energy of the valence-shell electrons in ground-state free atoms. *J. Am. Chem. Soc.* **111,** 9003–9014 (1989).

23. Allred, A. L. Electronegativity values from thermochemical data. *J. Inorg. Nucl. Chem.* **17,** 215–221 (1961).
24. Shi, S.-Q. *et al.* Multiscale materials computational methods. *Sci. Technol. Rev.* **33,** 20–30
25. Kresse, G. & Joubert, D. From ultrasoft pseudopotentials to the projector augmented-wave method. *Phys. Rev. B* **59,** 1758 (1999).
26. Kresse, G. & Furthmüller, J. Efficient iterative schemes for ab initio total-energy calculations using a plane-wave basis set. *Phys. Rev. B* **54,** 11169–11186 (1996).
27. Vitos, L. *Computational quantum mechanics for materials engineers: the EMTO method and applications*. (Springer, 2007).
28. Cottenier, S. Density Functional Theory and the family of (L) APW-methods: a step-by-step introduction. *Inst. Voor Kern-En Stralingsfysica KU Leuven Belg.* **4,** 41 (2002).
29. Li, C. M. Elastic properties and phase stability of shape memory alloys. (Institute of Metal Research, Chinese Academy of Sciences, 2011).
30. Payne, M. C., Teter, M. P., Allan, D. C., Arias, T. A. & Joannopoulos, J. D. Iterative minimization techniques for ab initio total-energy calculations: molecular dynamics and conjugate gradients. *Rev. Mod. Phys.* **64,** 1045–1097 (1992).
31. Hirschl, M. R. Binary Transition Metal Alloys and Their Surfaces - an Ab Initio Study. Part I: Methods. (University of Vienna, 2002).
32. Henkelman Group. Bader Charge Analysis. *http://theory.cm.utexas.edu/henkelman/code/bader/*
33. Zeng, J.-Y. *Quantum mechanics*. (Sientific Press, 1990).

34. Hohenberg, P. & Kohn, W. Inhomogeneous Electron Gas. *Phys. Rev.* **136,** B864–B871 (1964).

35. Kohn, W. & Sham, L. J. Self-Consistent Equations Including Exchange and Correlation Effects. *Phys. Rev.* **140,** A1133–A1138 (1965).

36. Perdew, J. P. & Zunger, A. Self-interaction correction to density-functional approximations for many-electron systems. *Phys. Rev. B* **23,** 5048–5079 (1981).

37. Slater, J. C. A Simplification of the Hartree-Fock Method. *Phys. Rev.* **81,** 385–390 (1951).

38. Vosko, S. H., Wilk, L. & Nusair, M. Accurate spin-dependent electron liquid correlation energies for local spin density calculations: a critical analysis. *Can. J. Phys.* **58,** 1200–1211 (1980).

39. Ceperley, D. M. & Alder, B. J. Ground State of the Electron Gas by a Stochastic Method. *Phys. Rev. Lett.* **45,** 566–569 (1980).

40. Barth, U. von & Hedin, L. A local exchange-correlation potential for the spin polarized case. i. *J. Phys. C Solid State Phys.* **5,** 1629 (1972).

41. Perdew, J. P., Burke, K. & Ernzerhof, M. Generalized Gradient Approximation Made Simple. *Phys. Rev. Lett.* **77,** 3865–3868 (1996).

42. Wang, Y. & Perdew, J. P. Correlation hole of the spin-polarized electron gas, with exact small-wave-vector and high-density scaling. *Phys. Rev. B* **44,** 13298–13307 (1991).

43. Andersen, O. K., Jepsen, O. & Krier, G. *Lectures on Methods of Electronic Structure Calculations*. (World Scientific, 1994).

44. Soven, P. Coherent-potential model of substitutional disordered alloys. *Phys. Rev.* **156,** 809 (1967).

45. Gyorffy, B. L. Coherent-potential approximation for a nonoverlapping-muffin-tin-potential model of random substitutional alloys. *Phys. Rev. B* **5,** 2382 (1972).

46. Vitos, L., Abrikosov, I. A. & Johansson, B. Anisotropic Lattice Distortions in Random Alloys from First-Principles Theory. *Phys. Rev. Lett.* **87,** (2001).

47. Korzhavyi, P. A., Ruban, A. V., Abrikosov, A. I. & Skriver, H. L. Madelung energy for random metallic alloys in the coherent potential approximation. *Phys. Rev. B Condens. Matter* **51,** 5773–5780 (1995).

48. Ruban, A. V. & Skriver, H. L. Screened Coulomb interactions in metallic alloys: I. Universal screening in the atomic sphere approximation. *Phys. Rev. B* **66,** (2002).

49. Blöchl, P. E. Projector augmented-wave method. *Phys. Rev. B* **50,** 17953–17979 (1949).

50. Rostgaard, C. The Projector Augmented-wave Method. *ArXiv09101921 Cond-Mat Physicsphysics* (2009).

51. Kresse, G. & Hafner, J. Norm-conserving and ultrasoft pseudopotentials for first-row and transition elements. *J. Phys. Condens. Matter* **6,** 8245 (1994).

52. Vanderbilt, D. Soft self-consistent pseudopotentials in a generalized eigenvalue formalism. *Phys. Rev. B* **41,** 7892–7895 (1990).

53. Andersen, O. K. Linear methods in band theory. *Phys. Rev. B* **12,** 3060–3083 (1975).

54. Marsman, M. VASP: Plane waves, the PAW method, and the Selfconsistency cycle. (2011).

55. Kresse, G. & Furthmüller, J. Efficiency of ab-initio total energy calculations for metals and semiconductors using a plane-wave basis set. *Comput. Mater. Sci.* **6,** 15–50 (1996).

56. Kresse, G., Marsman, M. & Furthmüller, J. Vienna Ab-initio Simulation Package: VASP the GUIDE. (2016).

57. Teter, M. P., Payne, M. C. & Allan, D. C. Solution of Schrödinger's equation for large systems. *Phys. Rev. B* **40,** 12255–12263 (1989).

58. Davidson, E. R. Matrix Eigenvector Methods. in *Methods in Computational Molecular Physics* **113,** 95–113 (Springer, Dordrecht, 1983).

59. Wood, D. M. & Zunger, A. A new method for diagonalising large matrices. *J. Phys. Math. Gen.* **18,** 1343–1359 (1985).

60. Pulay, P. Convergence acceleration of iterative sequences. the case of scf iteration. *Chem. Phys. Lett.* **73,** 393–398 (1980).

61. Monkhorst, H. J. & Pack, J. D. Special points for Brillouin-zone integrations. *Phys. Rev. B* **13,** 5188–5192 (1976).

62. Blöchl, P. E., Jepsen, O. & Andersen, O. K. Improved tetrahedron method for Brillouin-zone integrations. *Phys. Rev. B* **49,** 16223–16233 (1994).

63. Methfessel, M. & Paxton, A. T. High-precision sampling for Brillouin-zone integration in metals. *Phys. Rev. B* **40,** 3616–3621 (1989).

64. De Proft, F., Van Alsenoy, C., Peeters, A., Langenaeker, W. & Geerlings, P. Atomic charges, dipole moments, and Fukui functions using the Hirshfeld partitioning of the electron density. *J. Comput. Chem.* **23,** 1198–1209 (2002).

65. Bader, R. F. W. *Atoms in Molecules: A Quantum Theory*. (Oxford University Press, 1994).

66. Mulliken, R. S. Electronic Population Analysis on LCAO–MO Molecular Wave Functions. I. *J. Chem. Phys.* **23,** 1833–1840 (1955).

67. Tang, W., Sanville, E. & Henkelman, G. A grid-based Bader analysis algorithm without lattice bias. *J. Phys. Condens. Matter* **21,** 084204 (2009).

68. Bader, R. F. W., Anderson, S. G. & Duke, A. J. Quantum topology of molecular charge distributions. 1. *J. Am. Chem. Soc.* **101,** 1389–1395 (1979).

69. Henkelman, G., Arnaldsson, A. & Jónsson, H. A fast and robust algorithm for Bader decomposition of charge density. *Comput. Mater. Sci.* **36,** 354–360 (2006).

70. Sanville, E., Kenny, S. D., Smith, R. & Henkelman, G. Improved grid-based algorithm for Bader charge allocation. *J. Comput. Chem.* **28,** 899–908 (2007).

71. Kaufman, L. & Cohen, M. The Martensitic Transformation in the Iron-Nickel System. *JOM* **8,** 1393–1401 (1956).

72. Kaufman, L. & Bernstein, H. *Computer Calculations of Phase Diagrams*. (Academic Press, 1970).

73. Saunders, N. & Miodownik, A. P. *CALPHAD (calculation of phase diagrams): a comprehensive guide*. (Pergamon, 1998).

74. Lukas, H. L., Fries, S. G. & Sundman, B. *Computational thermodynamics: the CALPHAD method*. (Cambridge University Press, 2007).

75. Kjellqvist, L. Thermodynamic description of the Fe-C-Cr-Mn-Ni-O system. (KTH, 2009).

76. Hillert, M. The compound energy formalism. *J. Alloys Compd.* **320,** 161–176 (2001).

77. Sundman, B. & Ågren, J. A regular solution model for phases with several components and sublattices, suitable for computer applications. *J. Phys. Chem. Solids* **42,** 297–301 (1981).

78. Andersson, J.-O., Guillermet, A. F., Hillert, M., Jansson, B. & Sundman, B. A compound-energy model of ordering in a phase with sites of different coordination numbers. *Acta Metall.* **34,** 437–445 (1986).

79. He, Y.-L., Lu, X.-G., Zhu, N.-Q. & Sundman, B. CALPHAD modeling of molar volume. *Chin. Sci. Bull.* **59,** 1646–1651 (2014).

80. Inden, G. Project Meeting Calphad V. *Max Planck Inst. Für Eisenforsch. Düsseld.* 21–25 (1976).

81. Hillert, M. & Jarl, M. A model for alloying in ferromagnetic metals. *Calphad* **2,** 227–238 (1978).

82. Murnaghan, F. D. The Compressibility of Media under Extreme Pressures. *Proc. Natl. Acad. Sci.* **30,** 244–247 (1944).

83. Grover, R., Getting, I. C. & Kennedy, G. C. Simple Compressibility Relation for Solids. *Phys. Rev. B* **7,** 567–571 (1973).

84. Lu, X.-G., Selleby, M. & Sundman, B. Implementation of a new model for pressure dependence of condensed phases in Thermo-Calc. *Calphad* **29,** 49–55 (2005).

85. Lu, X., Selleby, M. & Sundman, B. Theoretical modeling of molar volume and thermal expansion. *Acta Mater.* **53,** 2259–2272 (2005).

86. Lu, X.-G., Selleby, M. & Sundman, B. Calculations of thermophysical properties of cubic carbides and nitrides using the Debye–Grüneisen model. *Acta Mater.* **55,** 1215–1226 (2007).

87. Lu, X.-G. & Chen, Q. A CALPHAD Helmholtz energy approach to calculate thermodynamic and thermophysical properties of fcc Cu. *Philos. Mag.* **89,** 2167–2194 (2009).

88. Andersson, J.-O., Helander, T., Höglund, L., Shi, P. & Sundman, B. Thermo-Calc & DICTRA, computational tools for materials science. *Calphad* **26,** 273–312 (2002).

89. Sundman, B., Jansson, B. & Andersson, J.-O. The thermo-calc databank system. *Calphad* **9,** 153–190 (1985).

90. Thermo-Calc User Guide. (2017).

91. Joubert, J.-M. & Dupin, N. Mixed site occupancies in the μ phase. *Intermetallics* **12,** 1373–1380 (2004).

92. Joubert, J.-M. & Phejar, M. Crystal chemistry and Calphad modelling of the χ phase. *Prog. Mater. Sci.* **54,** 945–980 (2009).

93. Liang, M. J., Chen, Z., Wang, Y. X., Zhang, J. X. & Lai, Q. B. Microscopic phase-field study on atomic site occupation probability in L12–Ni3(Al1−xFex) structure. *Mater. Lett.* **62,** 4332–4335 (2008).

94. Wu, Y. *et al.* The First-principles Study on the Occupation Behavior and the Ductility Mechanism of Zr in Ni–Ni3Al System with Lattice Misfit. *J. Mater. Sci. Technol.* **30,** 517–522 (2014).

95. Crivello, J.-C., Breidi, A. & Joubert, J.-M. χ and σ Phases in Binary Rhenium–Transition Metal Systems: a Systematic First-Principles Investigation. *Inorg. Chem.* **52,** 3674–3686 (2013).

96. Kasper, J. S. & Waterstrat, R. M. Ordering of atoms in the σ phase. *Acta Crystallogr.* **9,** 289–295 (1956).

97. Wilson, C. G. & Spooner, F. J. Ordering of atoms in the sigma phase FeMo. *Acta Crystallogr.* **16,** 230–231 (1963).

98. Spooner, F. J. & Wilson, C. G. Ordering in binary σ phases. *Acta Crystallogr.* **17,** 1533–1538 (1964).

99. Algie, S. H. & Hall, E. O. Site ordering in some σ-phase structures. *Acta Crystallogr.* **20,** 142–142 (1966).

100. Spor, R. W., Claus, H. & Beck, P. A. X-Ray diffraction study of ordering in two sigma phases. *Adv X-Ray Anal* **10,** 213–220 (1967).

101. Alte da Veiga, L. M., Costa, M., De Almeida, M. J. M., Andrade, L. R. & Matos Beja, A. The ordering of the σ phases Cr2Ru and Cr2Os. *Acta Crystallogr. B* **36,** 1750–1757 (1980).

102. de Freitas, J. M., Alte da Veiga, L. M. & Gonschorek, W. The ordering of the sigma phase V62Co38. *Portgal Phys* **13,** 113–119 (1982).

103. Yakel, H. L. Atom distributions in sigma phases. I. Fe and Cr atom distributions in a binary sigma phase equilibrated at 1063, 1013 and 923 K. *Acta Crystallogr. Sect. B* **39,** 20–28 (1983).

104. Sluiter, M. H. F., Esfarjani, K. & Kawazoe, Y. Site occupation reversal in the Fe-Cr σ phase. *Phys. Rev. Lett.* **75,** 3142–3145 (1995).

105. Berne, C., Sluiter, M., Kawazoe, Y. & Pasturel, A. Ordering effects in the Re–W and Re–Ta sigma phases. *J. Phys. Condens. Matter* **13,** 9433 (2001).

106. Berne, C., Sluiter, M., Kawazoe, Y., Hansen, T. & Pasturel, A. Site occupancy in the Re-W sigma phase. *Phys. Rev. B* **64,** (2001).

107. Sluiter, M. H. F. & Pasturel, A. Site occupation in the Cr-Ru and Cr-Os σ phases. *Phys. Rev. B* **80,** (2009).

108. Perdew, J. P. & Wang, Y. Accurate and simple analytic representation of the electron-gas correlation energy. *Phys. Rev. B* **45,** 13244–13249 (1992).

109. Crivello, J.-C., Souques, R., Breidi, A., Bourgeois, N. & Joubert, J.-M. ZenGen, a tool to generate ordered configurations for systematic first-principles calculations: The Cr–Mo–Ni–Re system as a case study. *Calphad* **51,** 233–240 (2015).

110. Yu, M. & Trinkle, D. R. Accurate and efficient algorithm for Bader charge integration. *J. Chem. Phys.* **134,** 064111 (2011).

111. Liu, W., Lu, X.-G., Boulet, P. & Record, M.-C. Influencing factors of atomic order in the binary sigma phase. *Submitted*

112. Berne, C., Pasturel, A., Sluiter, M. & Vinet, B. Ab initio study of metastability in refractory metal based systems. *Phys. Rev. Lett.* **83,** 1621 (1999).

113. Liu, W., Lu, X.-G., He, Y.-L. & Li, L. Modeling of molar volume of the sigma phase involving transition elements. *Comput. Mater. Sci.* **95,** 540–550 (2014).

114. Cieślak, J., Dubiel, S. M. & Reissner, M. Site occupancy and lattice parameters in sigma-phase Co-Cr alloys. *Acta Crystallogr. B* **68,** 123–127 (2012).

115. Cieślak, J., Dubiel, S. M., Przewoznik, J. & Tobola, J. Structural and hyperfine characterization of σ-phase Fe–Mo alloys. *Intermetallics* **31,** 132–136 (2012).

116. Cieślak, J., Dubiel, S. M., Zukrowski, J. & Tobola, J. Sigma-phase in the Fe-Re alloy system: experimental and theoretical studies. *ArXiv Prepr. ArXiv12062377* (2012).

117. Farzadfar, S. A., Levesque, M., Phejar, M. & Joubert, J.-M. Thermodynamic assessment of the Molybdenum–Rhenium system. *Calphad* **33,** 502–510 (2009).

118. Joubert, J.-M., Pommier, C., Leroy, E. & Percheron-Guégan, A. Hydrogen absorption properties of topologically close-packed phases of the Nb–Ni–Al system. *J. Alloys Compd.* **356–357,** 442–446 (2003).

119. Boulineau, A., Joubert, J.-M. & Černý, R. Structural characterization of the Ta-rich part of the Ta–Al system. *J. Solid State Chem.* **179,** 3385–3393 (2006).

120. Mathieu, R. *et al.* CALPHAD description of the Mo–Re system focused on the sigma phase modeling. *Calphad* **43,** 18–31 (2013).

121. Bonny, G., Bakaev, A., Terentyev, D. & Mastrikov, Y. A. Elastic properties of the sigma W-Re phase: A first principles investigation. *Scr. Mater.* **128,** 45–48 (2017).

122. Cieślak, J., Tobola, J. & Dubiel, S. M. Site occupancies in sigma-phase Fe–Cr–X (X=Co, Ni) alloys: Calculations versus experiment. *Comput. Mater. Sci.* **122,** 229–239 (2016).

123. Vitos, L. Total-energy method based on the exact muffin-tin orbitals theory. *Phys. Rev. B* **64,** (2001).

124. Dreizler, R. M. & Gross, E. K. U. *Density Functional Theory*. (Springer, 1998).

125. Hu, Q.-M., Vitos, L. & Yang, R. Theoretical investigation of the ω -related phases in TiAl – Nb /Mo alloys. *Phys. Rev. B* **90,** (2014).

126. Cieślak, J., Costa, B. F. O., Dubiel, S. M., Reissner, M. & Steiner, W. Magnetic ordering above room temperature in the sigma-phase of Fe66V34. *J. Magn. Magn. Mater.* **321,** 2160–2165 (2009).

127. Cieślak, J., Dubiel, S. M., Tobola, J. & Zukrowski, J. Experimental and theoretical study of the σ-phase Fe–Re alloys. *Mater. Chem. Phys.* **139,** 590–595 (2013).

128. Cieślak, J., Reissner, M., Steiner, W. & Dubiel, S. M. On the magnetism of the σ-phase Fe-Cr alloys. *Phys. Status Solidi A* **205,** 1794–1799 (2008).

129. Birch, F. Finite elastic strain of cubic crystals. *Phys. Rev.* **71,** 809 (1947).

130. Jacob, K. T., Raj, S. & Rannesh, L. Vegard's law: a fundamental relation or an approximation? *Int. J. Mater. Res.* **98,** 776–779 (2007).

131. Slagle, O. D. & McKinstry, H. A. The lattice parameter in the solid solution KCl–KBr. *Acta Crystallogr.* **21,** 1013–1013 (1966).

132. Sirdeshmukh, D. B., Sirdeshmukh, L. & Subhadra, K. G. *Micro- and macro-properties of solids: thermal, mechanical and dielectric properties*. **80,** (Springer, 2006).

133. Wang, J.-F. *Solid state physics*. (Shandong University press, 2013).

134. Jacobs, M. H. G. & Oonk, H. A. J. A realistic equation of state for solids. The high pressure and high temperature thermodynamic properties of MGO. *Calphad* **24,** 133–147 (2000).

135. Lu, X.-G., Selleby, M. & Sundman, B. Assessments of molar volume and thermal expansion for selected bcc, fcc and hcp metallic elements. *Calphad* **29,** 68–89 (2005).

136. Hallstedt, B. Molar volumes of Al, Li, Mg and Si. *Calphad* **31,** 292–302 (2007).

137. Brosh, E., Makov, G. & Shneck, R. Z. Application of CALPHAD to high pressures. *Calphad* **31,** 173–185 (2007).

138. Hallstedt, B. *et al.* Thermodynamic models for crystalline phases. Composition dependent models for volume, bulk modulus and thermal expansion. *Calphad* **31,** 28–37 (2007).

139. Andersson, J.-O., Guillermet, A. F., Hillert, M., Jansson, B. & Sundman, B. A compound-energy model of ordering in a phase with sites of different coordination numbers. *Acta Metall.* **34,** 437–445 (1986).

140. Andersson, J.-O. & Sundman, B. Thermodynamic properties of the Cr-Fe system. *Calphad* **11,** 83–92 (1987).

141. Xiong, W. *et al.* An improved thermodynamic modeling of the Fe–Cr system down to zero kelvin coupled with key experiments. *Calphad* **35,** 355–366 (2011).

142. Watson, A. & Hayes, F. H. Some experiences modelling the sigma phase in the Ni–V system. *J. Alloys Compd.* **320,** 199–206 (2001).

143. Jansson, B. *Evaluation of parameters in thermochemical models using different types of experimental data simultaneously*. **TRITA-MAC-0234 S10044,** (1984).

144. Härtwig, J., Grosswig, S., Becker, P. & Windisch, D. Remeasurement of the CuKα1 Emission X-Ray Wavelength in the Metrical System (Present Stage). *Phys. Status Solidi A* **125,** 79–89 (1991).

145. Mohr, P. J. & Taylor, B. N. CODATA recommended values of the fundamental physical constants: 2002. *Rev. Mod. Phys.* **77,** 1 (2005).

146. Greenfield, P. & Beck, P. A. Intermediate phases in binary systems of certain transition elements. *Trans AIME* **206,** 265–276 (1956).

147. Knapton, A. G. An X-ray survey of certain transition-metal systems for sigma phases. *J Inst Met* **87,** 28–32 (1957).

148. Predel, B. Ir-W (Iridium-Tungsten). in **5G,** 1–2 (Landolt-Börnstein - Group IV Physical Chemistry 5G, 1997).

149. Predel, B. Os-W (Osmium-Tungsten). in *Ni-Np – Pt-Zr* (ed. Madelung, O.) **I,** 1–3 (Landolt-Börnstein - Group IV Physical Chemistry 5I, 1998).

150. Predel, B. Cr-Os (Chromium-Osmium). in *Cr-Cs – Cu-Zr* 1–5 (Landolt-Börnstein - Group IV Physical Chemistry 5D, 1994). doi:10.1007/10086090_998

151. Predel, B. Os-Ta (Osmium-Tantalum). in *Ni-Np – Pt-Zr* (ed. Madelung, O.) **I,** 1–2 (Landolt-Börnstein - Group IV Physical Chemistry 5I, 1998).

152. Predel, B. Re-Ta (Rhenium-Tantalum). in *Pu-Re – Zn-Zr* (ed. Madelung, O.) **5 J,** 1–2 (Landolt-Börnstein - Group IV Physical Chemistry 5J, 1998).

153. Okamoto, H. Re-Ta (Rhenium-Tantalum). *J. Phase Equilibria* **21,** 573 (2000).

154. Predel, B. Ir-Mo (Iridium-Molybdenum). in (ed. Madelung, O.) **G,** 1–4 (Landolt-Börnstein - Group IV Physical Chemistry 5G, 1997).

155. Knapton, A. G. The niobium-rhenium system. *J -Common Met* **1,** 480–486 (1959).

156. Bucher, E., Heiniger, F. & Müller, J. Supraleitung und paramagnetismus in komplexen phasen der übergangsmetalle. *Helv Phys Acta* **34,** 843–858 (1961).

157. Predel, B. Nb-Re (Niobium-Rhenium). in *Li-Mg – Nd-Zr* (ed. Madelung, O.) **H,** 1–2 (Landolt-Börnstein - Group IV Physical Chemistry 5H, 1997).

158. Kasper, J. S., Decker, B. F. & Belanger, J. R. The Crystal Structure of the Sigma-Phase in the Co-Cr System. *J. Appl. Phys.* **22,** 361–362 (1951).

159. Dickins, G. J., Douglas, A. M. & Taylor, W. H. The crystal structure of the Co–Cr σ phase. *Acta Crystallogr.* **9,** 297–303 (1956).

160. Stüwe, H. P. Description of the sigma phase as a structure with sphere packing. *Trans Met. Soc AIME* **215,** 408–411 (1959).

161. Yukawa, N., Hida, M., Imura, T., Mizuno, Y. & Kawamura, M. Structure of chromium-rich Cr-Ni, Cr-Fe, Cr-Co, and Cr-Ni-Fe alloy particles made by evaporation in argon. *Metall. Trans.* **3,** 887–895 (1972).

162. Gudzenko, V. N. & Polesya, A. F. Structure of Ni-V and Co-Cr alloys rapidly cooled from the liquid state. *Fiz Met. Met.* **41,** 1106–1109 (1976).

163. Sokolovskaya, E. M., Tuganbaev, M. L., Stepanova, G. I., Kazakova, E. F. & Sokolova, I. G. Interaction of cobalt with chromium and rhenium. *J. Common Met.* **124,** L5–L7 (1986).

164. Naohara, T. & Shinohara, K. Sigma phase formation in Cr-Ni binary alloy system. *Scr. Metall.* **17,** 111–114 (1983).

165. Gupta, K. P. The Co-Cr-Mo (Cobalt-Chromium-Molybdenum) System. *J. Phase Equilibria Diffus.* **26,** 87–92 (2005).

166. Niemiec, J. & Trzebiatowski, W. The existence of σ- and χ- phases in rhenium alloys. *Bull Acad Pol Sci* **3,** 601–603 (1956).

167. Waterstrat, R. M. & Kasper, J. S. X-Ray diffraction study of the sigma phase in systems Re-Cr, Ru-Cr and Os-Cr. *Trans AIME* **209,** 872–873 (1957).

168. Raub, E. Die Osmium-chrom-legierngen. *Z Met.* **48,** 53–56 (1957).

169. Savitskii, E. M., Terekhova, V. F. & Birun, N. A. Equilibrium diagram of the chromium-ruthenium system. *Russ J Inorg Chem* **6,** 1002–1003 (1961).

170. Darby, J. B., Lam, D. J., Norton, L. J. & Downey, J. W. Intermediate phases in binary systems of technetium-99 with several transition elements. *J. Common Met.* **4,** 558–563 (1962).

171. Muheim, J. & Müller, J. Spezifische wärme im Cr-Re-system antiferromagnetismus und supraleitung. *Phys Kondens Mater.* **2,** 377–396 (1964).

172. Wopersnow, W., Raub, C. J. & Gmünd, S. Die Legierungen des rutheniums mit palladium und chrom sowie eigigen anderen übergangsmetallen. *Metall* **33,** 1261–1265 (1979).

173. Tuganbaev, M. L., Kazakova, E. F. & Sokolovskaya, E. M. Interaction of intermediate phases in the iron-chromium-rhenium system. *J. Common Met.* **124,** L9–L12 (1986).

174. Shoemaker, D. P. & Bergman, B. G. THE CRYSTAL STRUCTURE OF A SIGMA PHASE, FeCr. *J. Am. Chem. Soc.* **72,** 5793 (1950).

175. Dickins, C. J., Douglas, A. M. B. & Taylor, W. H. Sigma-phase in the Co-Cr and Fe-Cr systems. *J Iron Steel Inst* **167,** 27 (1951).

176. Bergman, G. & Shoemaker, D. P. The determination of the crystal structure of the σ phase in the iron–chromium and iron–molybdenum systems. *Acta Crystallogr.* **7,** 857–865 (1954).

177. Ageev, N. V. & Schekhtman, V. S. The Crystal Chemistry of the Compounds of Rhenium with Transition Metals. in *Rhenmium* 46–53 (Elsevier, 1962).

178. Sampathkumar, T. S., Mallya, R. M. & Hegde, M. S. Low temperature preparation and characterization of intermetallics–Fe, W, FeMo and some ternary. *Bull Mater Sci* **7,** (1985).

179. Costa, B. F. O., Caër, G. L. & Campos, N. Study of alpha-sigma phase transformation in mechanically alloyed Fe-Cr-Sn alloys. (2001).

180. Nevitt, M. V. & Downey, J. W. Sigma phases containing osmium and iridium. *Trans AIME* **209,** 1072 (1957).

181. Michalik, S. J. & Brophy, J. H. A constitution diagram for the molybdenum-iridium system. *Trans Met. Soc AIME* **227,** 1047–1053 (1963).

182. Tylkina, M. A., Polyakova, V. P. & Shekhtman, V. S. The iridium-tungsten system. *Russ J Inorg Chem* **8,** 1335–1338 (1963).

183. Ferguson, J. W. H., Giessen, B. C. & Grant, N. J. The constitution diagram tantalum-iridium. *Trans Met. Soc AIME* **227,** 1401–1406 (1963).

184. Giessen, B. C., Koch, R. & Grant, N. J. The niobium (columbium)-iridium constitution. *Trans Met. Soc AIME* **230,** 1268–1273 (1964).

185. Koch, C. C. & Scarbrough, J. O. Superconductivity in Mo-Re and Nb-Ir σ Phases. *Phys. Rev. B* **3,** 742–748 (1971).

186. Khan, (H. R. & Raub, C. J. Superconductivity of A15- and σ-Phase of Nb-Ir. *Appl Phys* **19,** 231–235 (1979).

187. Carlile. *quoted in the Power Diffraction File (PDF)*.

188. Pearson, W. B., Christian, J. W. & Hume-Rothery, W. New Sigma-Phases in Binary Alloys of the Transition Elements of the First Long Period. *Nature* **167,** 110–110 (1951).

189. Decker, B. F., Waterstrat, R. M. & Kasper, J. S. Formation of sigma phase in the Mn-Mo system. *J Met* **197,** 1476 (1953).

190. Greenfield, P. & Beck, P. A. *Trans AIME* **200,** 252 (1954).

191. Gupta, K. P., Rajan, N. S. & Beck, P. A. Effect of Si and Al on the stability of certain sigma phases. *Trans Met. Soc AIME* **218,** 617–624 (1960).

192. Savitskii, E. M. & Tylkina, M. A. Phase Diagrams of Rhenium with Transition Metals. in *Rhenmium* 67–83 (Elsevier, 1962).

193. Setz, S., Nowotny, H. & Benesovsky, F. Untersuchungen in den systemen: Mangan-(Vanadin, Rhenium, Eisen)-Silicium. *Monatsh Chem* **99,** 2004–2015 (1968).

194. Elliott, R. P. & Rostoker, W. Structure of the phase TiMn and the indexing of powder patterns of sigma type phases. *Trans AIME* **197,** 1203–1204 (1953).

195. Anderson, E. & Hume-Rothery, W. The equilibrium diagram of the system molybdenum-ruthenium. *J. Common Met.* **2,** 443–450 (1960).

196. Taylor, A., Doyle, N. J. & Kagle, B. J. The constitution diagram of the system molybdenum-osmium. *J -Common Met* **4,** 436–450 (1962).

197. Quinn, T. J. & Iium-Rotiiety, W. The equilibrium diagram of the system molybdenum-cobalt. *J -Common Met* **5,** 314–324 (1963).

198. Forsyth, J. B. & D'Alte Da Veiga, L. M. The structure of the σ-phase Co2Mo3. *Acta Crystallogr.* **16,** 509–512 (1963).

199. Niemiec, J. X-ray analysis of technetium-molybdenum alloys. *Bull Acad Pol Sci Ser Sci Chim* **11,** 305–309 (1963).

200. Rasmussen, S. E. & Lundtoft, B. New crystal data for Mo.63Ru.37(Mo5Ru3), a superconducting sigma phase. *Power Diffr* **2,** 29–30 (1987).

201. Cornish, L. A. & Pratt, J. N. Constitutional studies of the molybdenum-ruthenium-palladium ternary system. *J Alloy Compd* **247,** 66–71 (1997).

202. Gürler, R. Constitutional studies of molybdenum–ruthenium alloys using ultra-rapidly solidified samples. *J. Alloys Compd.* **285,** 133–136 (1999).

203. Mckinsey, C. R. & Faulring, G. M. A new intermediate phase in the niobium-aluminum system. *Acta Crystallogr* **12,** 701–702 (1959).

204. Gladyshevskii, E. I. Crystal structure of the compound Nb2Al. *J. Struct. Chem.* **2,** 148–151 (1961).

205. Gupta, K. P. Sigma phases with aluminum. *Trans Met. Soc AIME* **221,** 1047–1049 (1961).

206. Ritter, D. L., Giessen, B. C. & Grant, N. J. The niobium (columbium)-rhodium binary system. Part 1: The constitution diagram. *Trans Met. Soc AIME* **230,** 1250–1259 (1964).

207. Lundin, C. E. & Yamamoto, A. S. The equilibrium phase diagram, niobium (columbium)-aluminum. *Trans Met. Soc AIME* **236,** 863–872 (1966).

208. Brown, P. W. & Worzala, F. J. Resistivity and lattice parameter variations in Nb2Al type sigma phases. *J. Mater. Sci.* **11,** 760–766 (1976).

209. Kokot, L., Horyn, R. & Iliew, N. The niobium-aluminum binary system phase equilibria at 1100 °C and superconductivity of alloys. *J -Common Met* **44,** 215–219 (1976).

210. Waterstrat, R. M. & Manuszewski, R. C. The niobium-osmium constitution diagram. *J -Common Met* **51,** 55–67 (1977).

211. Khan, H. R. & Raub, C. J. Measurements of critical magnetic fields and resistance for σ phase Mo-Re. *J -Common Met* **69,** 361–367 (1980).

212. Waterstrat, R. M. & Giessen, B. C. The niobium (columbium)-platinum constitution diagram. *Met. Trans A* **16 A,** 1943–1949 (1985).

213. Tylkina, M. A., Povarova, K. B. & Savitskii, E. M. The sigma phase in the system rhenium-vanadium. *Proc Acad Sci USSR Chem Sec* **131,** 247–249 (1960).

214. Knapton, A. G. The molybdenum-rhenium system. *J Inst Met* **87,** 62–64 (1958).

215. Knapton, A. G. Sigma phases in rhenium alloys. *Bull Inst Met* **3,** 21 (1955).

216. Brophy, J. H., Schwarzkopf, P. & Wulff, J. The tantalum-rhenium system. *Trans Met. Soc AIME* **218,** 910–914. (1960).

217. Wilson, C. G. & Parselle, M. H. Structural changes caused by the neutron irradiation of σ phases. *Acta Crystallogr* **19,** 9–14 (1965).

218. Kuz'ma, Y. B., Lakh, V. I., Stadnyk, B. I. & Voroshilov, Y. V. Phase equilibria in the systems Zr-Re-B and W-Re-B. *Sov Powder Met. Met Ceram* **7,** 462–466 (1968).

219. Stewart, G. R. & Giorgi, A. L. A search for strong coupling superconductivity. *Solid State Commun.* **28,** 969–972 (1978).

220. Edshammar, L. E. & Holmbery, B. The σ-phase Ta2Al. *Acta Chem Scand* **14,** 1219–1220 (1960).

221. Nowotny, H., Brukl, C. & Benesovsky, F. Investigations in the systems Ta-Al-Si and Al-Si-W. *Monatshefte Chem* **92,** 116–127 (1961).

222. Raub, E., Besskow, H. & Menzel, D. Tantal-Gold Legierungen. *Z Met.* **52,** 189–193 (1961).

223. Darby, J. J. B., Downey, J. W. & Norton, L. J. Intermediate phases in the tantalum-palladium system. *Trans Met. Soc AIME* **227,** 1028–1029 (1963).

224. Giessen, B. C., Ibach, H. & Grant, N. J. The constitution diagram tantalum-rhodium. *Trans Met. Soc AIME* **230,** 113–122 (1964).

225. Rudman, P. S. Lattice parameters of tantalum-osmium alloys. *J. Common Met.* **9,** 77–79 (1965).

226. Hansen, R. C. & Raman, A. Alloy chemistry of σ (β-U)-related phases. III. σ-phases with non-transition elements. *Z Met.* **61,** 115–120 (1970).

227. Camacho, M. The binary Ta-Au system. (Univ Geneve, 1973).

228. Kimura, H., Nakano, O. & Ohkoshi, T. On the aluminum-tantalum system. *Keikinzoku* **23,** 106–112 (1973).

229. Khan, H. R., Lüders, K., Raub, C. J. & Roth, G. Superconductivity and resistance behaviour of σ-phase alloys: Nb-Rh and Ta-Rh. *Z Phys B-Condens Matter* **38,** 27–33 (1980).

230. Schuster, J. C. Phases and phase relations in the system Ta-Al. *Z Met.* **76,** 724–729 (1985).

231. Okamoto, H. Al-Ta (Aluminum-Tantalum). *J. Phase Equilibria Diffus.* **31,** 578–579 (2010).

232. Moseley, P. T. & Seabrook, C. J. The crystal structure of β-tantalum. *Acta Crystallogr. B* **29,** 1170–1171 (1973).

233. Arakcheeva, A., Chapuis, G. & Grinevitch, V. The self-hosting structure of β-Ta. *Acta Crystallogr B* **58,** 1–7 (2002).

234. Arakcheeva, A., Chapuis, G., Birkedal, H., Pattison, P. & Grinevitch, V. The commensurate composite σ-structure of β-tantalum. *Acta Crystallogr B* **59,** (2003).

235. Pearson, W. B. & Christian, J. W. The structure of the σ phase in vanadium-nickel alloys. *Acta Crystallogr* **5,** 157–163 (1952).

236. Martens, H. & Duwez, P. Phase relationships in the iron-chromium-vanadium system. *Trans Am Soc Met* **44,** 484–493 (1952).

237. Hanneman, R. E. & Mariano, A. N. Lattice-parameter and volumetric data of the iron-vanadium system. *Trans Met. Soc AIME* **230,** 937–939 (1964).

238. Prima, S. B., Tret'yachenko, L. A. & Kostrigina, G. I. Isothermal section of the vanadium-nickel-molybdenum system at 1150 °C. *Dokl Akad Nauk SSSR A* **3,** 229–233 (1979).

239. van der Kraan, A. M., de Mooij, D. B. & Buschow, K. H. J. Magnetic properties and 57Fe mössbauer effect in V1-xFex alloys. *Phys Status Solidi A* **88,** 231–237 (1985).

240. Lomnytska, Y. F. & Pavliv, O. P. Phase equilibria in the V-Ni-Sb system. *Inorg. Mater.* **43,** 608–613 (2007).

241. Chen, X. J., Zhou, H. Y., Wang, T., Yang, Y. Q. & Rao, G. H. The crystal structure of La-doped Co40V60 compound. *J. Alloys Compd.* **503,** 281–285 (2010).

242. Eremenko, V. N., Khar'kova, A. M. & Velikanova, T. J. Intermetallic compounds in the rhenium-vanadium system. *Dopovidi Akad Nauk URSR Fiz-Mat Ta Tekhnichni Nauk* **45,** 78–81 (1983).

243. Gupta, K. P. The Ni-Re-V (Nickel-Rhenium-Vanadium) System. *J. Phase Equilibria Diffus.* **31,** 475–477 (2010).

244. Rostoker, W. & Yamamoto, A. A survey of vanadium binary systems. *Trans Am Soc Met* **46,** 1136–1167 (1954).

245. Eremenko, V. N., Tretyachenko, L. A. & Golubenko, Z. P. On the existence boundary of the sigma-phase in the tantalun-vanadium system. *Dopovidi Akad Nauk URSR* **2,** 192–195 (1962).

246. Savitskii, E. M. & Efimov, J. V. Superconducting metallic compounds and their alloys. *Monatshefte Chem* **103,** 270–287 (1972).

247. Okamoto, H. Ta-V (Tantalum-Vanadium). *J. Phase Equilibria Diffus.* **26,** 298–299 (2005).

248. Khan, A. U. *et al.* The system Ta–V–Si: Crystal structure and phase equilibria. *J. Solid State Chem.* **187,** 114–123 (2012).

249. Obrowski, W. Eine σ-phase im system Ru-W. *Naturwissenschaften* **44,** 581 (1957).

250. Taylor, A., Kalge, B. J. & Doyle, N. J. The constitution diagram of the tungsten-osmium binary system. *J -Common Met* **3,** 333–347 (1961).

251. Niemiec, J. X-ray analysis of technetium binary alloys with tungsten and rhenium. *Bull Acad Pol Sci Ser Sci Chim* **11,** 311–316 (1963).

252. Rapperport, E. J. & Smith, M. F. The constitution diagram tungsten-ruthenium. *Trans Met. Soc AIME* **230,** 6–11 (1964).

253. Giorgi, A. L. Superconductivity in the W-Tc and W2C-Tc systems. *Phys BC* **135,** 420–422 (1985).

254. Raman, A. & Schubert, K. Strukturuntersuchungen in einigen zu T4-T9 homologen und quasihomologen legierungssystemen. *Z Met.* **55,** 704–710 (1964).

255. Eremenko, V. N., Semenova, E. L. & Shtepa, T. D. State diagram of the Zr-Ir system. *Russ Met.* **5,** 210–213 (1980).

256. Genzual, K. & Parthé, E. Zr3Ir with tetragonal α-V3S structure. *Acta Crystallogr C* **41,** 820–823 (1985).

257. Savitskii, E. M., Tylkina, M. A. & Tsyganova, I. A. Phase diagram of the zirconium-rhenium system. *At. Energy* **7,** 724–727 (1961).

258. Murphy, H. J., Sims, C. T. & Reltran, A. M. PHACOMP revisited. *J. Met.* 47–66 (1968).

259. Morinaga, M., Yukawa, N., Adachi, H. & Ezaki, H. New PHACOMP and its application to alloy design. *Superalloys 1984* 523–532 (1984).

260. Cieslak, M. J., Knorovsky, G. A., Headley, T. J. & Romig, A. D. The use of new PHACOMP in understanding the solidification microstructure of nickel base alloy weld metal. *Metall. Mater. Trans. A* **17,** 2107–2116 (1986).

261. Sluiter, M. H. F. Prediction of Site Preference and Phase Stability of Transition Metal Based Frank-Kasper Phases. *EPD Congr. 2005 Ed. ME Schlesinger TMS Miner. Met. Mater. Soc.* (2005).

262. Ageev, N. V. & Shekhtman, V. S. The nature of sigma phases. *Dokl Akad Nauk SSSR* **135,** 309–311 (1960).

263. Alte da Veiga, L. M. The ordering of the σ-phase Cr2Ru. *Portgal Phys* **4,** 205–214 (1966).

264. Decker, B. F. & Kasper, J. S. Evidence for order in the Mn-Mo sigma phase. *J Met* **200,** 1406–1407 (1954).

265. Ageev, N. V. & Shekhtman, V. S. X-ray diffraction studies of alloys of rhenium with molybdenum. *Bull Acad Sci USSR Phys Ser* **23,** 638–639 (1959).

266. Brown, P. J. & Forsyth, J. B. The structure of the σ-phase Nb2Al. *Acta Crystallogr.* **14,** 362–364 (1961).

Appendix

Appendix A.

Table S.1 : Order degree calculated from the experimental site occupancy of the sigma phase from the literature.

AxBy	X(A)	Vm,10^{-6} m^3/mol	T/°C	A site occupancies					Order degree						Reference
				2a	4f	$8i_1$	$8i_2$	8j	S_{2a}	S_{4f}	S_{8i1}	S_{8i2}	S_{8j}	S	
SMe															
$V_{19}Mn_{81}$	0.191	---	as cast	0.000	0.450	0.150	0.000	0.340	0.067	0.043	-0.013	0.267	0.049	0.412	[99]
$V_{13.7}Mn_{86.3}$	0.139	7.341	970_11d	**0.000**	**0.320**	**0.150**	**0.010**	**0.200**	0.067	0.028	0.004	0.247	0.019	0.365	[9]
$V_{26.8}Mn_{73.2}$	0.269	7.386	970_11d	**0.100**	**0.590**	**0.260**	**0.040**	**0.390**	0.042	0.059	-0.003	0.227	0.044	0.368	[9]
$V_{60}Fe_{40}$	0.599	---	700_70h	0.150	1.000	0.810	0.150	0.750	0.050	0.133	0.140	0.200	0.100	0.624	[96]
$V_{59}Fe_{41}$	0.590	7.535	700_25d	**0.141**	**0.936**	**0.814**	**0.079**	**0.815**	0.051	0.113	0.146	0.231	0.146	0.686	[10]
$V_{47.9}Fe_{52.1}$	0.479	7.405	700_25d	**0.072**	**0.838**	**0.662**	**0.037**	**0.660**	0.057	0.092	0.094	0.246	0.093	0.581	[10]
$V_{39.9}Fe_{60.1}$	0.399	7.317	700_25d	**0.047**	**0.739**	**0.543**	**0.029**	**0.543**	0.059	0.075	0.064	0.247	0.064	0.509	[10]
$V_{62}Co_{38}$	0.619	---	---	0.350	0.990	0.840	0.150	0.750	0.029	0.130	0.155	0.202	0.092	0.607	[102]
$V_{61.3}Ni_{38.7}$	0.613	7.445	500_120h	0.150	1.000	0.700	0.125	0.935	0.050	0.133	0.060	0.212	0.222	0.678	[96]
$V_{64.3}Ni_{35.7}$	0.644	7.511	500_120h	0.100	1.000	0.810	0.090	0.990	0.056	0.133	0.124	0.229	0.259	0.803	[96]
$V_{69}Ni_{31}$	0.693	7.661	500_120h	0.150	0.980	0.940	0.140	0.990	0.052	0.125	0.215	0.213	0.258	0.862	[96]
$V_{68}Ni_{32}$	0.680	7.592	850_32d	**0.000**	**1.000**	**0.840**	**0.500**	**0.710**	0.067	0.133	0.133	0.071	0.025	0.429	[9]
$V_{65}Ni_{35}$	0.649	7.584	600_34d	**0.320**	**0.970**	**0.700**	**0.200**	**0.970**	0.034	0.122	0.039	0.185	0.244	0.623	[9]
$Cr_{25}Mn_{75}$	0.252	---	850_24h	0.000	0.250	0.380	0.000	0.440	0.067	0.000	0.046	0.267	0.067	0.446	[96]
$Cr_{20}Mn_{80}$	0.200	---	as cast	0.100	0.350	0.150	0.050	0.350	0.033	0.025	-0.017	0.200	0.050	0.292	[99]
$Cr_{24}Mn_{76}$	0.232	7.234	1100_27d	**0.080**	**0.320**	**0.270**	**0.070**	**0.350**	0.044	0.015	0.013	0.186	0.041	0.299	[9]
$Cr_{23}Mn_{77}$	0.233	7.236	900_28d	**0.100**	**0.280**	**0.270**	**0.080**	**0.360**	0.038	0.008	0.013	0.175	0.044	0.278	[9]
$Cr_{44}Fe_{56}$	0.440	---	650	0.300	0.550	0.450	0.350	0.500	0.021	0.026	0.005	0.055	0.029	0.135	[99]
$Cr_{47.8}Fe_{52.2}$	0.477	7.083	790_350h	**0.100**	**0.730**	**0.600**	**0.150**	**0.650**	0.053	0.064	0.063	0.183	0.088	0.451	[103]
$Cr_{48.2}Fe_{51.8}$	0.487	7.081	740_170h	**0.100**	**0.700**	**0.590**	**0.130**	**0.730**	0.053	0.055	0.054	0.195	0.126	0.484	[103]
$Cr_{49.5}Fe_{50.5}$	0.495	7.080	650_1400h	**0.130**	**0.750**	**0.630**	**0.160**	**0.660**	0.049	0.067	0.071	0.181	0.087	0.455	[103]
$Cr_{48.2}Fe_{51.8}$	0.483	---	650	**0.110**	**0.730**	**0.620**	**0.110**	**0.690**	0.051	0.064	0.071	0.206	0.107	0.498	[103]
$Cr_{49.5}Fe_{50.5}$	0.495	7.073	700_25d	**0.113**	**0.751**	**0.638**	**0.100**	**0.715**	0.051	0.068	0.075	0.213	0.116	0.523	[10]
$Cr_{49.1}Fe_{50.9}$	0.492	7.078	700_25d	**0.144**	**0.755**	**0.616**	**0.116**	**0.698**	0.047	0.069	0.065	0.204	0.108	0.493	[10]
$Cr_{48}Fe_{52}$	0.481	7.066	700_25d	**0.151**	**0.723**	**0.608**	**0.122**	**0.673**	0.046	0.062	0.065	0.199	0.099	0.471	[10]
$Cr_{47.6}Fe_{52.4}$	0.477	7.070	700_25d	**0.132**	**0.729**	**0.601**	**0.124**	**0.668**	0.048	0.064	0.063	0.197	0.097	0.470	[10]
$Cr_{46.2}Fe_{53.8}$	0.463	7.066	700_25d	**0.087**	**0.740**	**0.587**	**0.099**	**0.657**	0.054	0.069	0.062	0.210	0.096	0.491	[10]

$Cr_{45.3}Fe_{54.7}$	0.453	7.069	700_25d	**0.124**	**0.704**	**0.574**	**0.100**	**0.643**	0.048	0.061	0.059	0.208	0.093	0.469	[10]
$Cr_{46.2}Fe_{53.8}$	0.462	---	600_31d	**0.104**	**0.726**	**0.583**	**0.090**	**0.672**	0.052	0.065	0.060	0.215	0.104	0.496	[10]
$Cr_{46.2}Fe_{53.8}$	0.463	---	700_70d	**0.106**	**0.704**	**0.596**	**0.102**	**0.659**	0.051	0.060	0.066	0.208	0.097	0.483	[10]
$Cr_{46.2}Fe_{53.8}$	0.462	---	700_35d	**0.125**	**0.717**	**0.609**	**0.093**	**0.642**	0.049	0.063	0.073	0.213	0.089	0.487	[10]
$Cr_{46.2}Fe_{53.8}$	0.462	---	700_277d	**0.124**	**0.733**	**0.607**	**0.087**	**0.642**	0.049	0.067	0.072	0.216	0.089	0.493	[10]
$Cr_{53.3}Co_{46.7}$	0.533	---	no	0.000	1.000	1.000	0.000	0.500	0.067	0.133	0.267	0.267	-0.019	0.714	[159]
$Cr_{61}Co_{39}$	0.610	---	as cast	0.350	0.950	0.850	0.375	0.500	0.028	0.116	0.164	0.103	-0.075	0.336	[99]
$Cr_{57}Co_{43}$	0.570	---	1000_6d	**0.070**	**0.797**	**0.801**	**0.111**	**0.809**	0.058	0.070	0.144	0.215	0.148	0.635	[114]
$Cr_{62.7}Co_{37.3}$	0.627	---	1000_6d	**0.107**	**0.823**	**0.852**	**0.172**	**0.889**	0.055	0.070	0.161	0.194	0.187	0.667	[114]
$Cr_{65.7}Co_{34.3}$	0.657	---	1000_6d	**0.240**	**0.816**	**0.903**	**0.196**	**0.898**	0.042	0.062	0.191	0.187	0.188	0.670	[114]
$W_{34}Re_{66}$	0.337	---	---	**0.050**	**0.600**	**0.460**	**0.020**	**0.470**	0.057	0.053	0.050	0.251	0.054	0.464	[106]
$W_{44}Re_{56}$	0.437	---	---	**0.070**	**0.720**	**0.620**	**0.080**	**0.560**	0.056	0.067	0.087	0.218	0.058	0.486	[106]
$W_{54}Re_{46}$	0.536	---	---	**0.160**	**0.920**	**0.750**	**0.060**	**0.700**	0.047	0.110	0.123	0.237	0.094	0.611	[106]
LAs															
$Re_{53}Mn_{47}$	0.533		1000_360h	0.000	1.000	0.750	0.000	0.750	0.067	0.133	0.124	0.267	0.124	0.714	[262]
$Re_{51.4}Mn_{48.6}$	0.512		1150_24h	**0.120**	**0.860**	**0.760**	**0.280**	**0.420**	0.051	0.095	0.136	0.121	-0.050	0.352	[9]
LAs-LAe															
$Ru_{33}Cr_{67}$	0.333	---	---	0.250	0.370	0.400	0.350	0.250	0.017	0.007	0.027	-0.014	-0.033	0.004	[263]
$Ru_{33}Cr_{67}$	0.332	7.821	1300_72h	0.200	0.350	0.400	0.450	0.170	0.027	0.004	0.027	-0.095	-0.065	-0.102	[101]
$Ru_{33}Cr_{67}$	0.330	7.733	1400_9h	**0.250**	**0.450**	**0.400**	**0.330**	**0.220**	0.016	0.024	0.028	0.000	-0.044	0.024	[9]
$Re_{60}Cr_{40}$	0.600	---	1000_500h	1.000	0.000	1.000	1.000	0.000	-0.044	-0.200	0.267	-0.178	-0.400	-0.556	[9]
$Re_{60}Cr_{40}$	0.599	8.420	---	0.250	0.750	0.690	0.500	0.620	0.039	0.050	0.060	0.044	0.014	0.207	[98]
$Re_{62}Cr_{38}$	0.624	---	---	0.320	0.920	0.860	0.400	0.540	0.032	0.105	0.167	0.096	-0.060	0.341	[100]
$Re_{54}Cr_{46}$	0.542	8.230	1000_7d	**0.210**	**0.860**	**0.780**	**0.320**	**0.450**	0.041	0.093	0.139	0.109	-0.054	0.328	[9]
$Re_{58}Cr_{42}$	0.581	8.348	1000_11d	**0.180**	**0.870**	**0.780**	**0.450**	**0.470**	0.046	0.092	0.127	0.060	-0.071	0.254	[9]
$Re_{69}Cr_{31}$	0.747	8.625	1000_11d	**0.320**	**0.940**	**0.860**	**0.840**	**0.550**	0.038	0.102	0.119	-0.033	-0.207	0.019	[9]
$Re_{78}V_{22}$	0.777	---	as cast	**0.86**	**0.78**	**0.83**	**0.91**	**0.57**	-0.007	0.002	0.063	-0.046	-0.248	-0.236	[9]
$Os_{33}Cr_{67}$	0.333	7.711	1400_24h	0.200	0.420	0.400	0.440	0.150	0.027	0.017	0.027	-0.085	-0.073	-0.088	[101]
$Os_{30.7}Cr_{69.3}$	0.307	7.777	1600_8h	**0.160**	**0.460**	**0.360**	**0.350**	**0.170**	0.032	0.029	0.021	-0.038	-0.053	-0.008	[9]
LAs-SMe															
$Mo_{40}Mn_{60}$	0.400	7.879	---	0.000	1.000	0.500	0.000	0.500	0.067	0.133	0.044	0.267	0.044	0.556	[264]
$Mo_{34}Mn_{66}$	0.341	7.969	1150_24h	**0.000**	**0.680**	**0.530**	**0.020**	**0.390**	0.067	0.069	0.076	0.251	0.020	0.482	[9]
$Mo_{50}Fe_{50}$	0.500	8.210	---	0.000	0.750	0.750	0.000	0.750	0.067	0.067	0.133	0.267	0.133	0.667	[97]
$Mo_{55.7}Fe_{44.2}$	0.555	8.289	1450_8h	**0.050**	**0.980**	**0.820**	**0.080**	**0.680**	0.061	0.127	0.159	0.228	0.075	0.650	[9]
$Mo_{45}Fe_{55}$	0.450	8.058	1430_6h	---	**0.884**	**0.719**	---	**0.524**	---	---	---	---	---	---	[115]
$Mo_{46}Fe_{54}$	0.460	8.090	1430_6h	---	**0.921**	**0.740**	---	**0.525**	---	---	---	---	---	---	[115]
$Mo_{47}Fe_{53}$	0.470	8.110	1430_6h	---	**0.881**	**0.738**	---	**0.584**	---	---	---	---	---	---	[115]
$Mo_{48}Fe_{52}$	0.480	8.129	1430_6h	---	**0.849**	**0.768**	---	**0.607**	---	---	---	---	---	---	[115]
$Mo_{49}Fe_{51}$	0.490	8.143	1430_6h	---	**0.874**	**0.782**	---	**0.621**	---	---	---	---	---	---	[115]
$Mo_{51}Fe_{49}$	0.510	8.188	1430_6h	---	**0.885**	**0.788**	---	**0.682**	---	---	---	---	---	---	[115]
$Mo_{53}Fe_{47}$	0.530	8.232	1430_6h	---	**0.909**	**0.825**	---	**0.707**	---	---	---	---	---	---	[115]
$Mo_{55}Fe_{54}$	0.550	8.274	1430_6h	---	**0.979**	**0.826**	---	**0.738**	---	---	---	---	---	---	[115]
$Mo_{55}Fe_{54}$	0.550	---	1430_6h	---	**0.978**	**0.835**	---	**0.750**	---	---	---	---	---	---	[115]
$Mo_{56.2}Fe_{43.8}$	0.562	8.298	1430_6h	---	**0.981**	**0.860**	---	**0.759**	---	---	---	---	---	---	[115]
$Mo_{60}Co_{40}$	0.603	8.252	1400	0.000	1.000	0.880	0.000	0.880	0.067	0.133	0.186	0.267	0.186	0.839	[198]

$Mo_{62.5}Co_{37.5}$	0.627	8.338	1350_8h	**0.000**	**1.000**	**0.920**	**0.030**	**0.900**	0.067	0.133	0.210	0.254	0.195	0.859	[9]
$Ta_{62.7}Rh_{37.3}$	0.627	9.801	1530_8h	**0.400**	**0.800**	**0.910**	**0.040**	**0.900**	0.024	0.062	0.202	0.250	0.195	0.733	[9]
$Ta_{74.4}Rh_{25.6}$	0.743	10.162	1570_8h	**0.470**	**0.960**	**1.000**	**0.200**	**0.990**	0.025	0.113	0.267	0.195	0.256	0.855	[9]
$Ta_{76.2}Pd_{23.8}$	0.764	---	1650_8h	**0.200**	**0.890**	**1.000**	**0.370**	**1.000**	0.049	0.071	0.267	0.138	0.267	0.791	[9]
$W_{63}Ru_{37}$	0.629	---	1750_3h	**0.420**	**0.830**	**0.900**	**0.140**	**0.800**	0.022	0.072	0.195	0.207	0.123	0.619	[9]
$Re_{40}Fe_{60}$	0.400	---	1500_6h	0.000	1.000	0.500	0.000	0.500	0.067	0.133	0.044	0.267	0.044	0.556	[9]
$Re_{49}Fe_{51}$	0.487	---	---	0.100	0.900	0.780	0.140	0.430	0.053	0.107	0.152	0.190	-0.029	0.473	[100]
$Re_{46.4}Fe_{53.6}$	0.468	---	1300_8h	**0.160**	**0.890**	**0.690**	**0.180**	**0.400**	0.044	0.106	0.111	0.164	-0.034	0.391	[9]
$Re_{42.8}Fe_{57.2}$	0.428	7.813	1527_5h	**0.119**	**0.827**	**0.685**	**0.085**	**0.395**	0.048	0.093	0.120	0.214	-0.015	0.459	[116]
$Re_{43}Fe_{57}$	0.430	7.819	1527_5h	**0.089**	**0.867**	**0.696**	**0.073**	**0.393**	0.053	0.102	0.124	0.222	-0.017	0.484	[116]
$Re_{45}Fe_{55}$	0.450	7.854	1527_5h	**0.064**	**0.873**	**0.724**	**0.115**	**0.4**	0.057	0.102	0.133	0.198	-0.024	0.467	[116]
$Re_{47}Fe_{53}$	0.470	7.888	1527_5h	**0.074**	**0.869**	**0.743**	**0.124**	**0.446**	0.056	0.100	0.138	0.196	-0.012	0.478	[116]
$Re_{49}Fe_{51}$	0.490	7.930	1527_5h	**0.096**	**0.881**	**0.743**	**0.163**	**0.467**	0.054	0.102	0.132	0.178	-0.012	0.455	[116]
$Re_{53}Fe_{47}$	0.530	8.009	1527_5h	**0.065**	**0.904**	**0.788**	**0.225**	**0.513**	0.058	0.106	0.146	0.154	-0.010	0.455	[116]
SMs-SMe															
$Nb_{45}Re_{55}$	0.448	9.808	---	0.000	1.000	0.590	0.000	0.590	0.067	0.133	0.069	0.267	0.069	0.604	[98]
$Nb_{42.6}Re_{57.4}$	0.426	9.788	as cast	**0.030**	**0.920**	**0.500**	**0.020**	**0.610**	0.062	0.115	0.034	0.254	0.085	0.551	[9]
$Nb_{60}Os_{40}$	0.600	---	---	0.000	1.000	1.000	0.000	0.750	0.067	0.133	0.267	0.267	0.100	0.833	[98]
$Nb_{60}Ir_{40}$	0.603	---	---	0.000	1.000	0.880	0.000	0.880	0.067	0.133	0.186	0.267	0.186	0.839	[98]
$Nb_{68.2}Pt_{31.8}$	0.683	---	1550_8h	**0.290**	**1.000**	**0.980**	**0.040**	**0.970**	0.038	0.133	0.250	0.251	0.241	0.914	[9]
$Mo_{40}Re_{60}$	0.400	---	1600_30h	0.000	1.000	0.000	0.000	1.000	0.067	0.133	-0.178	0.267	0.267	0.556	[265]
$Mo_{32}Re_{68}$	0.333	9.153	---	0.000	0.500	0.500	0.000	0.500	0.067	0.033	0.067	0.267	0.067	0.500	[97]
$Mo_{45}Re_{55}$	0.452	9.224	---	0.000	0.750	0.500	0.190	0.630	0.067	0.073	0.023	0.155	0.087	0.404	[97]
$Mo_{29.9}Re_{70.1}$	0.299	9.131	1600_4h	**0.000**	**0.560**	**0.370**	**0.010**	**0.460**	0.067	0.050	0.027	0.258	0.061	0.463	[117]
$Mo_{31.9}Re_{68.1}$	0.317	9.141	1200_17d	**0.030**	**0.680**	**0.350**	**0.010**	**0.480**	0.060	0.071	0.013	0.258	0.064	0.466	[117]
$Mo_{40.4}Re_{59.6}$	0.404	9.190	1600_35min	**0.080**	**0.750**	**0.480**	**0.120**	**0.520**	0.053	0.077	0.034	0.187	0.052	0.404	[117]
$Mo_{46}Re_{54}$	0.461	9.222	1200_17d	**0.090**	**0.830**	**0.510**	**0.120**	**0.660**	0.054	0.091	0.024	0.197	0.099	0.465	[117]
$Mo_{48}Re_{52}$	0.480	9.234	1600_7h	**0.000**	**0.780**	**0.640**	**0.150**	**0.620**	0.067	0.077	0.082	0.183	0.072	0.481	[117]
$Mo_{65}Os_{35}$	0.651	---	---	0.250	1.000	0.940	0.060	0.880	0.041	0.133	0.221	0.242	0.175	0.812	[98]
$Mo_{72}Ir_{28}$	0.719	---	---	0.500	1.000	1.000	0.190	0.880	0.020	0.133	0.267	0.196	0.153	0.769	[98]
X-Al															
$Nb_{67}Al_{33}$	0.667	10.292	---	0.000	1.000	1.000	0.000	1.000	0.067	0.133	0.267	0.267	0.267	1.000	[266]
$Nb_{59}Al_{41}$	0.587	10.221	1250_10d	0.500	1.000	0.656	0.170	0.750	0.010	0.133	0.045	0.189	0.105	0.482	[205]
$Nb_{65.8}Al_{34.2}$	0.659	10.245	1000_12d	**0.090**	**0.900**	**0.960**	**0.050**	**0.990**	0.058	0.094	0.235	0.246	0.259	0.892	[9]
$Nb_{71}Al_{29}$	0.708	10.302	850_30d	**0.140**	**1.000**	**1.000**	**0.120**	**1.000**	0.053	0.133	0.267	0.221	0.267	0.942	[9]
$Ta_{67}Al_{33}$	0.667	10.144	---	0.000	1.000	1.000	0.000	1.000	0.067	0.133	0.267	0.267	0.267	1.000	[220]
$Ta_{60}Al_{40}$	0.603	10.144	1460_9h	**0.060**	**0.810**	**0.900**	**0.050**	**0.890**	0.060	0.070	0.200	0.245	0.193	0.767	[119]
$Ta_{61}Al_{39}$	0.613	10.150	1000_7h	**0.050**	**0.790**	**0.920**	**0.050**	**0.920**	0.061	0.061	0.212	0.245	0.212	0.790	[119]
$Ta_{65}Al_{35}$	0.655	10.208	1460_8h	**0.040**	**0.950**	**0.980**	**0.030**	**0.960**	0.063	0.114	0.251	0.254	0.236	0.918	[119]
$Ta_{72.4}Al_{27.6}$	0.721	10.314	1460_8h	**0.170**	**1.000**	**1.000**	**0.160**	**1.000**	0.051	0.133	0.267	0.207	0.267	0.925	[119]
$Ta_{74}Al_{26}$	0.739	10.347	1460_7h	**0.210**	**1.000**	**1.000**	**0.220**	**1.000**	0.048	0.133	0.267	0.187	0.267	0.902	[119]
$Ta_{76}Al_{24}$	0.756	10.490	1460_8h	**0.320**	**0.970**	**0.960**	**0.340**	**0.970**	0.038	0.117	0.223	0.147	0.234	0.759	[119]

Appendix B.

To be consistent with the compound energy formalism (CEF), the molar volume is modeled as:

$$V_m = \sum y_i^{'} y_j^{''} y_k^{'''} V_{ijk} + V_m^E , \qquad \text{(B.1)}$$

where $y^{'}$, $y^{''}$ and $y^{'''}$ are the site fractions in the first, second and third SL, respectively. The subscripts i, j and k represent the constituent elements. V_m^E is the excess molar volume, and the molar volume of the end-member compound, V_{ijk}, is expressed as:

$$V_{ijk} = \frac{x}{x+y+z} V_i + \frac{y}{x+y+z} V_j + \frac{z}{x+y+z} V_k + V_{ijk}^E, \quad \text{(B.2)}$$

where for the sigma phase, the stoichiometric factor x, y and z are 10, 4 and 16, respectively. V_i, V_j and V_k represent molar volumes of pure elements in the hypothetic crystal structure of the sigma phase. Here we show that when both excess molar volumes, V_m^E and V_{ijk}^E, are zero, the molar volume of a non-stoichiometric compound is independent of site fraction.

To simplify the derivation, a ternary sigma phase $(A,B,C)_x(A,B,C)_y(A,B,C)_z$ is chosen to demonstrate the procedure. Its molar volume is composed of 27 end-member compounds as follows:

$$V_m = y_A^{'} y_A^{''} y_A^{'''} V_{AAA} + y_A^{'} y_A^{''} y_B^{'''} V_{AAB} + y_A^{'} y_A^{''} y_C^{'''} V_{AAC} + y_A^{'} y_B^{''} y_A^{'''} V_{ABA} + y_A^{'} y_B^{''} y_B^{'''} V_{ABB} + y_A^{'} y_B^{''} y_C^{'''} V_{ABC} + y_A^{'} y_C^{''} y_A^{'''} V_{ACA} + y_A^{'} y_C^{''} y_B^{'''} V_{ACB} + y_A^{'} y_C^{''} y_C^{'''} V_{ACC} + y_B^{'} y_A^{''} y_A^{'''} V_{BAA} + \cdots + y_C^{'} y_A^{''} y_A^{'''} V_{CAA} + \cdots + y_C^{'} y_C^{''} y_C^{'''} V_{CCC} \quad \text{(B.3)}$$

$$V_{ABC} = \frac{x}{x+y+z} V_A + \frac{y}{x+y+z} V_B + \frac{z}{x+y+z} V_C \quad \text{(B.4)}$$

where V_A, V_B and V_C are molar volumes of A, B and C, respectively, in the structure of the sigma phase. By expanding and regrouping in terms of V_A, V_B and V_C, and using the following constrains:

$$y_A^{'} + y_B^{'} + y_C^{'} = 1, y_A^{''} + y_B^{''} + y_C^{''} = 1, y_A^{'''} + y_B^{''}{}' + y_C^{'''} = 1 \quad \text{(B.5)}$$

We can obtain:

$$V_m = \frac{x y_A^{'} + y y_A^{''} + z y_A^{'''}}{x+y+z} V_A + \frac{x y_B^{'} + y y_B^{''} + z y_B^{'''}}{x+y+z} V_B + \frac{x y_C^{'} + y y_C^{''} + z y_C^{'''}}{x+y+z} V_C \quad \text{(B.6)}$$

Taking into account the relation between mole fraction and site fraction, i.e.

$$x_A = \frac{x y_A^{'} + y y_A^{''} + z y_A^{'''}}{x+y+z}, x_B = \frac{x y_B^{'} + y y_B^{''} + z y_B^{'''}}{x+y+z}, x_C = \frac{x y_C^{'} + y y_C^{''} + z y_C^{'''}}{x+y+z} \quad \text{(B.7)}$$

it finally arrives:

$$V_m = x_A V_A + x_B V_B + x_C V_C \quad \text{(B.8)}$$

It is straightforward however tedious to extrapolate to a n-component system, leading to:

$$V_m = \sum_{i=1}^{n} x_i V_i \qquad \text{(B.9)}$$

It is obvious that the molar volume of a compound is dependent on composition and independent of site fraction under the condition that both excess molar volumes, V_m^E and V_{ijk}^E, are zero, which means that the volume data for a compound can be separated from

its thermodynamic description. It is worth mentioning that, however, when databases for thermodynamics and volume are integrated as mentioned earlier, the stoichiometric ratio (10:6:14 for the sigma phase) should be the same. In other words, the models for molar volume and thermodynamic properties should be compatible.